Paleoenvironmental reconstructions in the Baltic Sea and Iberian Margin

Assessment of GDGTs and long-chain alkenones in Holocene sedimentary records

Lisa Alexandra Warden

Photography:
Cover photos: Dietmar Rüß
Inside photos: Dietmar Rüß, René Heistermann and Claudia Zell

Printed by:
Ridderprint, Ridderkerk

Paleoenvironmental reconstructions in the Baltic Sea and Iberian Margin
Assessment of GDGTs and long-chain alkenones in Holocene sedimentary records

Het gebruik van GDGTs en alkenonen in Holocene sedimentaire archieven van de Baltische Zee en kustzeeën van het Iberisch schiereiland voor paleomilieureconstructie

(met een samenvatting in het Nederlands)

Proefschrift

ter verkrijging van de graad van doctor aan de Universiteit Utrecht op gezag van de rector magnificus, prof. dr. G.J. van der Zwaan, ingevolge het besluit van het college voor promoties in het openbaar te verdedigen op vrijdag 31 maart 2017 des middags te 12.45 uur

door

Lisa Alexandra Warden

geboren op 24 januari 1982
te Philadelphia, Verenigde Staten van Amerika

Promotor: Prof. dr. ir. J.S. Sinninghe Damsté

This work has been financially supported by the European Research Council (ERC) and the NIOZ Royal Netherlands Institute for Sea Research.

“We are the first generation to feel the impact of climate change and the last generation that can do something about it.”

-President Obama

For Lauchlan, who was with me the whole time as I wrote this thesis.

Photo by Dietmar Rüß

Contents

Photo by Dietmar Rüß

CHAPTER 1

Introduction

1.1. The Importance of Reconstructing Past Environments

Understanding past climate variability is important for predicting how future climate systems will be affected by anthropogenic greenhouse gas emissions, which in turn can impact ecosystems and their organisms and human societies. The global climate is a very dynamic system, which makes predicting how the climate will react to current anthropogenic forcings difficult. Scientists are striving to gain more information on the climate system in order to try and better understand it. This will allow for proposals to be made on how to mitigate human impact on the climate system as well as to more accurately predict how the environment and human societies will be affected by future climate change. Some of the threats associated with climate change include prolonged increase in temperatures resulting in damage and irreparable loss of unique and threatened ecosystems, increased probability of extreme weather events such as floods, droughts, tropical cyclones and storms, regions and countries being adversely affected by these extreme events, increases in vector organisms (i.e. mosquitoes) and vector born infectious diseases (i.e. malaria) as well as projected sea level rise and the increased probability of large scale events like the collapse of the West Antarctic Ice sheet or the cessation of the North Atlantic thermohaline circulations (IPCC, 2007). Hypoxia, or low oxygen conditions that occurs in aquatic environments when oxygen concentrations dwindle can be harmful to aquatic organisms (Wieland and Zuzarte, 1991; Wieland et al., 1994; Bagge et al., 1994; Brander, 2005), is another example of a threat to ecosystems that can be intensified by global climate change and has far reaching effects. When fish die offs occur due to low oxygen conditions, animals higher up in the food web that rely on them, including humans, are negatively impacted (Bagge et al., 1994; Diaz, 2001; Karlson et al., 2002; Weeks et al., 2002; Chan et al., 2008). Since hypoxia can be exacerbated by warmer water temperatures (Matear & Hirst, 2003; Stramma et al., 2008; Hoegh-Guldberg & Bruno, 2010), hypoxic zones are occurring more often and persisting longer in some regions, such as in the Baltic Sea, due partly to global climate change (Wasmund, 1997; Kabel et al., 2012).

One way to determine how the climate and environment may respond to human induced forcings is through the use of models, which are created to predict future variability in the climate as well as the possible effects of changing climate on the environment, i.e. through the intensification of hypoxia. These models are based partially upon what we know of past climate variability. Since instrumental records are only available from the recent past, information from geological climate archives such as marine sediments, ice cores, tree rings and corals (e.g. Bradley and Jones, 1993; Alley et al., 1997; Jones et al., 1998; Jones and

Mann, 2004; Weijers et al., 2007a) are used to extend the climate record back in the past. Because we often cannot directly measure past environmental parameters we must use climate indicators called proxies (Jones et al., 1998), which provide measureable information about important climatic and environmental parameters such as temperature, salinity, nutrient availability, CO_2 concentration (Wefer et al., 1999 and references cited therein) and hypoxia (i.e. O'Sullivan 1983; Zillén et al., 2003; 2008). Data collected from these proxies can be used to improve the robustness of climate models, increase the understanding of how the climate reacted to past forcings, as well as how ecosystems have been affected by past climate change, all of which will help develop our knowledge of the climate system and its potential impacts. However, all of the current climate proxies used have limitations that need to be better understood and addressed.

The validation of climate proxies is imperative for the correct interpretation of climate archives. Since proxies can provide data about past environments and the availability of trustworthy temperature data from terrestrial and aquatic environments are essential for the development of reliable climate models, it is important to improve the reliability of proxies. This can be done by applying them in a variety of settings to determine when they can be successfully used as well as assessing their limitations. Since there is no instrumental climate data from before the 1880s, one way to determine the effectiveness of a proxy is by comparing the results to that of another independent proxy, particularly during times when conditions are known, to help assess why the results are different and what additional environmental controls exist on the proxy. Therefore, even though several paleoclimate proxies already exist, the more independent proxies that show an agreement the more reliable the reconstructed climate data is, making new proxies highly valuable to the scientific community.

1.2. Sedimentary Lipids Used in Paleoenvironmental Studies

As mentioned above there are different types of environmental proxies. Environmental proxies can be physical and based on the remnants or abundance of organisms such as fossilized pollen or leaves. Environmental proxies can also include geochemical indicators, such as $\delta^{18}O$ and Mg/Ca and Sr/Ca ratios, all of which are considered inorganic, and those produced through biological activity i.e. hydrocarbons, fatty acids, pigments, which are considered organic. This thesis will concentrate on organic proxies, specifically fossilized sedimentary lipids.

Lipid molecules found in marine sediments can be derived from terrestrial and aquatic sources. Since lipids are able to reach the seafloor fairly unaltered and can be rather well preserved in the sediments, these organic compounds are especially useful as biomarkers. Examples of marine lipid biomarkers that have been successfully applied to reveal information about climate include long chain alkenones (Prahl and Wakeham, 1987; Schneider et al., 1995; Volkman et al., 1995; Müller et al., 1998; Conte et al., 2006), glycerol dialkyl glycerol tetraethers (GDGTs; Huguet et al., 2006, 2013; Sluijs et al., 2006; Kim et al., 2008) and more recently long chain diols (Rampen et al., 2012; Rodrigo-Gámiz et al., 2014). Terrestrial environments play an important role in global climate, however, continental climate reconstructions are hindered by the much reduced availability of continental temperature proxies compared with the marine realm. Terrestrially derived lipid biomarkers include long-chain-n-alkanes (Eglington and Hamilton, 1967; Ternois, et al., 2001; Schefuß et al., 2003) and branched GDGTs (brGDGTs; Weijers et al., 2007a; 2007b; Bendle et al., 2010; Keating-Bitonti et al., 2011). Below I will provide some background information on the sedimentary lipids used in the research contained in this thesis.

1.2.1. Alkenones

Long-chain alkenones (C_{37}-C_{39}) are biolipids that are ubiquitous in aquatic environments and produced exclusively by a few species of marine (Volkman et al., 1980; 1995) and lacustrine or brackish (Marlowe et al., 1984; D'Andrea et al., 2006) haptophyte algae. Since a relationship was established between surface water temperature and the unsaturation ratios of long-chain alkenones (See Fig. 1a for global core top calibration for $U^{K'}_{37}$), these sedimentary lipids have been successfully used for reconstructing past sea surface temperatures (SST) worldwide (Brassell et al., 1986; Brassell, 1993; Prahl & Wakeham, 1987; Volkman et. al., 1995; Müller et al., 1998). Subsequent studies have made it apparent that in addition to growth temperature the alkenone unsaturation ratios are influenced by species composition (Volkman et al., 1995; Conte et al., 1998) and physiological factors (Epstein et al., 1998; Yamamoto et al., 2000) and these should be taken into account when using alkenone unsaturation indices for SST reconstructions.

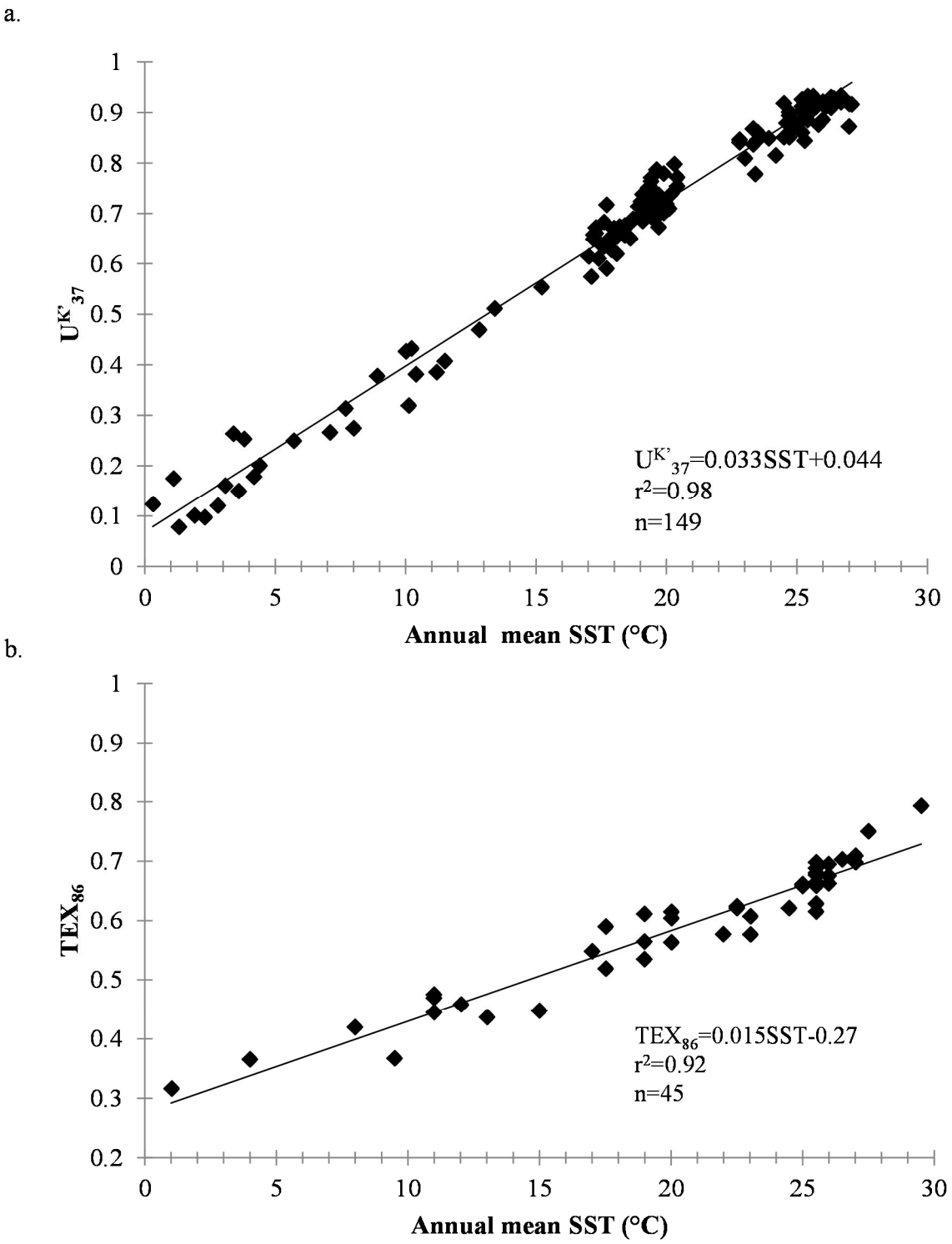

Fig.1. The relationship between the index and annual mean SST and resultant global core top calibrations for (a) the alkenone paleotemperature index $U^{K'}_{37}$ taken from Müller et al. (1998) and (b) the TEX_{86} paleothermometer taken from Schouten et al., 2002.

One environmental factor besides growth temperature that has been found to affect alkenone distribution is salinity (Chu et al., 2005; Ono et al., 2012; Chivall et al., 2014) and it is being explored for its possible application as a salinity proxy. However, Chivall et al.

(2014) found that although salinity can have an effect on the distribution of long-chain alkenones, whether alkenone distributions change in response to salinity changes can depend on other factors such as species composition and growth phase. Alkenones can be found in low salinity settings, but since salinity can affect alkenone distributions complications can arise when using the unsaturation indices to derive temperature estimates in lacustrine (Zink et al., 2001; Chu et al., 2005; Sun et al., 2007; Randlett et al., 2014; Song et al., 2016) and brackish (Rosell-Melé, 1998; Schulz et al., 2000; Coolen et al., 2004; 2009; Blanz et al., 2005) regions. Varying freshwater calibrations have been presented in order to obtain reliable water temperature estimates using long-chain alkenones (i.e. Chu et al., 2005; Sun et al., 2007; Zheng et al., 2016). Studies performed in coastal and brackish settings, such as the Baltic Sea, the North Altantic, and Nordic Seas, suggest that fluctuations in salinity can induce changes in haptophyte species composition creating difficulties using long-chain alkenones for paleoclimate applications (Rosell-Melé, 1998; Schulz et al., 2000; Blanz et al., 2005). In basins where salinity has evolved over time, such as Ace Lake and the Black Sea, it has been suggested that alkenone distributions changed as haptophyte species composition evolved triggered by salinity fluctuations. Consequently, this can result in erroneous SST estimates based on long-chain alkenones at times in the past (Coolen et al., 2004; 2009).

When applying long-chain alkenones for paleoclimate studies in areas where salinity changes in the past were possible, the hydrogen isotope composition (δD) of long-chain alkenones can be used to reconstruct relative changes in salinity in the past (M'boule et al., 2014). Schouten et al. (2005) demonstrated in culture experiments a relationship exists between the δD of long-chain alkenones and salinity. The δD of alkenones can also be characteristic of certain alkenone biosynthesizing haptophyte species and so the values can vary as haptophyte species composition alters with changing environmental conditions. Therefore, δD values can aid in assigning biological sources of sedimentary alkenones, i.e. coastal haptophytes tend to fractionate less than marine type haptophytes (Schouten et al., 2005; Chivall et al., 2014; M'boule et al., 2014).

1.2.2. GDGTs

Glycerol dialkyl glycerol tetraethers (GDGTs) are membrane lipids that can be synthesized by both archaea (isoprenoid GDGTs including crenarchaeol (isoGDGTs; Sinninghe Damsté et al., 2002) and bacteria (with branched carbon skeletons or branched GDGTs (brGDGTs; Sinninghe Damsté et al., 2000). These GDGTs are ubiquitous in marine and terrestrial environments (Schouten et al., 2000) and it was discovered that their

distribution reveals information about the environment in which they lived, i.e. terrestrial input (BIT index; Hopmans et al., 2004), sea surface temperature (TEX_{86} proxy; Schouten et al., 2002), and soil pH and mean annual air temperature (MBT/CBT proxy; Weijers et al., 2007b). Proxies based on GDGTs have been increasingly applied in paleoenvironmental studies and more recently they have found new applications in lacustrine environments (Zink et al., 2010; Blaga et al., 2010; Sun et al., 2011; Loomis et al., 2012). New proxies are still being discovered based on GDGTs as new GDGTs are being discovered, such as the hydroxylated GDGTs (Liu et al., 2012a) and additional branched isomers (De Jonge et al., 2013).

Isoprenoid GDGTs. Nitrifying Archaea called Thaumarchaeota use isoGDGTs as their membrane-spanning lipids. They are widespread in aquatic environments as well as soils and are estimated to make up 20% of the picoplankton in the world's oceans (Fuhrman, 1992; Karner et al., 2001). Isoprenoid GDGTs can have 0-4 cyclopentane moieties and are named according to the number of cyclopentane moieties they contain (GDGT-0 through 4; see Fig. 2a for structures). The most widespread isoGDGT, crenarchaeol, (Crenarchaeota has since been reassigned to the newly defined phylum, Thaumarchaeota; Brochier-Armanet et al., 2008; see Fig. 2a for structure) was isolated from Arabic Sea sediments and is unique in that it has a cyclohexane moiety in addition to four cyclopentane moieties (Sinninghe Damsté et al., 2002). Subsequently, a regio isomer of crenarchaeol was identified as well (see Fig. 2a for structure). Through culture studies with hyperthermophillic archaea it was established that the relative number of cyclopentane moieties increases with growth temperature (Gliozzi et al., 1983; Uda et al., 2001). The ability to change the amount of cyclopentane rings with temperatures is believed to be a response of the cell membrane to adapt to temperature changes (Gabriel and Chong, 2000; Gliozzi et al., 1983). Because of this mechanism it is possible to determine the temperature at which the isoGDGTs were produced in the membrane by calculating the distribution of the preserved isoGDGTs in marine sediments. Based upon this Schouten et al. (2002) introduced the TEX_{86} (tetraether index of tetraethers consisting of 86 carbons) proxy for reconstructing SSTs. This relationship between the number of cyclopentane moieties and SST is weaker in water temperatures below 15°C, and so a revised index termed TEX_{86}^{L} was developed for reconstructing SSTs in the lower temperature ranges (Kim et al., 2010; see Fig. 1b for global core top calibration for the TEX_{86}^{L} index). Additionally, it was determined that salinity did not have a large effect on the

TEX_{86} proxy (Wuchter et al., 2004) and so it could be applied in lacustrine sediments as well (Powers et al., 2004; 2005; 2010).

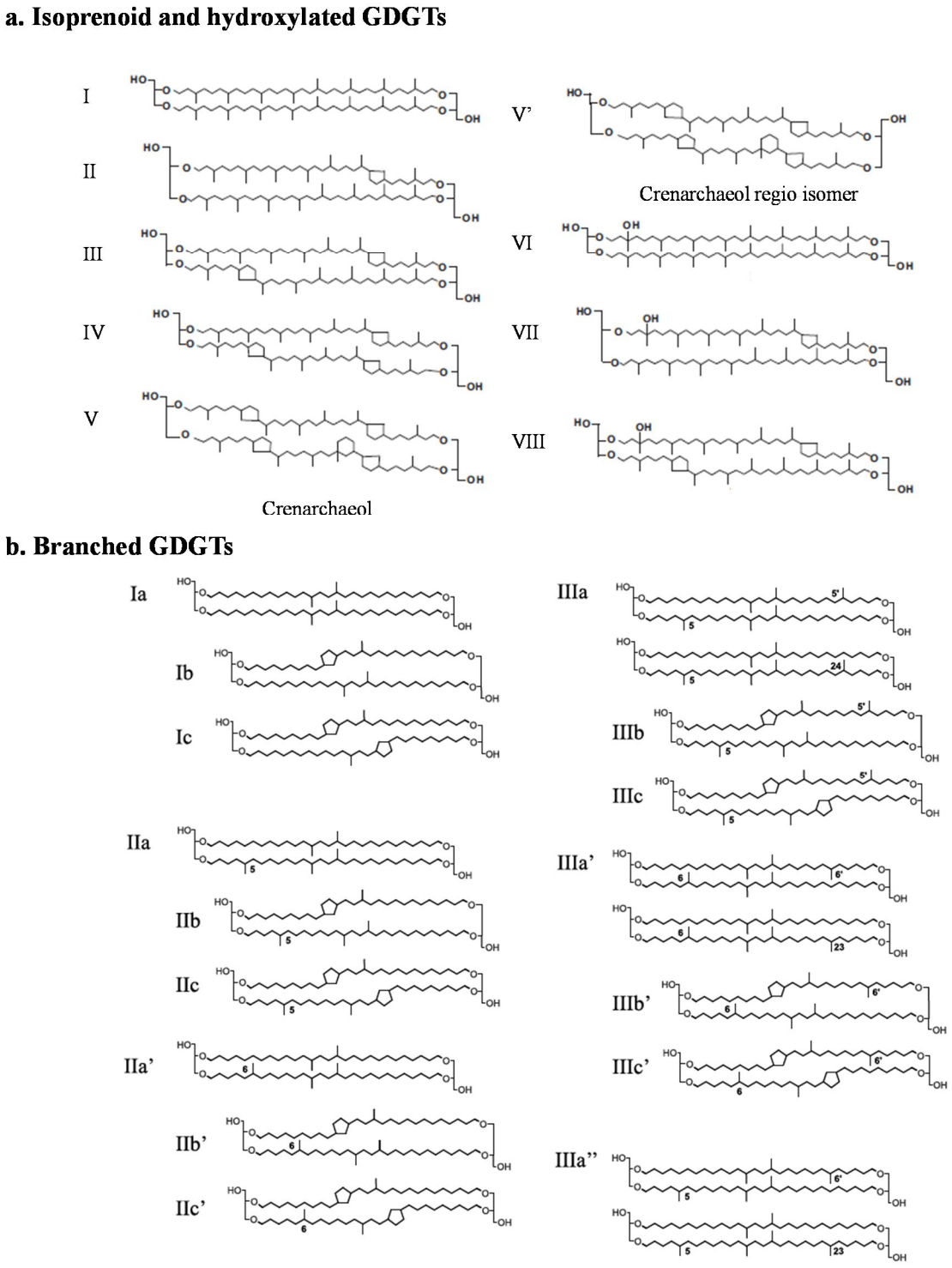

Fig. 2. Chemical structures of the (a) isoprenoid (I-IV) and hydroxylated (VI-VIII) GDGTs and (b) branched (br)GDGTs. The 6-methyl brGDGTs are denoted by an apostrophe (').

Even though the TEX_{86} proxy has been successfully used to reconstruct SSTs in an array of regions and on a wide variety of timescales (i.e. Huguet et al., 2006; Zachos et al., 2006; Kabel et al., 2012; Tierney and Tingley, 2014), issues still exist with the application of the proxy. A large input of soil organic matter into a region can contribute GDGTs produced by Thaumarchaeota and other soil archaea altering the GDGT distributions in the sediments and thus affecting TEX_{86} based temperature estimates (Weijers et al., 2006a; Sinninghe Damsté et al., 2012a). TEX_{86} derived SST estimates can also be biased by the contribution of GDGTs from methanogenic archaea (Pancost et al., 2000; Blaga et al., 2009). Furthermore, it is debated whether biases in SST reconstructions based on the TEX_{86} index can occur if a significant portion of the GDGTs in the sediments are not fossilized but are instead produced in situ in the sediments (intact polar lipids, IPLs, represent the faction from recently living sources) (Lipp and Hinrichs, 2009; Lengger et al., 2012).

Hydroxylated GDGTs. Recently, a new type of GDGTs, i.e. hydroxylated GDGTs (OH-GDGTs), were identified in marine sediments that can have up to two cyclopentane moieties (OH-GDGT-0, -1, and -2, where numbers refer to the amount of cyclopentane rings; see Fig. 2a for structures) and have a hydroxyl group located at a tertiary carbon atom of one of the biphytanyl chains adjacent to the glycerol moiety (Liu et al. 2012a). Liu et al. (2012a) postulated that the hydroxylation of the biphytanyl moiety could enhance membrane rigidity. Because of their relative abundance and widespread distribution in marine sediments, Liu et al. (2012a) suggested the OH-GDGTs had the potential to be useful as biomarkers. In a subsequent study, Huguet et al. (2013) demonstrated that the abundance of OH-GDGTs relative to non-hydroxylated GDGTs (%) increases with increasing latitude and lower SST and because of this strong correlation these compounds have potential for paleoclimate application. With this study the first SST calibrations based on OH-GDGTs were established (Huguet et al., 2013). It was also noted that OH-GDGTs occurred in lacustrine sediments (Huguet et al., 2013). Additional OH-GDGTs based indices were developed by Fietz et al. (2013) and applied to reconstruct SSTs in Nordic Seas. OH-GDGT indices have also been used for paleoclimate studies in the Arctic Ocean (Knies et al., 2014) and the Baltic Sea (Kaiser and Arz, 2016).

Branched GDGTs. Branched GDGTs are a group of membrane-spanning lipids likely biosynthesized by heterotrophic bacteria (Pancost and Sinninghe Damsté, 2003; Weijers et al., 2010), which were initially thought to be restricted to soils and peats (Sinninghe Damsté et

al., 2000; Weijers et al., 2006a; 2006b). The distribution of brGDGTs is expressed by their degree of methylation (methylation index of branched tetraethers; MBT) and cyclization (cyclization index of branched tetraethers; CBT) and depends on the soil pH and the growth temperature (Weijers et al. 2007b). MBT has more recently been modified as MBT', excluding those brGDGTs that rarely occur in soils (Peterse et al., 2012).

Originally it was believed that brGDGTs were produced predominantly in soils and that through runoff they are washed from the land into aquatic sediments where they are deposited. The preserved distribution of these fossilized membrane lipids in sediments has proven useful as a tool for obtaining continental air temperature reconstructions from coastal marine sediments (Weijers et al. 2007a; 2007b; Bendle et al. 2010), paleosoils (Peterse et al., 2011; Zech et al., 2012) and even lacustrine sediments (Zink et al., 2010; Loomis et al., 2012; Niemann et al., 2012). Problems using brGDGTs as a paleotemperature proxy have been noted in some settings and this makes it imperative to investigate how varying environmental conditions along with the transport and provenance of the brGDGTs affects their use as a proxy.

The branched vs. isoprenoid tetraether (BIT) index is the ratio of primarily terrestrially derived brGDGTs compared to the primarily aquatically derived isoprenoid GDGT crenarchaeol, and is used as an indicator for soil organic matter input (Hopmans et al., 2004). In areas with low terrestrial input as indicated by the BIT index, problems have been encountered using brGDGTs for mean annual air temperatures (MAT) estimates (Peterse et al., 2009; Zhu et al., 2011). Additionally, recent studies have demonstrated that the production of brGDGTs in the water column and even marine sediments could be affecting their distribution and therefore confounding the use of brGDGT based for temperature estimates (e.g. Sinninghe Damsté et al., 2009; Tierney and Russell, 2009; Zell et al. 2013; Sinninghe Damsté, 2016). Therefore, several studies have recommended performing a preliminary investigation in a region to determine the provenance of brGDGTs when attempting paleoclimate reconstructions (Zell et al., 2013; 2014; French et al., 2015; De Jonge et al., 2016).

Until recently, paleoclimate reconstructions using brGDGTs were believed to have been based on the collection of nine, 5-methyl brGDGTs. However, a set of six novel brGDGT isomers that differ from the original set of 5-methyl brGDGTs in the position of the methyl groups (6-methyl brGDGTs) were identified (see Fig. 2b for structures). It was also determined that these 6-methyl brGDGTs were co-eluting with the 5-methyl brGDGTs with the standard separation methods (De Jonge et al., 2013). Subsequently, the use of improved

chromatography methods has allowed for the separation and quantification of the 6-methyl brGDGTs (Hopmans et al., 2015) resulting in the development of new indices and the improvement of MAT reconstructions based on the global soil dataset, especially in arid regions (De Jonge et al., 2014). It was found that the relative abundance of these novel, 6-methyl brGDGT isomers are strongly dependent on pH and so the CBT index was amended to become CBT' and to include all of the 6-methyl brGDGTs resulting in a higher correlation with soil pH (De Jonge et al., 2014). Due to the strong relationship with pH, the 6-methyl brGDGT isomers are now excluded from the MBT' index (now defined as MBT'_{5ME}) improving the correlation with MAT (De Jonge et al., 2014).

1.3. Objectives and Outline of Thesis

The focus of this thesis is the application, development and validation of paleoclimate proxies based on the sedimentary lipids described above (long-chain alkenones and GDGTs) in Holocene sedimentary records. To accomplish this, proxies, both established and novel ones, were applied to marine sediment cores and the results were then compared to previously published results based on another independent proxy or by applying the proxy to different areas of the same region and comparing the results. When it appeared the proxy was not successful in a specific region, the causes and its limitations were explored. In some cases it was determined the development of a new calibration or index was appropriate and could improve the temperature estimates. In situations that the reconstructions seemed reliable, the environmental and historical implications were examined. Most of the chapters in this thesis are focused on the Baltic Sea environment, however, one chapter deals with the Tagus River basin and off the Portuguese continental shelf.

Chapter 2-6 are all based on sediments from the Baltic Sea (see Fig. 3 for map of the study site and sediment sample locations). The Baltic Sea is the world's largest brackish body of water and is fairly shallow and broken up into multiple sub-basins. The basin receives a substantial amount of terrestrial input as it is surrounded by land except for a narrow connection to the North Sea through the Danish Straits. The salinity varies greatly in the basin, ranging from ~3.5 PSU in the north to ~8 PSU in the central Baltic Sea and ~30 PSU in the region where the Baltic Sea connects to the North Sea (ICES). Due to it being persistently stratified, the modern Baltic Sea has anoxic bottom waters in the deeper basins as well as hypoxic coastal areas. The Baltic Sea has had a varied salinity history having experienced several phases since the last deglaciation; the Baltic Ice Lake, the Yolidia Sea, the Ancylus Lake, the Litorina Sea and the modern Baltic Sea.

In **Chapter 2** the impact of climate change on human societies during the Holocene in northern Europe is explored. This was done by examining a high resolution record with a detailed depth-age model of SST and anoxia from the central Baltic Sea and developing a marine ecosystem model, which together reveal that a sudden increase in summer temperatures at 6,000 BP improved farming conditions. Concomitantly, the intensification of anoxia in the Baltic Sea caused a reduction in the availability of marine resources, making the switch in economy from predominantly hunter-gather-fisher culture to agrarian enticing to the human populations in the region at the time. The results from this study suggest that rapid environmental changes drove a sudden increase in human population allowed by an economic transition to agriculture, likely influenced by people migrating up from the south to take advantage of the improved farming conditions. In **Chapter 3** a detailed age depth model for a sediment core from the central Baltic Sea (the Gotland Basin) is established and high-resolution TEX_{86}^{L} records from two separate sites in the Gotland Basin are obtained using a local SST calibration developed for this study. The records show that increased summer sea surface temperatures occur at the same time as laminations and increased organic carbon content in the sediment cores, signifying anoxic conditions. As anoxic conditions intensified with the start of marine influxes into the basin, cyanobacterial abundance and N_2-fixation both increased during the Holocene climatic optimum. A clear relationship between summer SSTs and anoxia is demonstrated by these geochemical records indicating that low oxygen conditions occurred naturally in the Baltic Sea during the Holocene. Also made apparent, though, is that anoxia could be intensified by increasing temperatures related to global climate change, which could create ecological havoc in the Baltic Sea ecosystem.

The fairly novel hydroxylated GDGTs (OH-GDGTs) were recently discovered in surface sediments in the Baltic Sea. In **Chapter 4** eleven surface sediment samples from around the Baltic Sea as well as two culture samples grown at different temperatures (4 and 22°C) were analyzed and the OH-GDGT distributions were compared with measured temperatures to assess the performance of the established OH-GDGT based indices. In this study a new OH-GDGT based index (OH-GDGT' index) and local calibrations were developed as well based on the results. Next, the OH-GDGT based indices that performed best in reconstructing SSTs in the surface sediments from the Baltic Sea and culture experiments were applied in two sediment records from different regions (the central Gotland Basin and the southern Arkona basin) in the Baltic Sea. They resulted in reliable SST estimates for the last 7,200 years that are in agreement with each other as well as previously published data. We determined that the use of the distribution of OH-GDGTs for SST

reconstructions in the Baltic Sea appears to be promising but that there is an effect of salinity on OH-GDGT based indices that can complicate the use for paleoclimate application in low salinity environments.

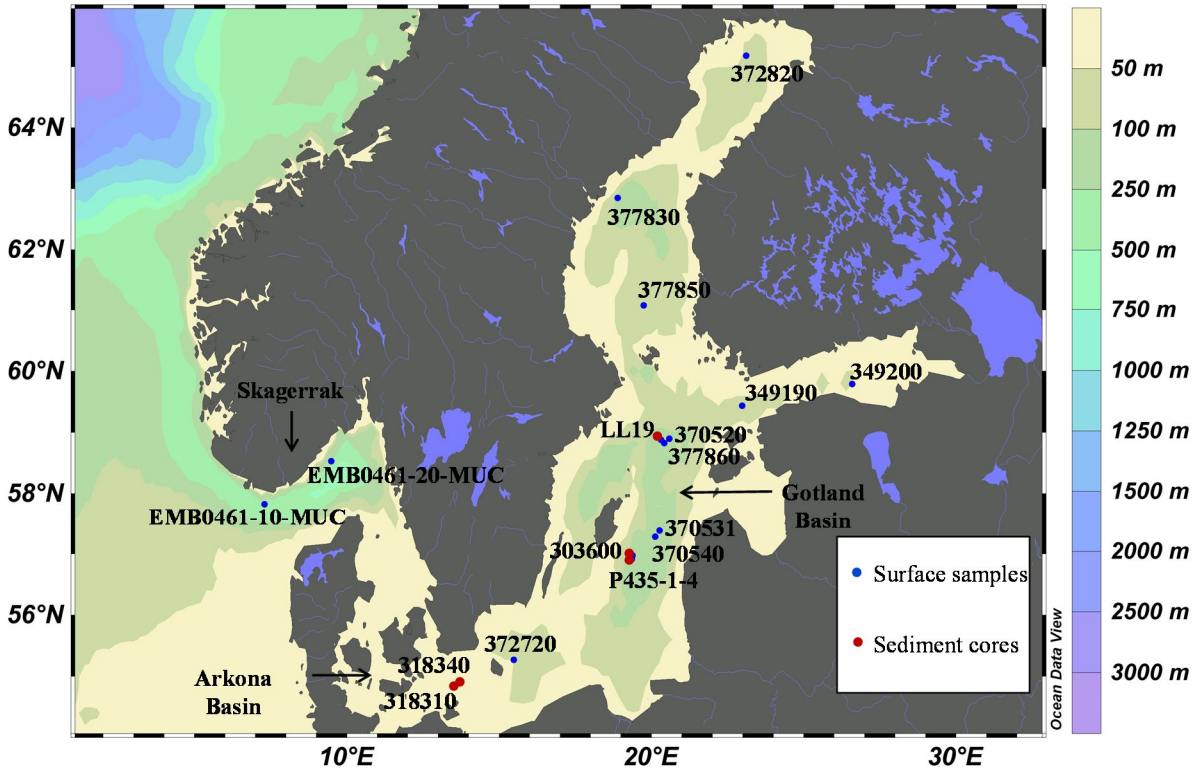

Fig. 3. A map of the Baltic Sea region with the locations of the sampling stations for the surface sediments (denoted by blue circles) and sediment cores (indicated by red circles). Bathymetry is indicated by the colors denoted in the bar to the right.

In **Chapter 5** changes in alkenone distributions are explored in two surface sediment samples from the Skagerrak (a region just outside of the Baltic Sea basin) and the sediment record from the Arkona Basin, but this time using long-chain alkenones. This study revealed that the distributions and concentrations of alkenones and their δD values co-varied with past salinity changes in the Baltic Sea over the Holocene. Additionally, the $C_{36:2}$ alkenone was found in the Baltic Sea sediments, which has not been reported in the Baltic Sea previously, and is believed to be an indicator of low salinity conditions. The Black Sea is a parallel to the Baltic Sea in that it also transformed from a freshwater lake to a brackish basin over the Holocene. Alkenone distributions and their δD values for the Black Sea from a previous study were used to demonstrate that the rare $C_{36:2}$ alkenone dominates the alkenone distribution at lower salinities (2-8 PSU) by reconstructing changes in surface water salinity over the Holocene in the Black Sea. This information was then transferred to the alkenone data presented for the Baltic Sea to make inferences about salinity changes and haptophyte species

composition in that basin over the Holocene. Both alkenone distributions and hydrogen isotopic composition suggest low and variable salinity waters in the Baltic Sea over the Holocene that have allowed for the production of alkenones by a mutable haptophyte community that includes low salinity adapted species. The contribution of alkenones from a variable haptophyte community is impeding the use of the indices based on long-chain alkenones for paleoclimate application; however, the long-chain alkenone amounts and distributions appear to be useful for examining salinity variations regionally as well as in the past.

In **Chapter 6** the provenance of brGDGTs in the Baltic Sea over the Holocene and the effect it has on the use of brGDGTs in paleoclimate applications is investigated by examining 13 surface sediments and two sedimentary records covering the Holocene from the Gotland and Arkona basins. The results from this study reveal that brGDGT distributions and the BIT index changed concomitantly with the re-established connection between the Baltic Sea and the North Sea between 7.8-7.3 cal kyr BP and also suggests that in situ production has occurred in the basin over the Holocene complicating the use of brGDGT based proxies. These results affirm that a preliminary study on the provenance of brGDGTs should be performed prior to the use of brGDGTs for paleoclimate applications in regions that have undergone environmental changes in the past.

Chapter 7 is the follow-up of a study performed on the Tagus River basin (see Fig. 4 for map of the study site and sample locations) that revealed that the MBT'/CBT proxy could not be used in the region because of the great diversity of brGDGT distributions in the sediments, which did not reflect the MAT in the region, and in situ production of brGDGTs was occurring in the river system. The results from re-analyzing samples (soil, riverbank sediment, and suspended particulate matter) from this previous study in the Tagus River basin with enhanced methods to test if the separation of the 5- and 6-methyl brGDGTs along with the newly developed indices to reconstruct MAT (MAT_{mrs}/ MAT_{mr}), thought to perform better in arid regions such as the Tagus River basin, resulted in more accurate temperature estimates. Additionally, the new indices were applied to four sediment cores in a transect from the continent to the deep ocean off the continental shelf to examine terrestrial input and derive temperature estimates over the Holocene. Unfortunately, the new method and indices did not result in much improvement in the MAT estimates as the application of the new indices on the soils did not even obtain accurate MAT estimates and the issue of in situ production of brGDGTs was complicating the use of the proxy. However, pH estimates were improved and new factors that should be considered when using this proxy were revealed. The results from

this study confirm the importance of examining the origin of the brGDGTs in a region before using them for paleoenvironmental application.

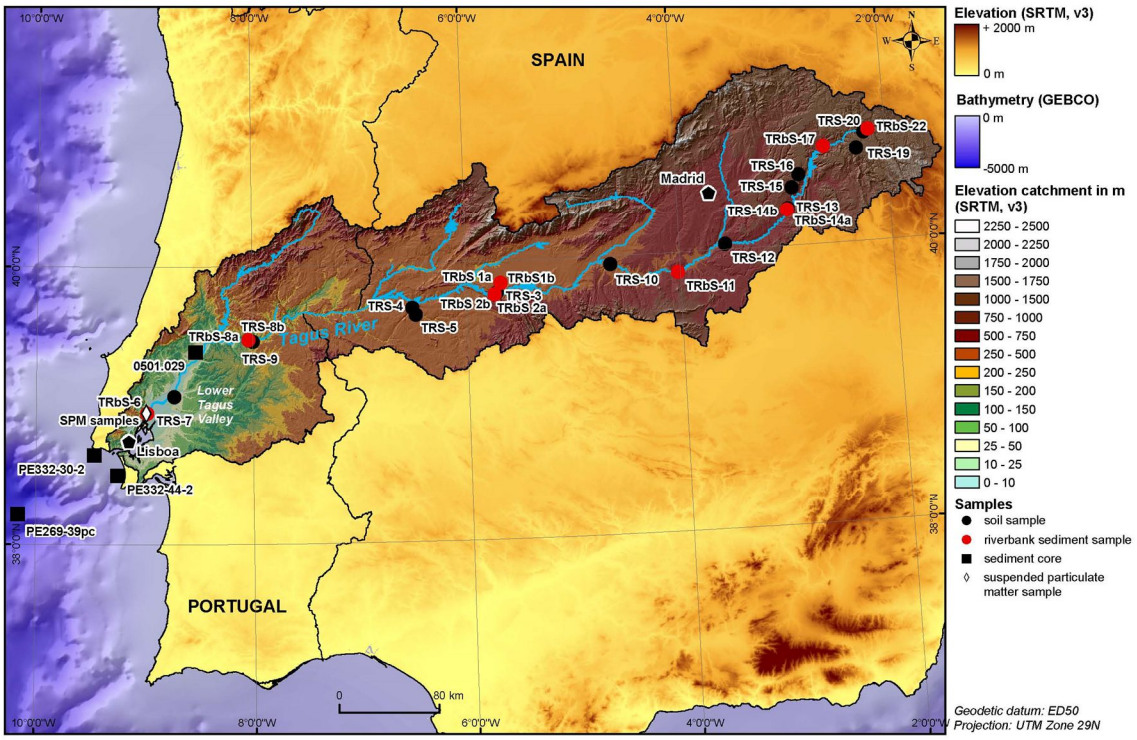

Fig. 4. Map of the study area on the Iberian Peninsula taken from Warden et al. (2016b) with the locations where the four sediment cores were sampled (indicated by black squares) along a transect from the Tagus River to off the Portuguese continental margin. The sampling sites of the river SPM (indicated by a white diamond), riverbank sediment (indicated by red circles), and soils (indicated by black circles), all collected in a previous study, are shown as well. Digital elevation data are from Jarvis et al. (2006) and bathymetry from IOC-IHO-BODC (2003).

This thesis highlights the importance of paleoenvironmental studies. By illuminating some successes as well as difficulties with using fossilized sedimentary lipids for plaeoenvironmental studies, the reliability of proxies based on these compounds can be improved. The results from these studies affirm the importance of examining the provenance of fossilized sedimentary lipids regionally as well as historically before applying proxies based on their distribution, as variable origins can complicate their application. The information contained in this thesis also emphasizes the importance of investigating environmental changes in a region's past, since environmental changes, such as salinity, can affect the distribution of fossilized lipids and thus their use for paleoclimate application. By looking at the whole picture, the provenance of the fossilized sedimentary lipids as well as environmental conditions they were produced under, other possible biomarker applications may be determined as well.


Photo by Dietmar Rüß

CHAPTER 2

Climate forced human demographic and cultural change in northern Europe during the mid-Holocene

L. Warden, M. Moros, T. Neumann, S. Shennan, A. Timpson, M. Sollai, L. Wacker, K. Perner, K. Häusler, T. Leipe, L. Zillén, A. Kotilainen, E. Jansen, R.R. Schneider, H. Arz, and J.S. Sinninghe Damsté

Submitted to Nature Geoscience

Climate change has played a key role in human evolution (Haug et al., 2003; Castañeda et al., 2009) . The transition from hunter-gatherer-fisher to agrarian societies is arguably the most significant change in recent human history (Bellwood, 2005). In the European plain there is evidence for fully developed agrarian societies by 7,500 cal. BP (Bonsall et al., 2002; Bogucki et al., 2012; Shennan et al., 2013), yet a well-established agrarian society does not appear in the north until 6,000 cal. BP (Bonsall et al., 2002; Shennan et al., 2013) for unknown reasons. Here we show a sudden increase in summer temperature at 6,000 cal. BP in northern Europe using a high resolution record of sea surface temperature (SST) from the Baltic Sea. Comparison with a summed probability distribution of radiocarbon dates from archaeological sites indicates that this temperature rise induced a dramatic population increase due to improved conditions for farming. In addition, paleoenvironmental sedimentary records in combination with marine ecosystem modeling indicate that the rapid increase of SST also resulted in a marked spread of hypoxia (so-called dead-zones; Diaz & Rosenberg, 2008) in the entire Baltic Sea, causing a reduction in the plentiful maritime resources in the region at that time (Price, 2007), and thus further contributing to the transition from hunting-gathering-fishing to farming as the more successful subsistence strategy. Our study demonstrates how climate change shaped human demographic and cultural history.

The transition from foraging to farming provided the basis for a massive increase in food production and human population density, which in turn drove the accumulation of technology and specialization, ultimately enabling the establishment of modern day societies (Haug et al., 2003). The reason and mechanism for this Neolithic Revolution occurring at different times in different places continues to be debated. In Northern Europe cereal agriculture with a full range of domestic animals did not begin until ca. 6,000 cal. BP (Bonsall et al., 2002; Shennan et al., 2013; Krause-Kyora et al., 2013), i.e. 1,500 years later than in neighboring populations to the south. It has been proposed that foraging societies were successful in relying largely on the marine resources from the Baltic Sea and had no incentive to adopt an agrarian lifestyle (Price, 2000), which required more intense labor with no immediate increase in living standards (Banks et al., 2013). This leaves the question of why the transformation did eventually occur at 6,000 cal. BP. It has been suggested that climate change may have been responsible for the late onset of farming in the northern European regions (Bonsall et al., 2002); however, due to the lack of high resolution climate reconstructions the effects of environmental change on human societies have been unclear. In

order to examine this at a fine temporal scale, we employed an approach combining sediment proxy studies with 3D ecosystem modelling to reconstruct climate conditions in northern Europe and environmental conditions in the Baltic Sea and compare this with human population and subsistence changes from archeological sites from the region.

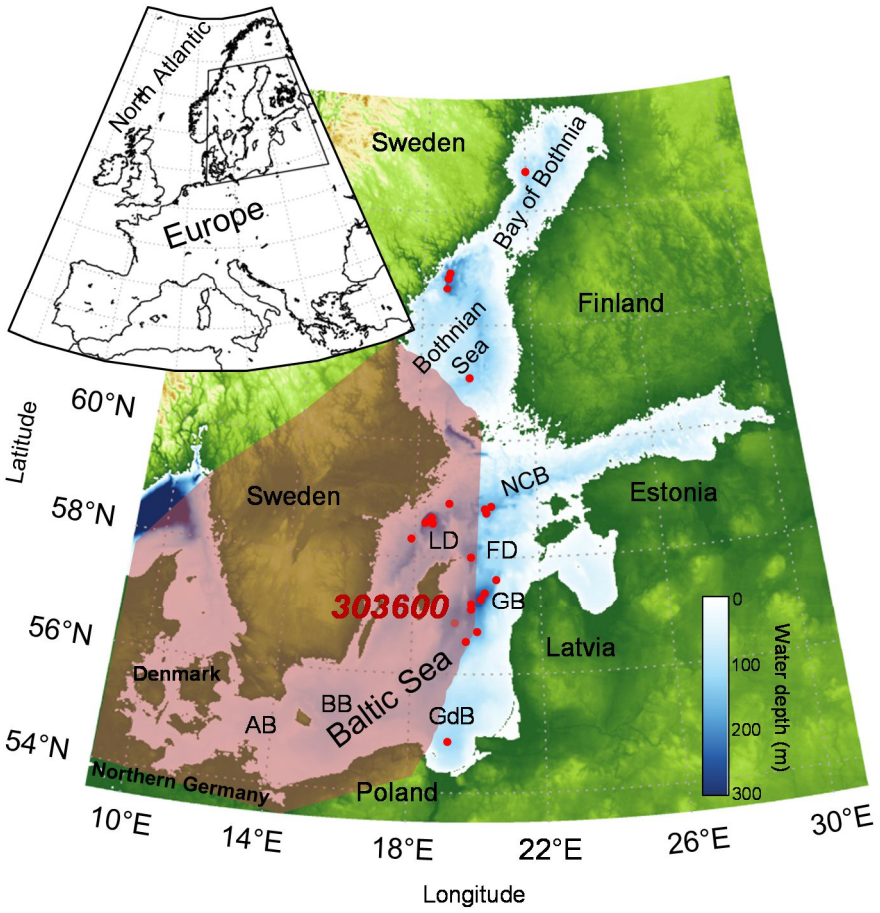

Fig. 1 Sediment coring stations and archaeological sites in the Baltic Sea region. Location of the sediment study sites are indicated with red dots with the location of the key-site 303600 is labelled. Areas with information on changes in population density and settlement activity are within the polygon shaded brown. The Baltic Sea´s modern bathymetry (see SI) is shown (inset: Baltic Sea area in Europe) along with the Baltic Sea basins: AB – Arkona Basin, BB – Bornholm Basin, GdB – Gdansk Basin, GB – Gotland Basin, FD – Fårö Deep, LD – Landsort Deep, NCB – Northern Central Basin.

We examined a key-sedimentary record from the central Baltic Sea (Fig. 1) from 7,000-3,000 cal. BP (Fig. 2 & Extended data Table 1). Complementary information for the entire Baltic was obtained from a number of other sediment cores (Fig. 1, Extended data Fig. 1 & Table 1). Our detailed age-depth model was developed based on radiocarbon (^{14}C) dating of fossil benthic foraminifera using accelerator mass spectrometry (Extended data Figs. 2 & 3; see also SI). The key-sediment core was analyzed in high resolution using the TEX_{86}-paleothermometer, a proxy for reconstructing past sea surface temperature (SST) based on the

distribution of Thaumarchaeotal membrane lipids (Schouten et al., 2002). We applied a local calibration of TEX_{86} to reconstruct summer SST in the Baltic Sea (Kabel et al., 2012). Our record shows that summer SST during the studied time interval varied between 14.5-17.5˚C (Fig. 2C). A distinct and rapid warming phase is evident at 6,000 - 5,500 cal. BP terminating a prolonged colder phase (Fig. 2C, Extended data Fig. 4). Subsequently, throughout the mid-Holocene the general summer SST trend declines, following summer solar insolation (Fig. 2C).

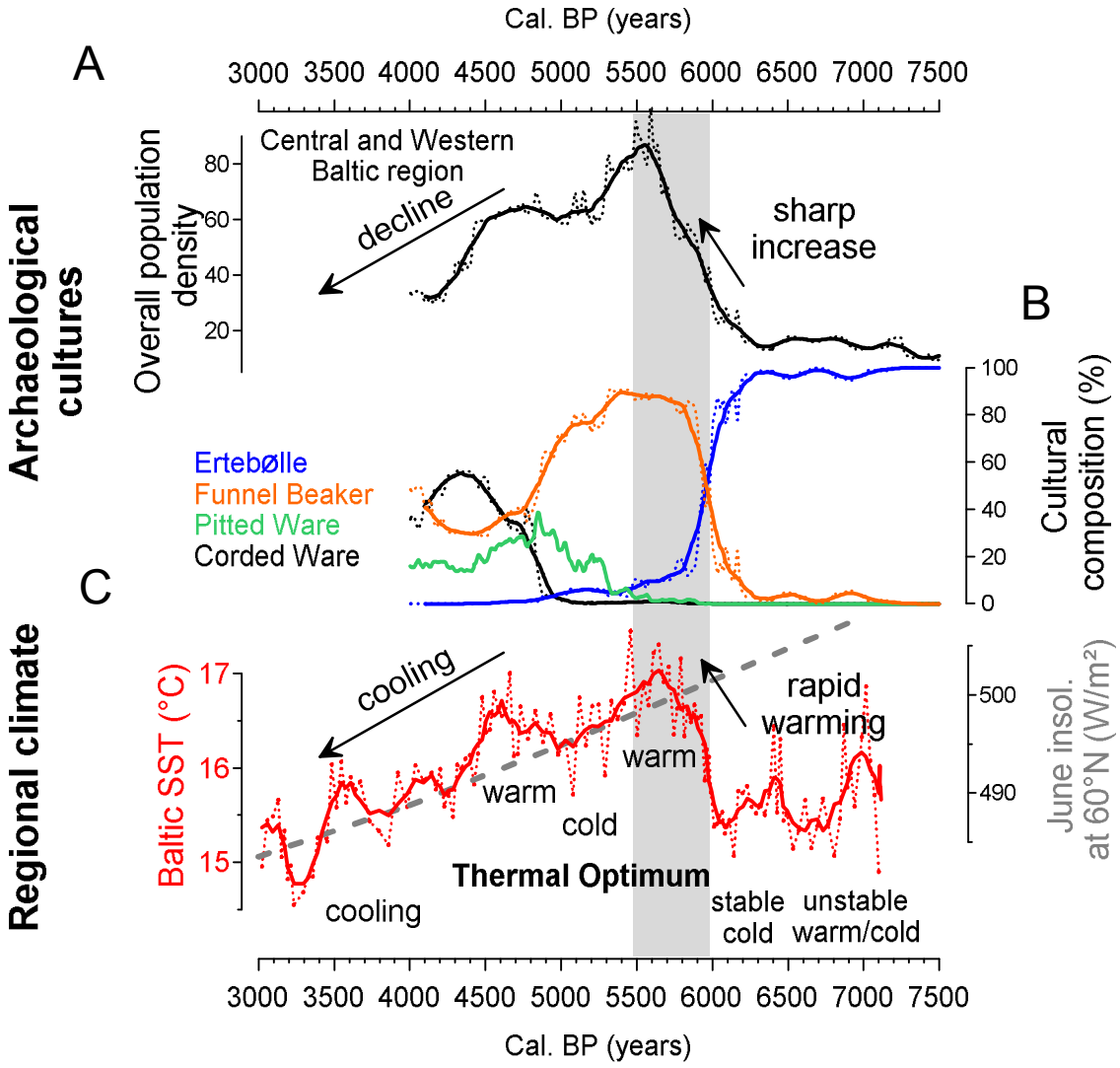

Fig. 2 Mid-Holocene SST and SPD records from the Baltic Region. (A) Population density (on a relative scale) based on an SPD from archaeological radiocarbon dates within the polygon indicated in Fig. 1. (B) Cultural composition (in %) based on a subset of the data used for the SPD analysis used for (A). Radiocarbon dates that been assigned to a culture by the original excavator (58% of the full dataset) were used. The archaeological data was smoothed (thick lines) with a 200 yr rolling mean. (C) Summer SST record based on TEX_{86} palaeothermometry. The red line plots the 5-point running mean. June insolation at 60˚N (in W m^{-2}) is plotted as a grey stippled line. The population density and settlement activity strongly increased during a period of marked warming in the Baltic Sea region (grey bar).

The present-day Baltic Sea is persistently stratified with anoxic bottom waters in the deep basins and oxygen-depleted (hypoxic) waters in coastal areas affecting food chain dynamics, marine habitats and reducing fish stocks (Karlson et al., 2002). Summer SST controls hypoxia in the Baltic Sea over the last 1000 yrs through various feedback loops (Vahtera et al., 2007; Kabel et al., 2012). A comparison of SST, the total organic carbon (TOC) content and the degree of lamination of the sediments clearly demonstrates that the critical temperature threshold for the occurrence of severe hypoxia at about 16 °C, assisted by the occurrence of cyanobacterial blooms (Vahtera et al., 2007), as proposed for the last 1000 yrs (Kabel et al., 2012), also acts earlier in the Holocene (Fig. 3B, Extended data Fig. 4, see also SI). A marked and rapid warming at 6,000 cal. BP co-occurs with the onset of bottom water anoxia (Extended data Fig. 4). This intensification of hypoxia at 6,000 cal. BP is evident in the sedimentary records from the entire Paleo-Baltic (Extended data Fig. 5). Our detailed analysis using a coupled hydrodynamic-biogeochemical model applying a reconstructed paleo-bathymetry (SI, Extended data Fig. 6) and forced by a delta change approach (SI, Extended data Fig. 7) indicates an increase of the hypoxic area in the Paleo-Baltic from only 20,000 before to more than 100,000 km^2 after 6,000 cal. BP (Fig. 3A). The likely strongly affected coastal areas are even not included in this calculation because of the coarse model grid.

We reconstructed fluctuations in the local human population through time using a Summed Probability Distribution (SPD) of 1,960 terrestrial radiocarbon dates from 608 archaeological sites (Fig. 2A), taken as a proxy for variation in human population levels in the Baltic region through time. The rationale behind this approach is that periods of increased population will leave more dateable material behind in the archaeological record (Bonsall et al., 2002; Timpson et al., 2014). Evidently, the large climatic and environmental change at 6,000 cal. BP that took place in northern Europe is concurrent with the start of a massive increase in population levels. Between 6,000 and 5,500 cal. BP the summer climate substantially increased by 2°C in parallel with a 3.3 fold increase in population levels (Fig. 2 and 3C). This represents a population growth rate of 6.1% per 25 year generation compared to 1.9% previously between 7,000 and 6,000 cal. BP. Additionally, the strong relationship between temperature and population is evident throughout the entire overlap in both time-series from 7,000 to 4,000 cal. BP (Pearson's $R = 0.73$, p-value < 0.00002; see SI for statistical tests). Furthermore, cross-correlation analysis shows the population lagged behind climate by 60 years, suggesting a rapid human response to climate changes (see SI).

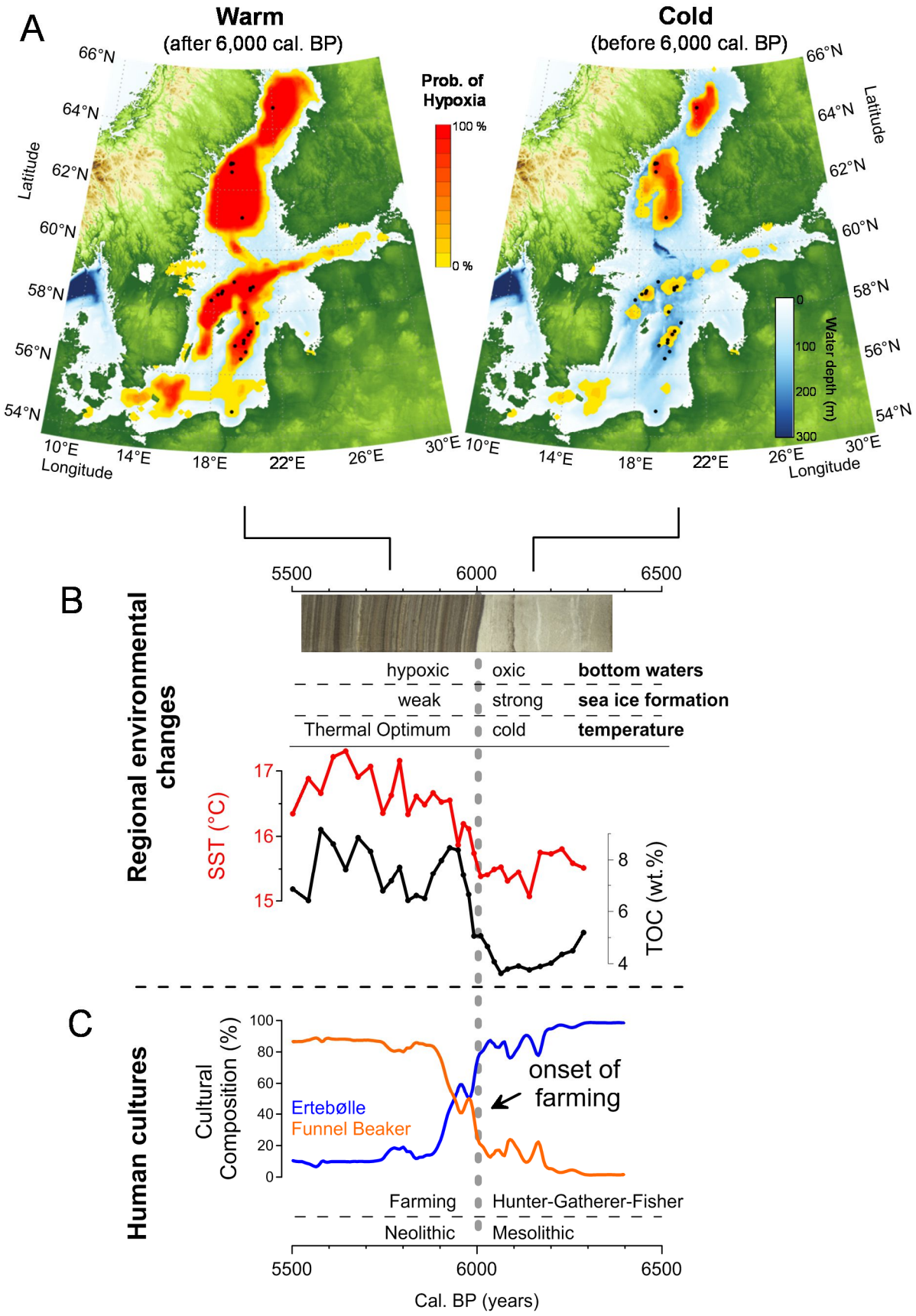
A
Warm
(after 6,000 cal. BP)
Cold
(before 6,000 cal. BP)
Prob. of Hypoxia
100 %
0 %
Water depth (m)
0
100
200
300
66°N
64°N
62°N
60°N
58°N
56°N
54°N
Latitude
10°E
14°E
18°E
22°E
26°E
30°E
Longitude
B
5500
6000
6500
hypoxic
oxic
bottom waters
weak
strong
sea ice formation
Thermal Optimum
cold
temperature
Regional environmental changes
SST (°C)
17
16
15
TOC (wt.%)
8
6
4
C
Human cultures
Cultural Composition (%)
100
80
60
40
20
0
Ertebølle
Funnel Beaker
onset of farming
Farming
Hunter-Gatherer-Fisher
Neolithic
Mesolithic
5500
6000
6500
Cal. BP (years)

⬅ Fig. 3 The 6,000 cal. BP event: Changes in ecosystem, climate and culture. Increasing summer temperature after 6,000 cal. BP likely improved conditions for farming in the region and thus prompted the establishment of the Funnel Beaker culture. (A), The extent of hypoxia in the Baltic Sea based on 3D ecosystem modelling for the cold phase (right panel) before 6,000 cal. BP and for the warm phase (left panel) after 6,000 cal. BP. Note the remarkable spreading of hypoxic areas to the whole basin after 6,000 cal. BP, which had severe consequences for marine life, therefore affecting the hunter-gatherer-fisher society. (B) Regional environmental changes at this time. The sequence from non-laminated to laminated sediments along with the significant increase in organic carbon content reveals that the development of anoxic bottom water conditions which is related to the substantial increase in summer SST. (C) Cultural composition (in %) showing the rapid change at the boundary between the Meso- and Neolithic. Note that this coincides with a substantial increase of the population (see Fig. 2A).

Importantly, the marked population increase starting at 6,000 cal. BP also coincides with the transition to an agrarian economy, which could indeed support a larger population in a given area by increasing food yields (Shennan et al., 2013). Evidence of this economic revolution is seen in archaeobotanical and faunal evidence showing the simultaneous introduction of wheat, barley and domestic animals throughout southern Scandinavia ca. 6,000-5,700 cal. BP (Sorensen & Karg, 2014). This corresponds with a rapid change ca. 6,000 cal. BP from a predominantly marine to a mainly terrestrial based diet as indicated by a shift in stable isotope values in ceramic residues and human remains from coastal areas of Denmark, and there continues to be evidence of only a small contribution from marine food throughout the Neolithic after the shift at ca. 6,000 cal. BP (Richards et al., 2003; Fischer et al., 2007; Craig et al., 2011). This transition also reflects a cultural shift, from the Ertebølle culture, representing hunter-gatherer-fisher societies, to the agricultural Funnel Beaker culture (Fig. 2B, Fig. 3C).

Modeling studies indicate that a warming climate in Scandinavia could induce shifts in the northern limit of cereal suitability by 100-150 km per °C (Carter et al., 1996). Ancient DNA (Skoglund et al., 2014) and archaeological evidence (Rowley-Conwy, 2011) suggests that the transition occurred as farming communities to the south responded to the warming climate by expanding north into southern Scandinavia. By around 5,500 cal. BP population levels and summer temperatures reach a maximum (Fig. 2) and farming is at its most extensive, with large areas of cleared land (Feeser et al., 2012).

In addition to temperature changes, the development of widespread hypoxia in the whole Baltic Sea including coastal areas may also have played a substantial role in the rapid transition from the Ertebølle to the Funnel Beaker culture in the Baltic region. At the beginning of the early Neolithic, ~6,000 cal. BP, summer SSTs started to increase rapidly and bottom water conditions in wide areas became persistently hypoxic (Fig. 3), a state that

continued for most of the next two millennia during a local Thermal Optimum (when SST > 16°C, Extended data Figs. 4 & 5). Hypoxia in the Baltic Sea has been shown to contribute to a reduction in fish populations (Breitburg et al., 2001) (see also SI) and consequently will affect other marine predators such as harp seals. Therefore, we can infer from the rapid introduction of hypoxia over the entire Baltic Sea beginning at 6,000 cal. BP that marine resources became scarce for the Ertebølle population, at a time when farming groups were migrating north and climate conditions for farming had improved substantially.

After the peak at 5,500 cal. BP, the SPD population reconstruction shows a steady decline throughout the remainder of the record (Fig. 2A), synchronous with the declining summer insolation at 60°N and summer SST (Fig. 2C), indicating that climatic deterioration played a role in the decline in human population, probably due in part to poorer conditions for farming. At this time there is evidence of woodland regeneration, which would result from a decrease in human activity (Feeser et al., 2012). This period also sees the southward expansion of the Pitted Ware Culture (Skoglund et al., 2014) (Fig. 2B), during a period when environmental conditions were worsening further north (Tallavaara & Seppä, 2012). This hunter-gatherer-fisher culture relied on marine resources for their main protein source, which is evidenced from stable isotope analysis of human bones from coastal areas Eriksson et al., 2008; Fornander et al., 2008), and so may have benefited from the long-term recovery of marine resources predicted by the decreasing SST trend and associated reduction in hypoxia (Extended data Figs. 4 & 5).

The Neolithic Revolution is widely considered to be the most consequential transition in recent human history. In Europe this transition spread north and west following its full establishment in SW Asia ca. 9, 000 cal. BP, and reached central Germany by 7,500 cal. BP. Remarkably this northerly spread was then delayed by 1,500 years. We show that climate change drove demographic and cultural changes by two key processes in northern Europe during the mid-Holocene. Firstly, rapid warming ca. 6,000 cal. BP improved terrestrial conditions for farming whilst simultaneously depleting marine resources. This incited an expansion of the agrarian groups from the south (Skoglund et al., 2014) causing the transition from foraging to farming and as a consequence a massive population increase in the Baltic region. Secondly, the long term cooling from ca. 5,500 cal. BP drove a gradual decrease in farming productivity causing a reduction in population size and contributed to a later resurgence of hunter-gatherer-fisher communities as marine resources returned to more productive levels. Our study indicates a rapid human reaction within only two to three

generations to changing conditions, emphasizing the remarkable plasticity humans can demonstrate in response to climate changes.

Methods

For a detailed description of the methods see Supplementary methods.

Sampling and preparation. Sediments were obtained by using a gravity-corer. The subsamples were freeze dried, ground and homogenized for further analysis.

Dating. The sediment cores were radiocarbon dated on picked benthic forminifera tests. A highly resolved age model was obtained analyzing 61 small-sized samples (0.3-1 µg carbonate) with a new sampling technique employing an accelerator mass spectrometer (AMS) equipped with a gas ion source, plus 8 normal-sized samples (3-5 mg) prepared with traditional AMS methods.

TEX_{86} analysis. Freeze dried sediments (1-3 g) were extracted with an accelerated solvent extractor. Glycerol dibiphytanyl glycerol tetraethers were analyzed by liquid chromatography-mass spectrometry as described previously (Schouten et al., 2007).

TOC and LOI. The TOC content was calculated as the difference between total carbon determined on a EA 1110 CHN analyzer (CE Instruments) and the total inorganic carbon (TIC) using the Multi EA- 2000 Elemental Analyzer (Analytic Jena). For measurement of LOI weighted aliquots of freeze dried sediments were ashed at 550°C for 3 h and the resulting mass difference was determined and expressed in wt.%.

Model Simulation. For the simulations the 3D circulation Modular Ocean Model (MOM v.5.1) with the integrated biological geochemical ecosystem model ERGOM was used, applying a paleo-bathymetry (see SI). A realistic forcing for cold and warm climate periods was derived from the coastDat project. For the warm and cold climate scenarios a delta change approach was applied. Temperature data was adjusted to our sediment proxy findings.

Human population probability. Based on the premise that periods of increased human population will leave behind more dateable archaeological artifacts (Karlson et al., 2002; Castañeda et al., 2009), local human population fluctuations in the Baltic region were reconstructed using a Summed Probability Distribution of 1,960 terrestrial radiocarbon dates from 608 archeological sites.

Author contributions. M.M. and J.S.S.D. designed the research. S.S. and A.T. analysed the archaeological data and generated the population reconstruction curves. T.N. performed the numerical modelling and paleobathymetry reconstruction. M.M. and H.A. conducted sampling campaigns. L.W., M.S. and J.S.S.D. obtained the biomarker data. T.L. and K.H. obtained TOC/LOI data. M.M., K.P., L.Z., A.K., R.R.S. and E.J. constructed the chronology. L.Wacker performed radiocarbon dating on small foraminifera samples. L.W., M.M., S.S., A.T., T.N. and J.S.S.D. interpreted the data, and wrote the paper with contributions from all other authors.

– SUPPLEMENTARY INFORMATION –

Part A: Proxy Data and Chronology

A1. Material, site selection and analytical methods

*Sediment core sampling and sample preparation for analysis***.** For this study the key sediment core 303600 was collected from the central Baltic Sea in the Gotland Basin just east of Gotland Island at 56˚55.02' N and 19˚19.98' W (Extended data Fig. 1, Extended data Table 1) using a gravity corer during a cruise of the research vessel (R/V) "Professor Albrecht Penck" in July 2009. The collected core was cut in 1-m sections and split lengthwise. The core halves were line-scanned (photographic documentation) and sampled at a 1 cm resolution. The samples were freeze dried, ground, and homogenized by mortar and pestle for analysis. The sediment chronology was developed using gravity cores 370540-7 and P435-2-1 taken during cruises with R/V "Aranda" in 2009 and R/V "Poseidon" (P435) in 2012, respectively, in the eastern Gotland Basin. For comparative studies a number of cores were taken during several cruises between 2005 and 2014 in almost all Baltic Sea basins W (Extended data Fig. 1, Extended data Table 1).

*Site selection for determining core chronology and sediment proxy studies***.** Benthic foraminifera (i.e. *Elphidium spp.*) were present in high numbers in cores P435-2-1 (220 m water depth) and 370540-7 (242 m water depth) taken in the deepest part of the eastern Gotland Basin as a result of strong saline water inflows (Lutze, 1965). They do not occur in sediments from shallower water sites of this basin. For example, at our key site 303600 (175 m water depth) benthic foraminifera are absent, likely because the inflowing saline water (vertical extent) did not reach this site. Cores P435-2-1 and 370540-7 were, therefore, selected for determining the chronology. However, the deep sites are influenced by lateral transport of fine grained material and, therefore, not suitable for sediment proxy studies of past in-situ surface water conditions using biomarker. For this purpose, site 303600, located outside the inflowing water pathway on the western side of the eastern Gotland Basin (Extended data Fig. 1), was chosen as it is only to a minor extent influenced by lateral matter transport.

Extended data Table 1 Details on the core sites studied located in almost all basins of the Baltic Sea (see Extended data Figure 1 for a map). The location, present-day and estimated paleo-water depths (6,500 cal. BP) are indicated, along with cruises and years of sampling of sites. Key-sites for chronology and proxy studies are marked in red. Loss on ignition (LOI) data are available from all sites. LOI data from cores marked with (X) are shown in Extended data Figures 2, 3 and 5.

Site	latitude	longitude	water depth (m)	paleo water depth (m)	Research vessel / Cruise	Sampling Year	LOI data
Gdansk Basin							
P475-12-6	54°49.38´N	19°11.16´E	105	101	Poseidon 475	2014	X
Gotland Basin							
303600	56°55.01´N	19°19.99´E	170	190	Prof. Albrecht Penck	2009	X
370540-6(-7) (349110) MSM16/1-052	57°17.01´N	20°07.25´E	243	264	Aranda (Maria S. Merian) Maria S. Merian 16/1	2009 (2008) 2010	X(X) (X) x
P435-2-1 (303620-3)	57°06.33´N	19°50.77´E	218	232	Poseidon 435 (Poseidon)	2012 (2005)	X (x)
372740 (370530) 211640-7	57°23.10´N	20°15.50´E	232	255	Maria S. Merian 12/4 (Aranda) Kotzov	2009 (2009) 1997	X (x) X
303630-3	57°00.37´N	19°50.08´E	185	199	Poseidon	2005	x
303640-6	56°43.66´N	19°57.49´E	153	165	Poseidon	2005	x
303650-5	56°30.05´N	19°40.46´E	141	155	Poseidon	2005	x
MSM16/1-057	57°38.88´N	20°38.75´E	139	165	Maria S. Merian 16/1	2010	x
Farö Deep							
F80	58°00.00´N	19°53.81´E	181	225	Aranda	2009	X
Northern Central Basin							
243060	58°46.90´N	20°15.30´E	190	211	Poseidon 282	2002	X
243070	58°46.10´N	20°15.30´E	195	211	Poseidon 282	2002	X
349140	58°48.99´N	20°25.07´E	189	222	Maria S. Merian	2008	X
P435-17	58°42.75´N	20°14.68´E	210	243	Poseidon 435	2012	X
Landsort Deep							
349210	58°33.51´N	18°13.83´E	258	314	Maria S. Merian	2008	x
M86/1-33	58°21.90´N	17°50.04´E	101	144	Meteor M86/1	2011	X
M86/1-37	58°40.39´N	18°31.07´E	250	323	Meteor M86/1	2011	X
M86/1-38	58°35.84´N	18°28.03´E	179	236	Meteor M86/1	2011	X
M86/1-39	58°58.42´N	19°14.43´E	104	154	Meteor M86/1	2011	X
Bothnian Sea							
P435-10	62°52.16´N	19°02.55´E	214	321	Poseidon 435	2012	X
P435-11	62°50.70´N	18°53.27´E	206	357	Poseidon 435	2012	x
P435-12	62°52.78´N	18°55.25´E	178	328	Poseidon 435	2012	x
P435-13	62°35.18´N	18°58.13´E	215	308	Poseidon 435	2012	X
P435-14	61°03.98´N	19°43.13´E	141	208	Poseidon 435	2012	X
Bay of Bothnia							
MSM16/1-93	64°42.00´N	22°03.72´E	130	211	Maria S. Merian 16/1	2006	X

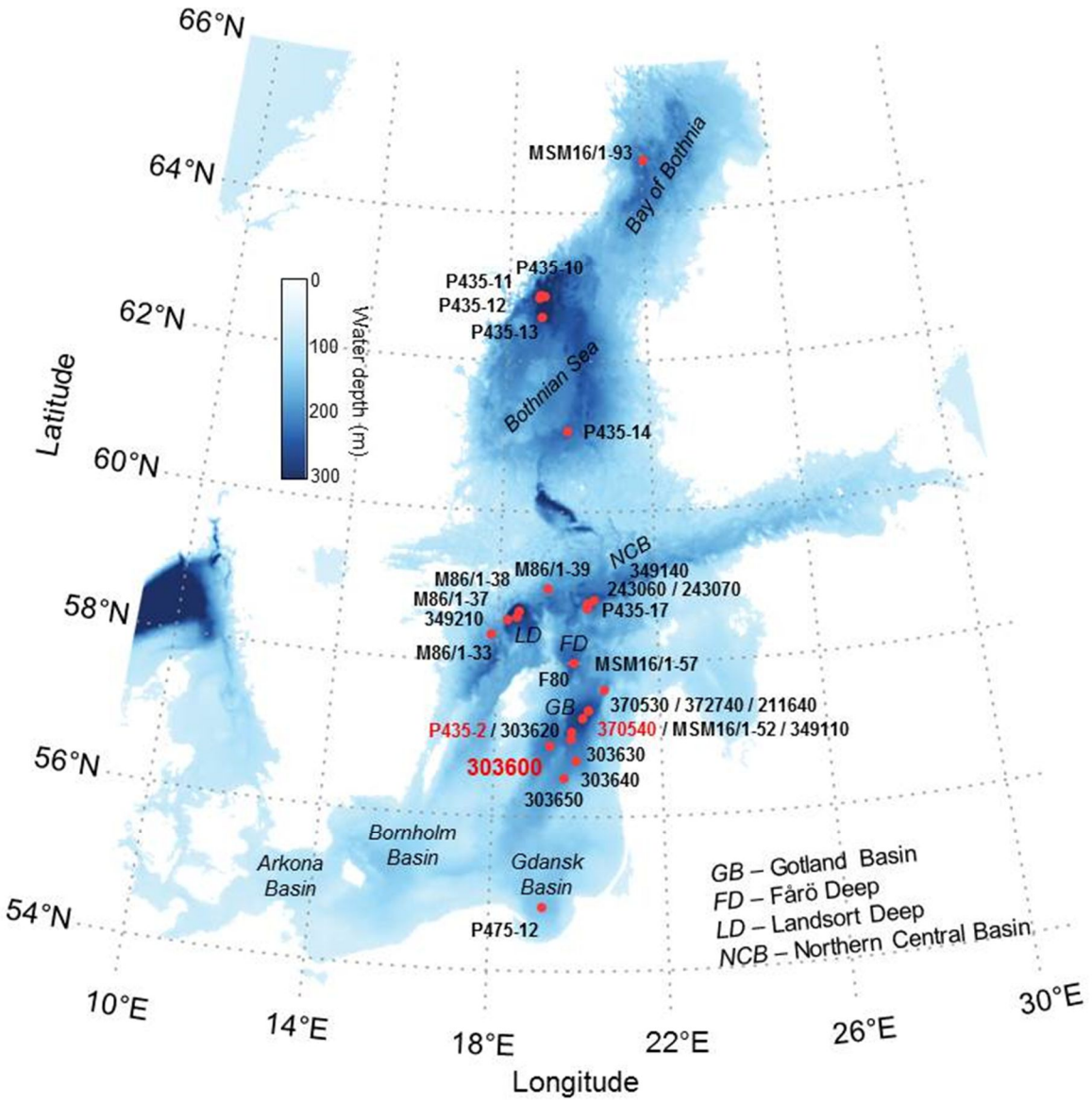

Extended data Fig. 1 Location of the sediment coring sites on a map of the Baltic Sea with the paleobathymetry at c. 6,500 cal. BP (see SI). For more details on the site location see Extended data Table 1.

*Radiocarbon dating***.** 69 individually picked benthic foraminifer samples from cores P435-2-1 and 370540-7 were radiocarbon dated with accelerator mass spectrometry (AMS) to obtain a detailed age model of the sediment cores. Eight samples of 3-5 mg foraminifera test were leached to remove any potential surface contamination, before the remaining 70% was decomposed to CO_2 under vacuum and converted to graphite for AMS ^{14}C measurement at the Poznan Radiocarbon Laboratory in Poland (see www.radiocarbon.pl). The majority of 61 samples was too small for routine AMS measurements on graphite and was dated with a new

technique at ETH Zurich employing an AMS system equipped with a sample introduction system based on a gas ion source (Wacker et al., 2013). Foraminifera tests of only 0.3 to 1 mg were leached with 100 µl of 0.02 M HCl to remove 100 µg carbonate (12 µg carbon), before the remaining carbonate was completely dissolved in phosphoric acid in 3 ml septa sealed vials and the formed CO_2 was introduced into the ion source of the AMS for ^{14}C measurement (Bard et al., 2015).

*Total organic carbon (TOC) content***.** The TOC content of sediments of core 303600 and P435-2-1 was determined as follows: After measuring the total carbon (TC) using the EA 1110 CHN analyzer from CE Instruments and the total inorganic carbon (TIC) using the Multi EA- 2000 Elemental Analyzer from Analytic Jena the TOC content was calculated as the difference between TC and TIC.

*Loss on ignition***.** All cores described in this study have been analyzed for loss on ignition (LOI); some record (cores F80, 373740, 370530, 370540-6) have previously been published (Lougheed et al., 2012; Reinholdsson et al., 2013). The LOI was determined by ashing freeze-dried samples at 550°C for 3 h and calculating the resulting mass difference in wt.%. For Baltic Sea sediments, the LOI provides a proper estimate of the TOC content of the sediments (Leipe et al., 2011) (see also Fig. S2).

*TEX_{86} analysis***.** Typically 1-3 g of sediment were extracted using the Dionex™ accelerated solvent extraction with dichloromethane/methanol (9:1; v/v) as solvent. The total lipid extract was dried over a Na_2SO_4 column and then separated using Al_2O_3 column chromatography. The polar fraction was obtained using dichloromethane/methanol (1:1. v/v) as the eluent. The polar fraction was concentrated under N_2 gas and then dissolved in hexane/isopropanol (99:1, v/v) before being filtered using a 0.4 µm PTFE filter as described previously (Hopmans et al., 2004). The sample was then analyzed by high-performance liquid chromatography coupled with atmospheric pressure chemical ionization-mass spectrometry (HPLC/APCI-MS) as described previously (Schouten et al., 2007). A local TEX_{86} calibration for the Baltic Sea was established by Kabel et al. (2012) using nine surface sediment samples from the Baltic Sea and comparing the TEX_{86} derived SSTs with satellite sea surface temperature (SST) data. The highest correlation was found using TEX_{86}^{L} and with the SST of the months July through October. The resultant Baltic Sea summer SST calibration equation is:

$$SST = 34.03 \times TEX_{86}^{L} + 36.73 \ (R^2=0.89, n=9)$$

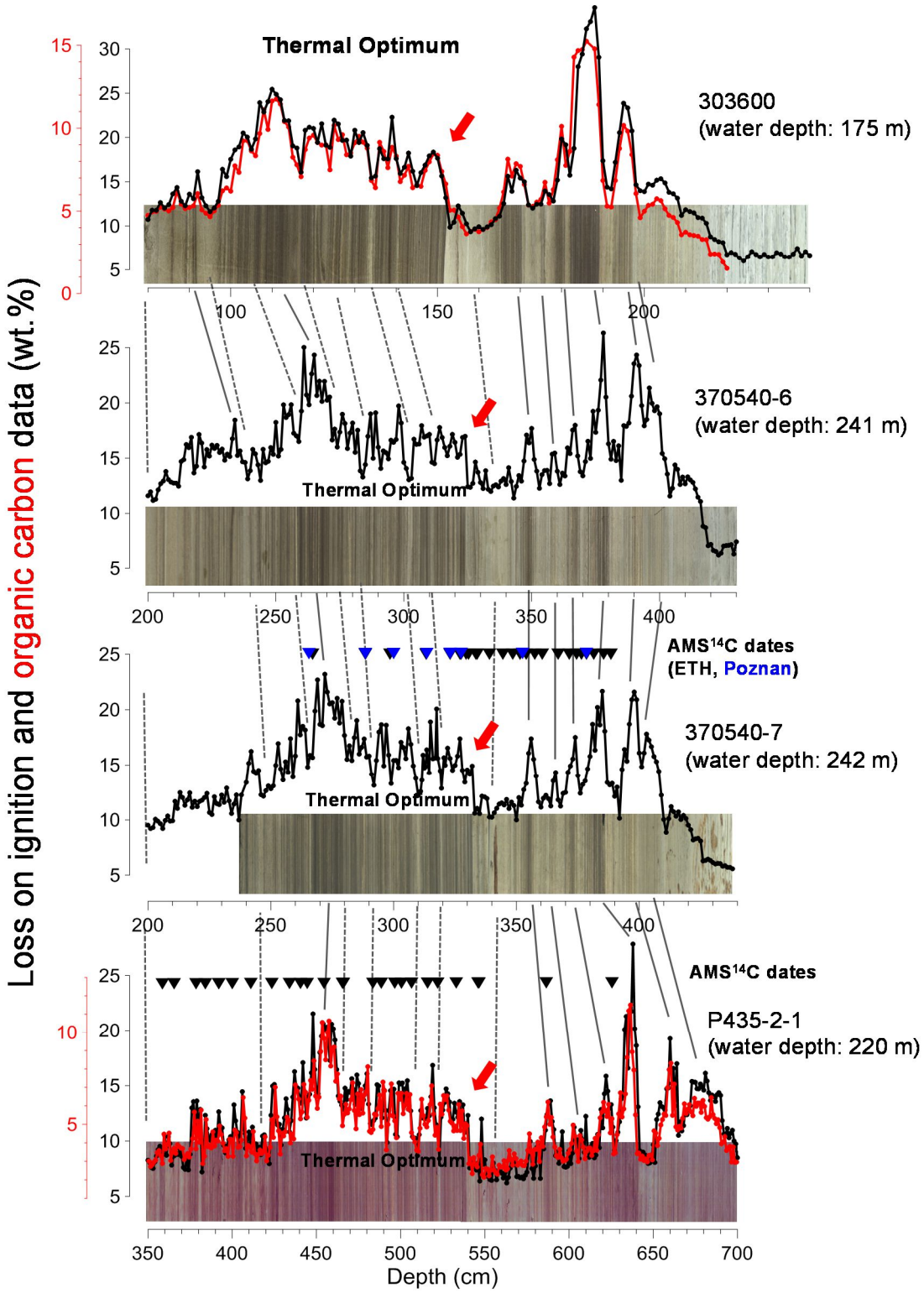

Extended data Fig. 2 Correlation of organic carbon (red curves) and LOI (black curves) data from the key-cores from the Gotland Basin in the central Baltic Sea (dashed grey lines: characteristic minima; grey lines: characteristic maxima). The chronology was developed based on 69 AMS ^{14}C dates of benthic foraminifera in core P435-2-1 and 370540-7. Depth positions of AMS ^{14}C dates are marked (black triangles: ETH Zürich, blue triangles: Poznan). The age-depth relationships were transferred onto core 303600 correlating the high-resolution LOI and TOC profiles.

A2. Sediment core age-depth relationships

High-resolution AMS ^{14}C dating was performed for the cores from sites P435-2-1 and 370540-7 (Extended data Table 2, Extended data Figs. 2 & 3). The foraminiferal abundance and quality in the lower core interval of 370540-7 is much higher than in the equivalent depth interval of P435-2-1. Therefore, high resolution dating of this older interval concentrated on 370540-7. Nevertheless, in order to secure a sound and robust high-resolution composite (P435-2-1 and 370540-7) age-depth model, overlapping depths intervals in P435-2-1 were dated too (Extended data Figs. 2 & 3). The raw AMS^{14}C dates of benthic foraminiferal samples were calibrated using the Marine13 database in the Calib7.01 (Reimer et al., 2013) and adjusted with a standard reservoir age of 400 years commonly used in western Baltic Sea studies (Extended data Table 2). As mentioned above, benthic foraminifera only occurred after strong saline water inflows in the saline, oxygen rich deep water body and therefore they very likely have the same reservoir age as Western Baltic / Skagerrak material.

The age-depth relationship developed on the central Baltic Sea cores from the deeper cores, P435-2-1 and 370540-7, can be easily transferred onto shallower cores from the central / southern Baltic by correlating LOI profiles, which are a good measure of organic carbon content changes in Baltic Sea sediments (Leipe et al., 2011) (Extended data Fig. 2), from the respective cores. This was demonstrated e.g. by Lougheed et al. (2012) and Kabel et al. (2012). Extended data Fig. 2 and 3 show how well the key cores for chronology (P435-2-1 and 370540-7) and proxy (303600) studies can be correlated to each other using LOI (TOC) profiles.

The 370540-7 depth scale was transferred onto P435-2-1 equivalent depth scale by correlating the LOI profiles using *Analyseries* Software. The resulting relationship for age versus P435-2-1 equivalent depth is shown in Extended data Fig. 3. A polynomial fit was applied for the age model and this model was transferred onto 303600 using high-resolution LOI data in *Analyseries* Software. AMS^{14}C dating in sediment cores from the northern Baltic Sea basins were performed in order to obtain information on the approximate duration of the early Littorina Sea Phase hypoxic stage (Extended data Table 2, Extended data Figs. 3 & 4).

Extended data Table 2 AMS ^{14}C dating results and calibrated ages (one sigma range, using Marine13 in Calib 7.01 program) from Gotland Basin key-site P435-2-1 and 370540-7, and other sites of the central and northern Baltic Sea. Core 370540-7: (*) denotes equivalent core depth in gravity core P435-2-1. Samples were measured as gas (ETH) and graphite samples (Poz), respectively.➡

Depth (cm) in core	Lab code	Material dated	^{14}C age	Calibrated age 1σ
P435-2-1, Gotland Basin (57°06.33′N, 19°50.77′E, water depth: 218 m)				
293-294	ETH-55053	*Elphidium* spp.	3090 ± 70	2770 – 2940
304-305	ETH-55054	*Elphidium* spp.	3150 ± 70	2840 – 3040
331-336	ETH-56921	*Elphidium* spp.	3345 ± 50	3130 – 3270
346-348	ETH-56922	*Elphidium* spp.	3465 ± 75	3240 – 3430
358-359	ETH-56231	*Elphidium* spp.	3570 ± 75	3380 – 3550
365-366	ETH-55057	*Elphidium* spp.	3615 ± 55	3440 – 3580
378-379	ETH-56923	*Elphidium* spp.	3710 ± 65	3540 – 3720
384	ETH-59705	*Elphidium* spp.	3815 ± 75	3660 – 3860
392	ETH-59706	*Elphidium* spp.	3860 ± 75	3710 – 3920
399-401	ETH-56233	*Elphidium* spp.	4030 ± 140	3860 – 4240
410-412	ETH-56924	*Elphidium* spp.	4010 ± 65	3930 – 4110
423-424	ETH-55059	*Elphidium* spp.	4095 ± 55	4060 – 4230
434	ETH-59707	*Elphidium* spp.	4185 ± 75	4170 – 4380
440-441	ETH-56925	*Elphidium* spp.	4190 ± 80	4160 – 4390
444-445	ETH-56926	*Elphidium* spp.	4290 ± 80	4290 – 4520
454-455	ETH-56927	*Elphidium* spp.	4375 ± 75	4410 – 4620
465-466	ETH-56928	*Elphidium* spp.	4500 ± 70	4610 – 4800
466	ETH-59708	*Elphidium* spp	4490 ± 110	4540 – 4810
473-474	ETH-55060	*Elphidium* spp.	4445 ± 65	4520 – 4720
482.5-484	ETH-56929	*Elphidium* spp.	46607 ± 75	4800 – 4980
488-489	ETH-56930	*Elphidium* spp.	4826 ± 80	5020 – 5250
496-497	ETH-55061	*Elphidium* spp.	5025 ± 75	5290 – 5460
500-501	ETH-56931	*Elphidium* spp.	5020 ± 80	5280 – 5460
505-508	ETH-56242	*Elphidium* spp.	5170 ± 170	5310 – 5700
516	ETH-59709	*Elphidium* spp.	5440 ± 100	5690 – 5920
521-523	ETH-56932	*Elphidium* spp.	5205 ± 65	5480 – 5630
533	ETH-59710	*Elphidium* spp.	5380 ± 110	5640 – 5870
545-547	ETH-56245	*Elphidium* spp.	5570 ± 190	5750 – 6170
586-587	ETH-55064	*Elphidium* spp.	5895 ± 65	6260 – 6380
625-626	ETH-55066	*Elphidium* spp.	6250 ± 70	6610 – 6790
370540-7, Gotland Basin (57°17.01′N, 20°07.25′E; water depth: 243 m)				
264-267 (450*)	Poz-73943	*Elphidium* spp.	4390 ± 50	4440 – 4610
266.5-267.5 (452*)	ETH-62230	*Elphidium* spp.	4450 ± 80	4550 – 4660
288-289 (479*)	Poz-73946	*Elphidium* spp.	4650 ± 80	4790 – 4990
288-289 (479*)	ETH-62231	*Elphidium* spp.	4755 ± 65	4880 – 5090
298-299 (493*)	ETH-62232	*Elphidium* spp.	4860 ± 75	5050 – 5270
299-301 (495*)	Poz-73944	*Elphidium* spp.	4470 ± 75	4580 – 4730
312.5-314.5 (513*)	Poz-73945	*Elphidium* spp.	5080 ± 75	5380 – 5510
313-313.5 (513*)	ETH-62233	*Elphidium* spp.	5230 ± 95	5480 – 5690
322-324 (529*)	Poz-73947	*Elphidium* spp.	5460 ± 75	5780 – 5890

322-324 (529*)	ETH-62234	*Elphidium* spp.	5395 ± 60	5700 – 5850
327 (538*)	ETH-59688	*Elphidium* spp.	5620 ± 85	5920 – 6120
327-328 (538.5*)	ETH-61284	*Elphidium* spp.	5725 ± 80	6030 – 6230
327-328 (538.5*)	Poz-70380	*Elphidium* spp.	5690 ± 60	6010 – 6170
333-334 (546*)	ETH-61286	*Elphidium* spp.	5690 ± 75	6000 – 6180
334 (546.5*)	ETH-59690	*Elphidium* spp.	5635 ± 70	5940 – 6120
338-340 (551*)	ETH-59691	*Elphidium* spp.	5565 ± 85	5870 – 6080
348-349 (568*)	ETH-59693	*Elphidium* spp.	5785 ± 70	6130 – 6280
351-352 (580*)	ETH-61287	*Elphidium* spp.	5960 ± 75	6290 – 6440
352.5 (581*)	Poz-68833	*Elphidium* spp.	5970 ± 50	6310 – 6430
354 (586*)	ETH-59694	*Elphidium* spp.	5900 ± 70	6260 – 6320
357-358 (594*)	ETH-59695	*Elphidium* spp.	6025 ± 75	6350 – 6530
360-361 (600*)	ETH-59696	*Elphidium* spp.	6210 ± 90	6540 – 6760
366-368 (616*)	ETH-59698	*Elphidium* spp.	6255 ± 90	6600 – 6830
371-372 (621*)	ETH-59699	*Elphidium* spp.	6220 ± 75	6570 – 6760
374-375 (629*)	ETH-61288	*Elphidium* spp.	6470 ± 75	6870 – 7080
376-377 (630*)	ETH-59700	*Elphidium* spp.	6475 ± 75	6880 – 7080
378-379 (631*)	ETH-61289	*Elphidium* spp.	6485 ± 80	6890 – 7100
378.5 (631*)	Poz-70381	*Elphidium* spp.	6320 ± 70	6700 – 6870
381.5 (636*)	ETH-59701	*Elphidium* spp.	6350 ± 75	6720 – 6910
385.5 (641*)	ETH-59702	*Elphidium* spp.	6415 ± 80	6780 – 7000
388.5 (650*)	ETH-59703	*Elphidium* spp.	6710 ± 75	7160 – 7310
P435-13-4, Bothnian Sea (62°35.18´N, 18°58.13´E; water depth: 215 m)				
282-285.5	ETH-56905	*Elphidium* spp.	3495 ± 80	3270 – 3470
303.5-305.5	ETH-56907	*Elphidium* spp.	4780 ± 110	4920 – 5220
P435-14-2, Bothnian Sea (61°03.98´N, 19°43.13´E; water depth: 141 m)				
578-580	ETH-59736	*Elphidium* spp.	4020 ± 70	3930 – 4140

610-611	ETH-59738	*Elphidium* spp.	5000 ± 85	5260 – 5460
624-625	ETH-59739	*Elphidium* spp.	6450 ± 70	6840 – 7040
MSM16/1-93, Bay of Bothnia (64°42.00′N 22°03.72′E; water depth: 130 m)				
441.5-442.5	ETH-56908	*Elphidium* spp.	4365 ± 65	4410 – 4590
464.5	ETH-59704	*Elphidium* spp.	4955 ± 80	5210 – 5440
495.5-497.5	ETH-56909	*Elphidium* spp.	6545 ± 110	6930 – 7180

Part B: Ecosystem modelling approach

B1. Model description

Circulation. To simulate the climatic impact on biogeochemistry, (for example on the redox conditions, hypoxic/oxic), we used a coupled three dimensional hydrodynamic and biogeochemical model. The hydrodynamic part of the model is based on the circulation model MOM (version 5.1) (Griffies, 2004) and has been adapted to the Baltic Sea with an open boundary condition to the North Sea, and freshwater riverine input. The MOM model is complemented with a sea ice model to estimate ice cover thickness and extent. Furthermore, a parametric surface wave model (Schwab et al., 1984) is coupled to MOM. The main purpose in this application is to account for the surface wave generated bottom shear stress, which in shallow seas is predominantly how the resuspension of sedimentary material occurs.

Biogeochemistry. The biogeochemistry was integrated using ERGOM (Leibniz-Institute for Baltic Sea Research, 2015). The ERGOM biogeochemical model, which has been developed for the Baltic Sea, describes the dynamics of nitrogen, oxygen and phosphorus including the inorganic nutrients nitrate, ammonium and phosphate, and particulate organic matter consisting of phytoplankton (autotrophs), dead organic matter (detritus) and zooplankton (heterotrophs). In ERGOM, in-situ organic matter is produced from the inorganic nutrients by three functional groups of phytoplankton: large cells, small cells and others, and cyanobacteria. Organic material sinks and enters the model sediment as benthic nitrogen and phosphorus. All model processes requiring electron acceptors (e.g. respiration) reduce the oxygen concentration in the water. When oxygen is depleted nitrogen is first used as an electron acceptor (denitrification) and then subsequently sulfate becomes the electron acceptor resulting in the formation of hydrogen sulfide.

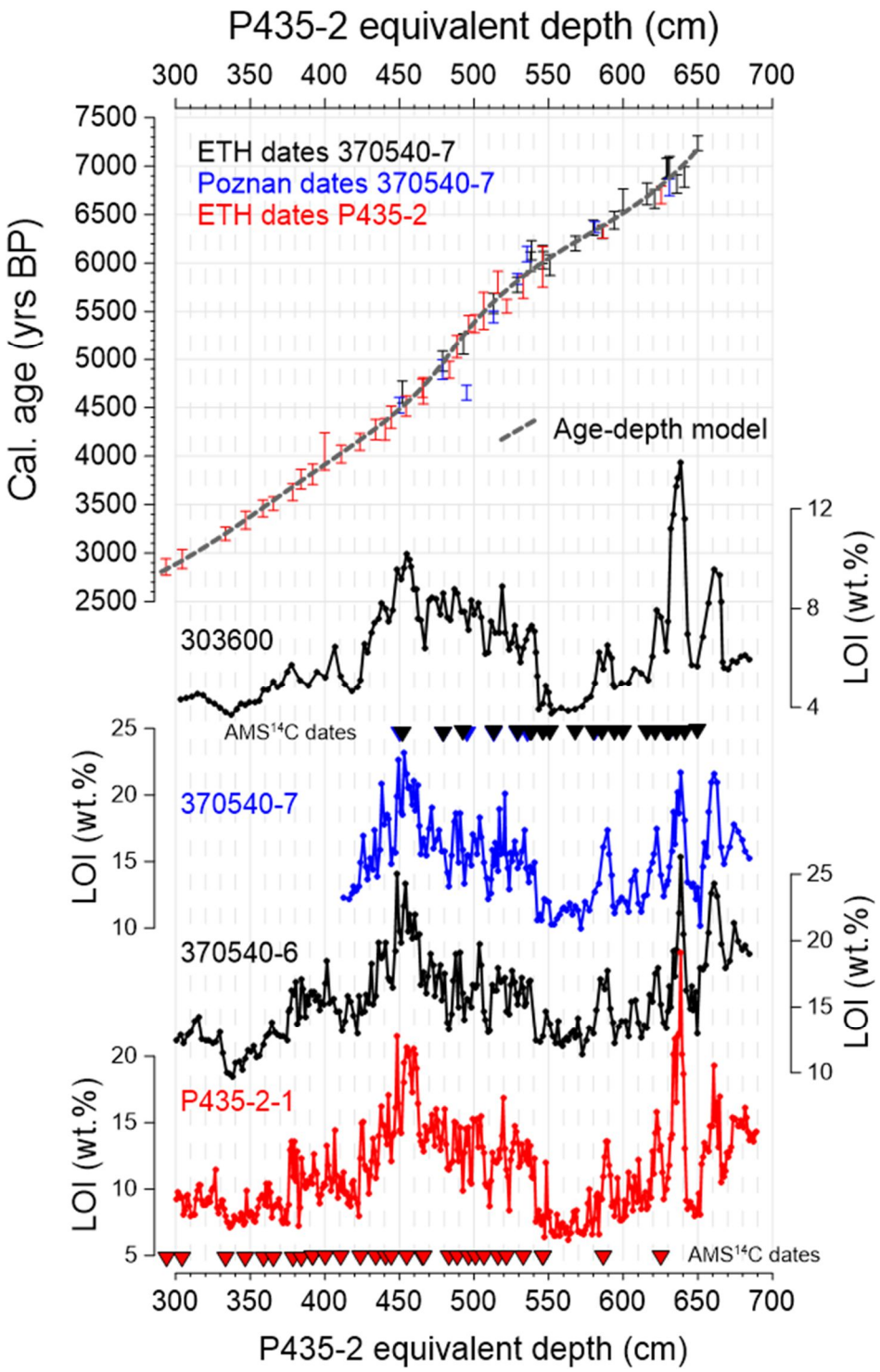

Extended data Fig. 3 Loss on ignition (LOI) records of 370540-6(-7) and 303600 were correlated to core P435-2-1 and transferred on P435-2-1 equivalent depth scale. AMS ^{14}C dates of benthic foraminifera in cores 370540-7 and P435-2-1 (blue triangles: ETH dates, blue: Poznan dates), calibrated ages (upper graph) are shown vs. P435-2-1 equivalent depth scale. The resulting age model is a polynomial fit (upper graph).

Bathymetry. The Baltic Sea bathymetry is not static. In particular the northern Baltic Sea lifts up and becomes shallower due to the glacio-isostatic rebound. To reconstruct the Baltic Sea bathymetry about 6,500 cal. BP, we made use of data for relative sea level change by Rosentau et al. (2012). These data were combined with a contemporary bathymetry of the Baltic region by Seifert et al. (2001). Extended data Fig. 6 shows the reconstructed paleo- (B) and contemporary (A) bathymetry for the Baltic Sea, respectively. The northern basins are sometimes more than 100 m deeper while the southern Baltic remains nearly unchanged.

Spatial resolution. Due to the tremendous computational load (2,000 years have been simulated), we applied a relative coarse model grid of 6 nautical miles. Extended data Fig. 6C shows the derived paleo bathymetry projected onto the model grid. Vertically the model is resolved into 80 layers. Close to the surface the vertical resolution starts with 0.25 m extending to the bottom to a maximum of 6 m.

Atmospheric forcing. Atmospheric forcing was reconstructed using via prescribed surface boundary conditions. We used the coastDat data set (Weisse et al., 2009), a dynamical downscaling re-analysis for the years 1948-2014. For the different climate states (warm vs. cold), we modified the atmospheric data by a delta change approach successfully applied earlier (e.g., Kabel at al., 2012). This approach is typically applied when meteorological data are not available in a sufficient temporal and spatial resolution. In order to simulate the biogeochemical consequences of the change in summer SST that occurred in the reconstructed SST record at 6,000 cal. BP, we applied the following conditions. For the warm climate state we increased the 10 m air temperature of the coastDat data by 1K, which results in a slight increase of the water temperature. To mimic a colder climate we reduced the 10 m air temperature by 2K and decreased the downwelling shortwave radiation. The effect is a mean SST difference of 2K between cold and warm climate periods. The temperature difference is higher in summer and amounts up to ca. 3K (Extended data Fig. 7). This temperature change reflects the temperature difference we reconstructed in the proxy studies for the transition at 6,000 cal. BP (Extended data Fig. 4).

Nutrient composition. The nutrient input has been compiled from HELCOM assessments (www.helcom.fi). Pre-industrial nutrient loads to the Baltic Sea due to riverine discharge and atmospheric deposition are derived from estimates by Gustafsson et al. (2012).

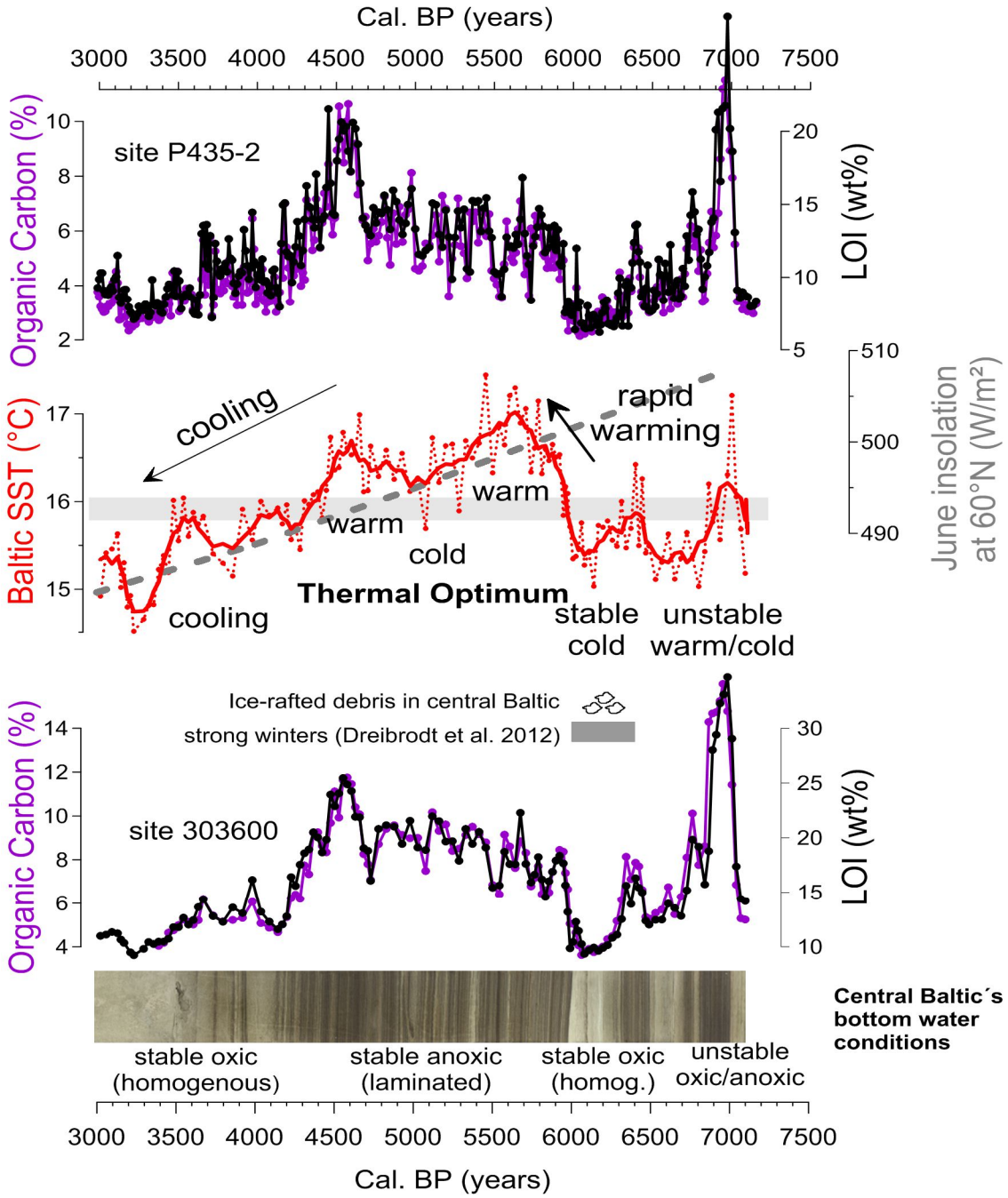

Extended data Fig. 4 Relationship of SST with bottom water anoxia in the Baltic Sea. Loss on ignition (LOI, black) and organic carbon (purple) data from two key-sites P435-2 and 303600 vs. age. Baltic SST reconstruction for Gotland Basin site 303600 is shown in red (5 point running mean: thick red line). June insolation at 60°N (in W m^{-2}) is plotted as a grey stippled line. Horizontal grey bar marks the presumed 16°C threshold temperature for cyanobacteria blooms. Note, anoxic conditions of bottom waters (i.e. laminated sediments and elevated LOI values) occurred when temperatures were above this threshold temperature. Ecosystem modelling results confirm this close relationship (see SI). A rapid warming with the sudden appearance/spread of anoxic conditions occurred at 6,000 cal. BP and is followed by a regional Thermal Optimum. The general temperature decline/cooling follows the summer insolation decrease finally leading to stable oxic bottom water conditions. The strong cold phase between 6,300 and 6,000 cal. BP is also evident from lake reconstructions (Dreibrodt et al., 2012) indicating strong winters, and an increase in coarse mineral fraction (ice rafted debris) in central Baltic Sea sediments.

We used their estimates for AD 1850 and reduced them by additional 10% to account for a smaller population density at 6,500 cal. BP. Total loads including riverine loads and atmospheric deposition for the whole model domain account for $1.2*10^7$ kg phosphorus and $3.9*10^7$ kg nitrogen.

We simulated the Baltic Sea ecosystem under our model as described in Part B1 in 50-year time slices, which were eventually concatenated into the complete simulated time-series. The first time slice was initialized using data from a pre-industrial reconstruction of the Baltic Sea´s environment(Gustafsson et al., 2012), which is characterized by low nutrient and high oxygen concentrations in the waters of the Baltic. The output of the preceding time slice was used as the starting condition for the next time slice in the simulation. Each time slice was forced by the modified meteorological data producing respective warm or cold climatic conditions (see Part B1). The modeled cold period (350 yr) mimics the cold climate before 6,000 cal. BP (Extended data Fig. 4) and the modeled warm phase (400 yr) the warm climate after 6,000 cal. BP (Extended data Fig. 4).

B3. Simulation Results

The simulations clearly demonstrate a tight coupling between SST, hence climate, and the oxygen concentrations in the Baltic Sea (Fig. 3A main text). During warm conditions the probability for the occurrence of hypoxia in wide areas of the entire Baltic increases to a large extent, while during cold periods most parts of the Baltic Sea are well oxygenated. An increase of the hypoxic areas from 20,000 to > 120,000 km² is estimated by our simulations at the transition from cold to warm climate at 6,000 cal. BP. It is worth noting that due to the rather coarse model grid the spread of hypoxia cannot be accurately estimated in the coastal regions. It is therefore likely that hypoxia increased significantly in all coastal regions at 6,000 cal. BP, but this is not shown in Fig. 3A as this represents the conservative estimate.

Our simulation results support the theoretical predictions by Vahtera et al. (2007). These authors argue that when hypoxic or anoxic conditions emerge, a positive feedback mechanism between temperature and hypoxia becomes established. This positive feedback loop has two major ingredients: i) bloom development by nitrogen-fixing cyanobacteria, and ii) enhanced phosphate availability. For an effective nitrogen fixation by cyanobacteria a certain minimum temperature is required. For the Baltic Sea a temperature threshold of 16°C has been estimated from observations (Kononen, 1992; Wasmund, 1997), therefore, when summer SSTs are >16°C cyanobacterial blooms can develop, substantially affecting the biogeochemistry of the Baltic Sea. Phosphorus mineralized in sediments under oxic

conditions becomes to a certain extent bound with iron, forms phosphorus-iron complexes and then is retained in the sediment and eventually buried. A change to hypoxic/anoxic conditions liberates the iron bound phosphorus and it is released as phosphate to the water column (Laima et al., 2001; Neumann & Schernewski, 2008). This surplus phosphate in the water column can then be taken up by cyanobacteria. Consequently, SSTs >16°C result in a substantial increase in primary productivity. This additional biomass (in modern times approximately half of the sedimentary organic carbon is estimated to be derived from these blooms in the central Baltic basins; Struck, et al., 2004) results in an increased carbon flux into the deeper water and in turn the oxygen demand for heterotrophic processes increases. Oxygen concentrations go down and increasingly larger sediment areas become covered by anoxic waters resulting in even more phosphate release from the sediment. Nutrient concentrations increase and as a final result of this positive feedback loop a eutrophic state of the Baltic Sea is established. This state is almost independent of external loading and can only be changed due to colder summer SSTs (below 16°C), which prevents cyanobacteria from forming heavy blooms.

Part C: Regional, basin wide environmental changes from 7,500 to 3,000 cal. BP and its consequences for the food web

C1. Basin wide environmental changes from 7,500 to 3,000 cal. BP

The climatic conditions after the Littorina Sea transgression (c. 7,500 cal. BP) in the Baltic region were characterized by high summer insolation at 60°N latitude, potentially leading to warmer summer SSTs in the entire Baltic region. Warming SSTs in summer are critical to the formation of cyanobacterial blooms in the Baltic Sea (Wasmund, 1997; Kabel et al., 2012), which stipulates the feedback loop discussed in Part B3. During periods of warmer climate, hypoxic conditions occur and laminated organic carbon rich (high LOI) sediments are deposited as transpired in the entire Baltic Sea basin when the climate significantly warmed at 7,500 cal. BP (Extended data Fig. 5). The Baltic Sea region experienced climatic oscillations (Fig. 2 main text, Extended data Fig. 4) between 7,500 and 6,500 cal. BP and effects of this are seen clearly in the central Baltic basin (alternating homogenous/oxic and laminated/hypoxic sediments (Zillén et al., 2008; Kabel et al., 2012), Extended data Figs. 4 and 5), but not in the formerly much deeper (> 150 m; Rosentau et al., 2012) northern areas (Extended data Fig. 5).

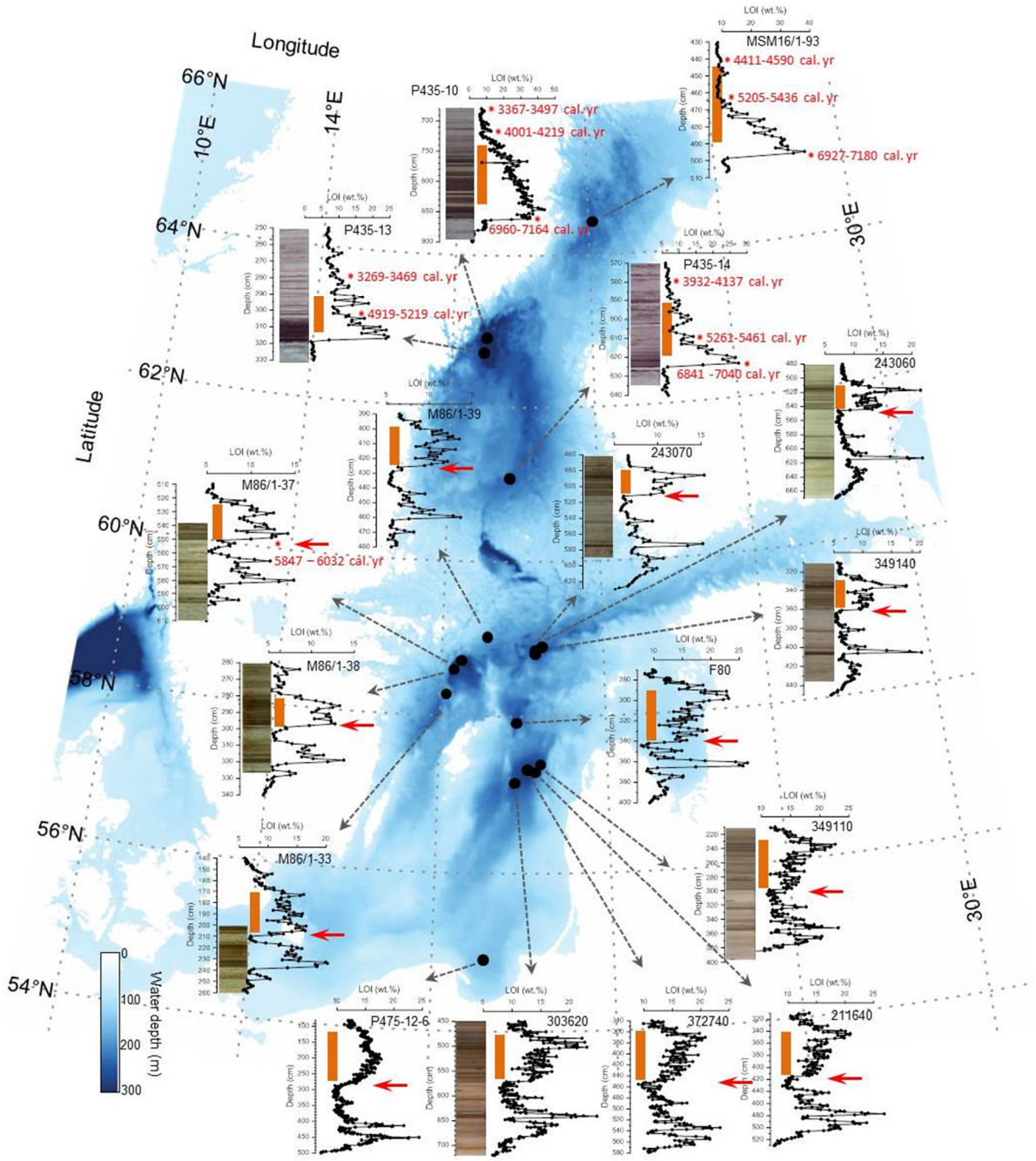

Extended data Fig. 5: Loss on ignition (LOI) profiles vs. depth from various sites from the entire deeper Paleo-Baltic. The sharp transition (red arrow) from a marked cold (oxic, low LOI, homogenous sediments) to a warm phase (hypoxic, high LOI, laminated sediments) at c. 6,000 cal. BP is clearly seen in all records from the central and southern Baltic. Only the deeper part of the northern Baltic (upper panel) was hypoxic before 6,000 cal. BP. During the Thermal Optimum (vertical orange bar) the almost entire Baltic Sea was hypoxic but conditions gradually changed to oxic after the Thermal Optimum. Records from the key-sites (Extended data Figure 2) are not included here but fit these LOI profiles very well. AMS ^{14}C are marked in profiles from the northern cores.

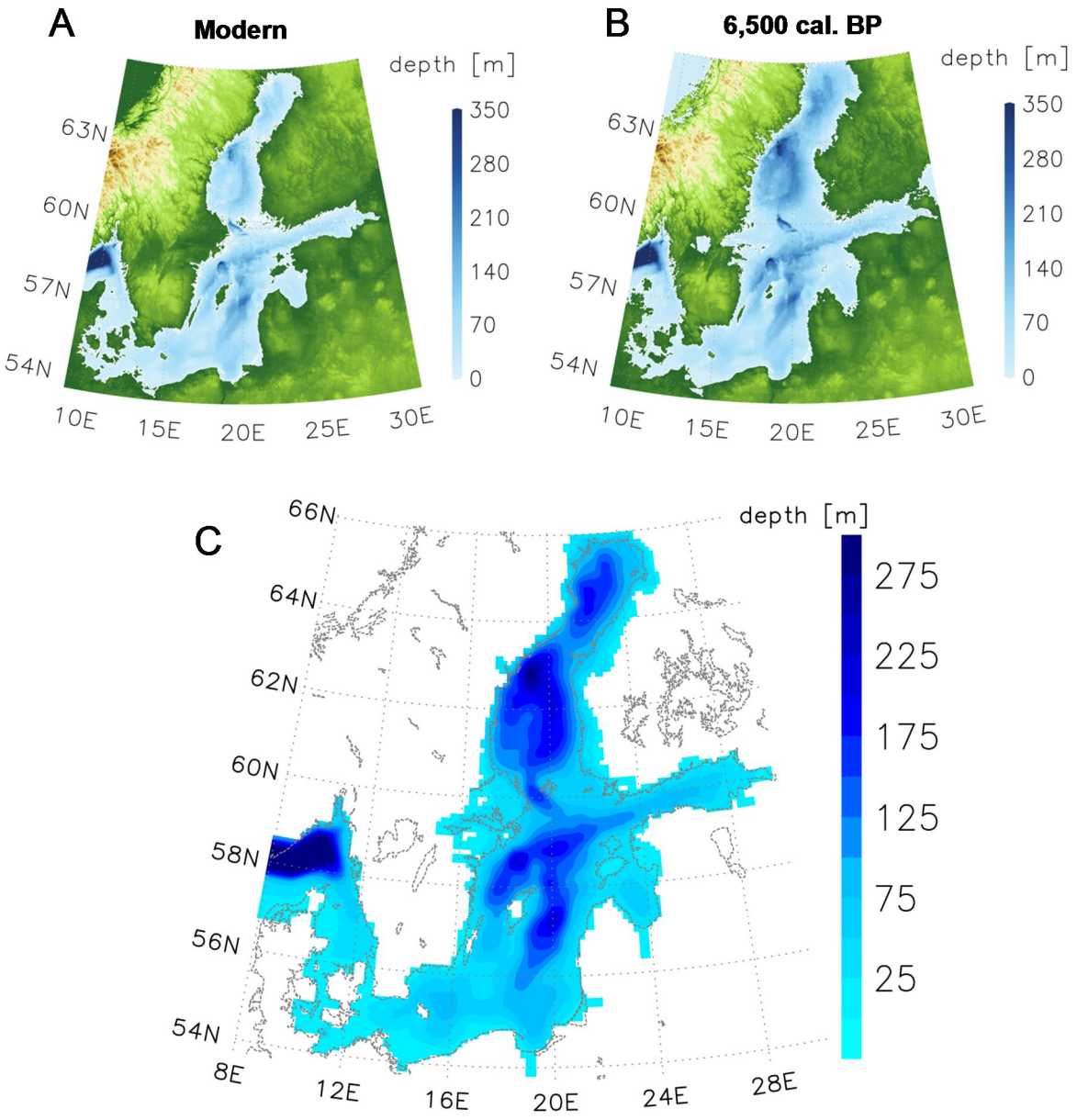

Extended data Fig. 6 Reconstructed contemporary (A) and paleo- (B - 6,500 cal. BP) bathymetry for the Baltic Sea. About 6,500 cal. BP the northern Baltic Sea basins were more than 100 m deeper than today due to the rapid galcio-isostatic land uplift in the region. The southern Baltic remained nearly unchanged. The derived paleobathymetry was projected onto the 6 nautical miles model grid and is shown in (C). Note that the contemporary coastline is marked by a dashed grey line in (C).

A strong cold phase is recorded between 6,500 and 6,000 cal. BP (Fig.2, main text, Extended data Fig. 4) with a pronounced transition from cooler/oxic conditions to warmer/anoxic conditions at 6,000 BP that is prevalent throughout the southern and central Baltic (Extended data Figs. 4 and 5). The marked transition from oxic to hypoxic conditions at c. 6,000 cal. BP had important implications for the marine fauna in the entire Baltic (basins and coastal waters) at that time (described below) and consequently affected the human

populations that relied upon them. The stable hypoxic conditions of the Thermal Optimum phase, when SSTs are persistently higher than 16°C, are widespread in the entire Baltic Sea (Extended data Figs. 4 and 5) and terminated parallel a marked cooling trend after 4,500 cal. BP when SSTs became lower than 16°C (Fig. 2 main text, Extended data Figs. 4 and 5).

Our model generates simulated results (Part B3) that are similar to the data observed in marine sediment cores, for example by successfully simulating the observed dramatic change at 6,000 cal. BP in the ecosystem. Therefore we can infer that the overall model is useful, and its mechanisms and dynamics are informative. The model nicely reproduces the remarkable spread of hypoxia from the northern basins (laminated sediments were restricted to the North) to the entire Baltic including coastal areas at/after 6,000 cal. BP (Fig. 3A, Extended data Fig. 5). A eutrophic ecosystem state was established during the local Thermal Optimum and changed to oligotrophic as cooling continued after 4,500 cal. BP (e.g. Extended data Fig. 4).

C2. Environmental changes and consequences for food web dynamics

Previous studies have shown that in the last three decades changes in climate have caused major restructuring of the upper trophic levels in the Baltic Sea (Möllmann et al., 2003; MacKenzie & Köster, 2004). In the late 1980s the North Atlantic Oscillation (NAO) shifted from a negative to a positive phase causing SSTs to increase by ~1°C, a temperature change that most likely drove ecological regime shifts in the central Baltic Sea (Alheit, et al., 2005; Möllmann et al., 2005). Warming SSTs can cause variations in phytoplankton populations in the Baltic Sea and since they are the prey of zooplankton these shifts can potentially create bottom-up changes in food web dynamics (Alheit, et al., 2005; Möllmann et al., 2008). Additionally, fluctuations in copepod abundances in the Baltic ecosystem are driven at least partially by temperature changes (Möllmann et al., 2000). Climate induced changes in copepod fecundity can both directly and indirectly affect fish stocks in the Baltic Sea dynamics (Alheit, et al., 2005; Möllmann et al., 2008). For example, contemporary warming in the Baltic in the late 1980´s shifted commercially important fish populations towards sprat (Alheit, et al., 2005; Möllmann et al., 2005).

Climate variability and oxygen availability have been shown to especially affect cod, a commercially important fish in the Baltic Sea. Cod spawn in late winter and early spring when SSTs are around 5-7°C and if SSTs fall outside of this range survival of the offspring is reduced (Brander, 2000). Oxygen depletion has also been found to be the limiting factor determining reproductive success of cod in the Baltic Sea and egg survival diminishes with decreasing oxygen concentrations (Wieland et al., 1994). Reduced oxygen conditions in the

Baltic Sea are frequently sufficient to prevent cod eggs from hatching as most eggs are below the halocline depth where hypoxia occurs (Wieland et al., 1994). Because the success of hatching for cod eggs is closely related to oxygen concentration at their depth, salinity is also a factor because it impacts the buoyancy of eggs and the depth at which they float (Wieland, & Zuzarte, 1991). Additionally, hypoxia can affect food web dynamics in the Baltic ecosystem by forcing fish living near the bottom to find prey alternatives or cause fish to feed in shallower water (Bagge et al., 1994). Furthermore, research shows that cod recruitment is more susceptible to the deleterious effects of climate change when stock biomass is already low due to other conditions (Brander, 2005) such as overfishing, hypoxia, and increased competition among other fish species.

Seals are an apex predator and their presence or absence would have a large top down impact on the food web in the Baltic Sea. Additionally, harp seals were important game to people living during the mid-Holocene (Eriksson, 2004; Fornander et al., 2008) as supported by the abundance of bones from this species in refuse from islands in the Baltic Sea (Bennike, et al., 2008; Stora & Ericson, 2008). When this species exactly arrived in the Baltic Sea is not known for sure, but the dating of bones places their appearance in the basin after 7,500 cal. BP (Ukkonen, 2002; Schmoelcke, 2008) succeeding the opening of the Danish Straits. Why a subarctic species would enter the Baltic Sea during the warmest periods of the Holocene has been a debated topic, but this study may shed some light on the debate as it is possible the harp seals entered during a cooler period between 7,500 and 6,000 cal. BP (Extended data Fig. 4). Once the connection with the North Sea was re-established, marine water and species were able to enter the Baltic Sea (Schmoelcke, 2008) making it a more productive marine environment that was favorable for potential prey of the seals such as cod, herring (Lougas, 1999; Forstén,& Alhonen, 1975) and oysters (Bennike, et al., 2008). Since cod and herring are prey to harp seals (Lawson et al., 1995; Lindstrøm, et al., 1998), it is reasonable to assume any changes in the fish populations based on changes in climate or oxygen availability would also affect the seals. Through examining archaeological evidence one study showed a correlation between oyster and harp seal remains in the Baltic Sea region and conjectured that when oysters were abundant during mid-Holocene, so were their predators, harp seals (Bennike, et al., 2008).

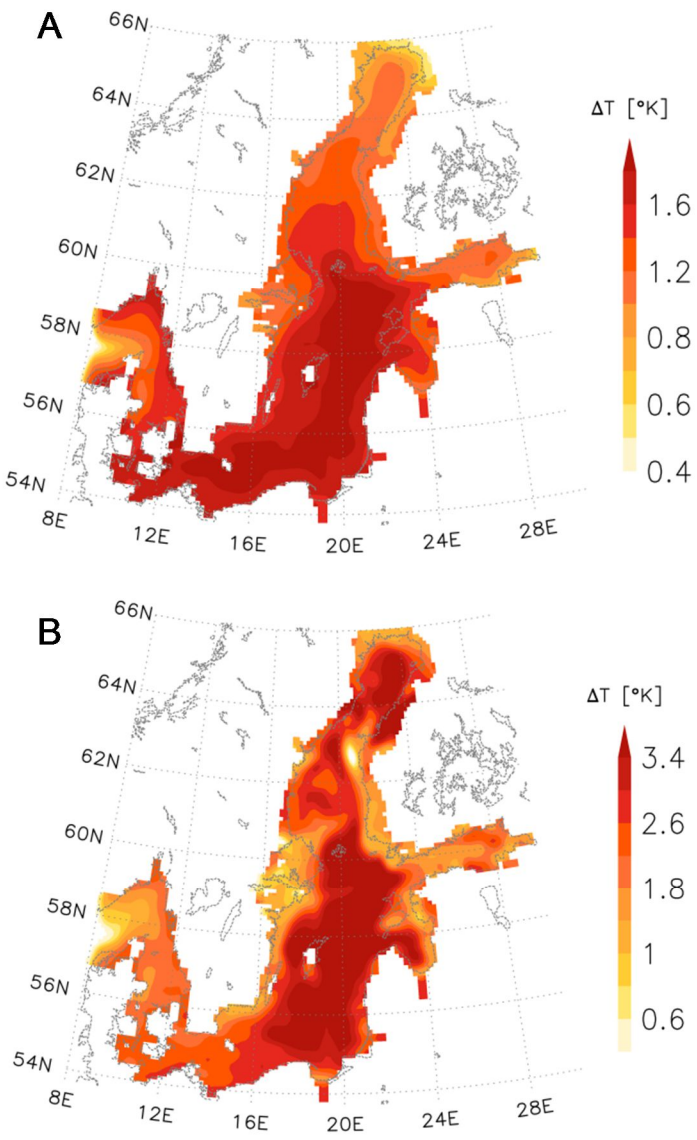

Extended data Fig. 7 Modeled mean annual (A) and summer (JJA, B) temperature difference between cold and warm climate states in the upper 15 m surface waters using the delta change approach (for details see SI).

Part D: Human population and cultures

D1. Construction of Central and Western Baltic Summed Probability Distributions (SPD)

Overall population proxy. We constructed an SPD using all ^{14}C dates (Fig. 2A black line, top) obtained from EUROEVOL radiocarbon database http://discovery.ucl.ac.uk/1469811/ that fall within the Central and Western Baltic kml polygon (brown polygon Fig. 1). All these ^{14}C dates have an anthropogenic association and

are of terrestrial origin from archaeological sites. The SPD was constructed using methods described in Shennan et al. (2013) and Timpson et al. (2014). At each site, similar dates (within 200 ^{14}C years) were binned, calibrated using Intcal13, summed and normalized to unity, such that multiple similar dates at a site had the same overall weighting in the SPD as a single date. This is a conservative approach to dealing with differential dating at sites due to, for example, a larger research budget permitting more samples to be radiocarbon dated. All binned SPDs were then summed and the final SPD was normalized to unity. The rationale behind this approach is that periods of increased population will leave more dateable material behind in the archaeological record. Therefore, the SPD provides a proxy for relative population levels through time within the polygon, but the density values are relative and therefore the units are arbitrary. The thin solid line represents a fine temporal resolution SPD and the thick dashed line represents a 200 year rolling mean.

The Polygon was specifically constructed to test the hypothesis of a demographic response to climatic change across the broad region of Central and Western Baltic. By utilizing the largest possible sample size (site n = 608, sample n = 1960) we can expect local variability (e.g. from endogenous causes) to destructively interfere, and any patterns common to the entire region to be maximized.

SPDs based on cultural assignment. We constructed SPDs from four subsets of ^{14}C dates (Fig. 2A colored lines, middle) from the Central and Western Baltic polygon, utilizing a total of 1144 of the 1960 ^{14}C dates (58%) which had been assigned to one of the following cultures by the original excavator: Ertebølle (or Lihult), TRB (Funnel Beaker), Corded Ware, Pitted Ware. Dates that were considered transitional between two cultures were not included, i.e. Ertebølle/TRB (n=79) and TRB/Bell Beaker (n=1). Also not included were 24 dates associated with cultures beyond the temporal interest of this study (for example Early Bronze Age). The remaining 712 excluded dates had not been associated with a specific culture. SPD analysis was performed as described above for all dates in the polygon, with the exception of the final step of normalization to unity. This ensures a fair comparison of the magnitudes of each cultural SPD. Again, the thin solid line represents a fine temporal resolution SPD and the thick dashed line represents a 200 year rolling mean.

D2. Correlation tests between Baltic Sea SST and Central and Western SPD

Overall correlation. Correlation between SST and Central and Western Baltic SPD was calculated using two methods. In both cases interpolation was required to simplify and

match the SPD time series to exactly the same 99 unequal discrete SST time points that overlap with the SPD, from 4,036 to 7,099 yrs BP inclusive. The first method uses Pearson's product moment correlation coefficient, r = 0.731 (95% CI = 0.624 to 0.812), p-value < 2.2e-16, t=10.56, df = 97. However, there is the possibility of some spurious shared information between the SST and SPD, which may exaggerate the p-value. For example, SST core time points were estimated using a ^{14}C time depth model from dates that were calibrated via the same Intcal13 curve. Similarly both time-series are subject to the same atmospheric variability in ^{14}C. Therefore a second method using a Monte Carlo simulation approach as employed in Shennan et al. (2013) generated 50,000 simulated radiocarbon datasets (using a uniform distribution between 4,000 and 8,000 cal. BP). An SPD was generated for each, which were then subjected to exactly the same correlation test with SST. This ensured each simulated SPD was processed using the same calibration and interpolation as the observed radiocarbon dataset and resulted in 50,000 Pearson's product moment correlation coefficients ranging from -0.735 to +0.721 (SD = 0.228), which were compared to the observed correlation coefficient. Not a single simulated correlation coefficient was equal or greater (1-tailed) and only one simulation was greater in magnitude but negative (2-tailed), providing a more conservative p-value estimate of 0.00002.

Cross-correlation and lag. Both the SPD and SST time series were interpolated to annual points between 4,036 and 7,099 yrs BP, allowing a fine resolution cross-correlation analysis using Pearson's product moment correlation coefficient in the lag range of +/- 15% (460 years). A peak correlation was obtained when the SPD lagged SST by 61 years (r = 0.862 compared to r = 0.839 at lag = 0). Note only the relative values are informative as the magnitude of these values are inflated compared to the correlation test since both time series were heavily interpolated and trimmed to ensure a constant window length.

D3. Archaeological sites and cultures

Although there is now evidence of the presence of domestic pigs in Ertebølle Mesolithic contexts in Baltic north Germany ca. 6,500 cal. BP (Krause-Kyora et al., 2013), the arrival of farming in southern Scandinavia is associated in material culture terms with the Funnel Beaker, or TRB culture, beginning ca. 6,000 cal. BP. Ancient DNA evidence has recently shown that it involved an expansion of farming populations from further south (Skoglund et al., 2014). In terms of the economy, farming is indicated by the presence of cereal remains and the bones of domestic animals. Direct radiocarbon dates on charred cereal grains of wheat and barley show their presence across southern Scandinavia as far north as

middle Sweden in the period 6,000-5,700 cal. BP and the same is true for directly dated domestic animal bones, including sheep/goat and cattle (Sørensen & Karg, 2014). However, this does not mean that wild resources ceased to be exploited. When coastal and lakeside sites are distinguished from inland ones they generally show very high proportions of wild fauna and even at inland sites wild fauna can represent a significant proportion at sites from the EN I phase (Sørensen & Karg, 2014) (Fig. 13), although there is a shift towards higher domestic proportions in later phases at all sites (Sørensen & Karg, 2014) (Fig. 14). The discussion continues and it remains unresolved whether local forager groups continued to exist in coastal zones side by side with incoming farmers or whether the latter exploited marine resources on a seasonal basis; however, there is evidence of some introgression of genes from hunter-gatherer lineages into the farming population but none in the opposite direction (Skoglund et al., 2014).

In recent years extensive stable isotope and lipid analyses have been carried out on both human bone and ceramic residues to examine dietary patterns during the Mesolithic and Neolithic of southern Scandinavia. A stable isotope study of human bone by Richards et al. (2003) indicated a wide-ranging diet for Mesolithic individuals, including partially terrestrially-based protein. Neolithic diets, on the other hand, were much more uniform and based entirely on terrestrial protein, most probably from domesticated resources. Fischer et al.'s (2007) isotope study of human and dog bones from Mesolithic and Neolithic sites found that Mesolithic samples indicated heavy dependence on marine resources, especially high trophic level fish, even at inland sites. With one exception, the Neolithic samples indicated a general shift towards a diet based on terrestrial foods with some low trophic level freshwater and marine food. However, early Neolithic samples from coastal sites have not yet been analyzed (Sørensen & Karg, 2014).

Isotope analyses by Craig et al. (2007) found that ceramic residues from late Mesolithic Ertebølle pottery from the coastal site of Tybrind Vig in Denmark indicated that the vessels were mainly used 'for processing marine products', and that marine products were strongly represented at the inland site of Ringklosters. The results of analyses of residues from TRB vessels indicated the processing of freshwater fish as well as terrestrial products including animal fats. A further study by Craig et al. (2011) of a much larger number of ceramic residues from Ertebølle and early Neolithic TRB vessels in Denmark and the Baltic coastal area of Germany found that EN vessels from coastal sites had been heavily used for marine animals while evidence of freshwater resources was found at inland sites. However, a third of the TRB vessels, including samples from the coastal sites, also had evidence of dairy

fats indicating the keeping of animals for milking. It seems then that there was not a complete switch to domesticated resources with the local beginning of farming and that, whoever the farmers were, they initially combined both marine and domestic animal resources. Analyses of TRB EN ceramic residues from the site of Skogsmossen in eastern middle Sweden (Isaksson & Hallgren, 2012) produced similar results to those of Craig et al. (2011), including evidence of both dairy fats and marine resources.

Isotopic analyses of human bones from the island of Oland in the Baltic show a contrast between the MN TRB site of Resmo, ca. 5,400-4,800 cal. BP, which has the pattern described above showing a mixture of marine and terrestrial resources, and the contemporary Pitted Ware Culture (PWC) site of Kopingvik, which shows a heavy reliance on marine mammals with a possible addition of marine fish, as in the Mesolithic phase at the site (Eriksson et al., 2008). This pattern is confirmed by results from the eastern Swedish coastal PWC site of Korsnas, dating to ca. 5,300-4,800 cal. BP, where the proportion of terrestrial protein in the diet was negligible and virtually all individuals analyzed had diets indicating seal consumption, with the outlier pointing to a diet of fish as well as seal (Fornander et al., 2008). The faunal assemblages from Pitted Ware sites on the island of Gotland (Ref. 56, table 15.1, p. 291) support this picture. Domestic animals are either completely or virtually absent, there are numbers of wild boar, and very large numbers of seals and fish. Further north, recent lipid analyses of ceramic residues from the Combed Ware site of Vantaa Stenkulla/Maarinkunnas in southern Finland ca. 5,900-5,300 cal. BP, thus contemporary with the TRB further south, show that they derive from resources of marine origin, in keeping with the archaeological remains from the site (Cramp et al., 2014).

The long-standing suggestion that the southward spread of the Pitted Ware to Denmark represents a re-expansion of hunter-gatherer populations from the north has been confirmed by a genomic analysis of ancient DNA samples from Pitted Ware skeletons from Gotland (Skoglund et al., 2008; Skoglund et al., 2012). This showed continuity from a late Mesolithic to the PWC samples, and that all belonged to a group of Mesolithic populations that was very widely distributed across Europe. At the same time the difference between the PWC samples and that from a TRB farmer burial in central southern Sweden was greater than that between the two present-day European populations that are most different from one another, Finns and Italians.

Finally, the Single Grave/Battle Axe/Corded Ware culture (all different regional names for essentially the same set of material culture) appears in southern Scandinavia and the Baltic area from ca. 4,800 cal. BP and succeeds the TRB, running alongside the later part

of the PWC. Like the TRB this is an agricultural culture, though with probably more emphasis than the latter on domestic animal exploitation. Like the latter, it may represent at least in part an expansion of new populations into southern Scandinavia (Haak et al., 2015). Recent stable isotope and lipid work on ceramic residues from Corded Ware sites in southern Finland (Cramp et al., 2014) dated c. 4,500 cal. BP has produced patterns corresponding to terrestrial ruminants at 60° degrees north even though the sites were close to the coast, and half of the patterns correspond to dairy fats indicative of milking, although a single vessel had evidence of marine product processing. In contrast, the subsequent Kiukainen culture, with pottery similar to both Corded Ware and local Late Comb Ware, had residues indicative of processing both marine and terrestrial ruminant products in the same vessels, thus a shift to use of both domestic and marine resources, after 4,500 cal. BP.

Photo by Dietmar Rüß

CHAPTER 3

Determining the predominant cause of anoxia in the Baltic Sea over the Holocene

By Lisa Warden, Martina Sollai, Ellen C. Hopmans, Nicole Bale, Anchelique Mets, Matthias Moros, Francien Peterse, Klaas G.J. Nierop, Vincent Kofman, Caroline P. Slomp, and Jaap S. Sinninghe Damsté

To be submitted to Nature Geoscience

The Baltic Sea is currently one of the most polluted seas in the world and the biggest disturbance is eutrophication, which causes anoxia and affects food chain dynamics, marine habitats and fisheries (Karlson et al., 2002). However, research indicates anoxia has been a natural feature of the Baltic Sea over the Holocene (Andren et al., 2000b) although such events and their possible triggers are poorly understood. Here we examine high-resolution records from two separate sites in the central Baltic Sea revealing that increased summer sea surface temperatures (SST), obtained using a local SST calibration developed for this study and based on the TEX_{86}^{L}-index, co-occur with laminations and increased organic carbon content indicating anoxic conditions in the basin. These results demonstrate that starting with the onset of brackish conditions in the Baltic Sea (~7,300 BP) anoxic events are initiated by higher summer SSTs and a threshold exists at ca. 16°C where above that anoxia persists. We also show that cyanobacterial abundance and N_2-fixation increases as anoxia intensifies in the Baltic Sea with the start of the Holocene climatic optimum. These geochemical records show a clear relationship between summer SSTs and anoxia over the Holocene, indicating that it is a natural feature of the Baltic Sea but it could be exasperated by global climate change, further threatening the ecological state of the Baltic Sea.

The Baltic Sea is the largest brackish body of water in the world with a drainage area that is four times larger than the basin itself and with a human population of 85 million (Karlson et al., 2002). The basin is mostly surrounded by land with limited water exchange through a narrow and shallow connection to the North Sea via the Danish Straits (Döös et al., 2004). Through the restricted connection to the North Sea, an inflow of denser, saline bottom waters creates a lateral salinity gradient in the Baltic Sea with a decreasing salinity trend towards the north where there is large freshwater input from rivers. The inflow of freshwater from the north and the limited influx of saline water from the south creates a halocline that keeps the Baltic Sea permanently stratified and prevents vertical mixing and oxygenation of the bottom waters (Matthäus & Schinke, 1999). Major inflows of marine water from the North Sea occur on a decadal timescale and are the main process that ventilates the oxygen depleted bottom waters (Reissmann et al., 2009). Overall, the physical setting of the present-day Baltic Sea with its restricted water exchange, relatively high river runoff, long water residence time, and strong density stratification is conducive to low-oxygen bottom water conditions in the basin. In conjunction with this there has been an increase in anthropogenic eutrophication in

the past few decades that has led to an intensification in primary production, including enhanced cyanobacterial blooms, which are now a characteristic feature of the Baltic Sea in the summer months and further contribute to the depletion of oxygen in the bottom waters (Wulff et al., 2007).

Many hydrological, geological and climactic changes characterize the environment of the Baltic Sea since the last phase of the deglaciation (~13-9 ka BP in Scandinavia; Björck, 1995) and various phases can be recognized (Björck, 1995; Jensen, 1995; Andren et al., 2000b). As a consequence of glacial retreat and melting along with isostatic rebound the Ancylus Lake formed, ~9.5-8.0 ka BP, and was the last extended freshwater stage (Jensen et al., 1999). The Ancylus Lake/Littorina Sea transition, ~7.8-7.3 ka BP, occurred when eustatic sea-level rise opened up a connection through the Danish Straits allowing salt water to flow into the southern part of the basin in pulses until gradually brackish conditions were established (Andren et al., 2000b). The Littorina Sea phase, ~7.2-3.5 ka BP, is characterized by a warmer climate and the most marine-like conditions in the basin during the Holocene (Andrén & Sohlenius, 1995). The modern Baltic Sea basin is a continuation of the Littorina Sea, except with a salinity almost half that of the Littorina Sea (Punning et al., 1988). During this time period the region has experienced several climatic extremes including the Medieval Warm Period (MWP), ~ 1250-900 AD, the Little Ice Age (LIA), ~1850-1250 AD, and the Modern Warm Period (MoWP), since ~1850 AD (Leipe et al., 2008).

With this study we examine the fluctuations in summer SST that occurred in the Baltic Sea over the Holocene and determine how this relates to the development of anoxia. To this end we used three sediment cores from the central Baltic Sea in the Gotland Basin (Fig. 1). The dating of the multi core (MUC) P435-1-4 and the brackish section of the gravity core (GC) 303600-N is based on a depth age model obtained by high resolution ^{14}C dating of benthic foraminifera (Warden et al., in review). The age model for the MUC LL19 record is based on the correlation of organic carbon profiles with a multi-core dated using ^{210}Pb (Funkey et al., 2014) and aligned with the GC 303600-N record using loss on ignition (LOI) profiles from both cores. Distinct lamination of the sediments, elevated TOC content and Mo/Al ratio (Funkey et al., 2014) all indicate anoxic conditions in the bottom waters occur during the MoWP, the MWP and the Litorina Sea Phase (Fig. 2). Contrastingly, sediments that accumulated during the Ancylus Lake period, during the post-Littorina Sea phase before the MWP, and throughout the LIA are homogeneous and have low TOC content and Mo/Al ratio (Fig. 2) designating periods of oxygenated bottom waters.

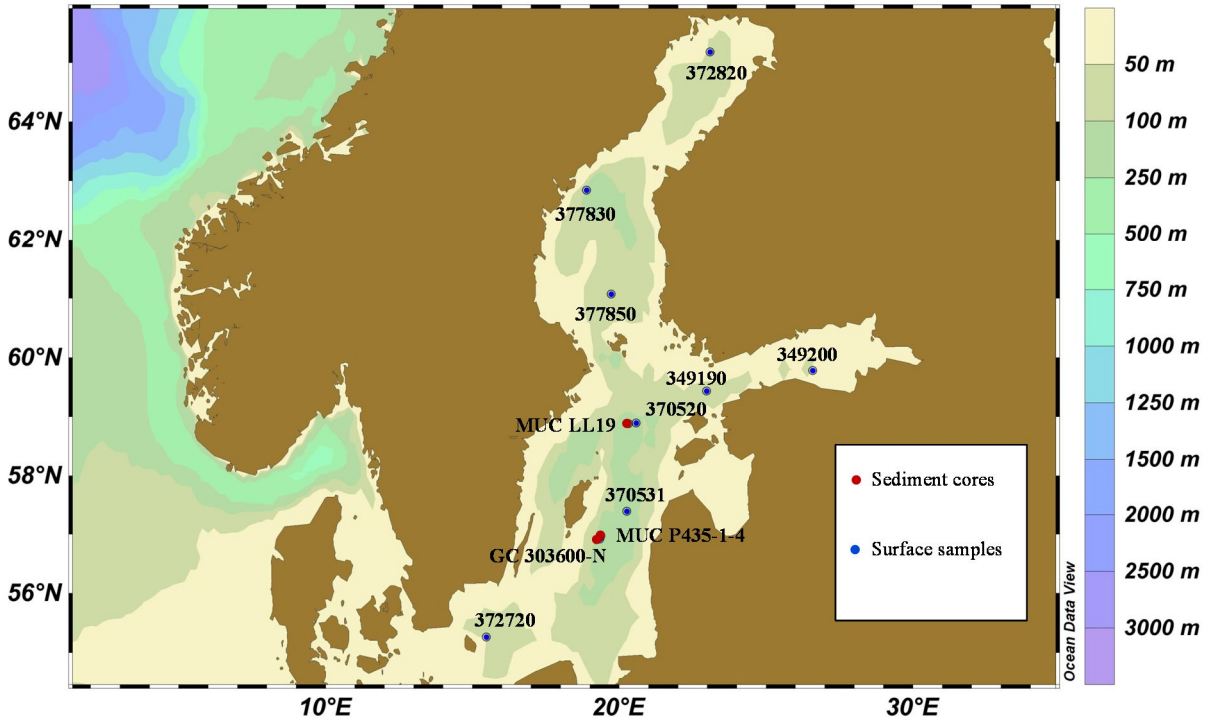

Fig. 1 Map of the Baltic Sea showing the location of the three sediment cores (indicated by red circles) from the Gotland Basin and the nine surface sediments samples (indicated by blue circles) used in this study.

To investigate if summer SST played a role in the development of anoxic conditions throughout the Holocene, we reconstructed temperatures using the TEX_{86}^{L}-paleothermometer and compared the reconstructions with laminations in the cores, TOC content and the Mo/Al ratio. The TEX_{86}^{L} proxy is based on the distribution of archaeal Thaumarchaeotal membrane lipids, i.e. isoprenoid glycerol diakyl glycerol tetraethers (Schouten et al., 2002). In order to increase the accuracy of the SST reconstructions we applied a local calibration that was developed for this study by comparing TEX_{86} data for nine surface sediment samples with instrumental SST data derived from satellites (Kabel et a., 2012). The best correlation was obtained using TEX_{86}^{L} with July SST. The TEX_{86}^{L} derived SST records show warmer SSTs by ~2°C during the Littorina Sea Phase, MWP and MoWP (Fig. 2). The increase of SST from the Ancylus Lake to the Littorina Sea phase, and also moving into the MWP and the MoWP is evident from both TEX_{86}^{L} records from the different locations in the Gotland Basin as is the decrease in SST during the LIA (Fig. 2). Comparing the SST reconstructions with the indicators for anoxia, the strong correlation is apparent (Fig. 2). Higher SSTs co-occur with laminations, increased TOC content and Mo/Al ratio all indicating anoxic conditions, whereas lower temperatures correlate with homogeneous sediments and lower TOC content and Mo/Al

ratio, signifying oxic periods. This suggests that the prevalence of anoxia in the Baltic Sea throughout the Holocene was linked to warmer summer SSTs. Additionally, throughout the Holocene a threshold appeared to have existed of ca. 16°C where above that anoxic conditions persisted in the Baltic Sea.

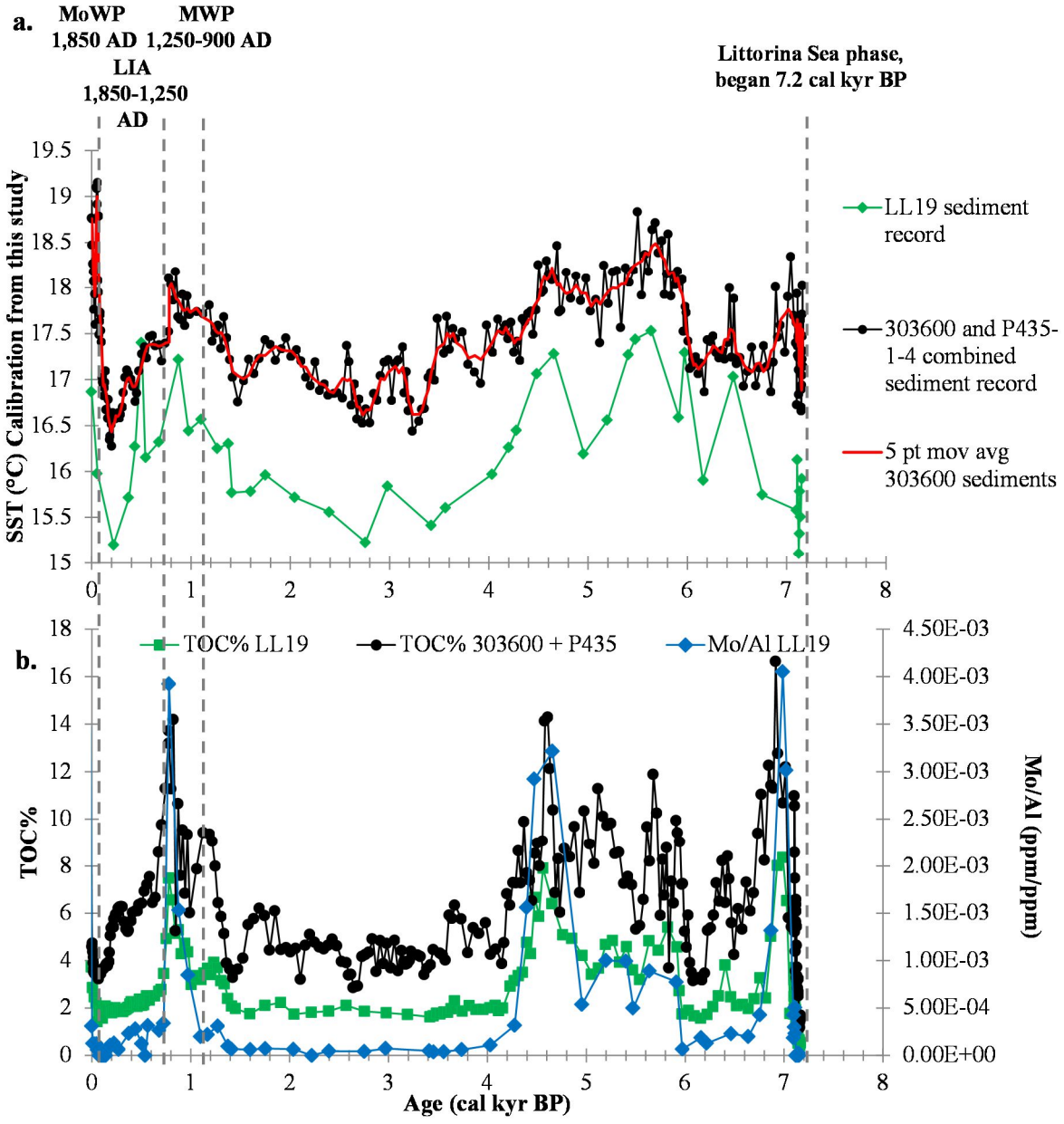

Fig. 2 (a) Reconstructed SSTs (°C) for the Gotland Basin over the last 7.2 cal kyr BP. The record from sediment core LL19 is shown in green, from 303600 is in black, and the five point moving average for the record from sediment core 303600 is in red. (b) TOC (%) and Mo/Al (ppm/ppm) for the Gotland Basin record over the last 7.2 cal kyr BP. The TOC record from sediment core LL19 is shown in green, the TOC record for sediment core 303600 is shown in black, and the Mo/Al record for sediment core LL19 is shown in blue.

Summer SST has been postulated as one of the main environmental controls on blooms of nitrogen-fixing cyanobacteria (Wasmund, 1997; Kabel et a., 2012; Funkey et al., 2014). In the present-day Baltic cyanobacterial blooms cause additional primary productivity and this aids in the development of anoxia in the bottom waters as the biomass degrades (Wasmund, 1997). A recent study proposed that over the past 1,000 years anoxia in the Baltic Sea was caused by the spread of cyanobacterial blooms, which are more likely to occur when SSTs are above ~16°C (Kabel et al., 2012). All bloom-forming cyanobacteria in the Baltic Sea have the ability to form heterocysts (Laamanen & Kuosa, 2005), differentiated cells that are sites for fixation of atmospheric dinitrogen (N_2) into ammonium (NH_4^+) (Walsby, 1985). Heterocyst Glycolipids (HGs) are specifically produced to surround the heterocyst cell to avoid oxygen diffusion into this compartment where N_2-fixation occurs and the O_2-sensitive enzymes involved are located (Walsby, 1985). Because these lipids are only produced by heterocystous N_2-fixing cyanobacteria they are specific biomarkers for the presence of nitrogen-fixing, heterocystous cyanobacteria (Bauersachs et al., 2010). An additional marker for increased N_2-fixation is the $\delta^{15}N$ record (Haug et al., 1998), because nitrogen-fixing cyanobacteria fix atmospheric nitrogen without significant fractionation resulting in ^{15}N-enriched OM (Cline & Kaplan, 1975). To determine if SSTs were the predominant cause of cyanobacterial bloom-induced anoxia during the Holocene, we compared the HG profile along with $\delta^{15}N$ record to the proxies for anoxia and reconstructed summer SSTs (Fig. 3). Both $\delta^{15}N$ record from the Gotland Basin decrease from ~4‰ to ~2‰ at the Ancylus Lake/Littorina Sea transition, indicating increased N_2-fixation in the Baltic Sea when marine inflows first began along with the initial increase in summer SSTs and the onset of anoxic events (Fig. 2 & 3). Starting at the Ancylus Lake/Littorina Sea transition the more depleted $\delta^{15}N$ values co-occur with a higher abundance of HGs revealing that N_2-fixation and cyanobacterial abundance increased at this time (Fig. 3). After the initial decrease in the $\delta^{15}N$ record, there is not much variation and no clear correlation with SST or TOC content. Although there is some variation in the HG profile, it does not directly correlate with SST or TOC content after the initial increase. Subsequently, both records indicate N_2-fixation and cyanobacterial abundance increased at the Ancylus Lake/Littorina Sea transition with the onset of warmer summer SSTs and anoxic events indicating that cyanobacterial blooms contributed to the spread of anoxia in the basin. However, the $\delta^{15}N$ and the HG profiles do not support the idea that past anoxic events were caused solely by cyanobacterial blooms that were induced by increased SSTs. Therefore, we must consider that other factors besides SST-induced cyanobacterial blooms are responsible for the development of anoxia.

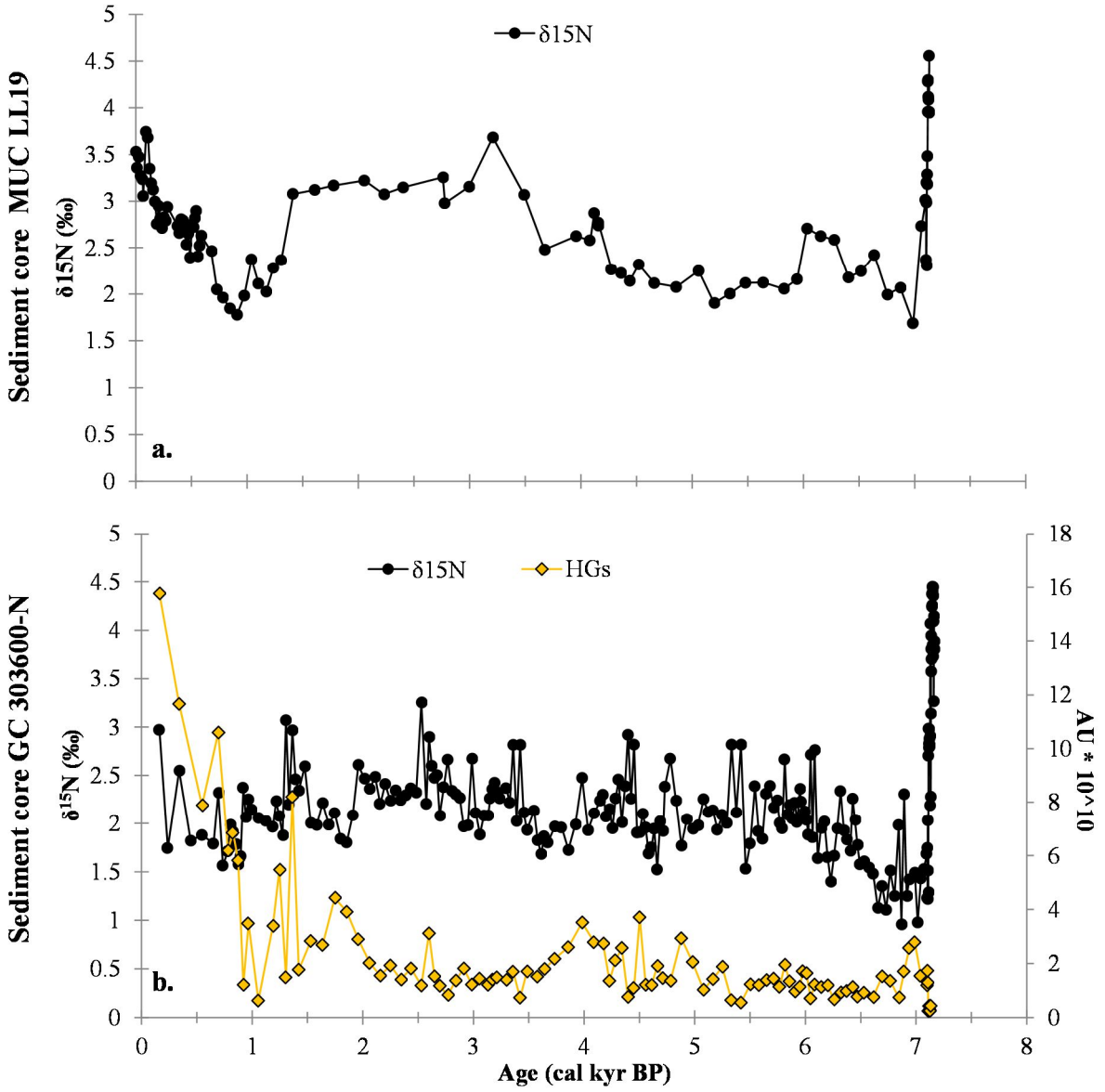

Fig. 3 The $\delta^{15}N$ (‰) record for two of sediment cores in the Gotland Basin, 303600-N (a) and LL19 (b), along with the HG profile for sediment record 303600-N (shown in gold).

Our results clearly show that the spread of anoxia in the Baltic Sea is controlled by summer SST and a threshold exists at around 16°C where above anoxic conditions occur. Since the 16°C threshold for the development of anoxia in the Baltic Sea over the Holocene does not appear to be directly due to enhanced cyanobacterial abundance, this leads us to question what other factors besides temperature are affecting N_2-fixation in the Baltic Sea. Hordoir & Meier (2012) demonstrated through a modeling experiment that stratification changes are predominantly controlled by SST in the Baltic Sea and that a warming of 2-3°C would intensify stratification in the water column in the springtime (Hordoir & Meier, 2012),

preventing ventilation except for when the occasional inflows of oxygenated waters from the North Sea arrive. Perhaps the anoxic conditions observed in the basin during the Littorina Sea phase, the MWP and the MoWP occurred because of the enhancement of stratification caused by the ~2°C increase in summer SSTs at those times. During cooler periods, as occurred after the Littorina Sea phase and during the LIA, stratification lessened allowing more frequent vertical mixing of the water column and, therefore, the oxygenation of the bottom waters.

Other interrelated aspects of climate should be considered as well. River runoff through thermal convection is usually responsible for lessening thermal stratification that occurs in the spring and summer. However, a warmer, drier climate such as is thought to have occurred during the Littorina Sea phase (Digerfeldt, 1988) would result in decreased river runoff allowing increased thermal stratification of the water column (Hordoir & Meier, 2012). A persistent positive North Atlantic Oscillation (NAO), like that which occurred during the MWP (Trouet et al., 2009), would indicate the climate was warmer as well as more humid. Increased precipitation could have led to increased river runoff, which has been shown to cause a decrease of inflows from the North Sea and consequentially a reduction in the ventilation of bottom waters (Matthäus & Schinke, 1999; Gustafsson, 2000). During the LIA the NAO had shifted to a more persistent negative phase (Trouet et al., 2009) leading to cooler SSTs and an increase in storm frequency (Hurrell, 1995), which could have disrupted the stratification in the water column and led to ventilation of the bottom waters and the oxic conditions.

This study demonstrates that in the Baltic Sea anoxia was controlled primarily by climate during the Holocene. Warmer summer SSTs correlate with periods of anoxic conditions and colder summer SSTs co-occur with more frequent oxygenated periods in the basin. Although the proxies for N_2-fixing cyanobacteria suggest that these blooms contributed to past anoxic events, the fossil molecular evidence suggests that there is no direct link between the occurrence of cyanobacterial blooms and the development of anoxia. We theorize that climate induced stratification could be responsible for the anoxic events that occurred throughout the Holocene after the basin became brackish. Since climate has the biggest effect on the spread of anoxia in the Baltic Sea, there could be consequences in regards to the ecological state of the basin considering projections of future climate warming over the region (HELCOM, 2010). Taking into account the large anthropogenic pressure already on the Baltic environment (HELCOM, 2010), local measures presently being taken to improve the condition of the basin may not be adequate as summer SSTs rise and anoxia intensifies.

– SUPPLEMENTARY INFORMATION –

Part A: Study Site

The Baltic Sea is the largest brackish body of water on Earth with an area of 413.10^3 km^2 and a drainage area that is four times larger than the basin itself with a human population of 85 million. Despite its large area the Baltic Sea is a shallow sea with an average depth of 52 m. The basin is mostly surrounded by land with only a narrow and shallow connection to the North Sea via the Danish straits that restricts water exchange. Through the restricted connection to the North Sea, denser saline bottom waters flow in creating a lateral salinity gradient in the Baltic Sea with a decreasing salinity trend towards the north where there is large freshwater input from rivers. There is also a salinity gradient within the water column as surface salinity in the Baltic Proper is 7-8 PSU, but beneath the halocline, located at 60-80 m depth, the salinity is 11-13 PSU (Samuelsson, 1996). Due to the halocline the Baltic Proper (from the Aland Sea to the Danish sounds) is permanently stratified which prevents vertical mixing of the water columns and oxygenation of the bottom waters (Matthäus and Schinke, 1999). Overall the physical setting of the Baltic Sea with its restricted water exchange, relatively high river runoff, long water residence time, and strong density stratification is conducive to low-oxygen bottom water conditions in the basin. Winter SSTs in the Baltic are between -1 and 2 °C and summer SSTs between 15-17 °C (http://helcom.fi/baltic-sea-trends/environment-fact-sheets/hydrography/development-of-sea-surface-temperature-in-the-baltic-sea).

Part B: Supplementary methods

B1. Materials, site selection, dating and analytical methods

Sampling. All three cores used in this study were recovered from the Gotland Basin in the central Baltic Sea, which is subdivided into several sub-basins (Fig. 1). Two of the cores, Gravity core (GC) 303600-N and multi core (MUC) P435-1-4, were collected from the Eastern Gotland Basin. GC 303600-N (0-377 cm length) was collected in July 2007 during R/V "Prof. Albrecht Penck" east of Gotland Island, at the site 56 ˚55.02 N and 19 ˚19.98 E and at 170 m water depth (wd). At a very near location (56°57.94 N, 19°22.21 E, 178 m water depth) in June 2012 during the R/V "Poseidon" cruise, MUC P435-1-4 (0 to 51.5 cm length) was also recovered. A third sediment core used in this study, the multi-core (MUC) LL19,

was recovered from the Northern Gotland Basin (58.8807°N, 20.3108°E, 169 m water depth) during a cruise with R/V Aranda in May/June 2009.

Sample preparation. GC 303600-N was cut into two halves before sampling to allow for photographic documentation and more precise sampling. Half of GC 303600-N arrived at the NIOZ in 2012 and was sub-sampled at high resolution from 0 to 377 cm length. The core was cut into 1 cm-thick slices between 0 and 241 cm depth and then into 2 cm-thick slices for the remainder of the core, from 241-377 cm. During the process depths 81-82 and 187-189 were missed. The samples were then freeze-dried and ground and homogenized with mortar and pestle for further analysis. MUC P435-1-4 was sub-sampled at 0.5 cm resolution and after being freeze-dried and grounded samples were sent to the NIOZ for further analysis. MUC LL19 was sliced at 0.5-2 cm resolution in a nitrogen- or argon-filled glovebox. Sediment samples were then freeze-dried before being returned to the glovebox to be ground in an agate mortar.

Dating. The depth age model for cores GC 303600-N and MUC P435-1-4 were obtained by high resolution ^{14}C dating of benthic foraminifera. The shallow (0-42.75 cm) sediment core MUC P435-1-4 covers from -0.06 to 0.64 cal kyr BP and sediment GC 303600-N (0-377 cm) spans 0.2 to 10.6 cal kyr BP. A detailed age model based on correlation with sediment cores from slightly deeper sediment cores that have been dated using radiocarbon dates of benthic foraminifera exists for the upper 210 cm of MUC P435-1-4 (Warden et al., in review). Sediment cores MUC P435-1-4 and GC 303600-N were correlated to each other using TOC (wt. %) profiles, LOI (%) and XRF data (Warden et al., in preparation). An age model for MUC LL19 was previously published (Funkey et al., 2014). The age model for this core was updated by correlation of organic carbon profiles with a multi-core dated using ^{210}Pb and correlated with cores GC 303600-N and MUC P435-1-4 for this study using LOI data.

Determination of the TOC content. For GC 303600-N, freeze dried and ground sediment was used for analysis to determine total organic carbon (TOC) content and stable isotopes analysis. About 2 mg of sediment per sample were de-carbonated by shaking for ~8 h in 2N HCl. Afterwards sediments were again freeze-dried and ground. The TOC along with the bulk stable nitrogen isotopes ($\delta^{15}N$) were analyzed in duplicate on a Thermo Finnigan Delta Plus isotope ratio mass spectrometer (irmMS) connected to a Flash 2000 elemental analyzer (Thermo Fisher Scientific, Milan, Italy). The $\delta^{13}C_{TOC}$ is expressed in relation to the

Vienna PeeDee Belemnite (VPDB) standard, whereas the $\delta^{15}N$ of each sample is relative to atmospheric dinitrogen. The isotope analysis precision was 0.1‰ for carbon and 0.2% for nitrogen measurements.

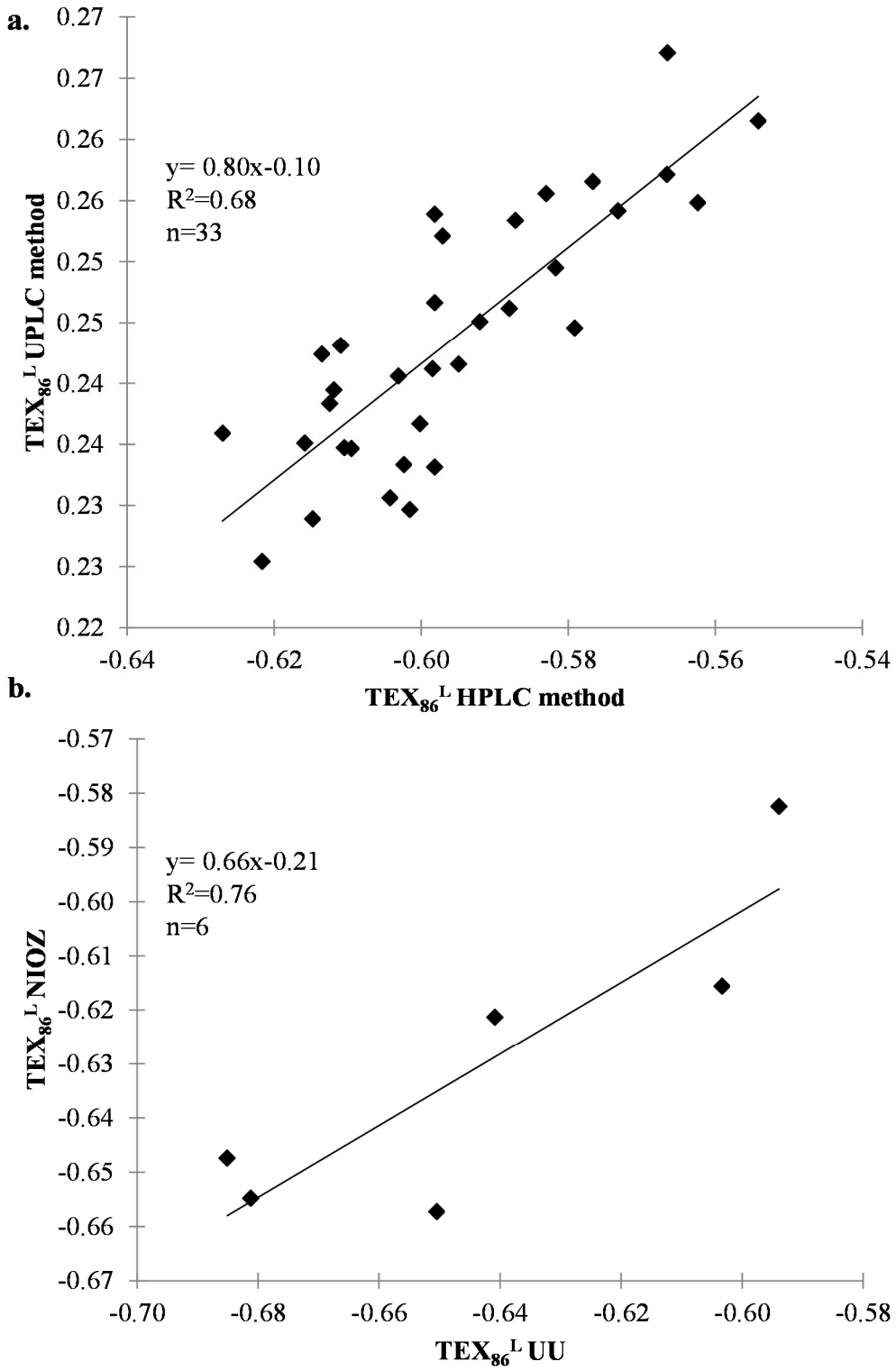

Fig. S1 (a) Correlation between TEX_{86}^{L} values for sediment samples from 303600 run on the HPLC method and the UPLC method (R^2=0.68, n=33). (b) Correlation between TEX_{86}^{L} values for sediment samples from LL19 analyzed at UU and the NIOZ (R^2=0.76, n=6).

The total carbon (TC) content of the MUC P435-1-4 sediments was determined using loss on ignition (LOI) analysis with an EA 1110CHN analyzer from CE Instruments, whereas a Multi EA- 2000 Elemental Analyzer (Analytic, Jena, DE) was used to determine the total inorganic carbon (TIC). The TOC content was ultimately calculated as the difference between TC and TIC (Kabel et al., 2012). The methods for TOC analysis for MUC LL19 were previously published (Funkey et al., 2014).

GDGT analysis. For GC 303600-N analysis was performed at 1 cm resolution and MUC P435-1-4 was analyzed at 0.5 cm resolution. Lipid analysis for both cores was performed at the NIOZ. Approximately 0.5-3 g of sediment per sample was extracted using an Automated Solvent Extractor (ASE 200, DIONEX; 100°C and 7.6*106 Pa) with a mixture of dichloromethane (DCM): methanol (MeOH) (9:1, v:v), to obtain a total lipid extract (TLE), which was dried under a gentle stream of N_2 air. After the TLE was dried over a $NaSO_4$ column it was split into three fractions over an activated Al_2O_3 column. The apolar fraction was obtained using Hexane (Hex):DCM (9:1; v:v) solvent, the ketone fraction with Hex:DCM (1:1; v:v) solvent, and the polar fraction by the solvent DCM:MeOH (1:1; v:v). The polar fraction was subsequently evaporated under a continuous flow of N_2 before being dissolved in in hexane:isopropoanol (99:1; v:v) solution via sonication at about 2 mg mL^{-1} concentration and then filtered through an Alltech 0.45 µm polytetrafluoroethylene filter before injection.

Even though GDGT analyses for GC-303600-N and MUC P435-1-4 were performed at the NIOZ, the analysis was done on different instruments and using different methods. Samples from GC 303600-N were analyzed using a high performance liquid chromatography-at-atmospheric pressure positive ion chemical ionization-mass spectrometry (HPLC-APCl-MS) with an Agilent 1100 series LC-MSD SL. The GDGTs were separated according to conditions described by (Schouten et al., 2007) on an Alltech Prevail Cyano column (150 mm x 2.1 mm; 3 µm). The polar fractions of the extracts of the sediments of core MUC P435-1-4 were analyzed with an Agilent 1290 Infinity ultra-high performance liquid chromatography (UHPLC) coupled to an Agilent 6130 single quadrupole mass detector using a two silica column according to Hopmans et al. (2015). The improved separation power of this method leads to small but significant changes in TEX_{86} values (Hopmans et al., 2015). In order to deal with this we analyzed 33 samples from core GC-303600-N with the new UPLC method as well. The correlation between the TEX_{86}^{L} values obtained with the UPLC method and those the older (HPLC) method was used to convert the TEX_{86}^{L} (HPLC) values into TEX_{86}^{L} (UHPLC) index values (Fig. S1):

$$TEX_{86}^{L}\ (UHPLC) = 0.80 * TEX_{86}^{L}\ (HPLC) - 0.10\ \ (R^2=0.68, n=33) \qquad (1)$$

Core MUC LL19 was analyzed at Utrecht University using an Agilent 1290 Infinity ultra-high performance liquid chromatography (UHPLC) coupled to an Agilent 6130 single quadrupole mass detector with the new UPLC method according to Hopmans et al. (2015). Even though MUC LL19 was analyzed on the same type of machine using the same method, a slight offset in TEX_{86} was observed. To deal with this offset six samples from MUC LL19 were also analyzed at the NIOZ with the UHPLC method. The equation resulting from the correlation of TEX_{86}^{L} values measured at Utrecht and NIOZ was used to deal with the offset in TEX_{86}^{L} values:

$$TEX_{86}^{L}\ (NIOZ)\ =0.66*TEX_{86}^{L}\ (UU)-0.21\ (R^2=0.76, n=6) \qquad (2)$$

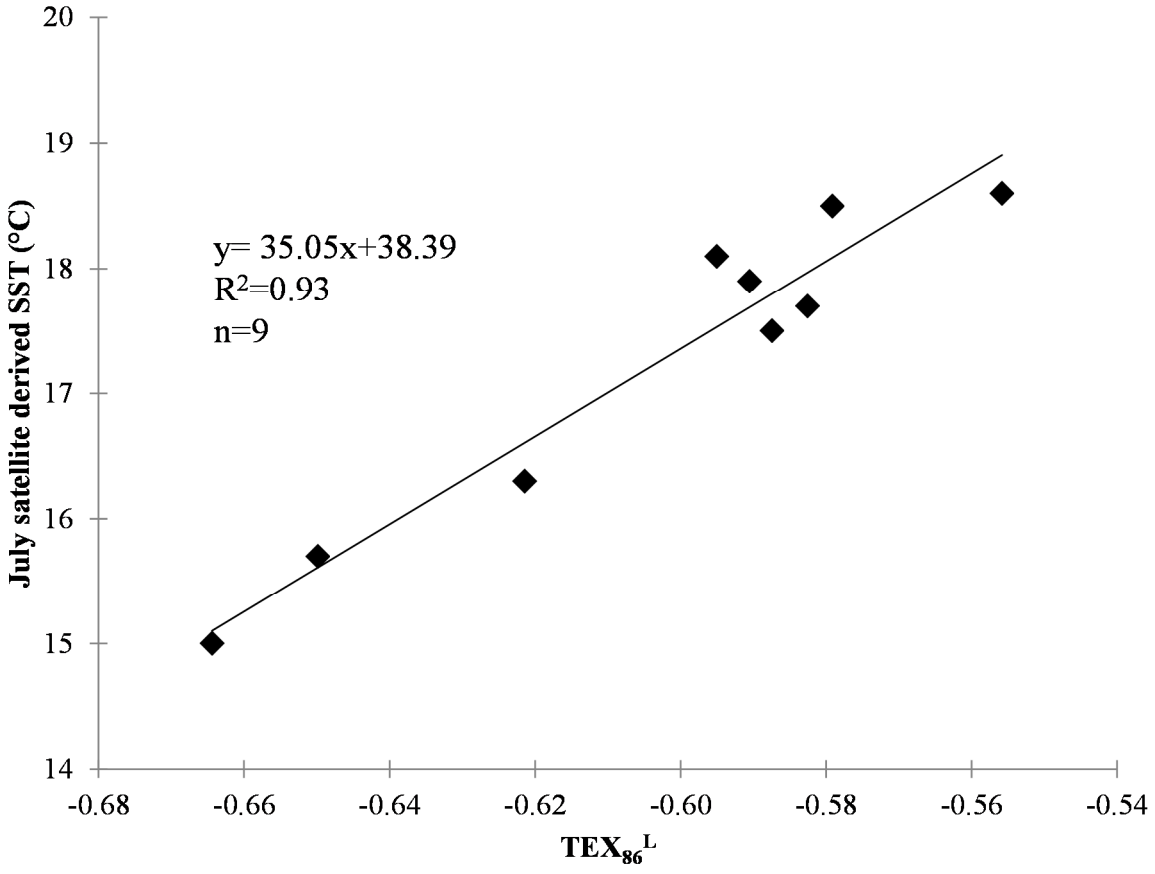

Fig. S2 Correlation of TEX_{86}^{L} values with previously published (Kabel et al. 2012) July satellite derived SSTs for nine surface sediment samples around the Baltic Sea basin (R^2=0.93).

Development of a new local SST calibration. The TEX_{86}-index reflects temperature – induced changes in the distribution of archaeal *Thaumarchaeota* membrane lipids (Schouten

et al., 2002) and the correlation of this index with SST has been demonstrated for global (Kim et al., 2010) as well as local data sets such as the Baltic (Kabel et al., 2012). For this study a local TEX_{86}-SST Baltic Sea calibration was developed based on nine surface sediment samples from around the Baltic Sea, which were analyzed using the new UPLC method (Hopmans et al., 2015). Isoprenoid GDGT distributions were compared to previously published satellite derived SSTs (Kabel et al., 2012). The highest correlation was found between SST of the month July and TEX_{86}^{L} making the following a summer SST calibration:

$$SST_{july} = 35.05 \times TEX_{86}^{L} + 38.39 \ (R^2=0.93, n=9) \quad (3)$$

Heterocyst glycolipids (HGs) analysis. After extraction the sediment samples were analyzed for HG content respectively at 2 cm resolution between 1-2 cm to 239-241 cm depth and at 4 cm resolution from this depth to the end of the core for the gravity core 303600, whereas for MUC P435-1-4 the resolution of analysis was 0.5 cm. Briefly, the total extract collected was sonicated for 10 min in DCM/MeOH (1:1, v:v). We prepared aliquots and dissolved them in hexane, isopropanol and water (72:27:1, v:v:v) to be filtered through a 0.45 μm regenerated cellulose syringe filter (4 mm diameter; Grace Alltech). Consequently, we analyzed the sediments by using a HPLC-MS2 system in the multi reaction monitoring (MRM) mode as modified by Bale et al. (2015), based on Bauersachs et al. (2010). For the analysis we employed an Agilent (Palo-Alto, CA, US) 1100 series LC equipped with a thermostat-controlled auto-injector, coupled to a Thermo TSQ Quantum EM triple quadrupole MS equipped with an Ion Max source with ESI probe. The MRM method here applied specifically targets C5 and C6 HGs (Bale et al., 2015). HGs were quantified as the integrated IPL area peak response per g of TOC (r.u. TOCg-1) as a result of the lack of a suitable standard.

Photo by Dietmar Rüß

CHAPTER 4

Evaluation of the distributions of hydroxylated isoprenoidal GDGTs in the Baltic Sea for reconstruction of sea surface temperature

Lisa Warden, Matthias Moros, Carlo Berg, Klaus Jürgens
and Jaap S. Sinninghe Damsté

To be submitted to Marine Chemistry

Abstract

Hydroxylated glycerol dialkyl glyceral tetraethers (OH-GDGTs) occur throughout the modern day Baltic Sea and have also been prevalent in the past. Known SST calibrations based on OH-GDGTs were applied to an thaumarchaeote culture enriched from the Baltic grown at known temperatures (4 and 22°C) and to surface sediments from around the Baltic Sea for which sea surface temperature data was available. The OH-GDGT $_{\text{Index 5}}$, the OH-TEX_{86} index, and the novel OH-GDGT' index (which was developed in this study) have the highest correlation with the measured temperatures when applied to both surface sediments and cultures. Calibrations based on these indices were then applied to sedimentary records in both the Arkona (12.5-0.1 cal kyr BP) and Gotland (10.6- -0.06 cal kyr BP) basins. The resultant reconstructed SSTs in the Gotland Basin captured the major SST fluctuations over the Holocene and gave reasonable SST estimates for the recent brackish phase (7.2- -0.06 cal kyr BP). The three reconstructions derived from different calibrations and indices were in good agreement with each other as well as previously published proxy based temperature data. In the Arkona Basin the reconstructed SSTs derived from calibrations based on the OH-GDGT $_{\text{Index 5}}$ and the OH-GDGT' index are in good agreement during the recent brackish phase (7.2-0.1 cal kyr BP), however, SSTs derived from the OH-TEX_{86} index in the Arkona Basin appear unreliable. Perhaps this is due to the proximity to the North Sea and an increased input of allochthonous OH-GDGTs. The calibrations based on the OH-GDGT' index resulted in unrealistically high SSTs during the lower salinity phases in both basins. Since this effect was not apparent with the OH-$GDGT_{\text{Index 5}}$ and the OH-TEX_{86} index, which both also incorporate isoprenoid GDGTs, this suggests that lower salinities may complicate the use of indices based solely on the OH-GDGT distributions for SST reconstructions, an issue that perhaps a freshwater calibration could assuage.

1. Introduction

Thaumarchaeota are nitrifying Archaea that occur ubiquitously in aquatic environments and soils. They are estimated to make up 20% of the picoplankton in the world's oceans (Fuhrman, 1992; Karner et al., 2001). Thaumarchaeota use isoprenoidal glycerol dialkyl glycerol tetraethers (isoGDGTs) as their membrane-spanning lipids. These lipids can contain a varying number of cyclopentane moieties. In addition, they contain crenarchaeol, a unique GDGT with one cyclohexane and four cyclopentane moieties (Sinninghe Damsté et al., 2002). Archaea adjust the number of cyclopentane moieties depending on growth temperature (De Rosa and Gambacorta, 1988). The increase in the production of cyclopentane rings with higher temperatures is thought to be a mechanism of temperature adaptation within the cell membrane, for example to maintain membrane permeability and fluidity at various temperatures (Gabriel and Chong, 2000; Gliozzi et al., 1983). Because of this physical adaptation, the distribution of Thaumarchaeotal isoGDGTs in marine and lacustrine sediments can be used to estimate past water temperature (Powers et al., 2004). Schouten et al. (2002) developed the TEX_{86}-index to be used as a SST proxy based on the relative abundance of isoGDGTs. This linear relationship between the number of cyclopentane moieties and SST is weaker in cooler waters, below 15°C, and a modified index termed TEX_{86}^{L} was developed to reconstruct SSTs for lower temperature ranges (Kim et al., 2010).

Recently, Liu et al. (2012a) identified a new type of GDGT, i.e. hydroxylated GDGTs (OH-GDGTs), in marine sediments from both tropical and temperate regions. These GDGTs contain 0-2 cyclopentane moieties with the hydroxyl group positions at a tertiary carbon atom of one of the biphytanyl chains that are closest to the glycerol moiety of the GDGT (Fig. S1). Liu et al. (2012a) postulated that their relative abundance and distribution could potentially be used as a proxy for SST. This premise was supported through the exploration of marine subsurface sediments that revealed their abundance in the marine environment may potentially be used as taxonomic biomarkers and geobiological proxies (Liu et al., 2012b). Huguet et al. (2013) showed that these OH-GDGTs can be found in lacustrine as well as marine sediments and that the abundance of OH-GDGTs relative to non-hydroxylated GDGTs increases with increasing latitude and lower SST. This study suggested that, because of the significant correlation between the relative abundance of OH-GDGTs and SST in surface sediments, these compounds have potential as a new paleotemperature proxy. Fietz et al. (2013) recently proposed two new indices based on OH-GDGTs, i.e. the so-called OH-GDGT-0/crenarchaeol ratio and OH-GDGT index, which were used to reconstruct SSTs in Nordic Seas. This same study also suggested that both the abundance of OH-GDGTs relative to non-hydroxylated

GDGTs (OH-GDGT%) and OH-GDGT index can be used as indicators of coastal ice-covered and less saline polar waters. These novel indices were also applied as paleotemperature proxies in the Arctic Ocean (Knies et al., 2014) and the Baltic Sea (Kaiser and Arz, 2016).

The Baltic Sea is an interesting study area for paleo SST studies since temperature has been shown to affect the occurrence of harmful cyanobacterial blooms, which have a large ecological and biogeochemical impact (e.g. Kabel et al., 2012). Due to the variable salinity within the Baltic Sea basin, complications arise when attempting to use the alkenone unsaturation indices to reconstruct SST (Blanz et al., 2005; Schulz et al., 2000; Warden et al., 2016b). Previous studies have successfully reconstructed summer SST in the Baltic using a calibration specific to the region based on the TEX_{86}^{L} index (Kabel et al., 2012; Warden et al., in review), however, there is a potential benefit to exploring additional paleotemperature proxies that could be utilized in the area. Since OH-GDGTs are relatively abundant in cold areas, it is desirable to further evaluate these compounds in the Baltic Sea (cf. Kaiser and Arz, 2016). In this study we describe the presence of OH-GDGTs in Baltic Sea surface sediments and evaluate the potential of previously published indices based on the OH-GDGTs to reconstruct SST in the Baltic Sea back to ~10.6 cal kyr BP in the Gotland Basin and to 12.5 cal kyr BP in the Arkona Basin.

2. Setting

The present day Baltic Sea (Fig. 1) is almost completely landlocked except for a narrow connection to the North Sea through the Straits of Denmark where an inflow of denser saline bottom waters occurs. These influxes of marine waters cause a lateral salinity gradient that decreases from the south to the north, where there is a large input of fresh water from rivers. The Baltic Sea has gone through several phases over the Holocene; the Ancylus Lake, the Litorina Sea and the modern Baltic Sea. Before the Ancylus Lake phase another freshwater period, known as the Baltic Ice Lake, existed when the Baltic Sea was disconnected from the ocean. A retreating ice sheet, however, allowed the re-connection to the ocean and caused an influx of marine water creating the slightly brackish conditions of the Yoldia Sea (Björck et al., 1996; Jensen, 1995). As the ice sheet melted, the land uplifted resulting in the basin once again being disconnected from the ocean (Jensen et al., 1999). This separation from the ocean produced an enclosed freshwater basin, the Ancylus Lake (Björck, 1995). Eustatic sea-level rise caused the connection to the ocean to become re-established and allowed once again for the inflow of saline water transforming the lake into the Litorina Sea (Winterhalter, 1992). The transformation of the Ancylus Lake to the Littorina Sea is

considered to be very complex consisting of pulses of marine waters entering the basin for nearly 2,000 years before becoming a fully brackish basin (Andren et al., 2000b).

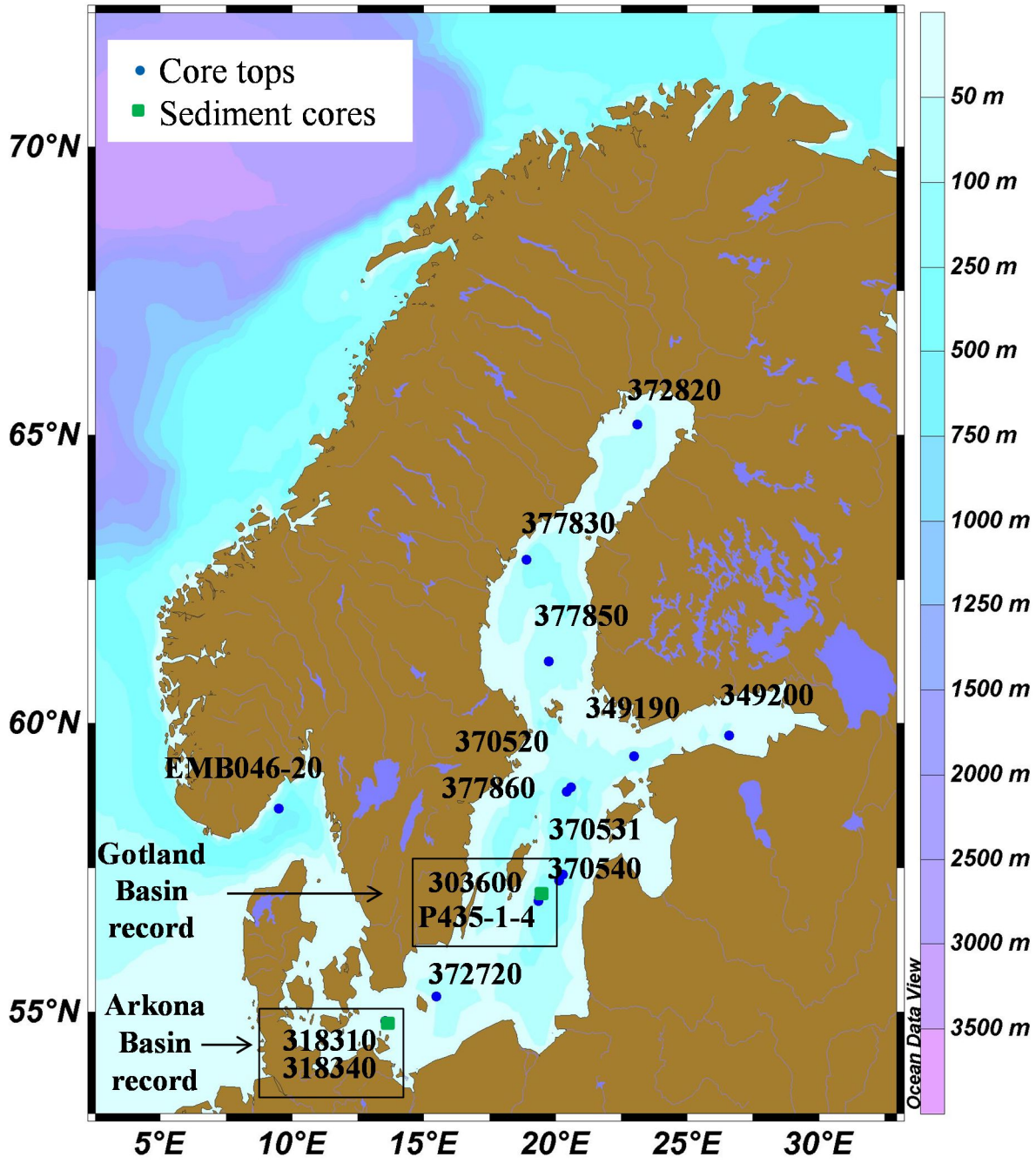

Fig. 1 Map of the Baltic Sea region showing the locations where the surface sediments (indicated by green squares) and sediment cores (indicated by blue circles) were collected.

3. Methods

3.1 Enrichment culture

A Thaumarchaeotal enrichment culture closely related to *Candidatus* Nitrosoarchaeum limnia obtained from the Landsort Deep in the Baltic Sea (Berg et al., 2014) was grown at

different temperatures (4 and 22ºC) but constant salinity (12 ppt) and other environmental factors to determine the effect of growth temperature on the relative abundance and distribution of OH-GDGTs. The cultures were filtered and the filters were stored at -20°C.

Table 1 Location, water depth, sea surface temperature and salinity of surface sediments and sediment cores for this study.

Station	Location	Latitude [N]	Longitude [E]	Water depth [m]	SST [°C]	SSS [ppt]
		Surface sediments				
EMB046-20	Skagerrak	58°31.59	09°29.09	457	10.2	n.a.
372720	Gotland Basin	55°15.67	15°28.21	96	9.7	10.5
303600	Gotland Basin	56°55.01	19°19.99	170	9.3	8.0
370540	Gotland Basin	57°17.04	20°07.26	243	9.4	9.8
370531	Gotland Basin	57°23.12	20°15.55	232	9.4	9.8
377860	Gotland Basin	58°48.92	20°25.17	195	9.1	8.2
370520	Gotland Basin	58°53.66	20°34.43	182	9.1	8.2
349190	Gulf of Finland	59°26.09	22°58.39	94	8.5	6.5
349200	Gulf of Finland	59°46.97	26°35.05	82	8.3	6.5
377850	Bothnian Sea	61°04.31	19°43.68	136	7.2	5.7
377830	Bothnian Sea	62°50.71	18°53.34	210	6.9	5.8
372820	Bothnian Bay	65°10.70	23°05.73	122	5.8	3.4
		Sediment cores				
303600-N	Gotland Basin	56°55.01	19°19.99	170	n.a.	n.a.
303600-3	Gotland Basin	56°55.01	19°19.99	170	n.a.	n.a.
P435-1-4MUC	Gotland Basin	56°57.94	19°22.21	178	n.a.	n.a.
318310	Arkona Basin	54°50.34	13°32.03	46	n.a.	n.a.

a SST was obtained from CTD measurements and reflect annual mean SST.
b SSS was an average of the years 2000-2006 obtained from the website, http://www.ices.dk/ and using the data from the closest HELCOM sampling site.

3.2 Sampling of sediments

Eleven surface sediments from different locations in the Baltic Sea basin (Table 1; Fig. 1) were studied; the sampling information has been described previously by Kabel et al. (2012). Additionally, a surface sediment sample from the Skagerrak, located northeast of the Arkona Basin where the Baltic Sea opens up to the North Sea, was collected using a multi corer during a cruise EMB046 of the R/V "Elisabeth Mann-Borgese" in May 2013.

Four sediment cores were used in this study (Table 1; Fig. 1). Two of the sediment cores, 303600-N and 303600-3, were obtained in July 2007 during the cruise campaign on the R/V "Prof. Albrecht Penck" from the Gotland Basin in the central Baltic Sea to the east of Gotland Island. Core 303600-N was cut into 1-cm sections from 0-237 cm and a sub-set of those samples were used in this study. In June 2012 a third sediment core, P435-1-4MUC, was also collected from the Gotland Basin using a multi corer during the R/V "Poseidon" cruise P435. The sediment core was taken from the location and then sub-sampled at 0.5 cm resolution. Sediment core 318310 was collected using a gravity corer on the R/V "Maria S. Merian" in April of 2006 from the Arkona Basin, which is located in the south-western part between the Bornholm Basin to the Danish Isles of Falster and Zealand. All sediment samples were freeze-dried and grounded before extraction.

3.3 Lipid extraction and GDGT analysis

The filters of the cultures were extracted with a modified Bligh and Dyer extraction and the extracts were base hydrolysed to release core isoprenoid GDGTs as previously described (Pitcher et al., 2011). All sediment samples were freeze dried and then subsequently ground and homogenized by means of a mortar and pestle. These samples were then extracted with the Dionex^{TM} accelerated solvent extraction (ASE) using 1-3 g of sediment and extracting with dilchloromethane (DCM):methanol (9:1, v/v) as the solvents at a temperature of 100°C and a pressure of 1,500 psi for 5 min with 60% flush and purge 60 s. The extract was collected and then dried using Caliper Turbovap®LV. Next, using DCM the lipid extract was dried over a column of anhydrous Na_2SO_4 and then blown down under a gentle stream of N_2. To quantify the amount of GDGTs, 1µg of an internal standard (C_{46} GDGT; Huguet et al., 2006) was added to the total lipid extract which was then separated over an Al_2O_3 column (activated for 2 h at 150°C) into three fractions using hexane:DCM (9:1, v:v) to obtain the apolar fraction, hexane:DCM (1:1, v:v) for the ketone fraction and DCM:MeOH (1:1, v:v) for the polar fraction.

The polar fractions of both the cultures and the sediments, which contain the GDGTs, were dried using N_2, re-dissolved in hexane:isopropoanol (99:1, v:v) at a concentration 10 mg ml^{-1} and then passed through a 0.45 µm PTFE filter and analyzed with an Agilent 1290 Infinity ultra-high performance liquid chromatography (UHPLC) coupled to an Agilent 6130 single quadrupole mass detector according to Hopmans et al. (2015).

Table 2 Fractional abundances of the isGDGTs and OH-GDGTs in a Thaumarchaeotal enrichment culture grown at different temperatures.

Growth temperature (°C)	GDGT-I	GDGT-II	GDGT-III	GDGT-IV	Crenarchaeol	Crenarchaeol'	OH-GDGT-0	OH-GDGT-1	OH-GDGT-2
4	66.37±2.73	2.89±0.19	0.60±0.01	0.36±0.08	26.99±2.81	0.37±0.01	1.95±0.01	0.38±0.03	0.09±0.02
22	23.00±1.38	22.70±0.34	18.83±0.18	2.86±0.04	30.87±1.87	0.45±0.02	0.18±3.0e-3	0.29±0.01	0.83±0.07

Average values from two LC/MS analyses are given with the standard deviation of the two measurements.

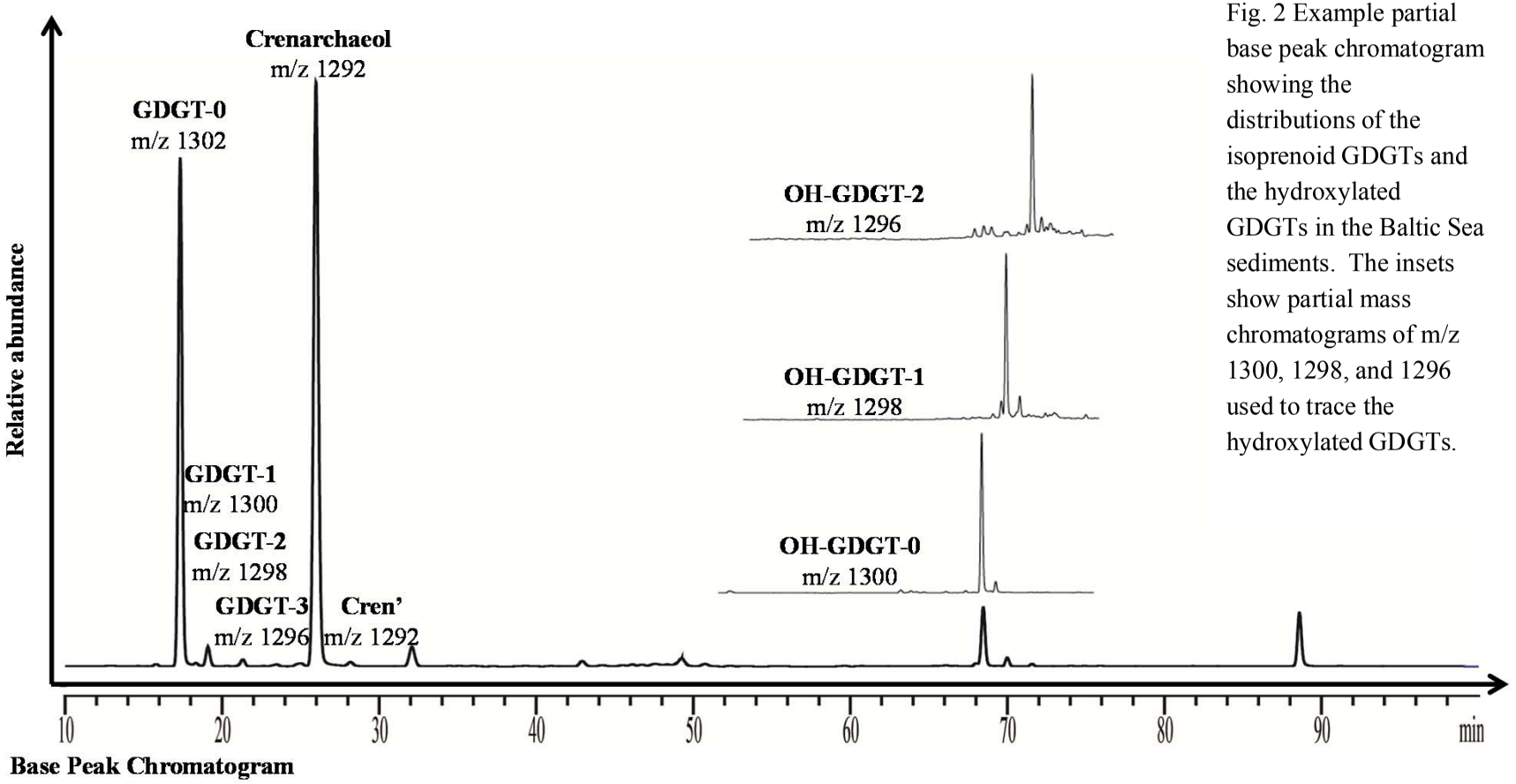

Fig. 2 Example partial base peak chromatogram showing the distributions of the isoprenoid GDGTs and the hydroxylated GDGTs in the Baltic Sea sediments. The insets show partial mass chromatograms of m/z 1300, 1298, and 1296 used to trace the hydroxylated GDGTs.

Table 3 Displays the OH-GDGT based indices and their correlation with measured SSTs from the nine surface sediments (excluding those from the Bothnian Sea and Bay) around the Baltic Sea basin as well as the average difference between estimated SST and measured SST(Δ, °C) based on that specified calibration and index from highest to lowest correlation.

Index	Correlation with measured SST	Calibration	Average ΔSST (°C)
General calibrations			
OH-GDGT $_{\text{Index 5}}$ [a]	0.92	SST (°C) = -0.34*OH-GDGT $_{\text{Index 5}}$+13.1 [a]	0.0±1.1
OH-TEX_{86} index [a]	0.88	SST (°C) = OH-TEX_{86} index/0.015-0.19 [a]	0.5±1.2
OH-GDGT% [b]	0.85	SST (°C) = (OH-GDGT%-8.60)/-0.67 [b]	-5.9±1.8
OH-GDGT $_{\text{Index 1}}$ [a]	0.83	SST (°C) = -0.24*OH-GDGT $_{\text{Index 1}}$+8.3 [a]	-1.9±1.2
OH-GDGT-0/crenarchaeol ratio [b]	0.82	SST (°C) = (OH-GDGT-0/crenarchaeol-0.25)/-0.025 [b]	-3.6±1.3
OH-GDGT index [b]	0.77	SST (°C) = (OH-GDGT index-0.93)/-0.0076 [b]	-1.5±3.7
OH-GDGT $_{\text{Index 3}}$ [a]	0.71	SST (°C) = -0.62*OH-GDGT Index 3+20.1 [a]	3.6±1.5
Baltic Sea calibrations			
OH-GDGT% [b]	0.85	SST (°C) = (OH-GDGT%-18.38)/-0.93 [d]	3.9±1.4
OH-GDGT-0/crenarchaeol ratio [b]	0.82	SST (°C) = (OH-GDGT-0/crenarchaeol-0.33)/-0.020 [d]	1.7±1.5
New calibrations			
OH-TEX_{86} index [a]	0.88	SST (°C) = 23.17* OH-TEX_{86} index+5.92 [c]	0.6±1.1
OH-GDGT' index [c]	0.82	SST (°C) = 11.40*OH-GDGT' index +7.38 [c]	0.6±1.1

[a] Huguet et al. (2013), [b] Fietz et al. (2013), [c] local calibration developed in this study, [d] Kaiser and Arz (2016)

Table 4 Shows calibrations tested in this study and the difference (Δ, °C) between estimated and growth temperature for culture samples using that specified index and calibration.

Index	Calibration	ΔT (°C)	
		4°C Growth	22°C Growth
OH-GDGT $_{Index\ 1}$ [a]	SST(°C) = -0.24* OH-GDGT $_{Index\ 1}$ +8.3 [a]	3.7	-14
OH-GDGT $_{Index\ 3}$ [a]	SST(°C) = -0.62* OH-GDGT $_{Index\ 3}$ +20.1 [a]	11	-4.4
OH-GDGT $_{Index\ 5}$ [a]	SST(°C) = -0.34* OH-GDGT $_{Index\ 5}$+13.1 [a]	8	-9.6
OH-TEX_{86} index[a]	SST(°C) = 23.17* OH-TEX_{86} index+5.92 [c]	6.6	-5.0
	SST(°C) = OH-TEX_{86} index/0.015-0.19 [a]	9.2	9.8
OH-GDGT index[b]	SST(°C) = (OH-GDGT index-0.93)/-0.0076 [b]	8.2	50.2
OH-GDGT' index [c]	SST (°C) = 11.40*OH-GDGT' index +7.38 [c]	5.6	-4.8
OH-GDGT-0/crenarchaeol ratio [b]	SST(°C) = (OH-GDGT-0/crenarchaeol-0.25)/-0.025 [b]	3.1	-12.2
	SST (°C) = (OH-GDGT-0/crenarchaeol-0.33)/-0.02 [d]	8.9	-5.8
OH-GDGT% [b]	SST (°C) = (OH-GDGT%-8.60)/-0.67 [b]	5.2	-11.1
	SST (°C) = (OH-GDGT%-18.38)/-0.93 [d]	13.2	-3.6

[a] Huguet et al. (2013), [b] Fietz et al. (2013), [c] local calibration developed in this study, [d] Kaiser and Arz (2016)

3.4 Age model and core correlation

The age depth models for all of the sediment cores in this study have been previously established and are based on picked forams. The correlation techniques and depth age model for sediment cores 303600-N, P435-1-4 MUC, and 303600-3 from the Gotland Basin are previously published in Warden et al. (in preparation). These three sediment cores were combined to form the record in the Gotland Basin from 10.6 cal kyr BP to 2008 AD, which covers the Ancylus Lake phase (10.6-7.8 cal kyr BP), the Ancylus Lake/Littorina Sea transition (7.7-7.3 cal kyr BP), and the recent brackish phase (7.2 cal kyr BP-2008 AD). The correlation methods and core depth age models for sediment cores 318310 and 318340 from the Arkona Basin are published in Warden et al. (2016b). The two sediment cores were combined to form a single long sediment record in the Arkona Basin spanning 12.5-0.1 cal kyr BP, which includes the Baltic Ice Lake (12.5-11.6 cal kyr BP), the Yoldia Sea phase (11.5-10.6 cal kyr BP), Ancylus Lake Phase (10.5-7.8 cal kyr BP), the Ancylus Lake/Littorina Sea transition (7.7-7.3 cal kyr BP) and the recent brackish phase (7.2-0.1 cal kyr BP).

3.5 Calculation of GDGT-based indices

The percentage of OH-GDGTs compared with the total isoGDGTs is calculated according to Huguet et al. (2013):

$$\text{OH-GDGT\%} = \Sigma\text{OH-GDGTs} / [\Sigma\text{OH-GDGTs} + \Sigma\text{isoGDGTs}] \times 100 \quad [1]$$

Where the OH-GDGTs include OH-GDGT-0, OH-GDGT-1 and OH-GDGT-2, and the isoGDGTs include GDGT-I, GDGT-II, GDGT-III, GDGT-IV, GDGT-V or crenarchaeol (a specific isoprenoid GDGT from Thaumarchaeota identified by Sinninghe Damsté et al. (2002) and GDGT-V', the crenarchaeol regio isomer (Refer to Fig. S1 for structures).
The OH-GDGT index used for SST determination was calculated according to Fietz et al. (2013):

$$\text{OH-GDGT index} = \text{OH-GDGT-0} / (\text{OH-GDGT-0} + \text{OH-GDGT-1}) \quad [2]$$

Huguet et al. (2013) reported three indexes based on the OH-GDGTs and isoprenoid GDGTs as well as modified the TEX_{86} index to include the OH-GDGTs in the denominator:

$$\text{OH-TEX}_{86}\text{ index} = (\text{GDGT-III+GDGT-IV+crenarchaeol'})/(\Sigma\text{OH-GDGTs} + \text{GDGT-II+GDGT-III+GDGT-IV+crenarchaeol+crenarchaeol'}) \quad [3]$$

$$\text{OH-GDGT}_{\text{Index1}}(\%) = 100 * \Sigma\text{OH-GDGTs}/(\Sigma\text{OH-GDGTs} + \Sigma\text{isoGDGTs}) \quad [4]$$

$$\text{OH-GDGT}_{\text{Index3}}(\%) = 100 * \Sigma\text{OH-GDGTs}/(\Sigma\text{OH-GDGTs} + \text{crenarchaeol}) \quad [5]$$

$$\text{OH-GDGT}_{\text{Index5}}(\%) = 100 * \Sigma\text{OH-GDGTs}/(\Sigma\text{OH-GDGTs} + \text{GDGT-I+GDGT-II+GDGT-III}) \quad [6]$$

4. Results

4.1 Occurrence and distribution of OH-GDGTs in the Thaumarchaeotal enrichment culture

A culture of a Thaumarchaeote enriched from Baltic Sea water and closely related to *Candidatus* Nitrosoarchaeum limnia (Berg et al., 2014) was grown at 4 and 22°C but otherwise identical conditions. The distribution of the core GDGTs was studied after base hydrolysis of intact polar lipids. It is dominated by GDGT-0 and crenarchaeol (Table 2) as is commonly observed for Thaumarchaeota (Blaga et al., 2009; Sinninghe Damsté et al., 2012b; Pitcher et al., 2011). A marked difference was noted between 4 and 22°C; in the latter case cyclopentane-containing GDGTs were relatively more abundant. This resulted in an increase of the TEX_{86} index from 0.32 at 4°C to 0.49 at 22°C. OH-GDGTs were detected in fairly low relative amounts (1.3-2.4%; Table 2) with higher relative amounts at low growth temperature. A marked change in the distribution of the OH-GDGTs was also apparent. At 4°C OH-GDGT-0 was most abundant, whereas at 22°C OH-GDGT-2 dominated (Table 2).

4.2 Occurrence and distribution of OH-GDGTs in surface sediments

All three known OH-GDGTs were found in the Baltic Sea sediments (Fig. 2). OH-GDGTs range between 3.8-8.6% of total isoprenoid GDGTs (isoGDGTs) in the Baltic Sea surface sediments and on average make up 6.8±1.4% (average±standard deviation). Surface sediments of the central Baltic (349190, 349200 and 377850; Fig. 1) contain a higher OH-GDGT% (8.5±0.2%) than the other surface sediments in the Baltic Sea (6.2±1.2%). OH-GDGT-0 made up the largest component of the OH-GDGTs in the Baltic Sea surface sediments with a fractional abundance of 0.84±0.04. OH-GDGT-1 was the second most abundant at 0.12±0.03 and OH-GDGT-2 had the lowest fractional abundance at 0.04±0.02. The average OH-GDGT index for the surface sediments is 0.88±0.04.

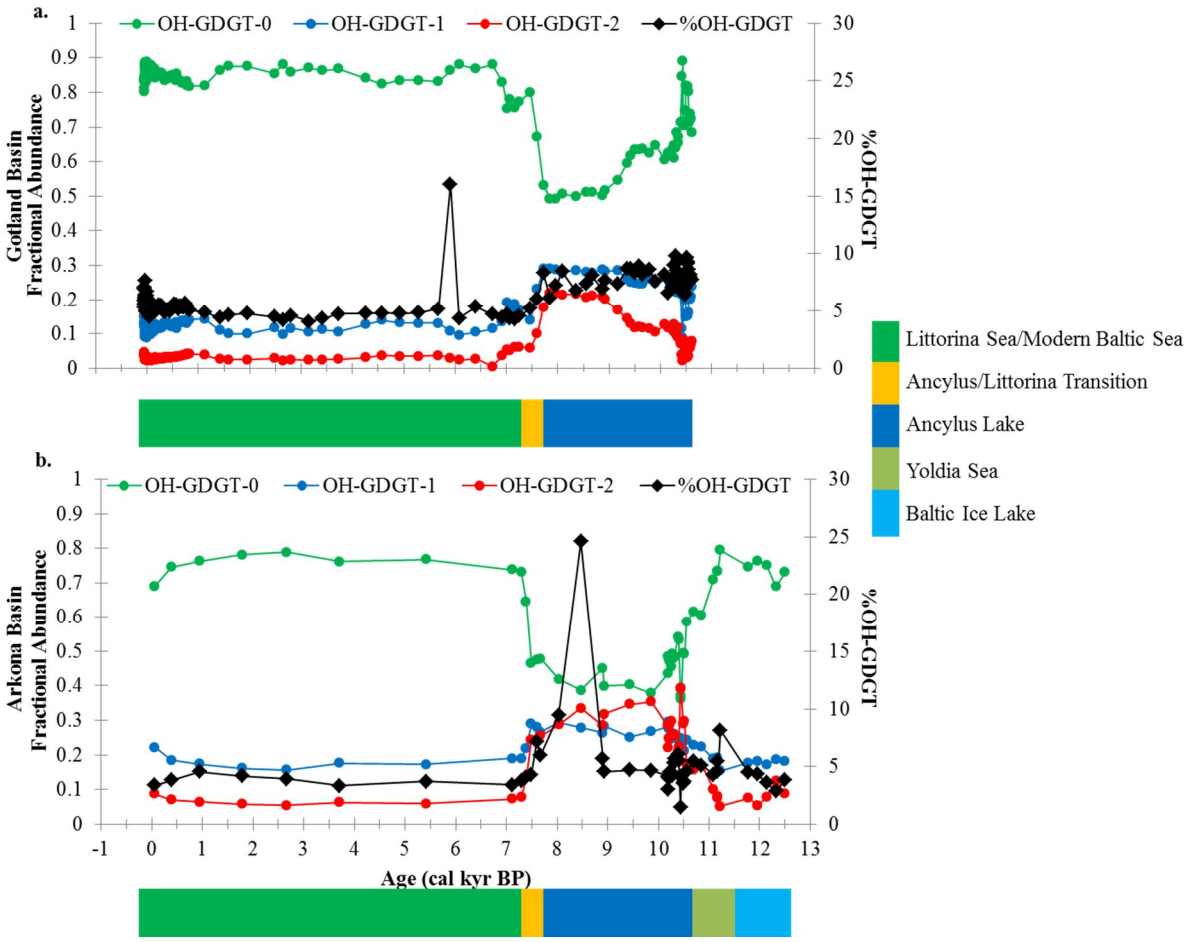

Fig. 3 The fractional abundance of OH-GDGT-0 (indicated in green), OH-GDGT-1 (indicated in blue), and OH-GDGT-2 (indicated in red) and the OH-GDGT% (indicated in black) plotted against age (cal kyr BP) for both the (a) Gotland and (b) Arkona basins. The various phases of the Baltic Sea are indicated.

4.3 Occurrence and distribution of OH-GDGTs in the sedimentary record

In the Gotland Basin the sediments deposited up to 7.8 cal kyr BP correspond with the low salinity period of the Baltic Sea, the Ancylus Lake phase, and the average OH-GDGT% (7.9±0.9%) are slightly higher than in the sediments deposited after 7.3 cal kyr BP, which corresponds to the brackish phase of the basin (5.4±1.2%) (Fig. 3a). An anomaly of much higher OH-GDGT% than the average (16.0±0.3%, triplicate analysis; Fig. 3a) occurs at 5.9 cal kyr BP. The OH-GDGT% for the sediments in the Arkona Basin record are statistically the same in all of the phases covered in the sediment record (Fig. 3b). During the Baltic Ice Lake period (12.5-11.8 cal kyr BP; 3.8±0.6%) and the recent brackish phase (from 7.2 cal kyr BP onwards; 3.8±0.4%), the OH-GDGT% are less variable than during the Yoldia Sea phase (11.2-10.7 cal kyr BP; 5.6±4.6%) and the Ancylus Lake phase (10.6-8.0 cal kyr BP;

5.5±1.4%) (Fig. 3b). An outlier also occurs in the Arkona Basin record with the sediment with an age of 8.5 cal kyr BP having a much higher than average OH-GDGT% (24.6%; Fig. 3b).

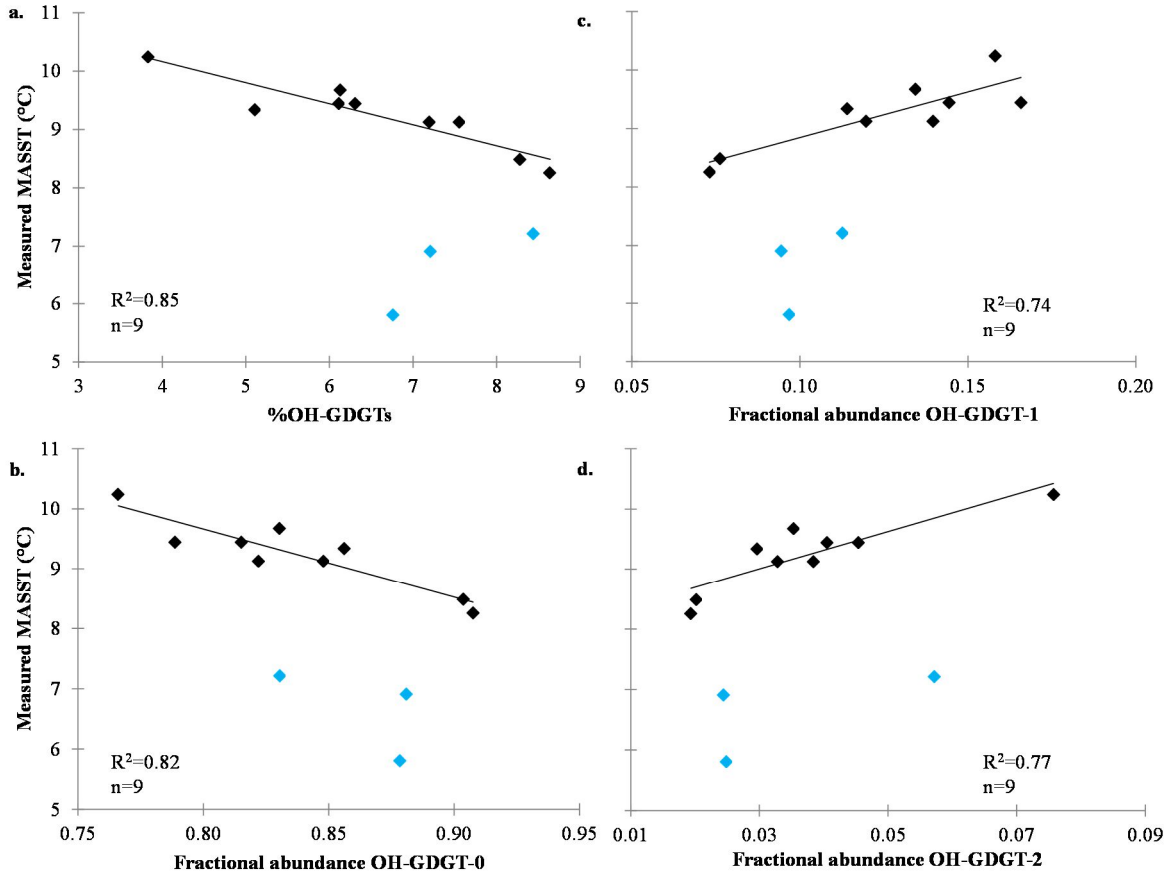

Fig. 4 Scatter plots of the measured mean annual sea surface temperature (MASST; °C) plotted against (a) OH-GDGT%, and fractional abundance of (b) OH-GDGT-0, (c) OH-GDGT-1, and (d) OH-GDGT-2. The blue symbols represent the sediments from the Bothnian Bay and Sea, which were left out of the regression analysis because they are considered as outliers (see text).

With respect to the distribution of the OH-GDGTs in the Gotland Basin record, OH-GDGT-0 always makes up the most abundant OH-GDGT (Figs. 3a-). The fractional abundance of OH-GDGT-0 increases moving from the Ancylus Lake phase, 0.66±0.10, into the brackish phase, 0.85±0.02 (Fig. 3a). The fractional abundance of OH-GDGT-1 decreases moving from the Ancylus Lake phase (0.23±0.05) into the brackish phase (0.12±0.02) (Fig. 3a). OH-GDGT-2 is always the least abundant component of OH-GDGTs and also decreases over the transition from the Ancylus Lake phase, 0.11±0.06, to the brackish phase, 0.03±0.01 (Fig. 3a).

OH-GDGT-0 is the most abundant OH-GDGT for the Arkona Basin record as well (Fig. 3b). OH-GDGT-1 is the second most abundant component of the OH-GDGTs during the Baltic Ice Lake phase (0.18±0.01) and recent brackish phase (0.18±0.02), but during the Yoldia Sea phase (0.19±0.03 v. 0.11±0.05) and the Ancylus Lake phase (0.26±0.02 v.

0.29±0.06) there is statistically no difference between the fractional abundance of OH-GDGT-1 and OH-GDGT-2 (Fig. 3b). During the Baltic Ice Lake period, the Yoldia Sea phase, and the recent brackish phase, there is statistically no change in the fractional abundances of OH-GDGTs-0 (0.73±0.05), -1 (0.18±0.02) and -2 (0.08±0.03) (Fig. 3b). However, during the Ancylus Lake phase the fractional abundance of OH-GDGT-0 (0.46±0.06) decreases as it did in the Gotland Basin record, and the fractional abundances of OH-GDGT-1 (0.26±0.02) and -2 (0.29±0.06) increases (Fig. 3b).

5. Discussion

5.1 Influence of temperature on the distribution of OH-GDGTs

Surface sediments. Previously it has been observed in marine sediments that OH-GDGT% increases with decreasing SST (Huguet et al., 2013). Although the correlation is low (R^2=0.28), the same trend is noted for the surface sediments of the Baltic Sea (Fig. 4a). The fractional abundance of the hydroxylated GDGT with no cyclopentane moieties, OH-GDGT-0, increased with decreasing SST (R^2=0.36) (Fig. 4b). The fractional abundances of the OH-GDGTs with one, OH-GDGT-1, and two, OH-GDGT-2, cyclopentane moieties increases with increasing SST (Figs. 4c-d), as has been observed in other marine sediments (Huguet et al., 2013). For all correlations, it was observed that if the three surface sediments from the Bothnian Sea and Bothnian Bay (stations 377850, 377830, and 372820; Fig. 1) were removed from the data set, the correlations increased substantially (e.g. for OH-GDGT% to R^2=0.85). These sediments probably represent outliers because the salinity of the Baltic Sea in this region is the lowest (5.0±1.4 ppt; Table 1) of the suite of surface sediments examined.

Enrichment culture. The increase in cyclopentane-containing GDGTs along with the resultant increase of the TEX_{86} index observed in the enrichment culture grown at the higher temperature (22°C) is in line with what has been previously demonstrated in marine sediments (Schouten et al., 2002). An earlier study also showed with marine sediments that with increasing SSTs, the OH-TEX_{86} index increases along with the increased abundance of cyclopentane-containing GDGTs (Huguet et al., 2013), and this is also observed in the enrichment culture grown at 22°C. Additionally, the higher value for OH-GDGT% in the enrichment culture grown at a lower temperature (4°C) is in agreement with what has been observed in marine sediments with the abundance of OH-GDGTs relative to non-hydroxylated GDGTs decreasing with increasing SST (Huguet et al., 2013). The change in the distribution of OH-GDGTs with growth temperature, from OH-GDGT-0 making up the

majority in the enrichment culture grown at 4°C to the predominance of OH-GDGT-2 in that grown at 22°C (Table 2), gives credence to the use of the distribution of OH-GDGTs as a proxy for SST.

5.2. Determining the potential application of existing OH-GDGT-based indices and the development of local calibrations for SST reconstruction

Surface sediments. Huguet et al. (2013) were the first to propose OH-GDGT-based indices for reconstructing SST and Fietz et al. (2013) has proposed some alternatives. Recently, another index based on OH-GDGTs, designed specifically for the Baltic Sea, was proposed by Kaiser and Arz (2016). To determine how the various OH-GDGT-based proxies perform in the Baltic Sea, we applied them to the GDGT distributions of the twelve examined surface sediments from around the Baltic Sea (Fig. 1) and regressed each proxy ratio with the mean annual SST data measured by CTD from the surface waters where the sediment was collected (Table 1). In this exercise, it was again (see section 5.1) observed that for all of the indices the correlation increased substantially if the three surface sediments in the north of the basin from the Bothnian Sea and Bay were removed from the dataset, yielding highly significant correlations with SST (R^2=0.92-0.71; Table 3). The two indices with the highest correlation were the OH-GDGT $_{\text{Index 5}}$ (R^2=0.92) and the OH-TEX_{86} index (R^2=0.88, Table 3; Figs. 5a).

Next, the suite of existing SST calibrations were assessed to determine how well they predict SST. In this exercise, we again omitted the surface sediments from the lower salinity Bothinian Bay and Sea. The SST estimates obtained from the calibration based on the OH-GDGT $_{\text{Index 5}}$ had the lowest average difference between reconstructed and measured SST (ΔSST = 0.0±1.1°C; Table 3). The SST estimates derived from the calibration based on the OH-TEX_{86} index (Huguet et al., 2013) also had a low ΔSST (0.5±1.2°C; Table 3). The calibration based on OH-GDGT% from Fietz et al. (2013) had on average the largest ΔSST (5.9±1.8°C; Table 3). Since the OH-GDGT $_{\text{Index 5}}$ and the OH-TEX_{86} index had the highest correlations with measured SSTs from surface sediments in the Baltic Sea from this study and both indices incorporate isoGDGTs, this suggests that the inclusion of the isoGDGTs, especially GDGT-II and GDGT-III, in the OH-GDGT indices results in better SST estimates using GDGT-derived proxies in the Baltic Sea. This broaches the question if using only isoGDGTs for SST reconstruction would lead to higher correlations with measured SSTs in the Baltic Sea. However, as Huguet et al. (2013) found in their study that the addition of the OH-GDGTs to the TEX_{86} index increased the correlation with SST, this was also the case

here. The correlation with the measured temperatures for the surface sediments was substantially higher using the OH-TEX_{86} index (R^2=0.88) than with the TEX_{86} index (R^2=0.40). Since it has been shown previously that the TEX_{86}^L index, that was developed by Kim et al. (2010) for use in regions with cooler temperatures and shown to have a good correlation with seasonal temperatures, has a high correlation to summer SST in the Baltic Sea (Kabel et al., 2012; Warden et al., in review). Therefore, this index was also compared to the mean annual measured temperatures for the surface sediments, however, resulting in an even lower correlation of R^2=0.23 (Fig. 5c).

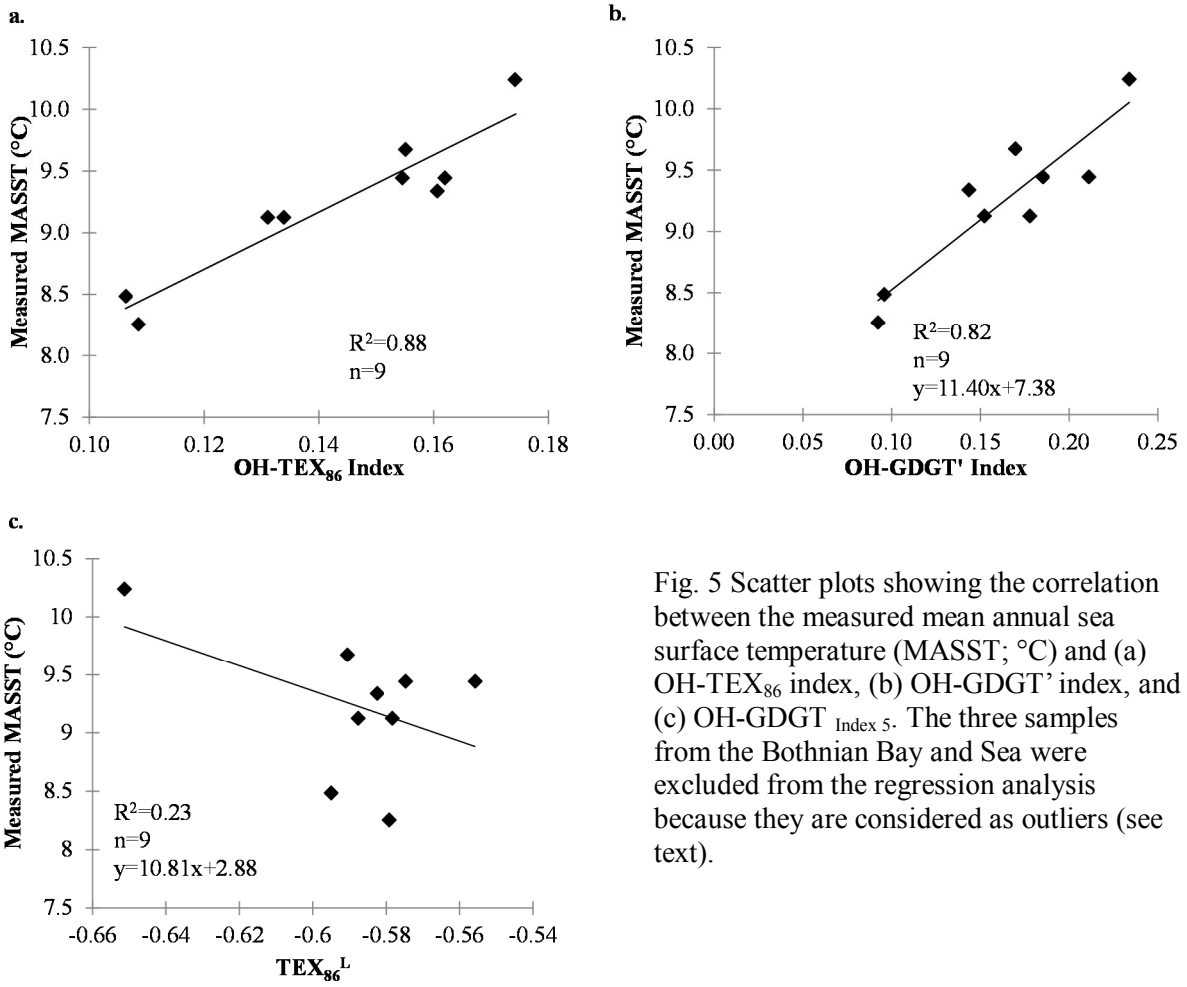

Fig. 5 Scatter plots showing the correlation between the measured mean annual sea surface temperature (MASST; °C) and (a) OH-TEX_{86} index, (b) OH-GDGT' index, and (c) OH-GDGT $_{Index\ 5}$. The three samples from the Bothnian Bay and Sea were excluded from the regression analysis because they are considered as outliers (see text).

Local calibrations may be expected to perform better than those based on global datasets or from other regions, so next the already existing calibrations based on Baltic Sea sediment developed by Kaiser and Arz (2016) were applied. The calibration based on the OH-GDGT-0/crenarchaeol ratio developed gave fairly accurate SST estimates (ΔSST = 1.7±1.5°C; Table 3), whereas that based on OH-GDGT% resulted in a much larger ΔSST. Additionally, two local calibrations based on the surface sediments from this study and their accompanying SST data were developed. One calibration, based on the OH-TEX_{86} index of

Huguet et al. (2013), resulted in the same average difference between reconstructed and measured SST (0.6±1.1°C; Table 3) as the general calibration. A modified version of the OH-GDGT index, which will be referred to as the OH-GDGT' index, had a slightly higher correlation with SST than the OH-GDGT index presented in Fietz et al. (2013) (Table 3; Fig. 5b).

OH-GDGT' index = (OH-GDGT-1+OH-GDGT-2) / (ΣOH-GDGTs) (n=9, R^2=0.82) [7]

This calibration also had a low average difference between reconstructed and measured SST (0.6±1.1°C; Table 3).

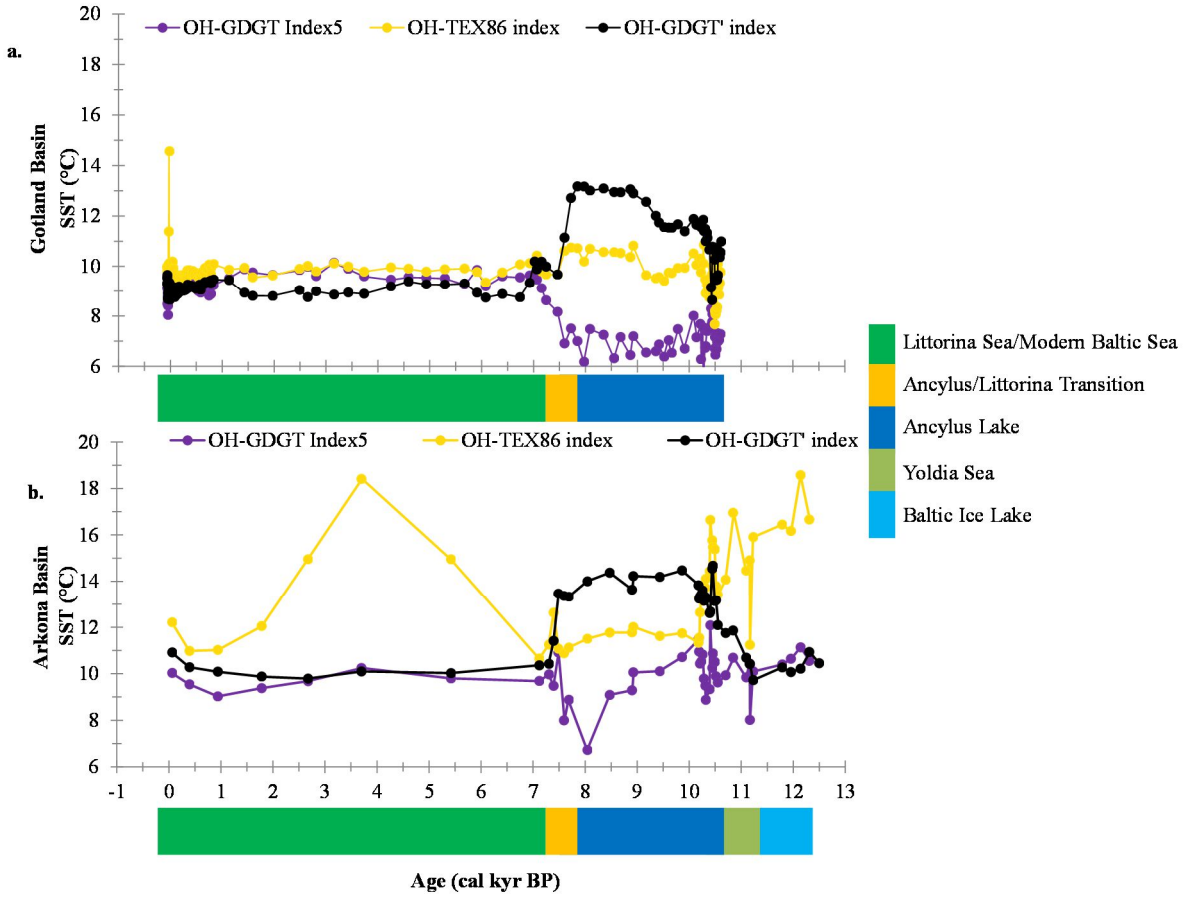

Fig. 6 Reconstructed sea surface temperatures (SST; °C) based on the OH-GDGT $_{Index\ 5}$ (designated in purple), OH-TEX_{86} index (designated in yellow), and the OH-GDGT' index (designated in black) plotted with age (cal kyr BP) for the (a) Gotland and (b) Arkona basins. The different phases of the Baltic Sea are indicated by the different colors in the bar below the x-axis as designated in the legend.

Enrichment culture. The indices OH-GDGT $_{Index\ 1}$, $_{Index\ 3}$, and $_{Index\ 5}$ (Eqns. 4-6) and the OH-TEX_{86} index (Eqn. 3) from Huguet et al. (2013) as well as two other indices applied in the Nordic Seas, the OH-GDGT-0/crenarchaeol ratio and the OH-GDGT index (Eqn. 2)

from Fietz et al. (2013), and the new OH-GDGT' index (Eqn. 7) developed in this study, were all applied to the GDGT distributions of the thaumarchaeotal enrichments grown at 4°C and 22°C (Table 4). All of the published calibrations applied resulted in an overestimation of temperature for the culture grown at 4°C (Table 4). For the culture grown at 22°C all of the calibrations gave temperatures that were an underestimation, with the exception of the calibration from Fietz et al. (2013) based on the OH-GDGT index, which greatly overestimated the temperature (ΔT = 50°C; where ΔT represents average difference between estimated and growth temperature) and the calibration based on OH-TEX_{86} index presented in Huguet et al. (2013), which also overestimated the temperature (ΔT c. 10°C) (Table 4). For the culture grown at 4°C, the calibration of Fietz et al. (2013) based on the OH-GDGT-0/crenarchaeol ratio (Eqn. 11; ΔT ca. 3°C) and of Huguet et al. (2013) the calibration based on the OH-GDGT $_{\text{Index 1}}$ (Eqn. 4; ΔT ca. 4°C), had the lowest difference between estimated temperature and actual growth temperature (Table 4). With respect to the enrichment culture grown at 22°C, the calibration from Kaiser and Arz (2016) based on the OH-GDGT% (Eqn. 1; ΔT ca. -4°C) and the calibration from Huguet et al. (2013) based on the OH-GDGT $_{\text{Index 3}}$ (Eqn. 6; ΔT ca. -4°C), had the smallest difference between estimated and actual growth temperature (Table 4). However, the calibration from Fietz et al. (2013) based on the OH-GDGT-0/crenarchaeol ratio (ΔT ca. -12°C) and from Huguet et al. (2013) based on OH-GDGT $_{\text{Index 1}}$ (Eqn. 4; ΔT ca. -14°C) both greatly underestimated the growth temperature for the enrichment culture grown at 22°C. The calibration of Kaizer and Arz (2016) based on the OH-GDGT% (Eqn. 1; ΔT ca. 13°C) and the calibration based on the OH-GDGT $_{\text{Index 1}}$ from Huguet et al. (2013) (Eqn. 4; ΔT ca 11°C) greatly overestimated the temperature for the sample grown at 4°C (Table 4). Therefore, the calibrations from this study based on the OH-TEX_{86} index (Eqn. 3) and the new OH-GDGT' index (Eqn. 7) performed the best overall for estimating growth temperatures for both culture samples (Table 4).

It may be expected that the calibrations from Fietz et al. (2013) based on ratio of OH-GDGT-0/crenarchaeol and OH-GDGT% (Eqn. 1) perform better for cooler SSTs since these are local calibrations for the Nordic Seas (Table 4). However, that the calibration from Kaizer and Arz (2016) based on OH-GDGT% is better for estimating higher SSTs is perplexing since it was developed on samples from the Baltic Sea where SSTs rarely, if ever, make it as high as 22°C (Table 4). Although the distribution of the GDGTs, both isoprenoid and hydroxylated, are behaving as expected with increasing number of cyclopentane moieties with increasing temperatures, the calibrations based on OH-GDGTs overall are not producing accurate temperature estimates. Perhaps a more extensive calibration based on cultures could

assuage this issue. Huguet et al. (2013) suggested that the OH-TEX_{86} index could be more effective as a SST proxy in colder waters, however, the results from this culture experiment do not support this as the reconstructed temperatures based on this index are more accurate for the culture grown at 22°C (5.0±0.0°C) than the one grown at 4°C (6.6±0.3°C) (Table 4).

5.3 Application of OH-GDGT-derived SST proxies to the Baltic Sea sedimentary record.

Next, the three SST calibrations (the OH-GDGT $_{Index\ 5}$, the OH-TEX_{86} index, and the OH-GDGT' index) that performed best in both predicting SST (set of surface sediments) and growth temperature (enrichment culture) (see section 5.2) were applied to the sedimentary records of both the Arkona Basin and the Gotland Basin (Figs. 6a-b). The results from the application of these SST calibrations will be examined below.

The values of the OH-GDGT' index are higher during the Ancylus Lake phase in both basins and decrease moving into the brackish phase (Figs. 6a-b). The decrease in OH-GDGT' index values that occurs over the Ancylus Lake/Littorina Sea transition in the Gotland Basin results in a decrease in estimated SSTs from 11.2±1.2°C during the Ancylus Lake phase to 9.1±0.3°C during the recent brackish phase (Figs. 6a). The SST average from the recent brackish phase is identical to today's measured SST in that area (9.3°C; Fig. 6a). However, a mean annual air temperature (MAT) reconstruction based on a pollen-climate calibration model from south central Sweden showed a ~2.5°C increase in MAT from the MAT (5.9°C) at c. 8,000 cal year BP (Seppä et al., 2005), whereas the OH-GDGT' index-derived SST record shows a decrease in temperatures (Fig. 6a; black line). The change in OH-GDGT' index-derived SST from the Ancylus Lake phase to the recent brackish phase in the Arkona Basin (Figs. 6b) also results in a decrease in estimated SST at this time (from 13.6±0.7°C to 10.2±0.4°C). The average reconstructed SST during the recent brackish phase in the Arkona Basin is similar to the measured SST from that area (9.7°C; Table 1). The OH-GDGT' index based SST estimates are statistically the same for the Baltic Ice Lake phase (10.4±0.3°C), the Yoldia Sea phase (10.8±0.8°C) and the recent brackish phase (Fig. 6b). The average OH-GDGT' index values and the resultant SSTs for the Ancylus Lake and recent brackish phases are similar for the Arkona Basin and Gotland Basin records (Figs. 6a-b).

The SST record of the Gotland Basin based on the OH-GDGT $_{Index\ 5}$ has an outlier at 5.9 cal kyr BP. This sample was run in triplicate and the resultant OH-GDGT $_{Index\ 5}$ values were similar (34.0±0.6). This sample is unique in that it has an OH-GDGT% ca. three times the amount in the other sediments, 16.0±0.3%. This outlier was removed from the SST record of the Gotland Basin presented in Fig. 6a. The average SST (outlier removed) based on the

OH-GDGT $_{Index\ 5}$ during the Ancylus Lake phase is 7.1±0.6°C and increases to 9.3±0.3°C in the recent brackish phase, which again is the same as today's measured SST in that area (9.3°C; Table 1) (Fig. 6a). This increase in temperature is consistent with the ~2.5°C from modern MAT (5.9°C) increase in MAT at c. 8,000 cal year BP (Seppä et al., 2005). In the Arkona Basin record there is also an outlier that occurs at 8.5 cal kyr BP, where again the OH-GDGT% is much higher than in the other sediments in the core (Fig. 6b). This outlier was also removed from the OH-GDGT $_{Index\ 5}$ based SST record. The average SSTs (with the outlier removed) in the Arkona Basin are quite similar for the four different phases (Baltic Ice Lake phase, 10.6±0.4°C; Yoldia Sea phase, 9.8±0.8°C; Ancylus Lake phase, 10.1±0.1°C; recent brackish phase, 9.7±0.4°C; Fig. 6b) and these SST estimates are similar to the measured SST in the Arkona Basin (9.7°C; Table 1). In the Arkona Basin the OH-GDGT $_{Index\ 5}$ based SST record, a cooling of ~2°C occurs at 8.0 cal kyr BP and then a warming of ~3°C (Fig. 6b). Such a temperature evolution was also demonstrated in the MAT reconstruction from south central Sweden (Seppä et al., 2005) and for Greenland ice cores (Alley et al., 1997). The estimated SSTs during the recent brackish phase are statistically the same in both basins, however, for the Ancylus Lake phase the reconstructed SST in the Arkona Basin is ca. ~3°C higher than in the Gotland Basin (Figs. 6a-b).

The observed change in values in the OH-GDGT $_{Index\ 5}$ and OH-GDGT' indices over the Ancylus Lake/Littorina Sea transition does not occur in the OH-TEX_{86} index record (Figs. 6a-b). The estimated SSTs for the OH-TEX_{86} index based calibration developed in this study are statistically the same throughout the record in both the Gotland (9.6±0.8°C during the Ancylus Lake phase and 9.8±0.5°C during the recent brackish phase; Fig. 6a) and Arkona (13.2±1.6°C during the Ancylus Lake phase and 13.2±2.7°C during the recent brackish phase; Fig. 6b) basins. In the OH-TEX_{86} index records there were "spikes" towards lower values in each record that occurred at the same time as the outliers in the OH-GDGT $_{Index\ 5}$ records. These outliers were removed. The SST average estimate from the recent brackish phase in the Gotland Basin based on the OH-TEX_{86} index is statistically the same as today's measured SST in that area (9.3°C), however, the average temperature estimate from the recent brackish phase in the Arkona Basin is higher than the measured SST from that area (9.7°C; Table 1). For the modern Baltic Sea in the Gotland Basin the SST estimate for the year 1975 AD (-0.025 cal kyr BP; 14.6°C) is ~4°C warmer than the temperature estimates for other recent sediments, and although this sediment was deposited during the modern warm period, this estimate seems too high for a mean annual temperature. In the Arkona Basin a distinct warming phase is observed from 5.41-2.67 cal kyr BP (16.1±2.0°C), which is not realistic for

a mean annual temperature estimate in this region. Since it is not also observed in the Gotland Basin OH-TEX_{86} index-derived SST record nor in any of the other SST records presented, it must be flawed for some unknown reason. In the Arkona Basin temperatures from the Ancylus Lake phase and recent brackish phase are similar to those during the Yoldia Sea phase (14.2±1.9°C) but SST estimates during the Baltic Ice Lake phase, 16.8±1.1°C, are higher (Fig. 6b). The reconstructed SSTs are statistically the same in each basin over the Holocene, although there is more variation in the Arkona Basin (Figs. 6a-b), which may be explained by the proximity of the Arkona Basin to the opening with the North Sea allowing a greater influence of allochthonous GDGTs brought in by the marine influxes and settling in the sediments.

For the portion of the record when the Baltic Sea was brackish, from c. 7.2 cal kyr BP onward, the OH-GDGT $_{Index\ 5}$, the OH-GDGT' index, and OH-TEX_{86} index temperature estimates are in good agreement and capture the major temperature fluctuations over the Holocene in the Gotland Basin (Fig. 6a), including the Medieval Climate Anomaly (MCA, from 950-1250 AD) and the Little Ice Age (LIA, from 1400-1700 AD) (Mann et al., 2009), as well as the warming trend occurring in recent times (from 1840 AD –present; Kabel et al., 2012) (Figs. 6a-b). However, the changes in SST are smaller than those observed in the TEX_{86}^{L} record (Kabel et al., 2012; Warden et al., in preparation). This may be due to the fact that the TEX_{86}^{L} index based reconstructions record summer temperatures, whereas the OH-GDGT ratios are calibrated against MAT and changes in summer SST may be larger than for annual mean SST. Due to the lower resolution in the more recent times in the Arkona Basin it is difficult to assess if these OH-GDGT based indices have captured the LIA and MCA, although, the recent warming period appears to be captured (Fig. 6b). In the Arkona Basin record the OH-GDGT' index and OH-GDGT $_{Index\ 5}$ SST estimates are in good agreement with each other. The temperature estimates are higher in the Arkona Basin record and since it is located more to the south than the Gotland Basin, it would be expected that SSTs would be slightly warmer (station 372720 is close to the Arkona Basin record and the measured mean annual SST is 9.7°C compared with 9.3°C from station 303600 in the Gotland Basin; Table 1), however, the differences in the estimated SSTs between the Gotland and Arkona basin for the recent brackish phase based on the OH-TEX_{86} index is too large (Figs. 6a-b).

For the lower salinity phases in both basins the SST estimates based on the OH-GDGT $_{Index\ 5}$, the OH-GDGT' index, and OH-TEX_{86} index are for the most part not in agreement with each other, however, the SST estimates based on the OH-GDGT $_{Index\ 5}$ during the Ancylus Lake phase for the Gotland Basin is in agreement with the MAT reconstruction from south

central Sweden (Seppä et al., 2005; Figs. 6a-b). The correlation between OH-GDGT based indices and measured SSTs increased when the lower salinity sediment samples from the northern region of the Baltic Sea basin (Bothnian Sea and Bay) were removed (Figs. 4a-d). This raises the question of whether salinity changes are affecting the distribution of OH-GDGTs and therefore the application of OH-GDGTs for SST estimates in the Baltic Sea during the Ancylus Lake phase. Therefore, it should be considered when applying the OH-GDGTs for SST reconstructions that low salinity environments may complicate their use.

Conclusions

The use of the distribution of OH-GDGTs for SST reconstructions in the Baltic Sea appears to be promising. The OH-GDGT $_{\text{Index 5}}$, the OH-GDGT' index, and OH-TEX_{86} index performed the best of the OH-GDGT based indices when reconstructing SSTs of both enrichment cultures and surface sediments samples. When these indices were applied to two sedimentary records in the Baltic Sea they resulted in reliable SST estimates for the last 7,200 years that were in agreement with each other as well as previously published data, except for the SST estimates based on the OH-TEX_{86} index in the Arkona Basin, which is perhaps due to the proximity of the North Sea allowing a greater influence of allochthonous GDGTs. It appears there is an effect of salinity when using the OH-GDGT based indices and it should be considered when applying these for paleoclimate application in low salinity environments.

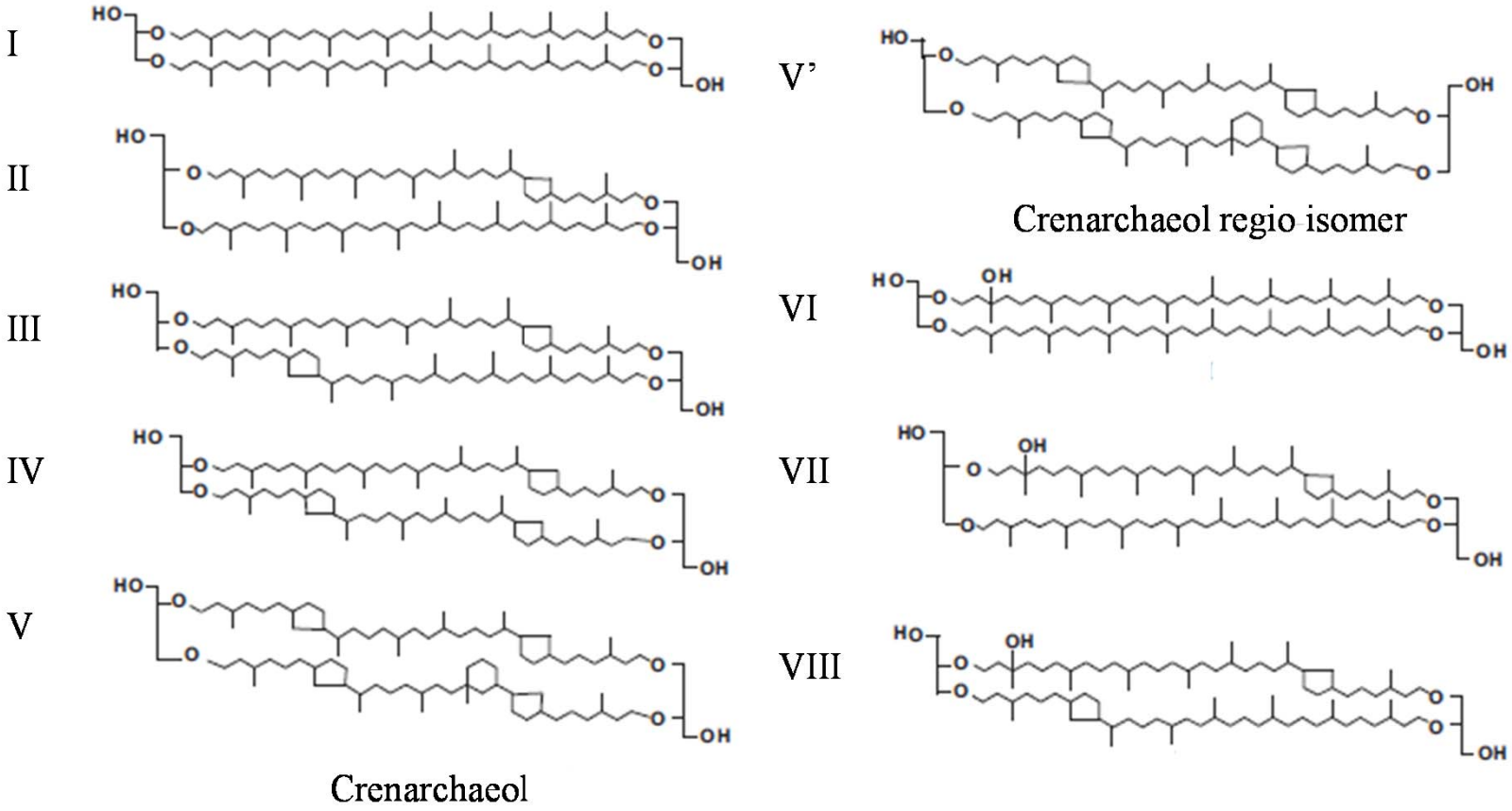

Fig. S1 Structures of the glycerol dialkyl glycerol tetraethers (GDGTs) found in the Baltic Sea sediments. GDGTs I-VI are the isoprenoid (iso)GDGTs and GDGTs VII-IX are the hydroxylated (OH-) GDGTs.

Photo by Dietmar Rüß

CHAPTER 5

Sedimentary alkenone distributions reflect salinity changes in the Baltic Sea over the Holocene

Lisa Warden, Marcel T.J. van der Meer, Matthias Moros,
and Jaap S. Sinninghe Damsté

Organic Geochemisty, 102, 30-44, 2016

Abstract

The Baltic Sea has had a complex salinity history since the last deglaciation. Here we show how distributions of alkenones and their δD values varied with past fluctuations in salinity in the Baltic Sea over the Holocene by examining a Holocene record (11.2 to 0.1 cal kyr BP) from the Arkona Basin. Major changes in the alkenone distribution, i.e. changes in the fractional abundance of the $C_{37:4}$ alkenone, the $C_{38:2}$ Et alkenones and the $C_{36:2}$ alkenone, the latter which has not been reported in the Baltic Sea previously, correlated with known changes in salinity. Both alkenone distributions and hydrogen isotopic composition suggest a shift in haptophyte species composition from lacustrine to brackish type haptophytes around 7.7-7.2 cal kyr BP, corresponding with a salinity change that occurred when the connection between the basin and the North Sea was re-established. A similar salinity change occurred in the Black Sea. Previously published alkenone distributions and their δD values from the Black Sea were used to reconstruct Holocene changes in surface water salinity and, hence, it was shown that the unusual $C_{36:2}$ alkenone dominates the alkenone distribution at salinities of 2-8 PSU. This information was used to corroborate the interpretations made about salinity changes from the data presented for the Baltic Sea. Low and variable salinity waters in the Baltic Sea over the Holocene have allowed for alkenones derived from a variable haptophyte community composition, including low salinity adapted species, hindering the use of the unsaturation ratios of long-chain alkenones for sea surface temperature reconstruction. However, these alkenone based indices are potentially useful for studying variations in salinity, regionally as well as in the past.

1. Introduction

Long chain alkenones, biolipids composed of predominantly C_{37}- C_{39} n-alkyl chains with di-, tri- or tetra unsaturations and a keto functionality at position C-2 or C-3 (de Leeuw et al., 1980; Rechka and Maxwell, 1988) are produced exclusively by only a few species of haptophyte algae in both open marine (i.e., *Emiliania huxleyi* and *Geophyrocapsa oceanica*; Volkman et al., 1980, 1995; Group III following the phylogenetic classification of Theroux et al., 2010) and coastal marine or lacustrine settings (i.e. algae of the genera *Isochrysiss, Ruttnera (*formerly *Chrysotila),* and *Tisochrysis;* Marlowe et al., 1984; Nakamura et al, 2016; Group II) and the more recently discovered 'Greenland haptophyte' species, so far exclusively found in Greenland and Alaskan lakes (D'Andrea et al., 2006; Longo et al., 2013; Group I). This latter group has a distinctly different alkenone distribution relative to alkenones produced by all other haptophytes since they all contain tri-unsaturated alkenone isomers not observed in other species (Longo et al., 2013; Dillon et al., 2016). An unusual C_{36} diunsaturated alkenone was identified by Xu et al. (2001) in Holocene sediments from the Black Sea. Coolen et al. (2009) reported its biological origin as a specific strain of *E. huxleyi* based on the analysis of fossil DNA.

Since field sampling and culture experiments demonstrated a relationship between surface water temperature and the unsaturation ratios of long-chain alkenones (Prahl and Wakeham, 1987; Müller et al., 1998), the unsaturation ratios of sedimentary alkenones have been extensively used as a paleotemperature proxy in marine settings. Two alkenone unsaturation ratios have been predominantly used in sea surface temperature (SST) reconstructions, the U^{K}_{37} (which includes the relative abundance of di-, tri- and tetra- unsaturated alkenones; Brassell et al., 1986) and the $U^{K'}_{37}$ (which excludes the tetra-unsaturated alkenone; Prahl and Wakeham, 1987). Even though this proxy has been successfully applied in marine settings, uncertainties still exist due to increasing evidence of non-thermal effects on alkenone distribution patterns such as species and strain composition (Volkman et al., 1995; Conte et al., 1998) and salinity (Chu et al., 2005; Ono et al., 2012; Chivall et al., 2014). For example, Rosell-Melé (1998) demonstrated that the amount of $C_{37:4}$ alkenone compared to the abundance of the other C_{37} alkenones ($\%C_{37:4}$) in particulate organic matter from Nordic Seas had a stronger correlation to sea surface salinity (SSS) than SST. Despite these results, the correlation between salinity and $\%C_{37:4}$ in surface water and sediment trap samples worldwide varies greatly and so there is no evidence supporting the application of a linear relationship (Sikes and Sicre, 2002), which would make the use of $\%C_{37:4}$ as a salinity proxy possible.

Alkenones are common biomarkers in marine sediments, but also occur in lake sediments (e.g. Cranwell, 1985; Volkman et al., 1988; Thiel et al., 1997; Zink et al., 2001; Chu et al., 2005; Sun et al., 2007; Randlett et al., 2014; Nelson and Sachs, 2014; Song et al., 2016) although not as widespread. In these lake settings, complications applying long chain alkenone unsaturation patterns as a temperature proxy have often been noted. Alkenone biosynthesizing haptophyte algae are much more genetically diverse in lacustrine settings than marine (e.g. Coolen et al., 2004; Theroux et al., 2010; Randlett et al., 2014) and this affects alkenone composition and has implications for lake surface temperature (LST) reconstruction since alkenone calibrations for Group I and II Isochrysidales vary substantially (e.g. Versteegh et al., 2001; Theroux et al., 2013; Nakamura et al., 2014, 2016; Longo et al., 2016). In many lakes the fractional abundance of the $C_{37:4}$ methyl ketone is much higher (up to 96% of the sum of C_{37} alkenones) than has been observed in marine settings (e.g. Chu et al., 2005; Nelson and Sachs, 2014). The predominance of the $C_{37:4}$ methyl ketone and the observed negative relationship with salinity suggested that its production may be a response to low salinity conditions (Chu et al., 2005; Song et al., 2016). Consequently, it was suggested that the long chain alkenone unsaturation ratio omitting $C_{37:4}$ ($U^{K'}_{37}$) may yield more accurate LST/SST estimations when used in lacustrine, brackish and estuarine waters. However, it is more likely that salinity influences the haptophyte composition, in turn affecting alkenone distributions, i.e. in freshwater and oligohaline lakes Group I Isochrysidales dominate and their alkenone distribution is dominated by the $C_{37:4}$ alkenone (Toney et al., 2012). Based on this finding, a new temperature index has been proposed for lacustrine, brackish and estuarine settings that includes the $C_{37:4}$ alkenone and instead excludes $C_{37:2}$ ($U^{K''}_{37}$; Zheng et al., 2016). This study suggests that the di-unsaturated alkenones play a less important role than the tri- and tetra-unsaturated alkenones in regards to regulating cell functions in accordance with temperature fluctuations in lower salinity settings.

Previous studies in brackish settings have shown that since alkenone distributions co-vary with salinity driven changes in haptophyte species composition, the use of long chain alkenones is complicated in areas with low and/or fluctuating salinity such as in the Black Sea (Coolen et al., 2009), Ace Lake in Antarctica (Coolen et al., 2004), the Baltic Sea (Rosell-Melé, 1998; Schulz et al., 2000; Blanz et al., 2005) and the North Atlantic and Nordic Seas (Rosell-Melé, 1998). In Ace Lake, Coolen et al. (2004) demonstrated that as lake chemistry changed over time, particularly the salinity as it evolved from a freshwater basin to a marine inlet, the alkenone distributions changed reflecting differences in the haptophyte population as evident from palaeogenetic signatures. Similarly, in the Black Sea, Coolen et al. (2009)

showed that as salinity increased over the Holocene in the basin that the haptophyte composition changed as well resulting in erroneous alkenone-derived SST estimates at times.

Culture experiments indicate that alkenone distribution patterns can vary with changing salinity and that this should be taken into account when using the alkenone unsaturation indices for SST reconstructions (Chu et al., 2005; Ono et al., 2012; Chivall et al., 2014). The results from Chivall et al. (2014) indicate salinity has an effect on alkenone distributions, but that other factors such as growth phase and species composition also play a role in whether the long chain alkenone distributions are affected by salinity. This culture study found a positive correlation between $\%C_{37:4}$ and salinity, however, they found growth phase has a larger effect on the $\%C_{37:4}$ than salinity. Further complicating the use of long chain alkenones for SST and LST reconstructions, Ono et al. (2012) established using culture experiments that salinity had an effect on alkenone unsaturation ratios at 20°C, but not at 15°C.

In addition to looking at alkenone distributions to infer salinity changes, culture studies have shown the hydrogen isotopic composition (δD) of long chain alkenones strongly depends on salinity as well in batch culture (Schouten et al., 2005) and recently also in continuous culture where salinity was the environmental parameter that was changed (Sachs et al., 2016). M'boule et al. (2014) also found a strong linear relationship between δD and salinity in culture experiments involving both *I. galbana* (a coastal species) and *E. huxleyi* (an open ocean species), suggesting that δD of alkenones might indeed be used to reconstruct relative shifts in paleosalinity. However, coastal species, such as *I. galbana* and *Ruttnera (Chrysotila) lamellosa*, have been observed to fractionate almost 100‰ less against deuterium than more open marine species, such as *E. huleyi* and *G. oceanica*, in culture (Schouten et al., 2005; Chivall et al., 2014; M'boule et al., 2014). The δD of sedimentary alkenones might therefore also be indicative of specific alkenone producing haptophytes.

The present day Baltic Sea has a large range in salinities (~3.5-32 PSU), with fresher water in the northeastern part of the basin (including the Gulf of Bothnia and Gulf of Finland) and saltier water closer to the connection to the North Sea, making it an interesting site to study present-day salinity effects on alkenone production. Schulz et al. (2000) demonstrated that alkenone unsaturation ratios in surface sediments of the Baltic Sea have a low correlation to mean annual SST and instead primarily reflect salinity changes. The authors postulate that lower salinity in parts of the basin causes salinity stress induced changes in alkenone biosynthesis. This, together with the production of alkenones by haptophytes adapted to lower salinities, results in distinct alkenone patterns with lower salinity regions of the basin having patterns more characteristic of freshwater haptophytes or a mixture of freshwater and marine

haptophytes, and saltier regions having distributions that resemble more marine haptophyte derived alkenones. Blanz et al. (2005) also reported that in the Baltic Sea salinity-induced stress on *E. huxleyi* could alter the biosynthesis of alkenones, thus affecting the use of the alkenone unsaturation ratios as a proxy for SSTs. The absence of C_{38} methyl ketones observed in lower salinity water masses in the Baltic Sea has been observed in Chinese Lakes as well (Song et al., 2016). This may be an indication for the presence of brackish alkenone producers of the Group II Isochrysidales. However, it should be noted that the freshwater and oligohaline species of the Group I Isochrysidales do produce C_{38} methyl ketones like *E. huxleyi* (Toney et al., 2012; Zheng et al., 2016).

Here we determine how alkenone distributions and concentrations, along with the δD of alkenones, varied with past changes in salinity in the Baltic Sea over the Holocene. Not only does salinity vary regionally over the Baltic Sea basin today, but the Baltic Sea also has had a complex salinity history since the last deglaciation and has gone through two fresh water and two brackish water stages (see Section 2.1 for more details). In this study we examined a Holocene record from the Arkona Basin to determine if changes in alkenone distribution patterns that exist today and correlate with salinity around the basin also existed in the past and co-varied with historical salinity changes.

2. Methods

2.1. Historical setting of the Baltic Sea and description of the study site

The Baltic Sea (Fig. 1) is the world's largest brackish body of water with an area of about 377,000 km^2 that is partitioned into multiple sub-basins. The Baltic is almost entirely enclosed by land with a large freshwater contribution (including precipitation) of 660 km^3 yr^{-1} from a drainage basin that is 1.6 million km^2 (Björck, 1995). An inflow of 475 km^3 yr^{-1} of saltwater pours in through the only connection to the North Sea, the narrow Straits of Denmark (Tikkanen and Oksanen, 2002). The Baltic Sea is a fairly shallow basin and on average only about 54 m deep. The salinity varies greatly in the Baltic Sea ranging from ~3.5 PSU in the north to ~8 PSU in the Baltic proper and ~32 PSU in the region where the Baltic connects to the North Sea. A permanent halocline exists at about 13-15 m depth, separating a relatively fresh surface and saline bottom waters.

The development of the Baltic Sea since the last deglaciation has been the focus of many studies in the last decades (Winterhalter, 1992; Björck, 1995; Jensen, 1995, Jensen et al., 1999; Andrén et al., 2000). Reasons for such intense scientific interest include the shifting bathymetry, dynamic hydrology and the resulting fluctuating salinity of the Baltic Sea over

the Holocene as the basin went through several different phases. Following deglaciation and before its present state, the Baltic Sea transformed from the freshwater Baltic Ice Lake (c. 12.6-10.3 ka BP) to the slightly brackish Yoldia Sea (c. 10.3-9.5 ka BP) into the freshwater Ancylus Lake (c. 9.5-8.0 ka BP) and then into the brackish Littorina Sea (c. 8.0-3.0 kyr BP) and subsequently into the Post-Littorina Sea/modern Baltic Sea (Winterhalter, 1992; Björck, 1995; Andrén et al., 2000). The Baltic Ice Lake formed as large areas of the southern Baltic basin became ice free. Rapid deglaciation resulted in the uplift of the seabed, bringing the connection of the basin with the North Sea above sea level and causing a large influx of fresh melt-water into the system (Björck, 1995). A climatic cooling resulted in less meltwater and the gradually receding ice sheet allowed drainage of the Baltic Ice Lake to occur, lowering the water level and resulting in a short period of seawater ingression, which characterized the very slightly brackish Yolidia Sea (Björck et al., 1995; Jensen, 1995). Continued isostatic rebound caused the basin to be once again cut off from the ocean and resulted in the Ancylus Lake (Jensen et al., 1999). Then, at around 8,000 years ago, eustatic sea level rise re-opened the connection with the North Sea through the Danish Straits allowing salt water to flow into the Ancylus Lake and transforming it into the brackish Littorina Sea (Winterhalter, 1992). The Ancylus Lake/Littorina Sea transition is a complex period characterized by different phases of brackish-water pulses, initially weak and eventually resulting in fully established brackish conditions (15-20‰ in the Baltic proper; Hyvärinen et al., 1988) only after ~2,000 years (Andren et al., 2000b). The Littorina Sea phase, which lasted from ~8,000-3,000 BP, is characterized by a warmer climate and thought to reflect the most marine-like conditions in the Baltic Sea since deglaciation (Andren et al., 2000b). The Post-Littorina Sea/modern Baltic Sea are a continuation of the Littorina Sea, but with a salinity thought to be almost half (7-8‰ in the Baltic proper; Hyvärinen et al., 1988) that of the Littorina Sea (Punning et al., 1988).

2.2. Sampling

Two sediment cores were retrieved from the Arkona Basin, which extends from the Bornholm Basin to the Danish Isles of Falster and Zealand (Fig. 1; Table 1). This basin represents a boundary between the Straits of Denmark, where high salinity water flows in, and the lower salinity Baltic Sea basin. The total discharge of brackish water from the basin is on the order of 950 km^3/yr (Björck, 1995). Both sediment cores were 12 m long and collected using a gravity corer on the R/V "Maria S. Merian" in April of 2006. Sediment core 318310 was recovered at 46 m water depth at 54°50.34'N and 13°32.03'E and core 318340 was collected nearby at 54°54.77'N and 13°41.44'E at 47 m water depth.

Table 1 Alkenone concentrations and distributions in Baltic Sea sediments

Site	Depth (cm)	Age (cal kyr BP)	Phase[a]	Summed concentration (µg g TOC)	Fractional abundance							
					$C_{36:2}$ Me	$C_{37:4}$ Me	$C_{37:3}$ Me	$C_{37:2}$ Me	$C_{38:3}$ Et	$C_{38:3}$ Me	$C_{38:2}$ Et	$C_{38:2}$ Me
Skagerrak (EMB0461 -10)	0-1	n/d	n.a.	n.d.	0	0.01	0.26	0.2	0.13	0.14	0.2	0.07
Skagerrak (EMB0461 -20)	0-1	n/d	n.a.	n.d.	0	0.01	0.27	0.19	0.13	0.14	0.2	0.07
Arkona (core 318310)	20.0	0.1	PS/MB	24	0.13	0.01	0.18	0.17	0.14	0.07	0.24	0.06
	50.0	0.4	PS/MB	32	0.09	0.03	0.23	0.22	0.09	0.09	0.18	0.07
	100.0	0.9	PS/MB (MCA)	156	0.05	0.00	0.10	0.26	0.07	0.05	0.37	0.10
	200.0	1.8	PS/MB	17	0.09	0.02	0.23	0.20	0.12	0.09	0.20	0.06
	300.0	2.7	PS/MB	25	0.11	0.02	0.24	0.20	0.09	0.10	0.17	0.07
	400.0	3.7	LS	2.6	0.56	0.03	0.10	0.05	0.07	0.02	0.09	0.07
	500.0	5.4	LS	2.9	0.57	0.02	0.09	0.06	0.06	0.02	0.11	0.07
	600.0	7.1	LS	5.6	0.38	0.03	0.22	0.13	0.08	0.02	0.11	0.04
	625.0	9.0	AL	3.6	0.00	0.09	0.38	0.10	0.21	0.08	0.11	0.02
	642.5	10.2	AL	3.7	0.01	0.10	0.35	0.09	0.24	0.08	0.10	0.04
Arkona (core 318340)	400.5	7.3	AL/LS TP	16	0.07	0.02	0.23	0.06	0.31	0.02	0.27	0.02
	420.5	7.4	AL/LS TP	42	0.01	0.03	0.49	0.13	0.15	0.02	0.17	0.01
	440.5	7.5	AL/LS TP	6.0	0.02	0.13	0.38	0.11	0.15	0.10	0.09	0.02
	464.5	7.6	AL/LS TP	4.8	0.00	0.10	0.37	0.10	0.11	0.06	0.16	0.10
	480.5	7.7	AL/LS TP	6.9	0.11	0.08	0.28	0.11	0.22	0.05	0.12	0.02
	500.5	8.0	AL	8.1	0.04	0.09	0.37	0.10	0.20	0.07	0.12	0.02
	520.5	8.5	AL	0.0	n.a.	n.a.	n.a.	n.a.	n.a.	n.a.	n.a.	n.a.
	540.5	8.9	AL	15	0.00	0.09	0.35	0.11	0.19	0.11	0.13	0.02
	584.5	9.9	AL	55	0.00	0.04	0.36	0.14	0.25	0.07	0.11	0.03
	643.5	10.3	AL	n.d.	n.a.	n.a.	n.a.	n.a.	n.a.	n.a.	n.a.	n.a.
	705.5	10.5	AL	n.d.	0.00	0.04	0.24	0.12	0.27	0.05	0.25	0.03
	750.5	10.6	AL	n.d.	0.01	0.03	0.30	0.09	0.33	0.02	0.21	0.01
	800.5	10.9	YS	n.d.	n.a.	n.a.	n.a.	n.a.	n.a.	n.a.	n.a.	n.a.
	840.5	11.2	YS	n.d.	n.a.	n.a.	n.a.	n.a.	n.a.	n.a.	n.a.	n.a.

n.a. = not applicable; n.d. = not determined because TOC content for these sediments was not measured [a] PS/MB = post Littorina/modern Baltic, MCA = Medieval Climatic Anomaly, LS = Littorina Sea, TP = transitional phase, AL = Ancylus Lake, YS = Yoldia Sea

Table 2 Alkenone fractional abundances and alkenone based indices as well as the δD values of alkenones used in this study to examine salinity changes in the Baltic Sea sediments through time.

Site	Depth (cm)	Phase[a]	$\%C_{37:4}$	Summed fractional abundance C_{38} Et alkenones	UK'_{37}	δD $C_{36:2}$ alkenones	δD C_{37} alkenones	δD C_{38} alkenones
Skagerrak (EMB0461 -10)	0-1		1.9	0.3	0.44	n.a.	-175.6	-184.2
Skagerrak (EMB0461 -20)	0-1		1.8	0.3	0.41	n.a.	-174.9	-183.7
Arkona (core 318310)	20	PS/MB	3.8	0.4	0.48	-173.4	-207.5	-216.8
	50	PS/MB	5.5	0.3	0.48	n.d.	n.d.	n.d.
	100	PS/MB (MCA)	0.7	0.4	0.72	n.a.	-214.5	-220.5
	200	PS/MB	3.5	0.3	0.47	-166.1	-207.4	-216.4
	300	PS/MB	5.2	0.3	0.46	-169	-205.4	-209.2
	400	LS	0.1	0.2	0.35	n.d.	n.d.	n.d.
	500	LS	13.6	0.2	0.41	n.d.	n.d.	n.d.
	600	LS	8.9	0.2	0.36	-182.4	-168.7	-170.3
	625	AL	16.3	0.3	0.21	n.d.	n.d.	n.d.
	642.5	AL	18.2	0.3	0.21	n.d.	n.d.	n.d.
Arkona (core 318340)	400.5	AL/LS TP	7.5	0.6	0.22	n.d.	n.d.	n.d.
	420.5	AL/LS TP	4.6	0.3	0.22	n.d.	n.d.	n.d.
	440.5	AL/LS TP	20.4	0.2	0.23	n.d.	n.d.	n.d.
	464.5	AL/LS TP	17.8	0.3	0.21	n.d.	n.d.	n.d.
	480.5	AL/LS TP	17.1	0.3	0.28	n.d.	n.d.	n.d.
	500.5	AL	15.4	0.3	0.21	n.d.	n.d.	n.d.
	540.5	AL	15.9	0.3	0.25	n.d.	n.d.	n.d.
	584.5	AL	7.5	0.4	0.28	n.d.	n.d.	n.d.
	705.5	AL	9.1	0.5	0.32	n.d.	n.d.	n.d.
	750.5	AL	6.7	0.5	0.22	n.d.	n.d.	n.d.

[a] PL/MB = post Littorina/modern Baltic, MCA = , LS = Littorina Sea, TP = transitional phase, AL = Ancylus Lake

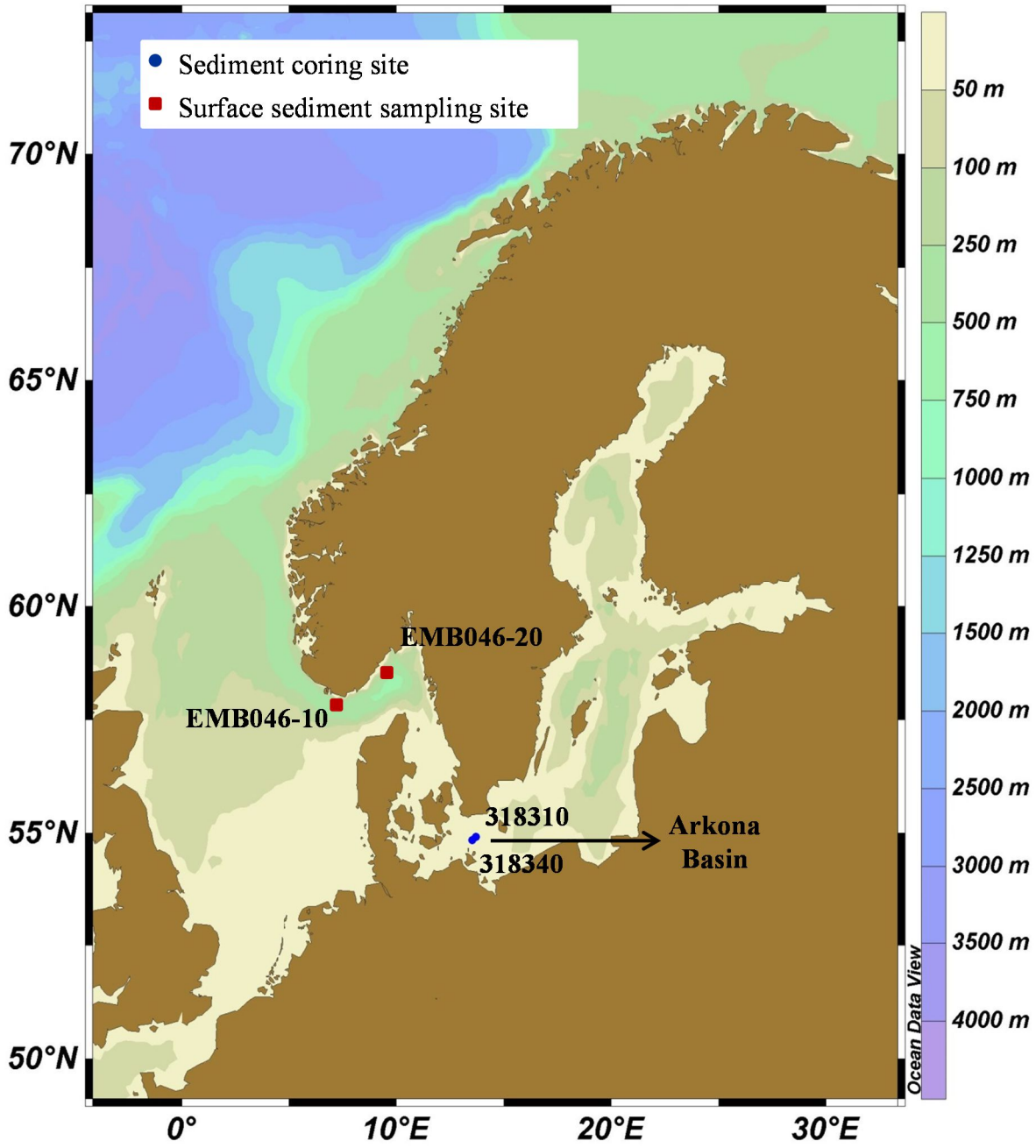

Fig. 1 A map of the Baltic Sea region and sampling sites. The sediment coring sites 318310 and 318340 in the Arkona Basin are designated by blue circles and the two stations in the Skagerrak where surface sediment samples were collected are indicated by red squares.

Two surface sediment samples from the Skagerrak obtained using a multi-corer provided a marine end member for comparison with our Baltic Sea sediment core samples. The surface sediment samples were collected during R/V "Elisabeth Mann-Borgese" cruise EMB046 in May 2013. The sampling site for EMB046-10 was positioned at 57°49.74′N and 07°17.66′E from 457 m water depth. Site EMB046-20 was situated a bit to the east of EMB046-10 at 58°31.60′N and 09°29.09′E from 532 m water depth.

2.3. Loss on ignition (LOI)

The LOI was determined by ashing freeze-dried sediments at 550°C for 3 h. The resulting mass difference was then calculated in wt.%. Previously, it was demonstrated that LOI provides an accurate estimate of the total organic carbon content of the sediments in the Baltic Sea (Leipe et al., 2011). In order to obtain estimates for the total organic carbon (TOC; %) content to normalize the concentration of ketones in the sediments, LOI values were divided by 2.5 (i.e. assuming that the organic matter contains on average 40% C; Dean, 1974).

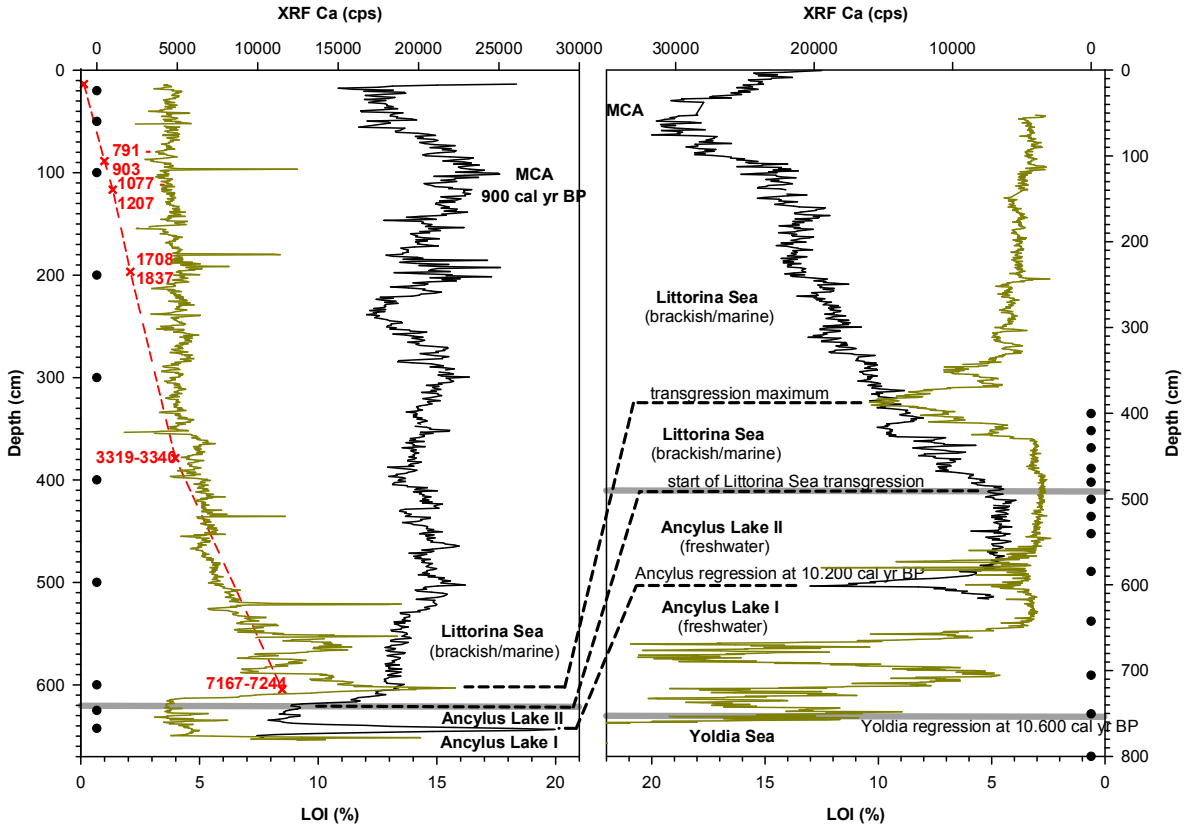

Fig. 2 Correlation of sediment cores 318310 (left panel) and 318340 (right panel) using Ca data obtained from XRF analysis (cps; designated by the gold line) and LOI (wt%; designated by the black line). The red numbers indicate the radiocarbon dates (in cal yr BP) of carbonate fossils from specific horizons in core 318310. The blue lines indicate tie points used for correlating both cores (see text). The closed circles along the depth axes indicate the depths of the sediments analyzed for alkenones in this study.

2.4. X-ray fluorescence (XRF) core scanning

XRF elemental scanning of sediment cores 318310 and 318340 was performed with an Avaatech XRF scanner (Avaatech, n.d.) at a resolution of 0.5 cm.

2.5. Correlation of sediment cores and age model

Sediment cores 318310 and 318340 were correlated to each other on the basis of LOI and XRF-Ca records (Fig. 2). The transition of the Ancylus Lake phase to the Littorina Sea phase is marked by a substantial increase in the TOC content, coinciding with color change of the sediment (e.g. Moros et al., 2002; Rößler et al., 2011). Just after the large increase in TOC (here reflected in the LOI record), there is a maximum in the carbonate content (here reflected in the maximum in the elemental XRF- Ca record) (Fig. 2), which is caused by the occurrence and preservation of benthic foraminifera (Moros et al., 2002; Rößler et al., 2011). The Ancylus Lake regression is also characterized by a clear peak in the LOI (TC) records, which can be used for correlation purposes (Fig. 2). The transitions, Baltic Ice Lake/Yoldia Sea and Yoldia Sea/Ancylus Lake are revealed by marked changes in the elemental XRF-Ca (carbonate) and bulk density records (Fig. 2; see Moros et al., 2002), and by basin-wide traceable sandy layers (Moros et al., 2002).

The age model for sediment core 318310 is based on a previous AMS^{14}C date (7.2 cal kyr BP) on *Mytilus edulis* close to the base of the Littorina phase (Rößler et al., 2011) and five additional dates on mollusc shells (Fig. 2). The age model of the section of sediment core 318340 that was studied (400-840 cm) is based on the carbonate maximum at 380 cm (7.2 cal kyr BP; Moros et al., 2002; Rößler et al., 2011). The start of the Ancylus Lake/Littorina Sea transitional phase at 7.7 cal. kyr BP (unpublished results) is revealed by the increase in the LOI record at 485 cm, and the Ancylus Lake regression at 10.2 cal kyr BP is denoted by the sharp peak in the LOI record (sandy layer; Moros et al., 2002) at 600 cm. The boundary between the Yoldia Sea phase and the Ancylus Lake phase (10.6 cal kyr BP; Moros et al., 2002) at 768 cm, and the boundary between the Baltic Ice Sea and Yoldia Sea phases (11.6 cal. kyr BP; Moros et al., 2002) at 895 cm.

2.6. Lipid extraction and analysis

The sediments were freeze dried and ground and homogenized by mortar and pestle for extraction. In general, 1-3 g of sediment was extracted using a Dionex^{TM} accelerated solvent extractor with dichloromethane/methanol (9:1; v/v) as extraction solvent. The total lipid extract was dried over a Na_2SO_4 column and then separated into three fractions using Al_2O_3 column chromatography: apolar (eluted with 9:1 v/v hexane/DCM), ketone (1:1 v/v hexane/DCM), and polar (1:1 v/v DCM/MeOH) fractions. The ketone fraction was then base hydrolyzed by refluxing the dry fraction in a 1 N KOH in MeOH solution for 1 h after which the pH was adjusted using a 2 N HCL/MeOH solution. DCM was added and the solution was

washed twice with DCM. The DCM layers were removed and combined to be dried over a Na_2SO_4 column. After the addition of a nonadecan-10-one internal standard, the alkenone fraction was analyzed using gas chromatography (GC) with an Agilent 6890 instrument equipped with an Agilent CP-Sil 5 CB column (50 m x 0.32 i.d.; 0.12 µm film thickness) and a temperature program from 70°C increasing at 20°C/min to 200°C and then at 3°C/min to 320°C where it remained stable for 44 min. Alkenones were identified by GC-mass spectrometry (GC-MS), including the $C_{36:2}$ alkenone, using an Agilent 7890A GC instrument equipped with a Agilent 5975C VL mass selective detector (MSD) and by comparing relative retention times with those of known alkenones of a culture of *E. huxleyi*. Peak areas were used to calculate alkenone unsaturation indices and alkenone concentrations were determined based on peak responses relative to the nonadecan-10-one internal standard.

2.7. Compound specific hydrogen isotope compositions

Alkenone hydrogen isotope analyses were carried out on a subset of the samples, i.e. those containing sufficient amounts of alkenones, on a Thermo Scientific DELTA$^+$ xl GC/TC/irMS. The temperature conditions of the GC increased from 70 to 145˚C at 20˚C min^{-1}, then at 8˚C min^{-1} to 200˚C and to 320˚C at 4˚C min^{-1}, at which it was held isothermal for 20 min using an Agilent CP Sil-5 column (25 m x 0.32 mm) with a film thickness of 0.4 µm and helium as carrier gas at 1 ml min^{-1} (constant flow). The high temperature conversion reactor was set at a temperature of 1425°C. The H_3^+ correction factor was determined daily and was constant at 5.6±0.2 before and 3.8±0.1 after a scheduled power outage and retuning of the irm. A set of standard n-alkanes with known isotopic composition (Mixture B prepared by Arndt Schimmelmann, University of Indiana) was analyzed daily prior to analyzing samples in order to monitor the system performance. Samples were only analyzed when the alkanes in Mix B had an average deviation from their off-line determined value of <5‰. Squalane was co-injected as an internal standard with each sample to monitor the accuracy of the alkenone isotope values. The δD of long chain C_{37} alkenones were measured as the combined C_{37} alkenones ($\delta D_{alkenone}$) (van der Meer et al., 2013) and the same applies to the C_{38} alkenones. The squalane standard yielded an average $\delta D_{alkenone}$ value of -160.7±2.7, which is stable but relatively enriched in D compared to its offline determined δD value of -170 ‰, potentially due to co-eluting compounds in this sample set.

2.8. Calculation of alkenone based proxies

$\%C_{37:4}$ is the contribution of the tetra-unsaturated 37-carbon methyl alkenone ($C_{37:4}$) to total C_{37} alkenone concentrations and calculated according to Rosell-Melé (1998):

$$\%C_{37:4} = C_{37:4} / (C_{37:2} + C_{37:3} + C_{37:4}) \times 100 \quad (1)$$

The U^{K}_{37} index represents the relative abundance of the diunsaturated ($C_{37:2}$), triunsatured ($C_{37:3}$), and tetraunsaturated ($C_{37:4}$) methyl ketones (Brassell et al., 1986). Later, the tetraunsaturated methyl ketone ($C_{37:4}$) was removed from the equation because this compound was rarely found in open-sea sediments or suspended water column particles and the equation was modified by Prahl and Wakeham (1987):

$$U^{K'}_{37} = C_{37:2} / (C_{37:2} + C_{37:3}) \quad (2)$$

2.9. Statistical analysis

Utilizing the R software package for statistical analysis, principle component analysis (PCA) based on the correlation matrix was executed on the fractional abundances of the eight alkenones quantified in the sediments studied. Four sediment samples from sediment core 318340 with no alkenones present were omitted from the PCA.

3. Results

3.1. Phases of the Baltic Sea covered in the Arkona Basin record

The XRF (Ca) and LOI (TC) data were used to distinguish different phases captured by each sediment core in this study (Fig. 2) and to correlate the two sediment cores (see methods). The sedimentary record for sediment core 318310 covers the upper section of the freshwater Ancylus Lake stage starting at 10.2 cal kyr BP (642.5 cm), but mostly spans the brackish phase of the basin beginning from 7.1 cal kyr BP (600-20 cm) (Fig. 2a). From sediment core 318310 we studied eight sediment samples representing the brackish phase including the Littorina Sea and Post-Littorina Sea/modern Baltic Sea stage and two samples representing the Ancylus Lake stage (Fig. 2a; Table 1). To obtain more information on alkenone occurrence and distribution during the Ancylus Lake stage, we also studied samples from another sediment core. This core (318340) includes the Yoldia Sea stage (11.2-10.6 cal kyr BP; 840.5-780.5 cm), the Ancylus Lake stage (10.6-7.8 cal kyr BP; 750.5-500.5 cm), and the Littorina Sea and Post-Littorina Sea/modern Baltic Sea stage (7.2-0.1 cal kyr BP; 400.5-20 cm) (Fig. 2b). We analyzed 14 sediment samples from this core spanning depths 840.5-400.5 cm (Fig. 2b; Table 1).

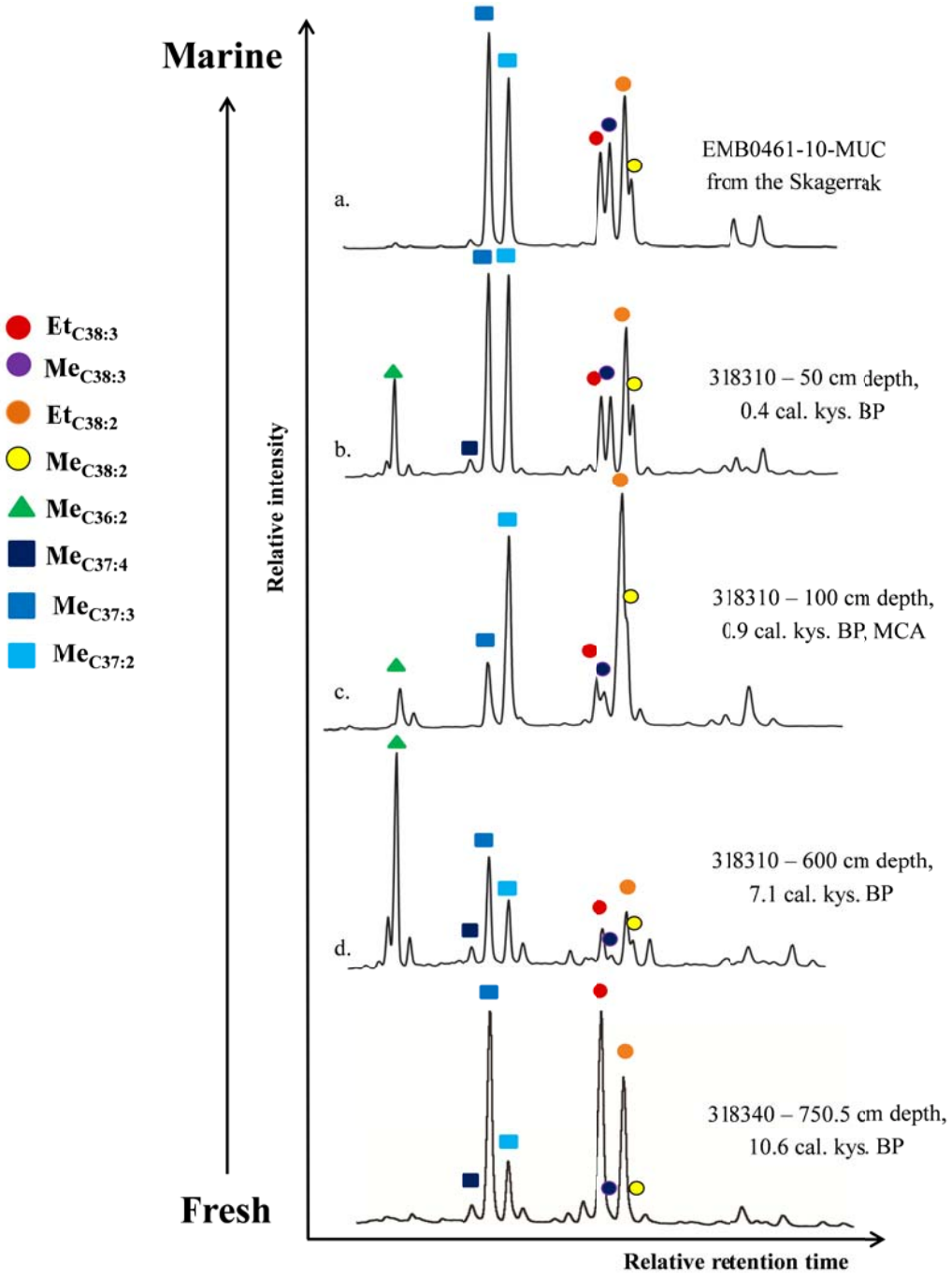

Fig. 3 Partial GC-FID chromatograms displaying alkenone distribution from various sediment horizons. (**a**) Sample EMB0461-10-MUC from the Skagerrak shows a typical marine distribution, (**b**) a sediment interval from 0.4 cal kyr BP (50 cm depth from core 318310) is from a brackish period and displays a distribution similar to the marine distribution except with the additional presence of the $C_{36:2}$ alkenone, (**c**) the sediment interval from 0.9 cal kyr BP (100 cm depth from core 318310) has a different distribution from the other depths in both cores with no $C_{37:4}$ alkenone, $C_{37:3} < C_{37:2}$, and a lower contribution of the $C_{36:2}$ alkenone relative to the C_{37} alkenones, (**d**) the sediment interval from 7.1 cal kyr BP (600 cm depth from core 318310) is from the period immediately following the Ancylus Lake/Littorina Sea transition and has an alkenone distribution characteristic of lower salinity haptophytes. Note the high relative abundance of the $C_{36:2}$ alkenone at this time. The alkenones are color coded according to the legend with circles designating the C_{38} alkenones, triangles signifying the $C_{36:2}$ alkenone, and squares indicating the C_{37} alkenones.

freshwater portion of the record (14±21 µg/g C; Table 1). In the latter case, there were also sediment horizons that did not contain detectable concentrations of alkenones. In the sediments of the Yoldia Sea phase no alkenones were detected (Table 1). Fig. 3 shows some typical alkenone distributions from sediment sample set. Alkenones are comprised of the more common $C_{37:2}$, $C_{37:3}$, and $C_{37:4}$ methyl (Me) ketones, $C_{38:2}$ and $C_{38:3}$ methyl (Me) and ethyl (Et) ketones, and the uncommon $C_{36:2}$ Me ketone. This latter alkenone has not been previously reported in sediments of the Baltic Sea. It is especially relatively abundant in sediments deposited during the Littorina Sea period. Skagerrak surface sediments (Fig. 1) were analyzed as a marine end member for comparison with the results obtained from the Arkona Basin record. We did not detect the presence of the $C_{36:2}$ alkenone in the Skagerrak sediments (Fig. 3a; Table 1). In sediment core 318310 a large difference in the relative abundance of C_{36}, C_{37} and C_{38} alkenones is observed from 600 cm depth (c. 7.1 cal kyr BP; Fig. 3d), which is close to the Ancylus Lake/Littorina Sea transitional phase, to more recent sediments from the brackish phase of the Baltic Sea, i.e. at 100 cm (0.9 cal kyr, BP) and 50 cm (0.4 cal kyr BP) depth (Fig. 3b-c). For the Skagerrak surface sediments the alkenone distribution is representative of a more open ocean setting (Fig. 3a). The alkenone distribution at 50 cm depth (Fig. 3b) is more similar to that of the Skagerrak sample than any of the other alkenone distributions shown (Fig. 3d), however, there are still a few differences between the two, such as the absence of the $C_{36:2}$ alkenone and the lower relative abundance of $C_{37:4}$ Me in the Skagerrak sediments.

For a statistical evaluation of alkenone distribution changes, PCA was performed on the distributions of C_{36}, C_{37} and C_{38} alkenones in the different sediments studied. Most of the variation is explained by principle component 1 (PC1; expressing 41% of the variance), which is related to the degree of unsaturation of the alkenones with the most unsaturated alkenones scoring negatively on PC1 (Fig. 4a). This is confirmed by the good correlation ($r^2 = 0.86$) of the score on PC1 with $U^{K'}_{37}$ (Fig. 4e). The variation in PC2 (27%) appears to be mostly explained by the fractional abundance of the $C_{36:2}$ alkenone, which scores negatively on PC2 (Fig. 4a). Indeed, the score on PC2 significantly ($r^2 = 0.77$) negatively correlates with the fractional abundance of the $C_{36:2}$ alkenone (Fig. 4f). PC3 explains 18% of the variance with the C_{38} Et ketones scoring negatively on PC3 (Fig. 4c). PC3 correlates significantly ($r^2 = 0.77$) negatively with the summed fractional abundance of the $C_{38:3}$ and $C_{38:2}$ Et ketones (Fig. 4g).

Most sediments score between -1 and +1 on PC2, however, the Skagerrak sediments plot more positively (ca. 2.0) and sediments from the core 318310 from the Littorina Sea phase (sediment core depths 400, 500 and 600 cm) plot more negatively on PC2 (ca. -3.2)

(Fig. 4b). Fig. 5a shows the scores of PC1-3 plotted as a function of age. This reveals that the score on PC1 is mostly negative for sediments older than 7.2 cal kyr BP and is mostly positive during the more recent phases of the Baltic Sea (after 7.2 cal kyr BP) (Fig. 5a). The score on PC2 consistently plots positively throughout the combined record from the Arkona Basin except for the sediment depths that correspond to the Littorina Sea phase (sediment core depths 400-600 cm from core 318310, which spans 7.1-3.7 cal kyr BP) and the end of the Ancylus Lake phase (sediment core depth 400.5 cm in core 318340, which spans 7.1-3.7cal kyr BP; Fig. 5a-b (Fig. 5a). Two other core 318340 samples that plot slightly negatively for PC2 are depths 480.5 cm (7.7 cal kyr BP) and 750.5 cm (10.6 cal kyr BP) (Fig. 5a). PC3 scores mostly between -1 and 1 throughout the sediment record and for the Skagerrak samples, however, some samples that fall within the Ancylus Lake phase plot outside of this range as does sediment sample 100 cm from record 318310 (0.9 cal kyr BP; Figs. 4d and 5a).

3.3. δD of alkenones

We also determined δD values of alkenones on a subset of the samples from sediment core 318310 (Table 2), which can be an indicator of environmental conditions, mainly salinity and potentially haptophyte species composition (Schouten et al., 2005; van der Meer et al., 2008, 2015; Chivall et al., 2014; M'boule et al., 2014). The surface sediment samples from the Skagerrak have similar δD values for the C_{37} and C_{38} alkenones that fall between -175 and -185‰ (Fig. 6; Table 2). In the Arkona Basin the C_{37} and C_{38} alkenones have lower δD values during the more recent brackish phase going back to about 2.7 cal kyr BP, (-212.2±5.5‰) (Fig. 6; Table 2). However, at the base of the Littorina Sea phase (7.1 cal kyr BP, 600 cm sediment depth from sediment core 318310), the δD values for C_{37} (-182.4‰) and C_{38} alkenones (-170.3‰) are much higher and, in contrast to the other samples, the C_{37} are more depleted in D than the C_{38} alkenones. The obtained δD values of the $C_{36:2}$ alkenone deposited during the brackish portion of the record in the Arkona Basin are enriched in D relative to the C_{37} and C_{38} alkenones from the same samples, but similar to those of the C_{37} and C_{38} alkenones encountered in the modern day Skagerrak (-169.3±3.0‰). Just after the Ancylus Lake/Littorina Sea transition, the δD values of the $C_{36:2}$ alkenone (-168.7‰) is similar to that of the C_{38} alkenones (-170.3‰; Fig. 6; Table 2).

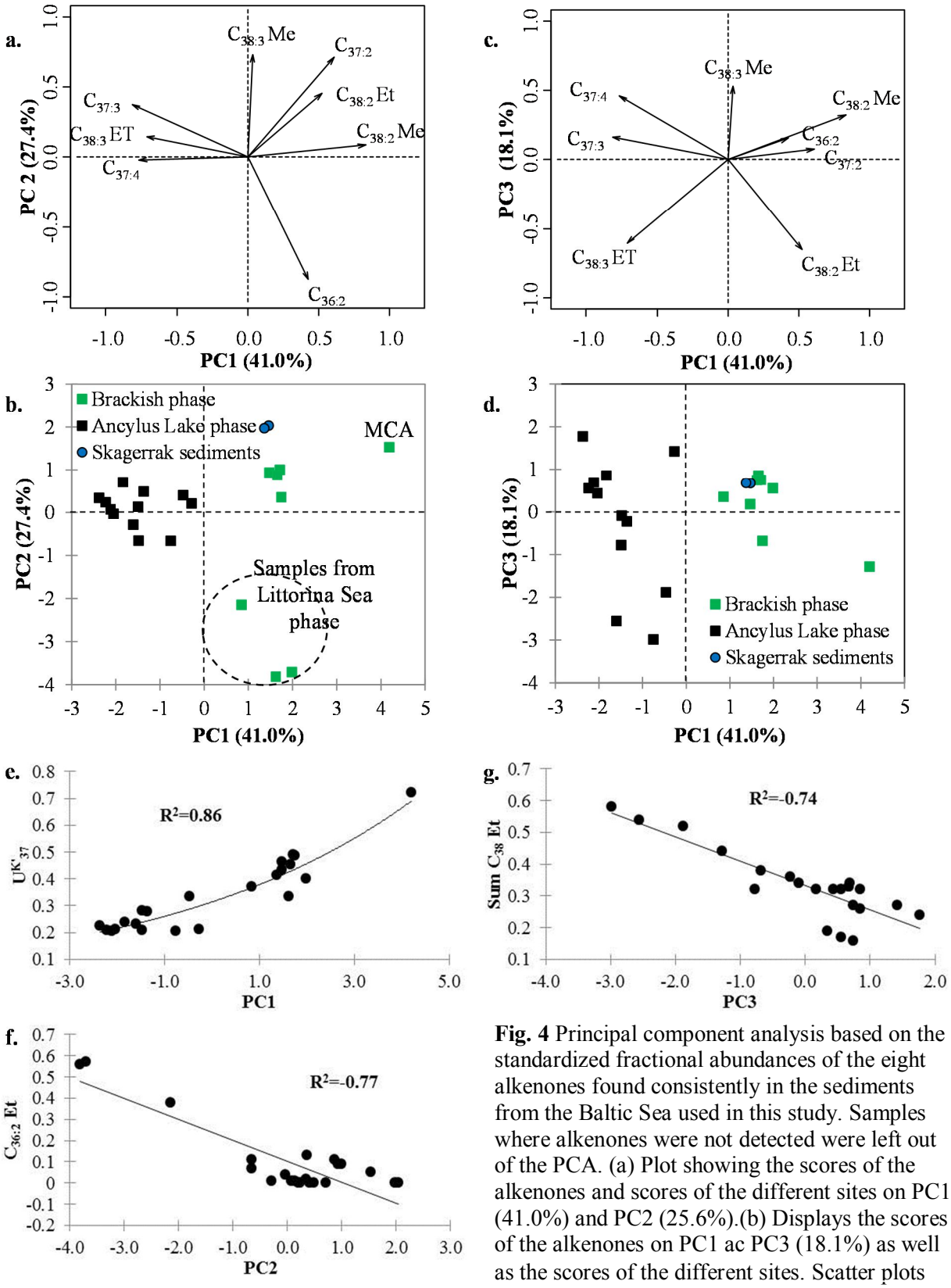

Fig. 4 Principal component analysis based on the standardized fractional abundances of the eight alkenones found consistently in the sediments from the Baltic Sea used in this study. Samples where alkenones were not detected were left out of the PCA. (a) Plot showing the scores of the alkenones and scores of the different sites on PC1 (41.0%) and PC2 (25.6%).(b) Displays the scores of the alkenones on PC1 ac PC3 (18.1%) as well as the scores of the different sites. Scatter plots displaying the correlation of (c) PC1 with $U^{K'}_{37}$ (R^2=0.86) (d) negative correlation of PC2 and $C_{36:2}$ Et (R^2=0.77) (e) and negative correlation with PC3 and the sum of the C_{38} Et (R^2=0.74).

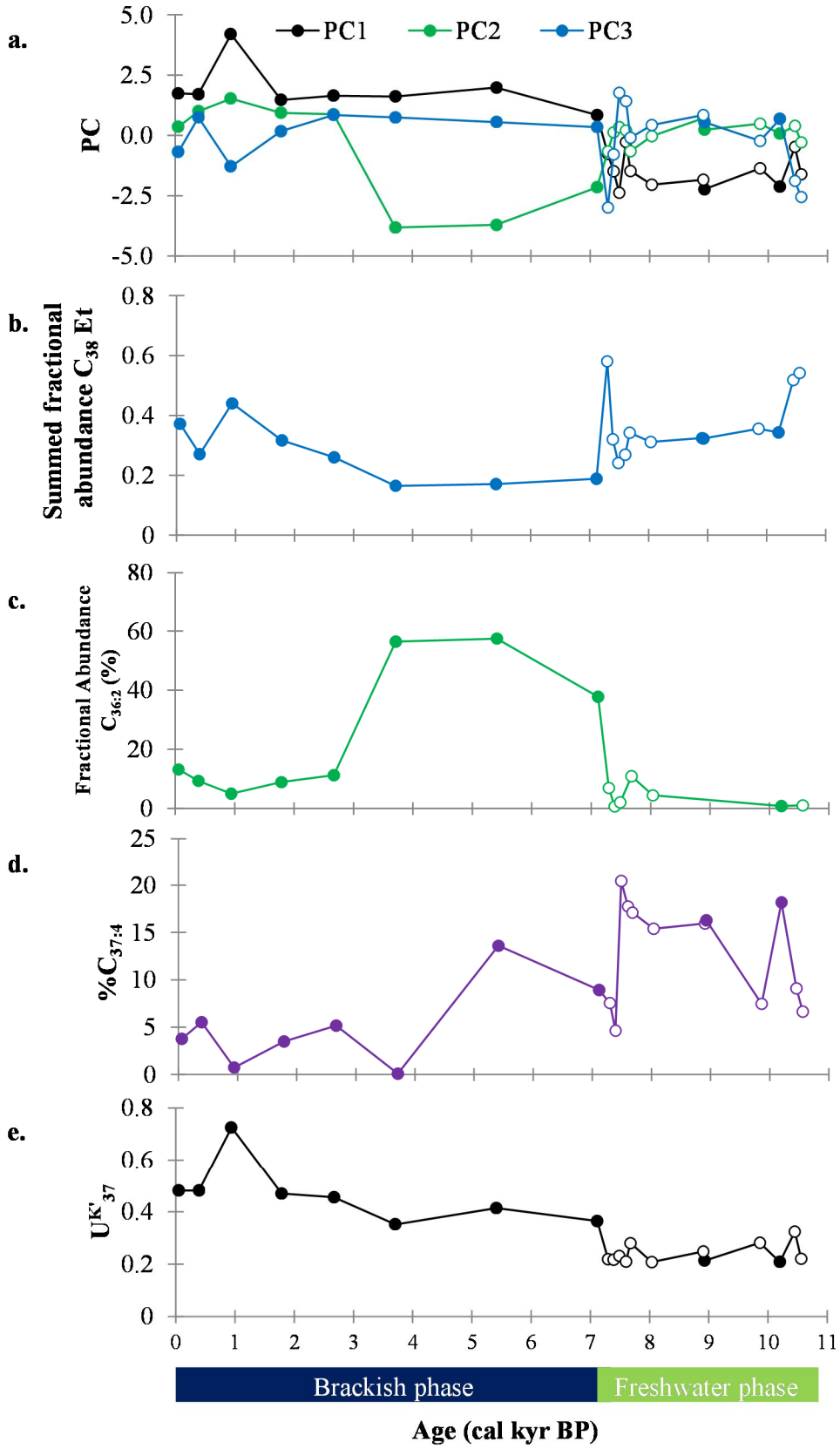

Fig. 5 Plots of the combined Arkona Basin record (sediment core 318310 designated by closed symbols and 318340 by open symbols) with age (cal kyr BP) for (a) PC1-PC3 (b) summed fractional abundance of the C_{38} Et alkenones, (c) fractional abundance of the $C_{36:2}$ alkenone (%) (d) $\%C_{37:4}$, and (e) $U^{K'}_{37}$.

4. Discussion

4.1. Changes in sources of alkenones and its relation to changes in salinity

The observed changes in the relative abundances of the different alkenones through time may be a direct response of alkenone biosynthesis to changing environmental conditions of the Baltic Sea over the Holocene, or alternatively, the changing conditions could result in changing species composition leading to different alkenone distributions. There are many characteristics of alkenones that have been linked to haptophyte species composition and/or environmental conditions. The most important are:

(i) The degree of unsaturation of alkenones is commonly interpreted to be predominantly dependent on growth temperature (Brassell et al., 1986; Prahl and Wakeham, 1987).

(ii) The relative abundance of the $C_{37:4}$ alkenone is generally higher in coastal haptophytes that thrive at lower salinities and this predominance is even more extreme in freshwater systems (Rosell-Mele, 1998; Schulz et al., 2000; Blanz et al., 2005; Liu et al., 2008, 2011).

(iii) The ratio of C_{37}/C_{38} alkenones might be indicative of haptophyte species since different C_{37}/C_{38} values were observed for different haptophytes with coastal haptophytes generally showing higher ratios compared to more open ocean species (Prahl et al., 1988; Conte et al., 1998; Schulz et al., 2000). However, it has also been shown that environmental conditions, e.g. temperature, also affect the C_{37}/C_{38} ratio (Conte et al., 1998; Sun et al., 2007).

(iv) The presence of the uncommon $C_{36:2}$ alkenone, which only has been reported in the Black Sea (Xu et al., 2001; Prahl et al., 2006), Japan Sea (Fujine et al., 2006), and in an estuary in Florida (Van Soelen et al., 2014). Previous studies suggested it to be an indicator of brackish conditions (Xu et al., 2001; Fujine et al., 2006) and more recently, Coolen et al. (2009) proposed its biological origin in the Black Sea is likely a strain of low salinity-adapted *E. huxleyi*.

(v) The δD of alkenones are characteristic of certain types of haptophytes, but can also change with changing environmental conditions. Coastal haptophytes tend to fractionate less than more open marine haptophytes (Schouten et al., 2005; Chivall et al., 2014; M'boule et al., 2014), therefore, δD values can aid in assigning biological sources of sedimentary alkenones. However, hydrogen isotope fractionation also depends on environmental factors such as salinity, light intensity and growth rate (Schouten et al., 2005; Prahl et al., 2006; van der Meer et al., 2008, 2015; Wolhowe et al., 2015).

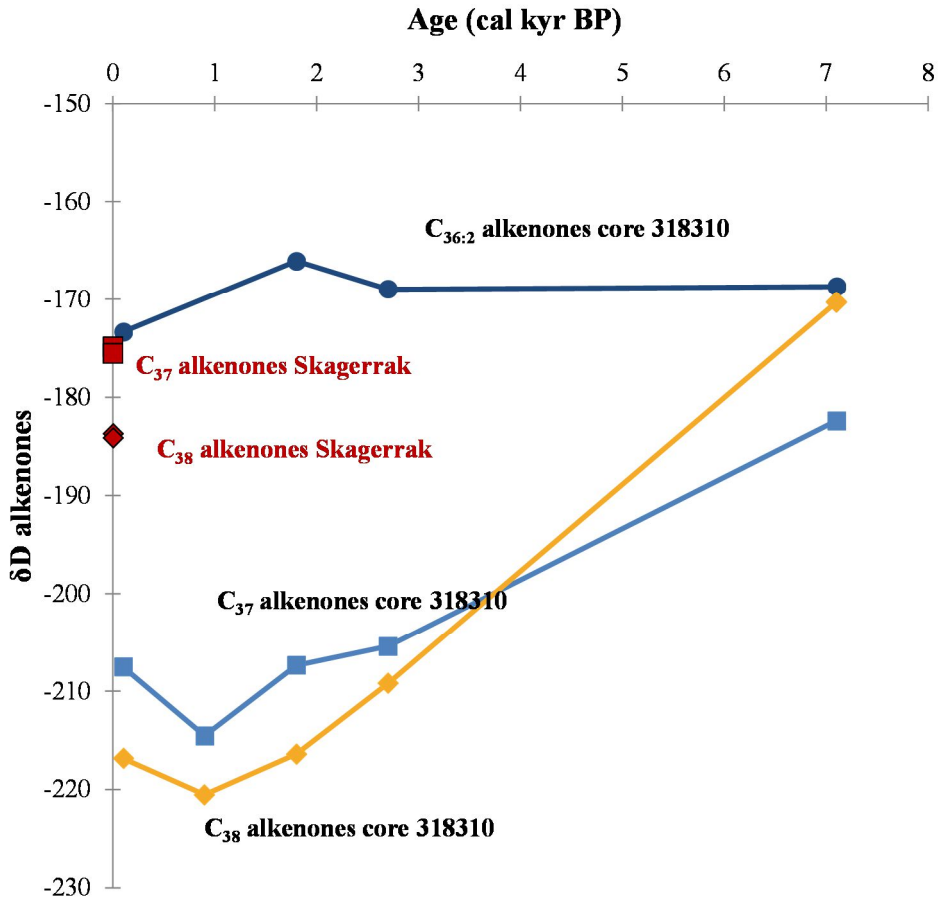

Fig. 6 δD values of the $C_{36:2}$, C_{37} and C_{38} alkenones plotted against age (cal kyr BP) from the record 318310 and the two Skagerrak surface sediment samples. In the Arkona Basin conditions were fresh until 7.8 cal kyr BP and brackish from 7.1 cal kyr BP onwards. The red squares designate the C_{37} alkenones and the red diamonds represent the C_{38} alkenones from the Skagerrak surface sediments. From the Arkona Basin sediment record (core 318310) dark blue circles denote the δD of the $C_{36:2}$ alkenones, the light blue squares signify the δD values C_{37} alkenones and the gold diamonds represent the δD of the C_{38} alkenones.

Some of these parameters were used to assign potential biological sources of the Baltic Sea sedimentary alkenones. To this end, the Arkona Basin data was compared with that from surface sediments of the Skagerrak (Figs. 4 and 6). Marine haptophytes, such as *E. huxleyi*, living at higher salinities and in more open ocean settings (like the Skagerrak; Egge et al., 2015) with a salinity of approximately 34 PSU (Danielssen et al., 1996) will fractionate at approximately 190‰ against D. Using a δD of Skagerrak water of ca. 0‰ (Frohlich et al., 1988) the δD values for the C_{37} and C_{38} alkenones are predicted to be ca. -190‰ (Englebrecht and Sachs, 2005; Schouten et al., 2005; M'boule et al., 2014). The δD value of the C_{37} and C_{38} alkenones in the Skagerrak surface sediments is -180±5‰ (Fig. 6; Table 2), indicating the

haptophyte species in this region are predominantly of the marine type, most likely derived from *E. huxleyi*.

The alkenones in the sedimentary record of the Arkona Basin up to ca. 2.7 cal kyr BP have a distribution that is quite similar to that observed in Skagerrak surface sediments (Figs. 3a-c), which is typical of a marine haptophyte such as *E. huxleyi*. The low $\%C_{37:4}$ during this time (3.1±2.3%) would also suggest that these alkenones are derived from marine type haptophytes (i.e. *E. huxleyi*) (Fig. 5d). However, the C_{37} and C_{38} alkenones have substantially lower δD values (-212±6‰) than found in the Skagerrak surface sediments for the alkenones (-180±5‰; Fig. 6; Table 2). There are two main factors to consider. Firstly, the present-day δD of surface waters in the Arkona Basin is ca. -40‰ averaged over the photic zone (Frohlich et al., 1988), i.e. 40‰ depleted relative to the Skagerrak waters. This will shift the δD values of alkenones to substantially lower values (e.g., Englebrecht and Sachs, 2005). Secondly, culture studies have shown that hydrogen isotope fractionation is dependent on salinity, among other factors, with increased fractionation at lower salinities (e.g. M'boule et al., 2014). The present-day salinity of surface waters of the Arkona Basin is ~10 PSU (ICES-CIEM, n.d.). If *E. huxleyi* would be able to grow at these low salinities, the alkenone δD value is estimated at ca. -270‰, which is substantially lower than the measured values for the C_{37} and C_{38} alkenones (-212±6‰). This value was arrived upon by extrapolating the isotope fractionation (α)-salinity relationship to these low salinities (M'boule et al., 2014), and using the δD value for surface waters of -40‰ over the photic zone (Frohlich et al., 1988). Consequently, this indicates that an *E. huxleyi* only origin for the C_{37} and C_{38} alkenones in the sedimentary record of the Arkona basin up to ca. 2.7 cal kyr BP, is unlikely. Haptophyte species adapted to lower salinities, such as *I. galbana* or *C. lamellosa*, fractionate less against D (Chivall et al., 2014; M'Boule et al., 2014), and the alkenones produced will have a less negative δD value. For *I. galbana* (M'boule et al., 2014) a δD value of alkenones of ca. -180‰ can be estimated using a salinity of 10 PSU and a δD of surface waters of -40. This value is higher than the values observed for the C_{37} and C_{38} alkenones in the Arkona Basin up to ca. 2.7 cal kyr BP (i.e. between -205 and -220‰). This suggests that these sedimentary alkenones represent a mixture of alkenones produced by low salinity adapted haptophytes such as *I. galbana* and higher salinity adapted haptophytes such as *E. huxleyi*, with a more substantial contribution from the low salinity adapted haptophytes.

The $C_{36:2}$ alkenone was detected in the Arkona Basin sediments, but not in the Skagerrak surface sediments (Fig. 3; Table 1). This supports the premise that the $C_{36:2}$

alkenone is exclusively produced by a low-salinity adapted haptophyte (Coolen et al., 2009). PCA revealed that the fractional abundance of the $C_{36:2}$ alkenone is an important factor in the changing alkenone distributions in the Baltic Sea (Figs. 4a and f); i.e. PC2, explaining 27% of the total variance, is predominantly determined by the fractional abundance of the $C_{36:2}$ alkenone (Fig. 4a). In the sedimentary record of the Arkona Basin up to ca. 2.7 cal kyr BP, the fractional abundance of the $C_{36:2}$ alkenone amounts to 0.10±0.03 (Figs. 5c; Table 1). From 7.1-3.7 cal kyr BP in the sediment record the fractional abundance of the $C_{36:2}$ alkenone increases to 0.51±0.11 and it dominates the alkenone distribution (Figs. 3d and 5c; Table 1). For the entire period of 7.1-0.1 cal kyr BP the δD values for the $C_{36:2}$ alkenone show only minor variation and are similar to the δD values for the C_{37} and C_{38} alkenones from the modern day Skagerrak (-170±3‰; Fig. 6; Table 2). However, for most of the record the δD value of the $C_{36:2}$ alkenone is significantly higher than those of the C_{37} and C_{38} alkenones. Since the δD value of the $C_{36:2}$ alkenone is close to that (-180‰) calculated for *I. galbana* using a salinity of 10 PSU and a δD of surface waters of -40‰ (see above), this suggests that it is derived from a single low-salinity adapted haptophyte species. Previous studies (Coolen et al., 2009; Van Soelen et al., 2014) have also reported a substantial offset in δD values for C_{37} and $C_{36:2}$ alkenones with that of the $C_{36:2}$ alkenone being significantly higher. Van Soelen et al. (2014) concluded that the offset in δD values for C_{37} and $C_{36:2}$ alkenones found in an estuary in Florida is evidence that different haptophytes, yet still unknown, are producing the $C_{36:2}$ alkenone. Interestingly, close to the Ancylus Lake/Littorina Sea transition (7.1 cal kyr BP, 600 cm sediment depth from core 318310), which falls within the period characterized by the high fractional abundance of the $C_{36:2}$ alkenone, the δD values for C_{37} (-182.4‰) and C_{38} (-170.3‰) alkenones are much higher than in the other Arkona Basin samples and similar to the δD values of the $C_{36:2}$ alkenone (Fig. 6; Table 2). This suggests a similar origin for most of the C_{36}, C_{37} and C_{38} alkenones at this time, most likely a low salinity adapted haptophyte species. This is strongly supported by the deviating alkenone distribution at this time (Fig. 3d) dominated by the $C_{36:2}$ alkenone. The observed trends in δD values of alkenones over the period between 7.1 and 0.1 cal kyr BP, thus, corroborate the idea that during this period in the Baltic Sea there is more than one alkenone producing haptophyte species.

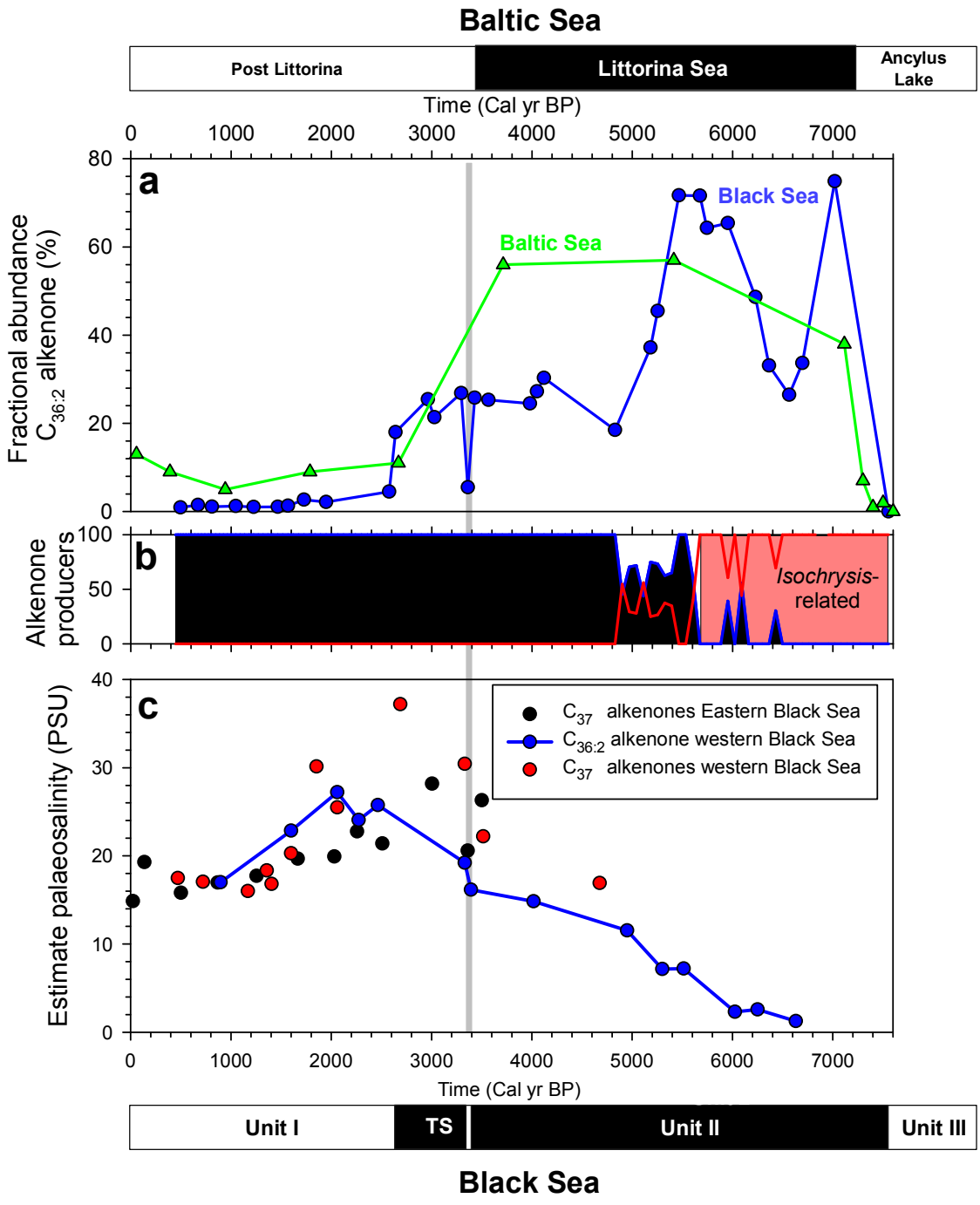
Baltic Sea
Post Littorina
Littorina Sea
Ancylus Lake
Time (Cal yr BP)
0
1000
2000
3000
4000
5000
6000
7000
a
Fractional abundance C36:2 alkenone (%)
Black Sea
Baltic Sea
b
Alkenone producers
Isochrysis-related
c
Estimate palaeosalinity (PSU)
C37 alkenones Eastern Black Sea
C36:2 alkenone western Black Sea
C37 alkenones western Black Sea
Unit I
TS
Unit II
Unit III
Black Sea

Fig. 7 Comparison of $C_{36:2}$ alkenone abundance data for the Baltic Sea and the Black Sea over the Holocene. Top panel (**a**) shows the fractional abundance of the $C_{36:2}$ alkenone relative to the C_{36}-C_{38} alkenones for the Black Sea (blue circles; data from Coolen et al., 2009) and Baltic Sea (green triangles; this study). The middle panel (**b**) shows the haptophyte community composition in the Black Sea as reconstructed based on DGGE analysis of partial 18S rRNA genes amplified with a specific haptophyte primer set with *Isochrysis*-related haptophytes in red and *E. huxleyi* in blue (data modified from Coolen et al., 2009; note that in their Fig. 3 relative abundance data is shown based on the relative abundance of all DGGE bands not only those related to alkenone-producing haptophytes, Coolen, personal communication). These data are in agreement with earlier haptophyte 18S rRNA gene work on a box core just penetrating Unit 2 from a deep water site in the eastern Black Sea (Coolen et al., 2006). The bottom panel (**c**) shows reconstructed salinities for the Black Sea based on the hydrogen isotopic compositions of the $C_{36:2}$ and C_{37} alkenones. For all data the fractionation factor α was calculated using a water hydrogen isotopic composition of -20 permille (Swart, 1991). Salinities were reconstructed based on the α-salinity relationship for *Isochrysis galbana* ($\alpha=0.0019*S+0.836$; M'Boule et al., 2014) for the $C_{36:2}$ alkenone and *E. huxleyi* ($\alpha=0.0021*S+0.740$; M'Boule et al., 2014) for the C_{37} alkenones. Original alkenone hydrogen isotope data are for the eastern Black Sea from van der Meer et al. (2008) and for the western Black Sea from Giosan et al. (2012). The stratigraphy for the Baltic Sea (top) and Black Sea (bottom) is indicated. TS denotes transition sapropel. Note that the stratigraphy described for the Black Sea core in the study of Coolen et al. (2009) and Giosan et al. (2012) has been adjusted to fit the commonly applied stratigraphy for the Black Sea (see lowermost part of the figure), i.e. the layer of the first invasion of *E. huxleyi* (grey bar in the other panels) is taken as the start of Unit 1 deposition (Hay et al., 1992; Arthur et al. 1994; Jones and Gagnon, 1994). In the sediment core used in the work of Coolen et al. (2009) this layer is not clearly revealed by an increase of the carbonate content but the alkenone distribution shows a distinct change at ca. 3,350 cal yr BP (see sudden decrease of the relative abundance of the $C_{36:2}$ alkenone in panel **a**; in addition this horizon is also characterized by a 3-4 fold increase in total alkenone concentration and the detection of C_{39} alkenones; Coolen et al., 2009) towards a composition highly comparable to the upper part of Unit I that is composed of coccolithic ooze. Their reported radiocarbon date for this section (3,360±68 cal yr BP) is by this adjustment in good agreement with the reported age of the base of Unit I at other locations in the Black Sea (Hay et al., 1992; Arthur et al. 1994; Jones and Gagnon, 1994).

From circa 7.1-3.7 cal kyr BP, during the Littorina Sea phase in the Baltic Sea, the $C_{36:2}$ ratio is highest demonstrating the greatest contribution from these low-salinity adapted haptophytes and the $\%C_{37:4}$ is more variable during this period ranging from 0.1-13.6%. This suggests mutable input from non-marine type haptophytes and therefore potentially fluctuating salinities (Fig. 5d; Table 2). The enrichment in the δD of the C_{37} and C_{38} alkenones corroborates the contribution from non-marine haptophytes as well (Fig 6). Why the $\%C_{37:4}$ and the fractional abundance of the $C_{36:2}$ alkenone is higher and the C_{37} and C_{38} alkenones are more enriched in D during the Littorina Sea phase than after is not clear since they are both brackish water periods. Possibly this is related to the period after the Ancylus Lake/Littorina Sea transition being a time of not only low, but also variable salinity. Perhaps the haptophytes producing the $C_{36:2}$ alkenone had a competitive advantage over other haptophytes at this time because they were better adapted to changing salinities, or alternatively, certain haptophyte species biosynthesize this compound in response to changing salinities or marine haptophytes

brought in from the North Sea were not yet established. These possibilities suggest that variable salinity was a characteristic of the Littorina Sea phase.

Prior to 7.1 cal kyr BP in the Arkona Basin sediment record we do not have δD values of alkenones to report, however, some remarkable changes in the alkenone distributions are observed. Firstly, the $U^{K'}_{37}$ is lower prior to the Ancylus Lake/Littorina Sea transition (Fig. 5e) potentially due to a change in the composition of the haptophyte community as indicated by the somewhat higher fractional abundance of the $C_{37:4}$ at this time (Fig. 5d; Table 1). Secondly, the fractional abundance of the $C_{36:2}$ alkenone is relatively low from 10.7 cal kyr BP up to the transition (0.02±0.03; Fig. 5c; Table 1). Thirdly, during the transitional phases of this time period, both the Yoldia Sea phase to Ancylus Lake transition (c. 10.7-10.6 cal kyr BP) and at the Ancylus Lake/Littorina Sea transition (c. 7.3 cal kyr BP), the alkenone distributions are dominated by C_{38} ethyl alkenones (i.e. a low score on PC3; Figs. 4c-d and i.e. summed average fractional abundance of 0.55±0.03; Fig. 5b; Table 1). The lower fractional abundance of the $C_{36:2}$ alkenone during the Ancylus Lake phase, (Fig. 5c; Table 1) suggests that most likely a change in haptophyte species composition occurred related to salinity. Additionally, the $C_{36:2}$ alkenone is absent in the Arkona Basin sedimentary record from 10.2-8.0 cal kyr BP (Fig. 5c; Table 1). Since it is a potential indicator for the low salinity adapted, but not freshwater haptophyte species, the presence of the $C_{36:2}$ alkenone prior to the Anyclus Lake phase ending suggests marine influxes had already begun in the basin at that time. A diatom study by Witkowski et al. (2005) reported that the first brackish water inflows began just before this time period, i.e. between 8.9 and 8.4 cal kyr BP. The presence of the $C_{36:2}$ alkenone from 10.6-10.2 cal kyr BP aligns with the ending of the slightly brackish Yoldia Sea phase. Lastly, the higher $\%C_{37:4}$ during the Ancylus Lake phase verifies that there was an increase in freshwater haptophytes during this time.

4.2. Comparison with the Holocene alkenone record of the Black Sea

A previous study of alkenones in the Black Sea (Coolen et al., 2009) reported similar trends with respect to the fractional abundance of the $C_{36:2}$ alkenone to those reported here for the Baltic Sea. The Black Sea experienced a somewhat comparable geological history to the Baltic Sea. In the early Holocene it was a freshwater lake until a connection was established with the Aegean and Mediterranean Seas due to the global transgression allowing the influx of more saline waters (Ryan et al., 1997). The permanent establishment of this connection is dated at c. 7.2 cal kyr BP (Ryan et al., 1997; Ballard et al., 2000). The resultant increase in salinity is reflected by the sedimentary sequence revealing a transition from banded clay with

graded sand and silt layers (Unit III) to sapropel mud (Unit II) (Ross et al., 1970). As the influx of salty Mediterranean waters continued it caused an increase in the surface salinity of the Black Sea allowing a massive growth of *E. huxleyi* (Jones and Gagnon, 1994) in the basin c. 2.7 cal kyr BP, resulting in deposition of a coccolith ooze (Jones and Gagnon, 1994). The abundance in *E. huxleyi* at this time has been attributed to a surface water salinity increasing above 11 PSU and the base of Unit I is generally defined as the horizon that reveals the first invasion of *E. huxleyi*, ca. 700 yr earlier (Fig. 7) (Arthur and Dean, 1998; Hay, 1988).

Since the salinity changes in the Baltic Sea and Black Sea occurred around the same time (~7.2 cal kyr BP), we compared the relative abundance of the $C_{36:2}$ alkenone from the Baltic Sea directly to that in the Black Sea reported by Coolen et al. (2009) (Fig. 7a). In both the Baltic Sea and Black Sea the fractional abundance of the $C_{36:2}$ alkenone is rapidly increasing to values of 40-70% just after the inflow of more saline waters started. Subsequently, a period of sustained high fractional abundances follows in both basins up to ca. 2.6 cal kyr BP. The higher resolution record of the Black Sea shows that the period between 7.0-5.4 cal kyr BP is characterized by the highest values (up to 75%), followed by a drop to a fractional abundance of ca. 25% for the period 5.0-2.6 cal kyr BP. This latter period is interrupted by the horizon of the first invasion of *E. huxleyi* at 3.5 cal kyr BP when the fractional abundance drops to 5%. For the Baltic Sea the fractional abundance of the $C_{36:2}$ alkenone is high throughout the 7.0-2.6 cal kyr BP period although this is based on a small dataset. In both basins the fractional abundance of the $C_{36:2}$ alkenone is substantially reduced in the most recent period (2.6-0.0 cal kyr BP) although for the Baltic Sea it does not drop to the low values seen in the Black Sea (i.e. 1%) and it increases towards the present day situation (Fig. 7a). In conclusion, we note a quite similar behavior for the fractional abundance of the $C_{36:2}$ alkenone in both enclosed basins with limited connection to the open ocean. This may relate to a somewhat comparable response to the global sea level transgression during the Holocene. For the Black Sea substantial additional data is available for the interpretation of this trend and this may help, by analogy, to provide a more detailed interpretation of the Baltic Sea record.

Coolen et al. (2006, 2009) provided through ancient DNA analysis clues on the biological origin of the sedimentary alkenone in the Black Sea. The most extensive record comes from a site in the western Black Sea. It reveals that during deposition of the base of Unit II *Isochrysis*-related haptophytes thrived (Fig. 7c). This fits with the time of the newly established connection with the Mediterranean since these type of haptophytes are adapted to low salinity. Subsequently, there is a short period (5.7-4.8 cal kyr BP) where Coolen et al.

(2009) detected both *Isochrysis*-related haptophytes and *E. huxleyi*, followed by a period where only ancient DNA of *E. huxleyi* was found. When this information is combined with the record of the fractional abundance of the $C_{36:2}$ alkenone (Fig. 7a), it is evident that this alkenone must have been produced by *Isochrysis*-related haptophytes since the period of highest fractional abundance (up to 75%) falls in the period where only ancient DNA of *Isochrysis*-related haptophytes is detected (Fig. 7). However, the $C_{36:2}$ alkenone also occurs (albeit at a substantially reduced fractional abundance) in more recent periods when only ancient DNA of *E. huxleyi* is detected, suggesting that this haptophyte may also produce this alkenone. However, this latter conclusion is at odds with the large difference (90-100‰) in δD composition of the $C_{36:2}$ and C_{37} alkenones as reported by Giosan et al. (2012) for this section, which indicates clearly distinct biological sources for these alkenones. In fact, when the δD record of the $C_{36:2}$ alkenone is combined with the recent determination of the isotopic fractionation factor α for *Isochrysis galbana* (M'boule et al., 2014) to estimate palaeosalinity of the surface waters of the Black Sea over the Holocene, we obtain a record (Fig. 7c; blue line) that is in good agreement with our general concept of the development of surface salinity of the Black Sea. In the lowermost part of Unit II the estimated palaeosalinity is only a few PSU, it subsequently rises to 15 PSU at the Unit I/II transition, reaches a maximum of ca. 26 PSU at 2.0 cal kyr BP and then declines to 17 PSU for the most recent period. These data are in good agreement with salinity calculations (Fig. 7c) based on δD data of C_{37} alkenones in cores from both the western and eastern Black Sea (van der Meer et al., 2008; Giosan et al., 2012) in combination with the isotopic fractionation factor α for *E. huxleyi* (M'boule et al., 2014). For the period where the fractional abundance of the $C_{36:2}$ alkenone is still elevated (i.e. up to 2.6 cal kyr BP) these estimations of palaeosalinity are on the high end (except for the horizon reflecting the first invasion of *E. huxleyi* in the Eastern Basin). This is most likely caused by the fact that the $C_{36:2}$ alkenone-producing haptophytes are also contributing D-enriched C_{37} alkenones to the total pool of C_{37} alkenones, influencing the palaeosalinity calculation that is based on a 100% origin from *E. huxleyi*. Hence, the δD data of the $C_{36:2}$ alkenone in combination with the salinity calculations strongly suggest that the $C_{36:2}$ alkenone has been produced by an *Isochrysis*-related haptophyte and not by a lower salinity adapted strain of *E. huxleyi* as suggested previously (Coolen et al., 2009). It remains unclear why ancient DNA of this haptophyte is only detected for the period 7.4-4.8 cal kyr BP. However, it is known that Denaturing Gradient Gel Electrophoresis (DGGE), the method used by Coolen et al. (2009) to detect ancient DNA is only able to quantify the predominant DNA sequences.

Combining the fractional abundance record of the $C_{36:2}$ alkenone (Fig. 7a) with the palaeosalinity record (Fig. 7c) now makes it possible to determine the optimal salinity for the *Isochrysis*-related haptophyte producing the $C_{36:2}$ alkenone. In the Black Sea at salinities from 2-8 PSU, the $C_{36:2}$ alkenone dominates the alkenone distribution. At a salinity of up to ca. 19 PSU the $C_{36:2}$ alkenone can still contribute substantially (25%) and above this level it becomes a minor alkenone. It is clear that salinity is not the only environmental control on the $C_{36:2}$ alkenone-producing haptophyte since when in recent times salinities drop to ca. 17 PSU, the $C_{36:2}$ alkenone still remains a minor alkenone (Fig. 7).

The $C_{36:2}$ alkenone data of the Black Sea allow the interpretation of the $C_{36:2}$ alkenone record of the Baltic Sea in term of changes in salinity. This should be done cautiously since it is clear that other environmental factors also may have an effect. Nevertheless, the sudden increase of the fractional abundance of the $C_{36:2}$ alkenone record at the Ancylus Lake/Littorina Sea transition is highly comparable to what happened in the Black Sea at the Unit III/II transition and indicates an incursion of marine waters into the freshwater lakes most probably by the worldwide sea level transgression, resulting in a modest increase in surface water salinity to ca. 2 PSU. In the Baltic Sea the fractional abundance of the $C_{36:2}$ alkenone remains high until ca. 3.0 cal kyr BP, suggesting that the salinity of the surface waters of the Arkona Basin increased at a lower rate than in the Black Sea. The lowest fractional abundance of the $C_{36:2}$ alkenone is recorded in the Arkona Basin at 0.9 cal kyr BP, suggesting that the salinity was highest at that time, which corresponds to the medieval climate anomaly (MCA, which occurred between 950 and 1,250 AD). This trend is similar to salinity records for the whole Baltic Sea based on combined proxies and modelling (Gustafsson and Westman, 2002) although the maximum salinity is thought to be earlier even when we correct for the different age models. Generally, it is believed that the Littorina phase of the Baltic Sea was more saline than the post-Littorina phase, however, other studies do not reveal this difference (Andren et al., 2000b; Westman and Sohlenius, 1999; Andrén et al, 2002; Witkowski et al., 2005) or show the opposite (Emeis et al., 2003).

4.3 Potential uses of alkenones as environmental indicators for SST/LST

The indices and ratios we have presented in this study all corroborate that a haptophyte species composition change, most likely driven by a salinity shift, occurred during the Yoldia Regression (10.6 cal kyr BP), the Ancylus Lake/Littorina Sea transition (7.7-7.2 cal kyr BP), and at the MCA (0.9 cal kyr BP). The results also indicate that the haptophyte species composition since 7.2 cal kyr BP in the Baltic Sea basin is a combination of marine (*E.*

huxleyi type) and low-salinity adapted haptophytes. This designates that higher salinity conditions have prevailed since the Ancylus Lake/Littorina Sea transition.

To determine how shifts in haptophyte species composition in the Baltic Sea could affect paleoclimate reconstructions using long chain alkenones, we examined the $U^{K'}_{37}$ index over the Holocene. $U^{K'}_{37}$ values changed across the Ancylus Lake/Littorina Sea transition with lower values (0.24±0.04) during the Ancylus Lake phase and an increase in the $U^{K'}_{37}$ index after 7.2 cal kyr BP (0.47±0.12; Fig. 5e; Table 2). This resulted in an increase in average estimated SST/LST based on the $U^{K'}_{37}$ index from ~6°C during the Ancylus Lake phase to ~13°C during the brackish phase. We believe that variations in haptophyte community composition resulting from fluctuating salinity is most likely responsible for this change in $U^{K'}_{37}$ values and the corresponding unrealistic increase in SST/LST over the Ancylus Lake/Littorina Sea transition. The highest contribution of the $C_{36:2}$ alkenone occurred during the Littorina Sea phase, which indicates salinity was relatively low at that time. The presence of this alkenone even in the more recent phase of the Baltic Sea is evidence of the continued contribution from low salinity adapted haptophytes, which are most likely complicating the use of alkenone unsaturation ratios for SST reconstructions in this region. Schulz et al. (2000) demonstrated in a study performed in the Baltic Sea that $U^{K'}_{37}$ varied regionally depending on salinity and that higher salinity areas in the Baltic had higher $U^{K'}_{37}$ values and vice versa. Since previous studies have also shown that alkenone distributions co-vary not only with temperature changes, but also with salinity driven changes in haptophyte species composition (Coolen et al., 2004, 2009) we cannot apply the $U^{K'}_{37}$ index for SST/LST reconstructions in the Baltic Sea basin over the Holocene.

Interestingly, we observed that during the brackish phase the alkenone distribution at 0.9 cal kyr BP (100 cm depth) is unique compared to the other sediment samples (Fig. 3) from the brackish phase. This sediment horizon has the lowest contribution of the $C_{36:2}$ alkenone, the lowest $\%C_{37:4}$ and the highest fractional abundance of the C_{38} Et alkenone (Fig. 5b-d; Tables 1-2), all indicating the increased presence of marine type haptophyte species and therefore that more marine conditions prevailed in the Baltic Sea at this time. This sample falls within the MCA, also known as the Medieval Warm Period. The lower contribution of the $C_{37:3}$ alkenone compared with $C_{37:2}$ corroborate that warmer temperatures (Fig. 3c) occurred during this time, although the minor contribution of *Isochrysis*-related haptophytes do not allow absolute SST determination.

5. Conclusions

This research demonstrates the usefulness of alkenone distributions along with the δD of the alkenones for paleosalinity studies in the Baltic Sea and other environments as well. Both alkenone distributions and hydrogen isotopic composition indicate a shift in haptophyte species composition in the Arkona Basin of the Baltic Sea from the Ancylus Lake to the Littorina Sea phase, c. 7.2 cal kyr BP, from lacustrine to brackish type haptophytes, corresponding to the incursion of marine waters that occurred in the Baltic Sea at that time as a consequence of the global sea level rise. During the Littorina Sea Phase the fractional abundance of the $C_{36:2}$ alkenone remains high, suggesting that salinity did not rise above 8 PSU. From ca. 3.0 cal kyr BP onwards the fractional abundance of the $C_{36:2}$ alkenone is lower, suggesting a slightly higher salinity. During this phase there is a substantial offset in δD values with the $C_{36:2}$ alkenone substantially more enriched than the C_{37} alkenones. The presence of the $C_{36:2}$ alkenone in the Baltic Sea as well as the δD record suggest it is produced by a different species of haptophyte adapted to lower salinity conditions that is not contributing much to the production of C_{37} and C_{38} alkenones. The contribution of alkenones from lower salinity adapted species in the Baltic Sea hinders the use of the $U^{K'}_{37}$ index for SST reconstructions.

Acknowledgements

We thank M. Verweij for assistance with the GC analysis and A. Mets for help with the GC-MS analysis. This work was supported by the European Research Council under the European Union's Seventh Framework Programme (FP7/2007-2013) / ERC grant agreement n° [226600]. MvdM was funded by the Dutch Organisation for Scientific Research (NWO) through a VIDI grant (#864.09.011). JSSD receives funding from the Netherlands Earth System Science Center (NESSC) though a gravitation grant from the Dutch ministry for Education, Culture and Science.

Photo by Dietmar Rüß

CHAPTER 6

Change in provenance of branched glycerol dialkyl glycerol tetraethers over the Holocene in the Baltic Sea and its impact on continental climate reconstructions

Lisa Warden, Matthias Moros, Yuki Weber and Jaap S. Sinninghe Damsté

To be submitted to Organic Geochemistry

Abstract

The Baltic Sea is an enclosed brackish basin receiving freshwater from the northeast and marine water from the southwest that has experienced a number of different phases during the Late Pleistocene and Holocene. In this study we analyzed brGDGTs in surface sediments and Holocene sedimentary successions from the Gotland and Arkona Basins in the Baltic Sea, in order to examine their applicability as indicators for terrestrial input, as well as their suitability for paleoclimate reconstructions. Several geological phases have occurred since deglaciation and before the current brackish-water state of the Baltic Sea, which according to our record occurred between 7,700-7,300 cal kyr BP. These include the Ancylus Lake phase, a freshwater period that began around 10,600 cal kyr BP and lasted c. 2,500 years, preceded by the Yoldia Sea phase, a brief slightly brackish water period from 11,600-10,600 cal kyr BP, preceded by the Baltic Ice Lake phase, a freshwater period that ended around 11,600 cal kyr BP. Our results show a marked change in brGDGT distributions and the BIT index corresponding to the opening of the connection between the Baltic Sea and the North Sea. Through examining the fractional abundances and distributions of brGDGTs from the Baltic Sea sediments regionally in the modern Baltic Sea and over the Holocene it was established that although the extent fluctuated, autochthonous production of brGDGTs contributed to the total pool of brGDGTs in the Baltic Sea sediments complicating the use of brGDGTs for temperature reconstructions. Although it is evident from these results that in situ production is affecting the distribution of brGDGTs in the Baltic Sea sediments, it was determined a portion of the brGDGTs in the Ancylus Lake phase sediments of the Baltic Sea were terrestrially derived and so the novel MAT_{mr}/CBT' soil calibration was applied to reconstruct continental air temperatures in two sediment records from the Gotland and Arkona basins from about 12,500 BP ~ 7,800 BP. The resulting temperature estimates in both basins are similar to each other and a previously published climate reconstruction from the region based on a different proxy. As for the brackish sediments in the Baltic Sea where in situ produced brGDGTs appeared to dominate, a novel coastal marine sediment calibration for bottom water temperature was applied to the surface sediments and the resultant temperature estimates were in good argeement with instrumental measurements from the area and it was also applied to the two sediment records over the Holocene and the results from the two records are in good agreement with each other. The results from this study demonstrate that geological changes and salinity variations in a basin's past can complicate temperature reconstructions using brGDGTs and this must be considered when using brGDGTs for paleoclimate applications in regions that have experienced similar environmental changes in the past.

1. Introduction

Investigating climatic variability is important for predicting future climate change as well as how ecosystems, organisms and human society could be affected. To better understand past climate systems, more reliable continental climate data are necessary and so is further research on developing and improving terrestrial climate proxies. Branched glycerol dialkyl glycerol tetraethers (brGDGTs; see Fig. 1 for structures) are biosynthesized by bacteria, which were initially thought to be restricted to soils and peats (Weijers et al., 2006a). Their distribution, expressed by their degree of methylation (methylation index of branched tetraethers; MBT) and cyclization (cyclization index of branched tetraethers; CBT), has been shown to correlate with soil pH and mean annual air temperature (MAT) (Weijers et al., 2007b). The preserved distribution of these fossilized membrane lipids has been used for paleoclimate reconstructions in coastal marine sediments (Weijers et al., 2007a; Bendle et al., 2010), paleosoils (Zech et al., 2012; Peterse et al., 2011) and even lacustrine sediments (Zink et al., 2010; Loomis et al., 2012; Niemann et al., 2012). In marine sand lacustrine sediments the bacterial brGDGTs were assumed to originate predominantly from continental soil erosion and terrestrial runoff, whereas the isoprenoid GDGTs (isoGDGTs; includes crenarchaeol the GDGT specific to *Thaumarchaeota* (Sinninghe Damsté et al., 2002)) are thought to be mainly produced by aquatic ammonia oxidizing archaea. Capitalizing on their terrigenous origins, the branched vs. isoprenoid tetraether (BIT) index was developed, representing the ratio of the major brGDGTs over crenarchaeol, as a proxy for terrestrial input into a region (Hopmans et al., 2004). Complications using brGDGTs for climate reconstructions have arisen in areas with low terrestrial input as determined using the BIT index (Peterse et al., 2009; Zhu et al., 2011). Also, several studies have suggested in situ production of brGDGTs in aquatic environments could be altering their distribution and thus affecting the use of these proxies (Zhu et al., 2011; Zell et al., 2013) and so it is recommended to understand the provenance of brGDGTs in a region before attempting paleoclimate reconstructions (Zell et al., 2013; De Jonge et al., 2015a). To date, most paleoclimate reconstructions using brGDGTs have been thought to have been based on the suite of nine 5-methyl brGDGTs (Fig. 1). However, in addition to the nine 5-methyl brGDGTs, six novel 6-methyl brGDGTs were recently discovered and shown to be co-eluting with the 5-methyl brGDGTs employing the commonly used separation methods (De Jonge et al., 2013). Using improved chromatography methods (Hopmans et al., 2015) the separation and quantification of 6-methyl brGDGTs has led to the definition of new indices and the improvement of MAT reconstructions based on a global soil calibration (De Jonge et al., 2014a)

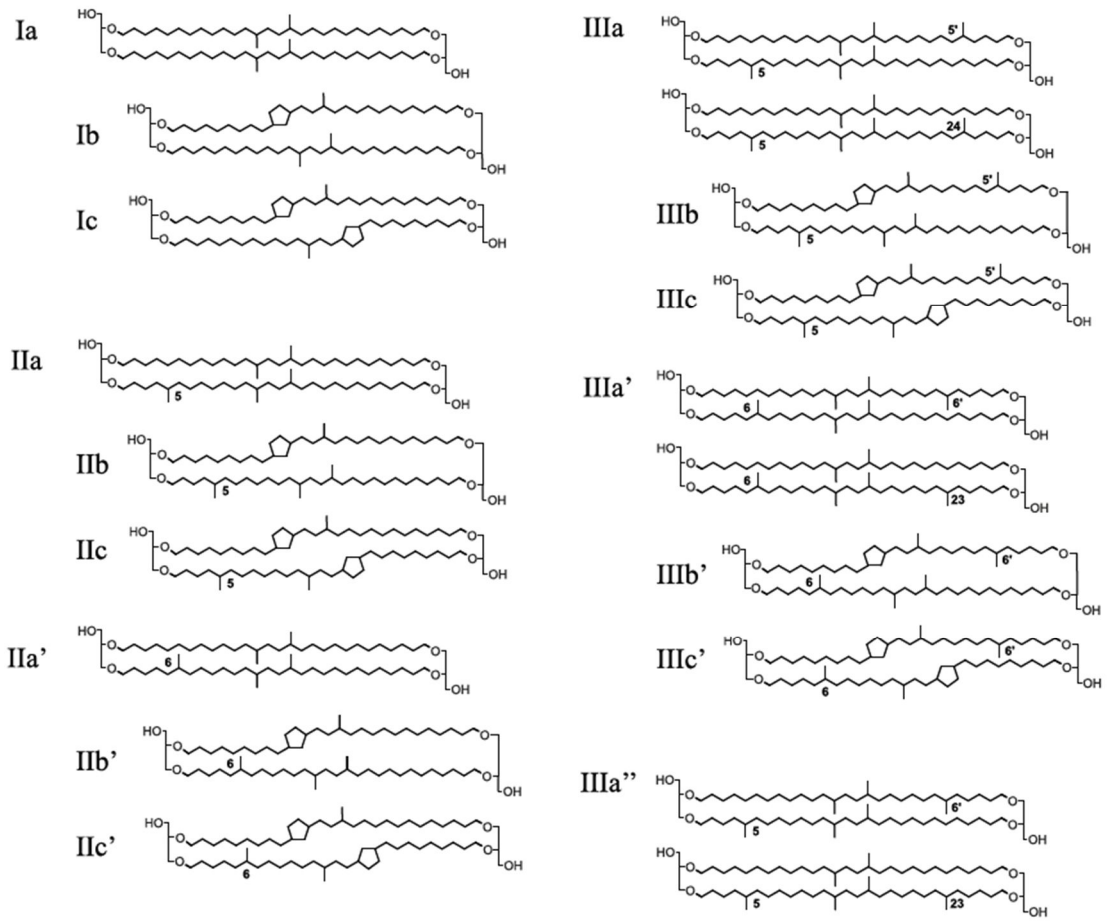

Fig. 1 Chemical structure of all 15 brGDGTs (I-III), crenarchaeol (IV) and the novel isomer IIIa''. The molecules designated with a prime symbol are referred to as the 6-methyl brGDGTs.

The Baltic Sea (Fig. 2) is a large, brackish body of water with high terrestrial influence, which makes it a promising region for investigating sedimentary brGDGT records. In this study we examine two sedimentary sections covering the Holocene from two locations in the Baltic Sea proper, covering varying time spans within different regions of the basin, as well as ten surface sediment samples from around the Baltic Sea and two from the Skagerrak. Through examining the brGDGT concentrations, GDGT distributions and the BIT index values we can gain further insight into how these lipid biomarkers are affected by physical changes in a basin. By making comparisons to present day conditions we gain new understanding about how certain physical changes in a system can affect paleotemperature reconstructions based on brGDGTs as well as whether these lipids can be indicators of other changes in the environment.

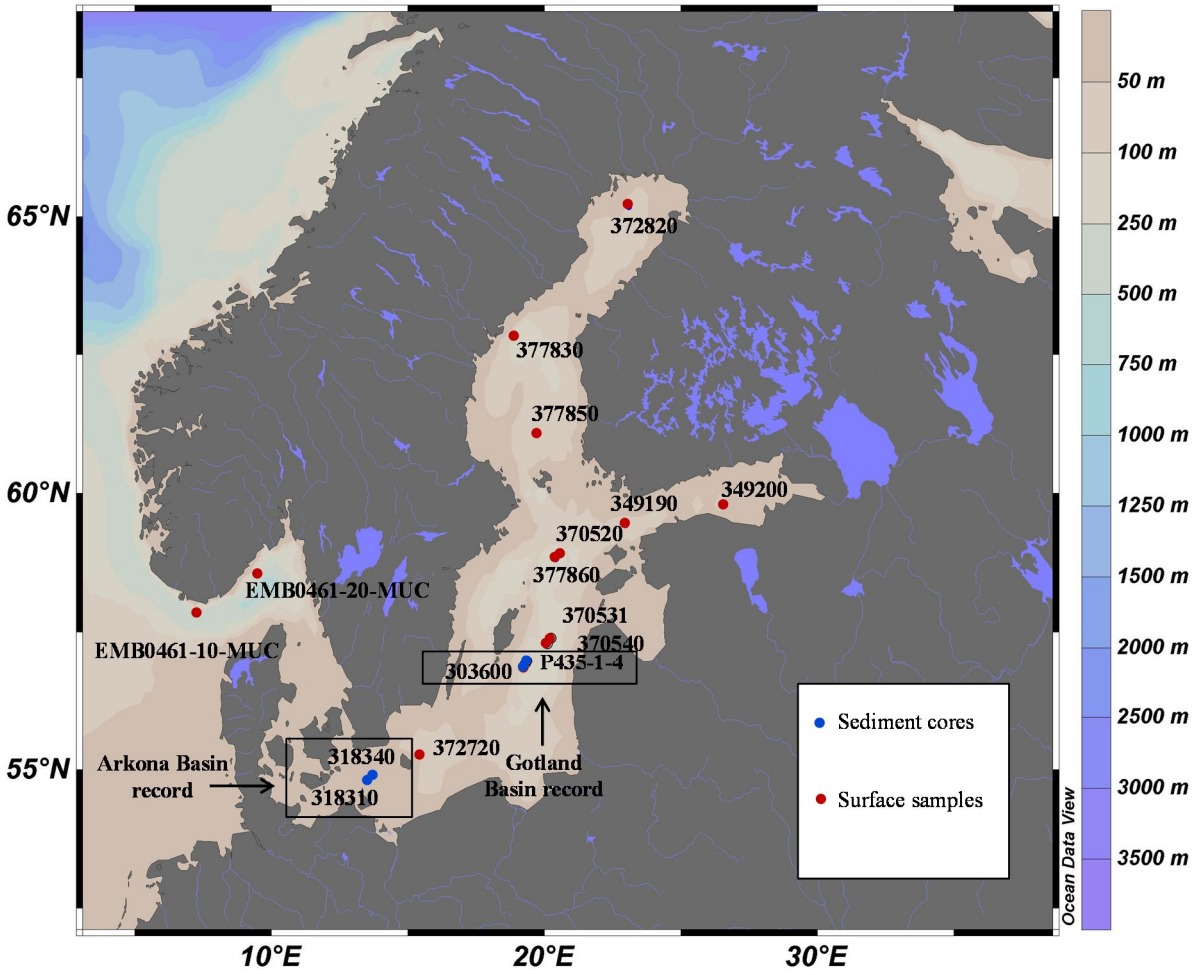

Fig. 2 The location of the study sites in the Baltic Sea including the 13 locations where surface sediments were collected, indicated by red circles, and the 5 locations where sediment cores were obtained in the Gotland and Arkona Basins, indicated by blue circles.

2. Study Site

The Baltic Sea (Fig. 2) and has an area of about 377,000 km^2 that is broken up into multiple sub-basins. It receives 660 km^3 of freshwater (including precipitation) per year from a drainage basin that has an area of 1.6 million km^2 (Björck, 1995). An influx of 475 km^2 yr^{-1} of saline water flows from the only connection to the North Sea through the narrow Straits of Denmark (Tikkanen and Oksanen, 2002). The total outflow of brackish water is of the order of 950 km^3 yr^{-1} (Björck, 1995). Although the Baltic Sea is the world's largest brackish body of water, it is fairly shallow and on average is only about 54 m deep (Emeis et al., 2003). Its salinity varies greatly ranging from ~3.5 PSU in the north to ~8 PSU in the central Baltic Sea and ~30 PSU in the Skagerrak, the region where the Baltic connects to the North Sea (ICES). A salinity gradient also exists between the surface and deep waters, separated by a permanent halocline at about 30 m depth. The air temperatures around the basin range from almost 0°C

in the winter to more than 20°C in the summer (Wasmund, 1997). Presently the Baltic Sea is persistently stratified resulting in anoxic bottom waters in the deeper basins as well as hypoxic coastal areas.

Table 1 Retrieval locations and water depths of surface sediments and sediment cores used in this study.

Station	Core or sediment sample name	Latitude [N]	Longitude [E]	Water depth [m]	Measured MAT (°C)
349190[a]	Baltic Sea surface sediments	59 °26.09	22 °58.39	94	6.9
349200[a]	Baltic Sea surface sediments	59 °46.97	26 °35.05	82	6.9
370520[a]	Baltic Sea surface sediments	58°53.66	20°34.43	182	6.9
370531[a]	Baltic Sea surface sediments	57°23.12	20°15.55	232	7.2
370540[a]	Baltic Sea surface sediments	57 °17.04	20 °07.26	243	7.2
372720[a]	Baltic Sea surface sediments	55°15.67	15°28.21	96	8.1
372820[a]	Baltic Sea surface sediments	65° 10.70	23° 05.73	122	1.4
377830[a]	Baltic Sea surface sediments	62°50.71	18°53.34	210	4.1
377850[a]	Baltic Sea surface sediments	61°04.31	19°43.68	136	4.5
377860[a]	Baltic Sea surface sediments	58°48.92	20°25.17	195	6.9
303600[a]	Baltic Sea surface sediments	56°55.01	19°19.99	170	7.2
EMB046-10	Skagerrak surface sediments	57°49.74	07°17.66	457	n.a.
EMB046-20	Skagerrak surface sediments	58°31.60	09°29.09	532	n.a.
303600-N	Gotland Basin record	56°55.01	19°19.99	170	n.a.
303600-3	Gotland Basin record	56°55.01	19°19.99	170	n.a.
P435-1-4MUC	Gotland Basin record	56°57.94	19°22.21	178	n.a.
318310	Arkona Basin record	54°50.34	13°32.03	46	n.a.
318340	Arkona Basin record	54°54.77	13°41.44	47	n.a.

[a] These sediments were used collected in a previous study (Kabel et al., 2012).
Measured MAT (°C) values are from the closest weather station and an average of temperatures from over the period of 1890-2016 obtained from: http://rimfrost.no/

The Baltic Sea has gone through several phases since the last deglaciation; the Baltic Ice Lake, the Yoldia Sea, the Ancylus Lake, the Littorina Sea and the modern Baltic Sea. The Baltic Ice Lake was created ~14,000 BP by a retreating ice sheet that blocked water exchange

with the North Sea (Björck, 1995). After the ice sheet retreated, the connection to the ocean was opened and an influx of marine water created the slightly brackish conditions of the Yoldia Sea (Jensen, 1995; Björck et al., 1996). The following post-glacial rebound and uplift of land once again restricted the connection between the basin and the ocean (Jensen et al., 1999), resulting in the freshwater Ancylus Lake (Björck, 1995). Eustatic sea-level rise initiated a reconnection to the ocean allowing the inflow of salt water and transforming the lake into the Littorina Sea (Winterhalter, 1992). The Ancylus Lake/Littorina Sea transition is considered to be very complex and consisted of weak pulses of higher salinity waters entering the basin for almost 2,000 years before fully brackish conditions were established (Andrén et al., 2000a). The Littorina Sea is considered to have had the most marine-like conditions of the Baltic Sea since deglaciation (Andrén et al., 2000b), while the present day Baltic Sea is regarded as a continuation of this phase with lower salinity (Punning et al., 1988). A previous study suggests that anoxic conditions in the Baltic Sea are likely controlled by climate and demonstrates that higher summer SSTs starting at around 6.0 cal kyr BP initiated the onset of anoxia in regions of the basin (Warden et al., in preparation). When summer SSTs subsequently decreased by 1-3°C during the post Littorina Sea phase (starting c. 4.3 cal kyr BP) anoxic conditions were not reestablished in the Baltic Sea for a period of about 3,000 years until a subsequent increase in summer SST at around 1.4 cal kyr BP (Warden et al., in preparation).

3 Experimental methods

3.1 Sampling.

Eleven surface (0-1 cm) sediment samples from various positions around the Baltic basin (Fig. 2) were used in this study and their sampling has been documented previously by Kabel et al. (2012). In addition, two surface (0.0-0.05 cm) sediment samples were collected from the Skagerrak (Table 1; Fig. 2), northeast of the Arkona Basin, where the Baltic Sea opens up to the North Sea, using a multi corer during a cruise EMB046 of the R/V "Elisabeth Mann-Borgese" in May 2013.

Five sediment cores from two locations within the Baltic Sea were used in this study (Table 1; Fig. 2). Two of the sediment cores, GC 303600-N and GC 303600-3, were collected during the cruise campaign on the R/V "Prof. Albrecht Penck" in the Gotland Basin to the east of Gotland Island in July 2007. The core was subsampled into 1-cm sections from 0-237 cm and into 2-cm slices for the remainder of the core (237-377 cm), A third sediment core, P435-1-4MUC, was also collected from the same region in the Gotland Basin using a multi

corer during the R/V "Poseidon" cruise P435 in June 2012. Two sediment cores were collected from the Arkona Basin, located in the south-western part between the Bornholm Basin and the Danish Isles of Falster and Zealand. Both cores were obtained using a gravity corer on the R/V "Maria S. Merian" in April of 2006.

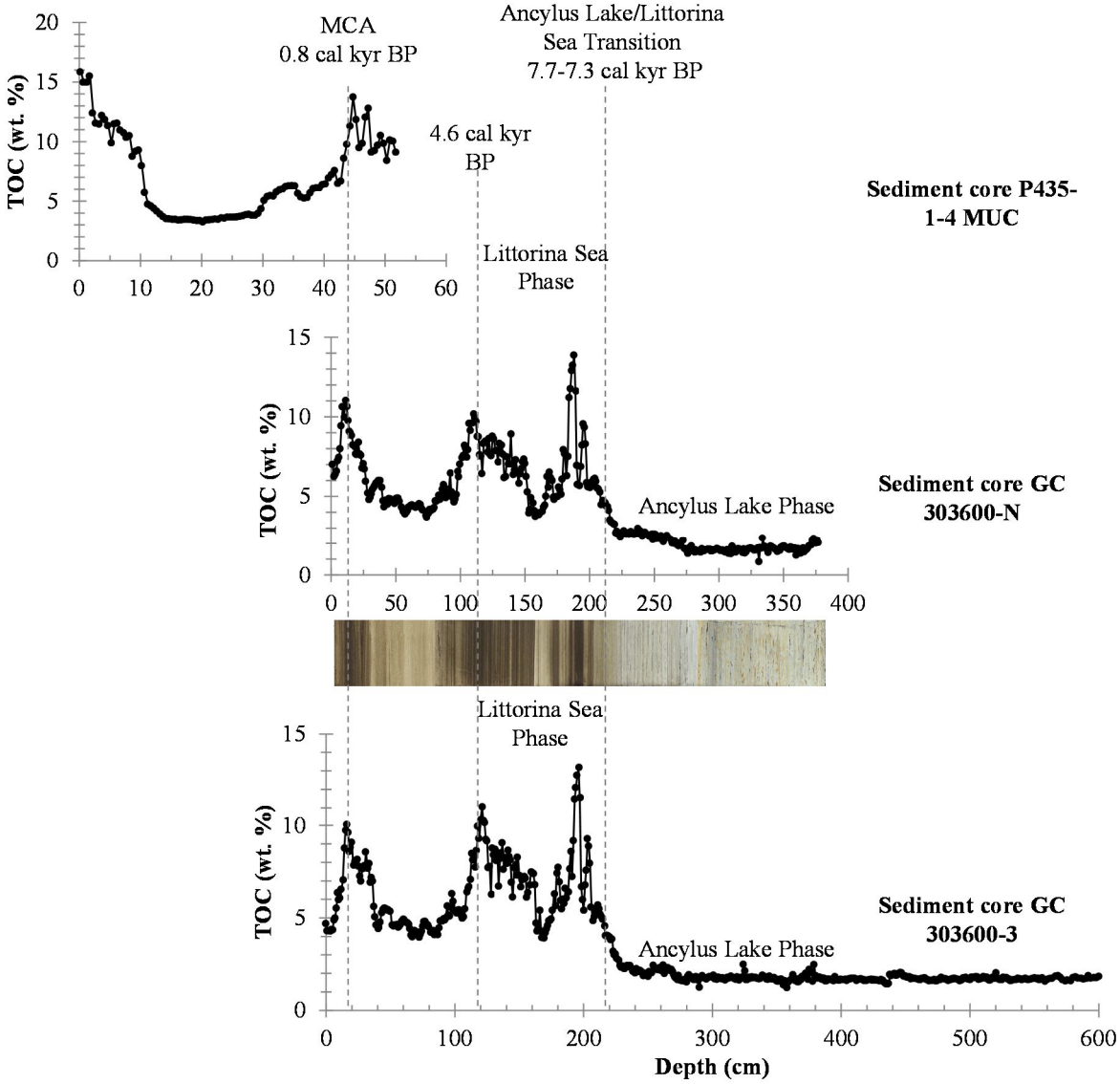

Fig. 3 TOC content (wt. %) vs. depth (cm) profiles for the three sediment cores (P435-1-4 MUC, GC 303600-N, and GC 303600-3) from the Gotland Basin. The TOC (wt. %) profiles were used to correlate the three cores as indicated and reveals the clear transition as TOC values increased from the Ancylus Lake to the Littorina Sea phase. A photo of sediment core GC 303600-N is displayed beneath its TOC profile. The different phases over the Holocene of the Baltic Sea are indicated. For sediment core 303600-N the TOC content was not measured but calculated from LOI data (see experimental).

3.2 Age models and correlation among cores.

Detailed age models based on picked foraminifera have been previously established for two of the sediment cores of the Gotland Basin studied here. The shallow (0-42.75 cm) sediment core P435-1-4 MUC is spanning from -0.06-0.64 cal kyr BP. Sediment core GC 303600-N (0-377 cm) covers most of the Holocene (0.2-10.6 cal kyr BP; Warden et al., in review). A detailed age model for the upper 210 cm of this sediment core was determined through correlation with slightly deeper sediment cores from this basin with age models that were previously established using radiocarbon dates of benthic foraminifera (Warden et al., in review). Sediment cores P435-1-4 MUC, GC 303600-3 and GC 303600-N from the Gotland Basin were correlated to each other by comparing TOC (wt. %) profiles (Fig. 3), LOI (%) and XRF data (Fig. S1). Based on this correlation the uppermost part of the analysed section (300-420 cm) of core GC 303600-3 overlaps with the lower part of core GC 303600-N (253-377 cm) with an age of c. 8.7-10.4 cal kyr BP. For the lowermost section (420-590 cm) of this core GC 303600-3 we applied a higher sedimentation rate of 10 mm yr^{-1}, which is relatively close to the average sedimentation rate of section 317-375 cm for core GC 303600-N (2.4 mm yr^{-1}), to generate tentative ages for the deeper section of this core. The reason a higher sedimentation rate than the average of the previous sediment section was used is because the base of core GC 303600-3 is believed to have recovered the beginning of the Ancylus Lake phase and exclude the Yoldia Sea phase, and this sedimentation rate when applied created a tentative age model that began right after the close of the Yoldia Sea phase and the start of the Ancylus Lake phase. Combining these three sediment cores from the Gotland Basin generates one long continuous sediment record spanning from10.6 to -0.1 cal kyr BP.

For the two sediment cores of the Arkona Basin (318340 and 318310) an age-depth model is also available (Warden et al., 2016b). The XRF (Ca) and LOI data were used to correlate and determine the different phases captured in each core. The sedimentary record for core 318310 spans the later part of the freshwater Ancylus Lake phase and most of the brackish phase of the Baltic Sea (10.2-0.1 cal kyr BP). For sediment core 318340 the part of the sedimentary record we analysed captures the Baltic Ice Lake period (12.5-11.6 cal kyr BP) the Yoldia Sea phase (11.3-10.7 cal kyr BP) the Ancylus Lake stage of the Baltic Sea (10.6-7.8 cal kyr BP), as well as a the Ancylus Lake/Littorina Sea transition (7.7-7.3 cal kyr BP). These two sedimentary records were correlated and combined to form a single, continuous sedimentary record of the Arkona Basin.

3.3 Total organic carbon (TOC).

TOC analysis was performed on the sediments subsampled from core 303600. To this end, the sediment was decalcified using a 2 N HCL solution for approximately 18 h. The sediment was subsequently rinsed three times with double-distilled water and then freeze-dried again. The TOC content of the decarbonated sample was analyzed in duplicate and measured using the Flash 2000 series Organic Elemental Analyzer (Thermo Scientific) equipped with a TCD detector and from this data and the carbonate content the TOC was calculated.

3.4 Loss on ignition (LOI).

In order to estimate the organic carbon content for sediment cores 303600-3, 318310, and 318340, freeze-dried samples were ashed at 550°C for 3 h and the resulting mass difference was then calculated in wt.%. Total organic carbon (TOC%) was calculated by dividing LOI values by 2.5 and then used to determine concentration of GDGTs in sediments. The factor of 2.5 is based on values for LOI and TOC for a large set of Baltic Sea sediments (Dean, 1974).

3.5 Lipid extraction and GDGT analysis.

All sediment samples were freeze-dried, and then after being ground and homogenized using a mortar and pestle, extracted using the Dionex^{TM} accelerated solvent extraction (ASE). For the ASE, 1-3 g of sediment was extracted with a solvent mixture of dilchloromethane (DCM):methanol (9:1, v/v) at a temperature of 100°C and a pressure of 1500 psi (5 min each) with 60% flush and purge 60 s. The collected extract was concentrated with a Caliper Turbovap®LV, then using DCM the lipid extract was dried over anhydrous Na_2SO_4 and blown down over a gentle stream of N_2. In order to quantify GDGTs, 1 µg of an internal standard (C_{46} GDGT; Huguet et al., 2006) was added to the total lipid extract before separating it over an Al_2O_3 column (activated for 2 h at 150°C) into three fractions using hexane:DCM (9:1, v:v) for the apolar fraction, hexane:DCM (1:1, v:v) for the ketone fraction and DCM:MeOH (1:1, v:v) for the polar fraction. The polar fraction containing the GDGTs was dried under N_2 and then re-dissolved in hexane:isopropoanol (99:1, v:v) at a concentration 10 mg ml^{-1} before being passed through a 0.45 µm PTFE filter and analysed with high performance liquid chromatography- atmospheric pressure positive ion chemical ionization –mass spectrometry (UHPLC-APCI-MS) using the method developed by Hopmans et al. (2015).

3.6 Compound specific stable C isotope analysis.

In order to constrain the source of brGDGTs in the sediments, we assessed their stable carbon isotope composition by analysis of their ether-bound alkyl moieties. To this end freeze-dried sediments from three different depth intervals from within the Ancylus Lake phase in sediment core 303600-N were pooled by equal amounts, homogenized in a mortar, and subsequently extracted by ASE and fractionated over Al_2O_3 as described above. The polar fractions were dissolved in hexane:isopropanol (99:1, v:v) and transferred to a column (4 cm) containing activated silica gel (3 h at 130°C). The column was eluted with (1) hexane:isopropanol (96:4, v:v) and (2) hexane:isopropanol (90:10, v:v). The brGDGT-containing second fraction was dried and subjected to 57 % HI in H_2O (Schouten et al., 1998) to cleave the ether bonds linking the alkyl chains with the glycerol backbone. The resulting alkyl iodides were reduced to hydrocarbons by H_2 in the presence of PtO_2 (Kaneko et al., 2011), and finally purified over activated Al_2O_3 by elution with hexane. The identity of the brGDGT-derived alkanes were confirmed by gas chromatography mass spectrometry (GC-MS) analysis and comparison of electron ionization (EI) mass spectra with previously published data (Sinninghe Damsté et al., 2000; Weijers et al., 2010; De Jonge et al., 2013b; Weber et al., 2015). Thereafter, the ^{13}C content of the alkyl chains was determined by GC/combustion-isotope ratio mass spectrometry (GC/C-IRMS) using a Delta V™ Advantage IRMS (Thermo Scientific, USA). Samples containing the hydrocarbons released by ether cleavage were injected at 50°C on a 50 m low-bleed Rxi®-5ms GC column (0.2 mm iD, 0.33 µm d_f, Restek, USA). After 2 min hold time, GC oven temperature was rapidly increased to 220 °C at 20 °C min^{-1}, held for 65 min to improve separation of alkanes and steranes, and finally increased at 4 °C min^{-1} to 320 °C (held for 35 min). The carbon isotopic composition of the analytes (reported in the δ-notation with respect to the V-PDB carbonate standard) were calibrated externally using an alkane mixture (C_{16} - C_{30}) with known isotopic compositions (n-alkane mixture B3 provided by A. Schimmelmann, Indiana University, USA). GC/C-IRMS performance was monitored by regular analysis of this standard mixture. All samples were analyzed in triplicate.

3.7 Calculation of GDGT-based proxies.

The Roman numerals refer to the GDGTs indicated in Fig. 1. The 5-methyl brGDGTs and 6-methyl brGDGTs are distinguished by an accent on the latter and IV is crenarchaeol. The BIT Index was calculated including the 6-methyl brGDGTs as according to De Jonge et al. (2016):

$$\text{BIT index} = (Ia+IIa+IIIa+IIa'+IIIa')/(Ia+IIa+IIIa+IIa'+IIIa'+IV) \quad [1]$$

The isomer ratio (IR) signifies the quantity of the penta- and hexa-methylated 6-methyl brGDGTs compared to the total brGDGTs (De Jonge et al., 2015a):

$$IR=(IIa'+IIb'+IIc'+IIIa'+IIIb'+IIIc')/(IIa+IIb+IIc+IIIa+IIIb+IIIc+IIa'+IIb'+IIc'+IIIa'+IIIb'+IIIc') \quad [2]$$

The relative abundance of the 6-methyl, hexa- and pentamethylated isomers compared with the 5-methyl are calculated according to (De Jonge et al., 2014b):

$$IR_{II} = IIa'/(IIa+IIa') \quad [3]$$

$$IR_{III} = IIIa'/(IIIa+IIIa') \quad [4]$$

The MBT was calculated according to (Weijers et al., 2007b) but without the inclusion of the novel isomers as in (De Jonge et al., 2014a):

$$MBT_{5me} = (I+Ib+Ic)/(I+Ib+Ic+IIa+IIb+IIc+IIIa+IIIb+IIIc) \quad [5]$$

The degree of cyclization, DC', was calculated according to Warden et al. (2016b), and was modified from (Sinninghe Damste et al., 2009) to include the 6-methyl, pentamethylated isomers:

$$DC' = (Ib+IIb+IIb')/(Ia+Ib+IIa+IIb+IIa'+IIb') \quad [6]$$

For the cyclopentane moieties the weighted average was calculated for the tetra- and pentamethylated brGDGTs according to Sinninghe Damste (2016):

$$\#rings_{tetra} = ([Ib]+2*[Ic])/([Ia]+[Ib]+[Ic]) \quad [7]$$

$$\#rings_{penta\ 5me} = ([IIb]+2*[IIc])/([IIa]+[IIb]+[IIc]) \quad [8]$$

$$\#rings_{penta\ 6me} = ([IIb']+2*[IIc'])/([IIa']+[IIb']+[IIc']) \quad [9]$$

The novel MAT_{mr} /CBT' calibration was used for the calculation of pH and MAT (De Jonge et al., 2014a):

$$CBT' = {}^{10}log[(Ic+IIa'+IIb'+IIc'+IIIa'+IIIb'+IIIc')/(Ia+IIa+IIIa)] \quad [10]$$

$$pH = 7.15 + 1.59 * CBT' \quad [11]$$

$$MAT_{mr} = 7.17 + 17.1 * [Ia] + 25.9 * [Ib] + 34.4 * [Ic] - 28.6 * [IIa] \quad [12]$$

The marine bottom water temperature (BWT) calibration designed for coastal marine sediments was calculated according to Dearing et al. (unpublished results):

$$BWT = (MBT'_{5me} – 0.3912)\backslash 0.0168 \quad [13]$$

For the calculation of mean summer air temperature (MST) using the distributions of aquatically produced brGDGTs we implemented the calibration from (Pearson et al., 2011) that was previously modified to account for the newly separated 6-methyl isomers in a study by (De Jonge et al., 2015b) :

$$MST\ (°C) = 20.9 + 89.1 \times [Ib] – 12 \times ([IIa] + [IIa']) -20.5 \times [IIIa] \quad [14]$$

The square brackets indicate the fractional abundances of the brGDGT within the brackets relative to the sum of all brGDGTs.

3.8 Statistical Analysis.

Principal component analysis (PCA) was executed using the software package R. The statistical analysis was completed using the fractional abundances of all 15 of the 5- and 6-methyl brGDGTs for the entire sample set from the Baltic Sea region.

4. Results

Three sediment cores from the central Gotland Basin were correlated (see experimental) and together provide a continuous record spanning the last 10.6 cal kyr BP. The

TOC content of the sediments varies from c. 3% to as high as 16% in the recent brackish phase (7.2– 0.1 cal kyr BP), while it is substantially lower (i.e. <2%) in the section representing the Ancylus Lake phase (10.6-7.8 cal kyr BP; Fig. 4).

Two sediment cores from the Arkona Basin were also correlated (see experimental) and together provide a continuous record spanning from at least 12.5 to 0.1 cal kyr BP. The LOI content of the sediments varies from c. 11% to as high as 17.7% in the recent brackish phase, while it is substantially lower (i.e. 5.5% on average) in the Ancylus Lake phase (Fig. 4). For the beginning of the Ancylus Lake phase (10.6-10.3 cal kyr BP) the Yoldia Sea phase (11.2-10.7 cal kyr BP) and the Baltic Ice Lake period (12.5-11.8 cal kyr BP) no LOI data are available (Fig. 4). The LOI-derived TOC content (wt. %) of Arkona Basin sediments deposited during the brackish phase (i.e. 5.8±0.7 wt. %, average±standard deviation) is highly comparable to that for the more recent brackish phase sediments from the Gotland Basin record (5.8±3.2 wt. %; Figs. 3-4). However, the TOC (wt. %) of sediments deposited during the Ancylus Lake phase in the Arkona Basin (3.1±1.8 wt.) is higher than those in the Gotland Basin (1.1±0.6 wt. %; Figs. 3-4).

4.1 GDGTs in the sedimentary records: concentrations, general distribution, and the BIT Index

The summed brGDGT concentrations (normalized to the TOC content) in both the Gotland and Arkona Basin sediment records were substantially higher during freshwater Ancylus Lake phase as compared to the brackish phase that followed (181±107 vs. 18±17 μg g^{-1} TOC, and 260±141 vs 37±5 μg g^{-1} TOC, respectively; Figs. 5a & d). The concentration of crenarchaeol is highly variable but the average amount remains the same in the Ancylus Lake phase and the brackish phase of both the Gotland (218±190 vs. 233±222 μg g^{-1} TOC) and Arkona Basin records (62±49 vs. 107±15 μg g^{-1} TOC) when the standard deviations are taken into account (Fig. 5b & e). The same holds true for the concentration of GDGT-0, which is also highly variable but the concentration is not significantly different from the Ancylus Lake to the brackish phase in both the Gotland (156±166 vs. 109±111 μg g^{-1} TOC) and Arkona (41±19 vs. 73±12 μg g^{-1} TOC) basins. In the last 0.5 cal kyr BP of the Gotland Basin record, a decrease occurs in both the concentration of crenarchaeol, 77±13 μg g^{-1} TOC, and the summed concentration of brGDGTs, 8.0±1.2 μg g^{-1} TOC (Figs. 5a & b).

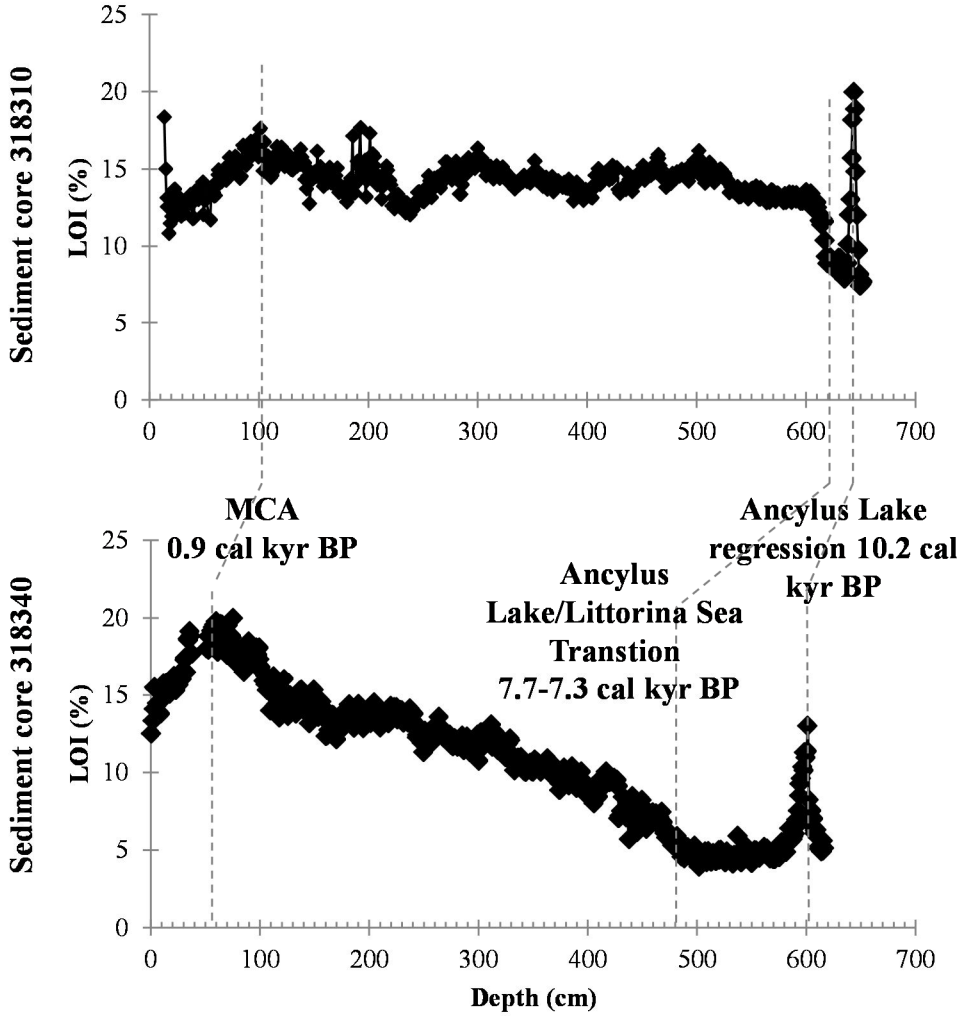

Fig. 4 The LOI (%) plotted with sediment core depth (cm) for the two sediment cores (318310 and 318340) from the Arkona Basin. Dotted lines illustrate how the LOI (%) profiles were used to correlate the two cores as well as designate the different phases that occurred in the Baltic Sea over the Holocene.

When these data are used to plot the fractional abundances of the three major classes of GDGTs, i.e. summed brGDGTs, crenarchaeol, and GDGT-0 (cf. Blaga et al., 2009), it is evident that there is a strong variation in this respect (Fig. 6). Included in this plot are data from surface sediments in the Baltic Sea and the nearby Skagerrak (for which we lack absolute concentration data). These surface sediments are all characterized by relatively low amounts of brGDGTs and the GDGT distributions of the sediments deposited during the brackish phase in both the Gotland and, to a lesser extent, Arkona Basin plot in the same area. Distributions such as this are more characteristic for marine sediments (Schouten et al., 2012). The sediments from both the Arkona and Gotland Basins deposited during the Ancylus Lake, and in the Arkona Basin sediments from the Yoldia Sea, and Baltic Ice Lake phases contain substantially higher relative amounts of brGDGTs (i.e. >20%; Fig. 6).

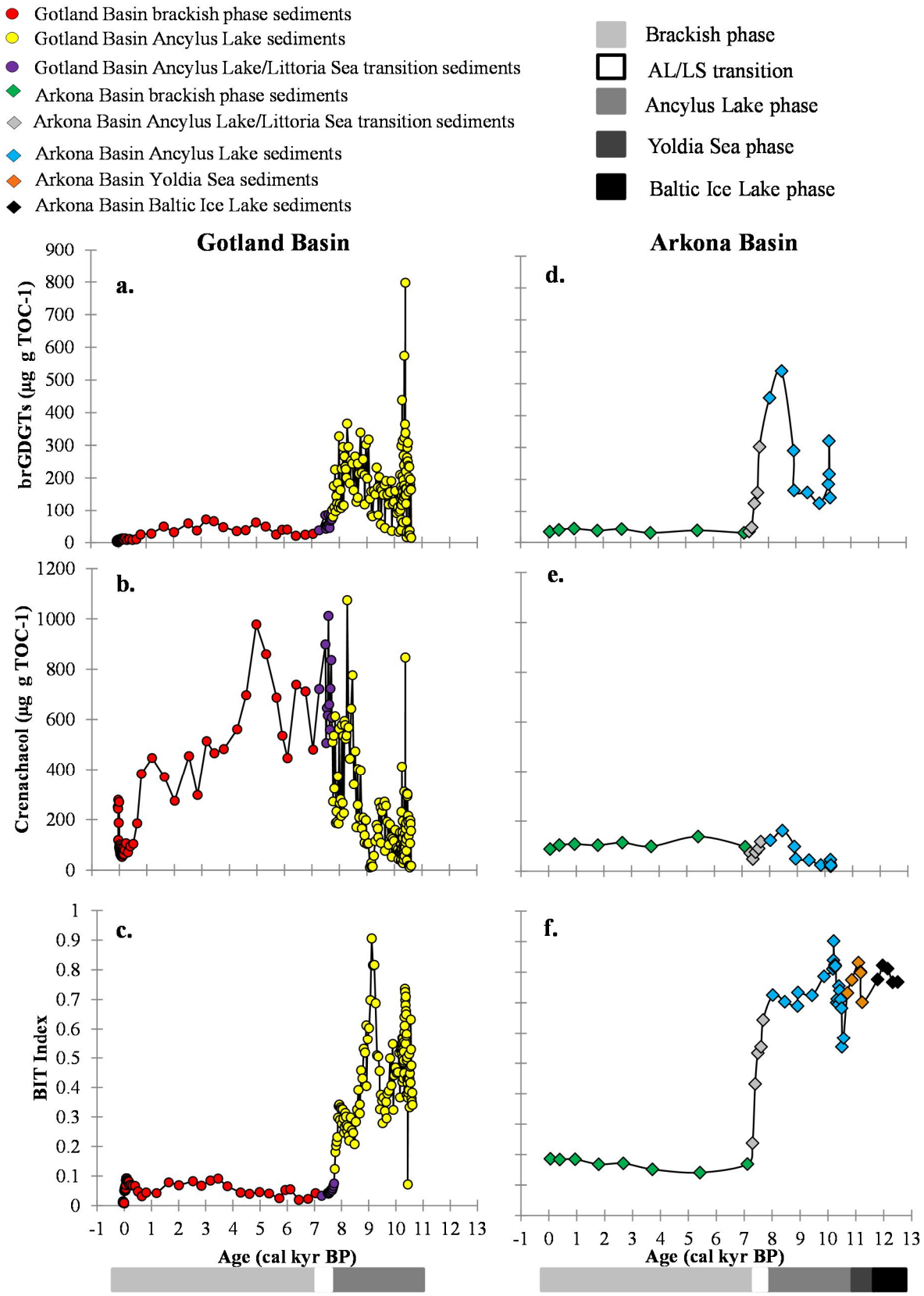
Gotland Basin brackish phase sediments
Gotland Basin Ancylus Lake sediments
Gotland Basin Ancylus Lake/Littoria Sea transition sediments
Arkona Basin brackish phase sediments
Arkona Basin Ancylus Lake/Littoria Sea transition sediments
Arkona Basin Ancylus Lake sediments
Arkona Basin Yoldia Sea sediments
Arkona Basin Baltic Ice Lake sediments
Brackish phase
AL/LS transition
Ancylus Lake phase
Yoldia Sea phase
Baltic Ice Lake phase
Gotland Basin
Arkona Basin
a.
b.
c.
d.
e.
f.
brGDGTs (µg g TOC-1)
Crenachaeol (µg g TOC-1)
BIT Index
Age (cal kyr BP)
Age (cal kyr BP)

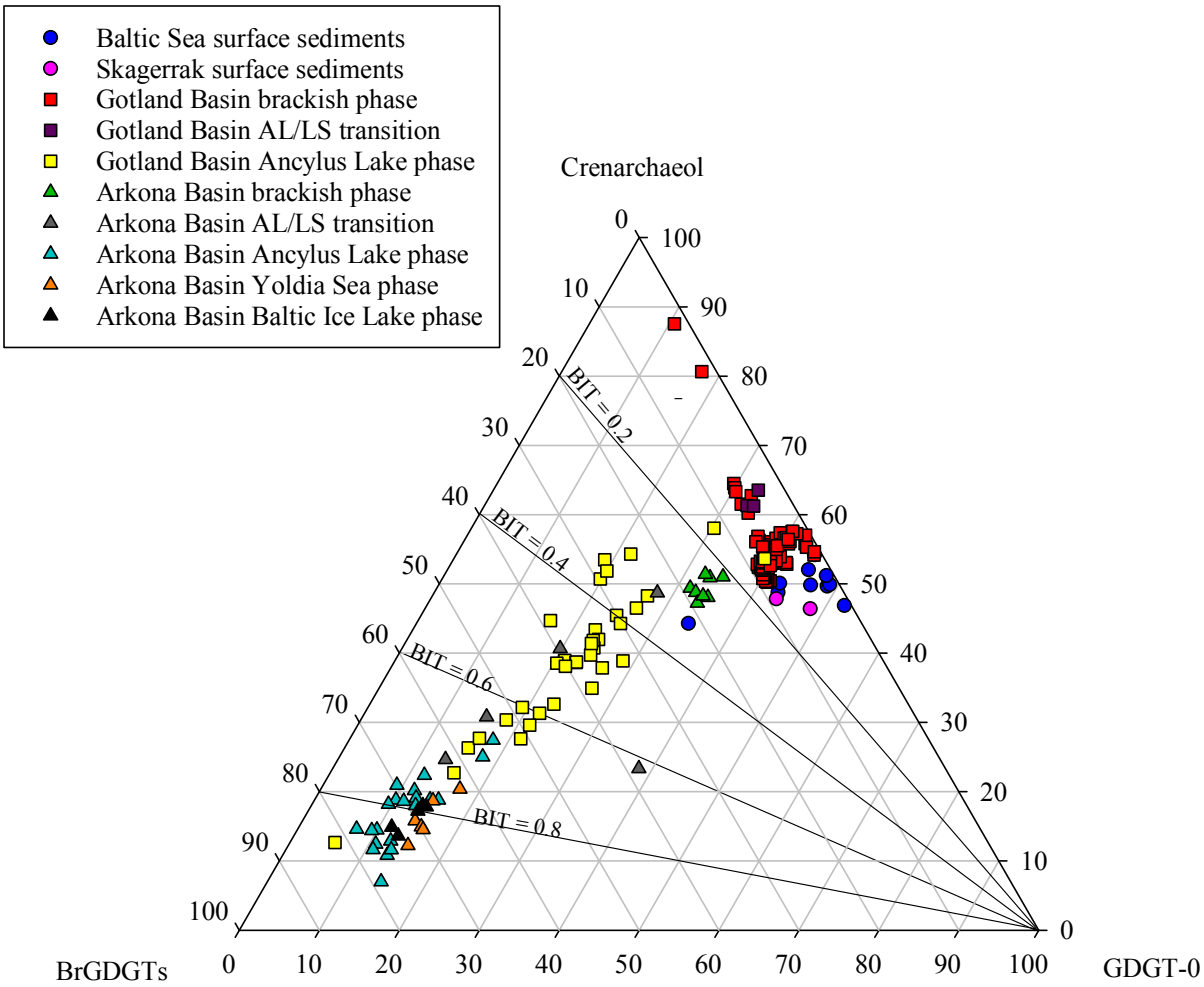

Fig. 6 Ternary diagram (after Blaga et al., 2009) illustrating the composition of the major isoprenoid and brGDGTs in the Baltic Sea sediments used in this study. Corresponding BIT values are indicated by black lines. The lines with constant values for the BIT are plotted to illustrate the wide variety in in the BIT index among these sediment samples. The different sediment samples from the Baltic Sea are represented by symbols with different colors and shapes as indicated.

⬅ Fig. 5 Variations in the concentrations of summed brGDGTs (in µg g^{-1} TOC) and crenarchaeol (in µg g^{-1} TOC) and the the BIT index for the Gotland Basin (**a-c**) and Arkona Basins (**d-f**). For the Gotland Basin the Ancylus Lake phase is designated in yellow, the Ancylus Lake/Littorina Sea transition in purple, and the brackish phase in red. For the Arkona Basin the Baltic Ice Lake is indicated in black, the Yoldia Sea phase in orange, the Ancylus Lake phase in light blue, the Ancylus Lake/Littorina Sea transition in gray and the brackish phase in green. There was no TOC or LOI data for the Baltic Ice Lake and Yoldia See phases to normalize the concentrations on and so the data from that phase is missing from plots (d) and (e).

The changes in the relative abundances of the GDGTs translate into distinct differences in the BIT index. The BIT index for both the Skagerrak surface sediments (0.08±0.02) and the Baltic Sea surface sediments (0.06±0.09) is low (Fig. 6). However, one of the Baltic Sea surface sediment from the Bothnian Sea, 377850 stands out with a significantly higher value for the BIT index, i.e. 0.31 (Fig. 2). With respect to the Gotland Basin sedimentary records, the BIT index decreases from the Ancylus Lake phase (0.44±0.16) to much lower values (0.06±0.02) in the brackish phase (Fig. 5c). These latter values are close to those of the Baltic Sea surface sediments. For the Arkona Basin record, the BIT index is highest in the Baltic Ice Lake phase (0.79±0.03), Yoldia Sea phase (0.77±0.05) and the Ancylus Lake phase (0.74±0.08) and is much lower in the brackish phase (0.17±0.02) (Fig. 5f). In the Gotland Basin sediments the BIT index is generally lower than in the Arkona Basin record (Figs. 5c & f). A period with higher BIT index values, (c. 10.3 cal kyr BP in the Gotland Basin and c. 10.20 cal kyr BP in the Arkona Basin; Figs. 5c & f) are observed and in both records this period is preceded by a "spike" towards lower BIT index values, i.e. 10.44 cal kyr BP in the Gotland Basin record and in the Arkona Basin record between 10.56-10.52 cal kyr BP (Figs. 5c & f), just after the Yoldia Sea/Ancylus Lake transition. In the Arkona Basin record, a BIT "spike" towards lower values also occurs at the start of the Yoldia Sea phase (11.2 cal kyr BP) (Fig. 5). A maximum in BIT index values (0.91) occurs at c. 9.1 cal kyr BP in the Gotland Basin record (Fig. 5c), and although the maximum does not occur at this time in the Arkona Basin record (maximum occurs at 10.20 cal kyr BP), BIT index values are high at this time as well (between 0.72-0.77) (Fig. 5f).

4.2 Distribution of branched GDGTs

All 15 brGDGTs (see Fig. 1 for structures) identified previously in soils with the UHPLC-MS method (De Jonge et al., 2013b) were detected in the examined sediments. The Baltic Sea and Skagerrak surface sediments and the sediments from the recent brackish phase of both the Gotland and Arkona Basins have similar brGDGT distributions (Figs. 7a, b, c, & d). The distribution of brGDGTs during the Ancylus Lake phase of the Gotland Basin is characterized by a higher fractional abundance of the brGDGTs IIIa and IIIa' than in the brackish phase (Figs. 7c & e). This is also true for the Arkona Basin but to a lesser extent (Figs. 7d & f). The Ancylus Lake phase of the Gotland Basin has the highest average fractional abundance of brGDGT IIIa' (0.26±0.09) out of all of the sample sets presented in this study (Fig. 7e).

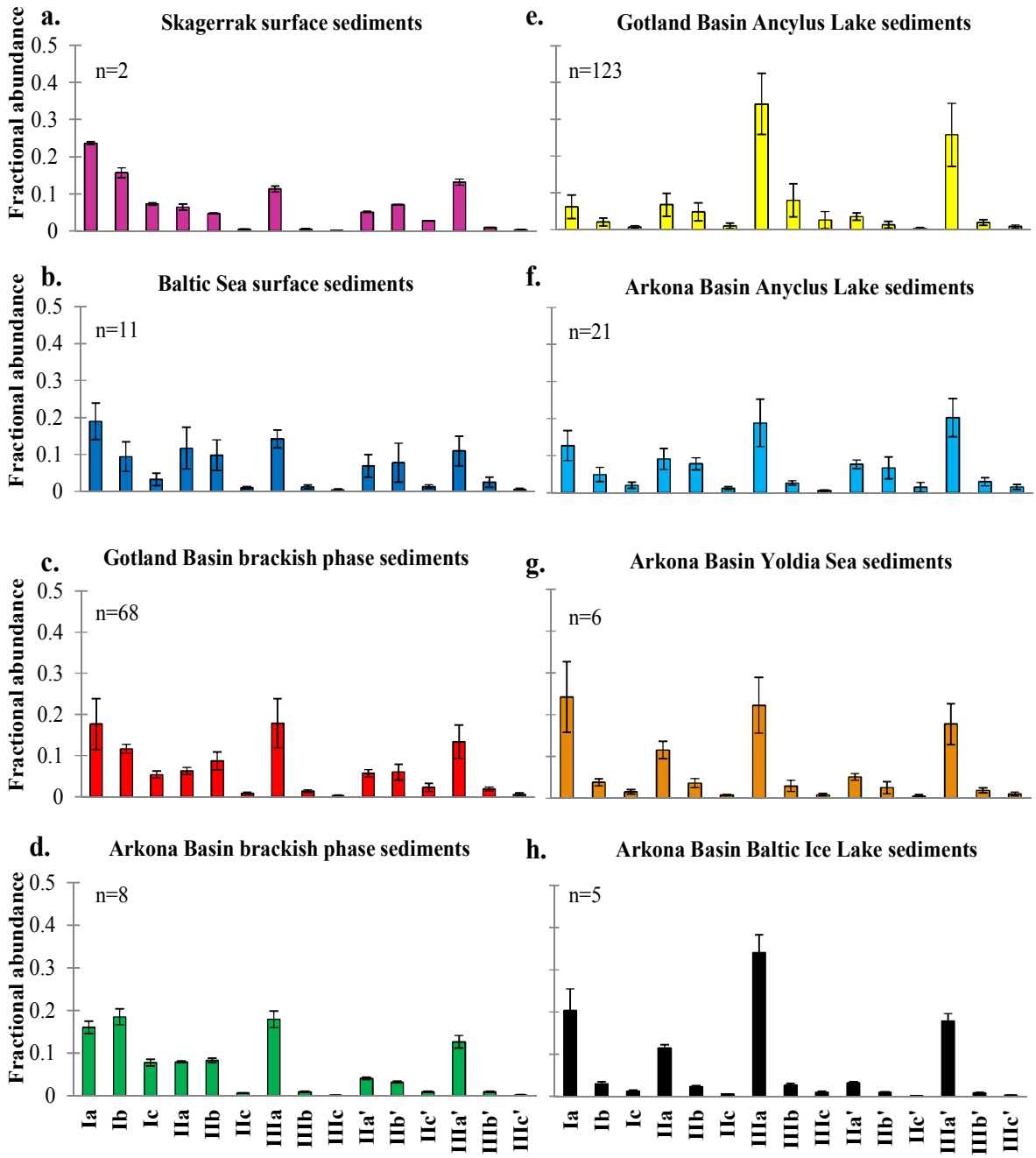

Fig. 7 The average distribution of brGDGTs for the various sets of sediments from the Baltic Sea used in this study, showing differences in brGDGT distribution between higher (a-d) and lower (e-h) salinity phases.

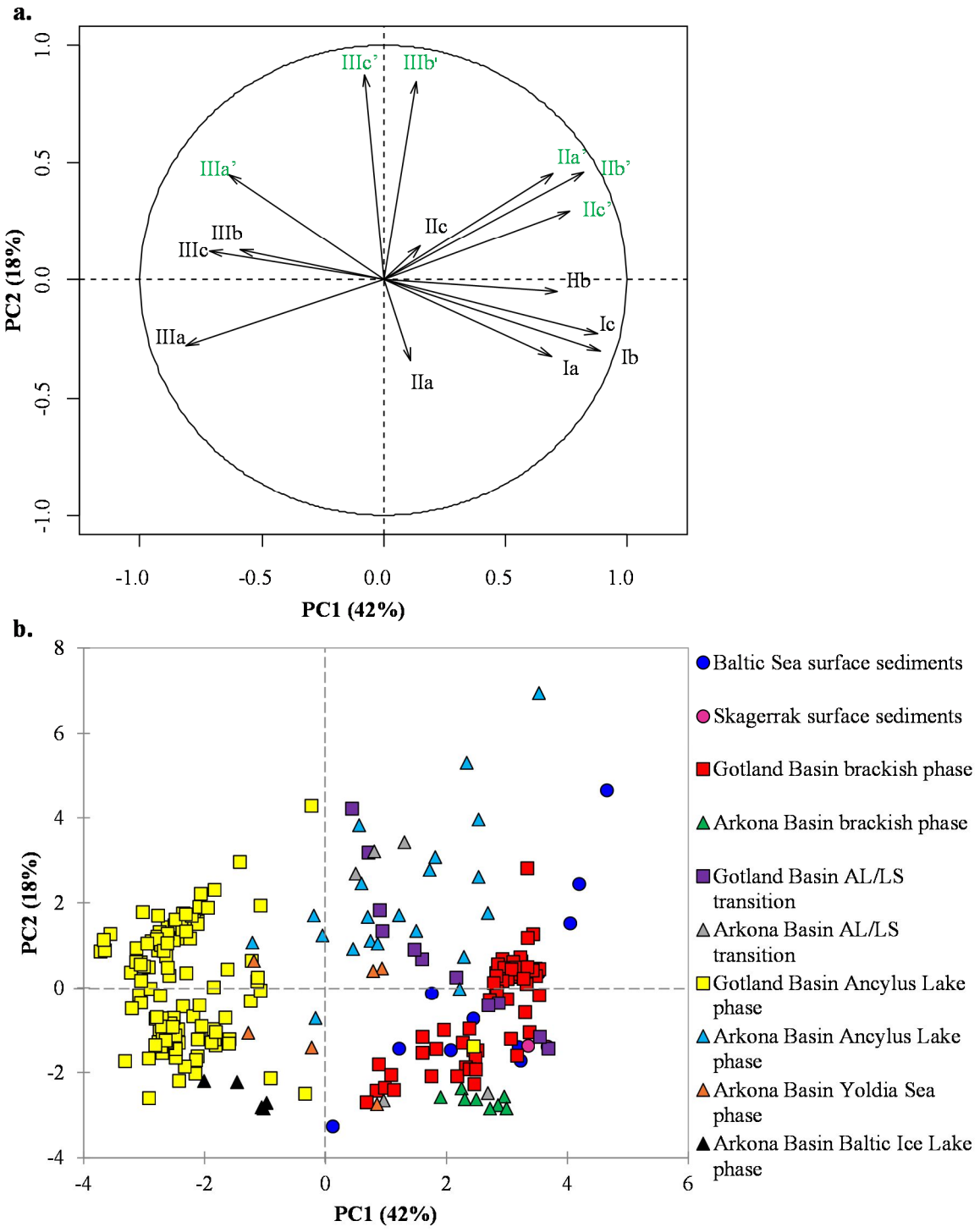

Fig. 8 Results of a principal component analysis (PCA) based on the fractional abundances of the 15 brGDGTs in sediments from the Baltic Sea, showing (a) variable loadings and (b) sample scores (b). The Roman numerals refer to brGDGT structures (Fig. 1). The different sample sets are designated by symbols with different color and shape as indicated.

The Ancylus Lake phase of the Gotland Basin and the Baltic Ice Lake phase of the Arkona Basin have the highest average fractional abundance of brGDGT IIIa (~0.34) (Figs. 7e & h). All of the lower salinity phase sediments from both basins (Ancylus Lake phase, Yoldia Sea phase and Baltic Ice Lake phase) are dominated by non-cyclic brGDGTs (Figs. 7e-h). This is mostly not the case with the higher salinity sediments such as the Baltic Sea surface sediments, the Skagerrak surface sediments, and the recent brackish phase in the Arkona Basin (Figs. 7a- d).

To better understand the factors controlling the distribution of brGDGTs in the sediments, PCA was performed on the fractional abundances of the 15 brGDGTs present in all sediments from this study. PC1 explained 42 % of the total variance and appears to be related to the degree of methylation of the brGDGTs, with most of the hexamethylated brGDGTs (IIIa, IIIa', IIIb, IIIc, IIIc') plotting negatively on PC1 and most of their less methylated counterparts (Ia, Ib, Ic, IIa, IIa', IIb, IIb', IIc, IIc') plotting positively (Fig. 8a). For the overall sample set, PC1 is highly correlated (R^2=0.89; Fig. 9a) with the MBT_{5Me}, i.e., the degree of methylation of the 5-methyl brGDGTs (De Jonge et al., 2014a).

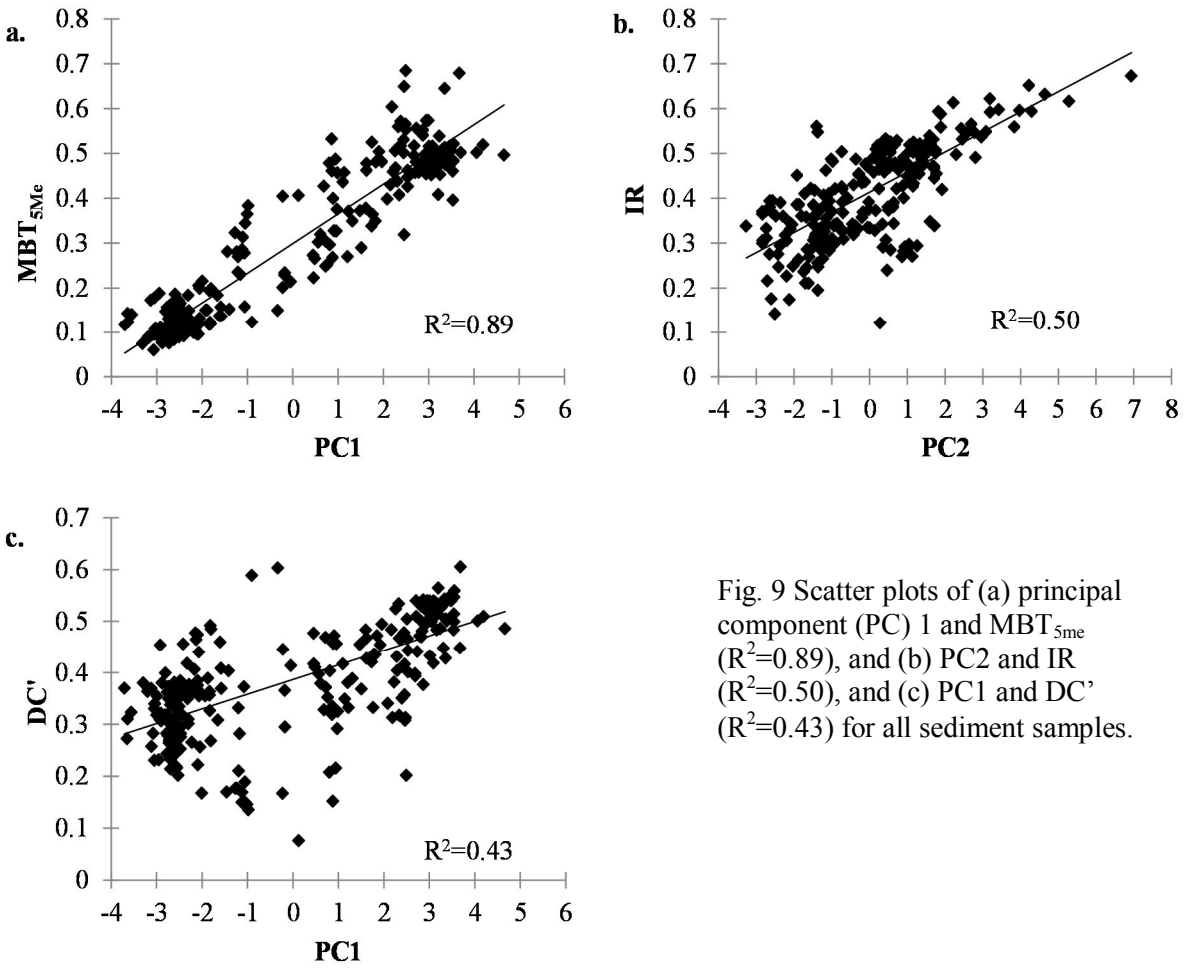

Fig. 9 Scatter plots of (a) principal component (PC) 1 and MBT_{5me} (R^2=0.89), and (b) PC2 and IR (R^2=0.50), and (c) PC1 and DC' (R^2=0.43) for all sediment samples.

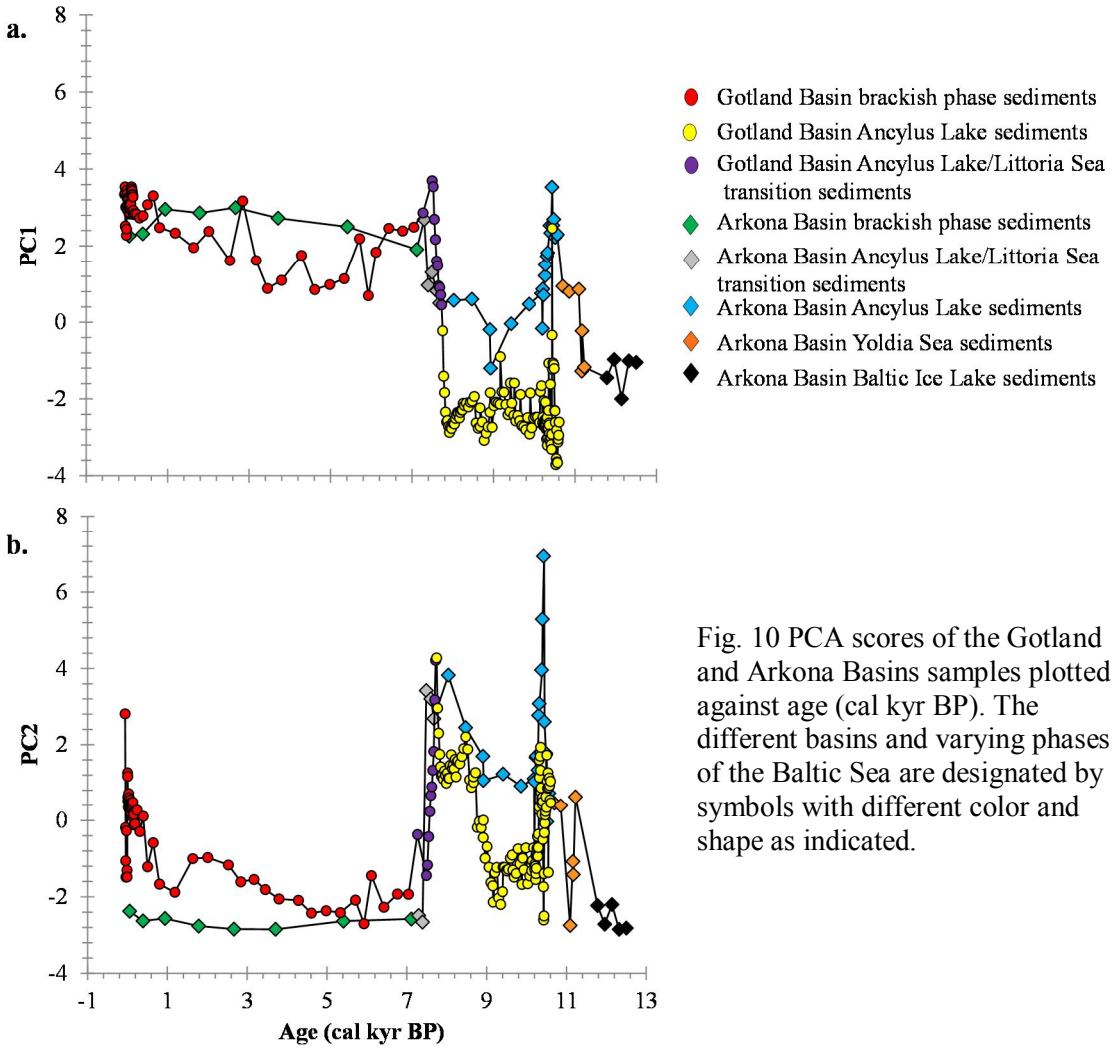

Fig. 10 PCA scores of the Gotland and Arkona Basins samples plotted against age (cal kyr BP). The different basins and varying phases of the Baltic Sea are designated by symbols with different color and shape as indicated.

With the exception of one sample (420.5 cm from core 303600-3, 10.44 cal kyr BP), all Ancylus Lake phase sediments from the Gotland Basin plot negatively on PC1 as do all of the sediments of the Baltic Ice Lake phase from the Arkona Basin (Fig. 8b). Additionally, the three sediments from the early Yoldia Sea phase (sediment depths 847.5, 840.5 and 839.5 cm from core 318340 corresponding to 11.23-11.16 cal kyr BP) as well as four sediments from the Ancylus Lake phase (sediment depths 540.5 and 564.5 cm depth from core 318340 and 625 and 642.5 cm depths from core 318310 corresponding with 9.43-8.91 and 10.20 cal kyr BP) in the Arkona Basin plot negatively as well (Fig. 8b). The remaining sediments all score positively on PC1, indicating that their brGDGT distributions are dominated by the less methylated brGDGTs (Figs. 8a & b). When plotted against age a sudden substantial increase in the scores on PC1 in the Gotland Basin record is observed during the Ancylus Lake/Littorina Sea transition (7.7-7.3 cal kyr BP; Fig. 10a). This transition takes place in c. 400 years. A less drastic increase occurs in the score on PC1 for the Arkona Basin

sedimentary record during this transition (Fig. 10a). Clearly, enhanced scores on PC1 are also noted for both records at 10.44 cal kyr BP, following the Yoldia Sea/Ancylus Lake transition (Fig. 10a). Overall, the score on PC1 for the Arkona Basin sediments is higher than for the Gotland Basin sedimentary record (Fig. 10a). The PC1 values increase from the Baltic Ice Lake phase, which has the lowest values in the Arkona Basin record, to the more recent brackish stage. This increasing trend in PC1 values going from the Ancylus Lake phase into the more recent brackish phase also occurs in the Gotland Basin (Fig. 10a).

PC2 explains 18% of the variance in the PCA and is related to the fractional abundance of the 5- versus 6-methyl brGDGTs (Fig. 8a). The 6-methyl brGDGTs all score positively on PC2, and except for some of the more minor 5-methyl brGDGTs, IIc, IIIc, and IIIb, the 5-methyl brGDGTs score negatively on PC2 (Fig. 8a). Indeed, for the overall dataset PC2 correlates with the IR (R^2=0.50; Fig. 9b), which is a reflection of the relative abundance of the 6-methyl brGDGTs (De Jonge et al., 2014b). The Baltic Sea surface sediments that score negatively on PC2 are mostly those from the northern part of the basin (372820, 377850, 377830, 349200& 349190) and those more in the south closer to the connection to the North Sea (372720 & 303600) as well as the surface sediment samples from the Skagerrak (Fig. 2). The sediments that plot negatively on PC2 include all of those from the Baltic Ice Lake, the brackish sediments from the Arkona Basin, two samples from later in the Ancylus Lake/Littorina Sea transition in the Arkona Basin (sediment core 318340 depths 420.5 and 400.5 corresponding to 7.39-7.30 cal kyr BP), and a portion of the Gotland Basin sediments from both the Ancylus Lake phase and the brackish phase as well as sediments from later in the Ancylus Lake/Littorina Sea transition (sediment depths 207-197 from core 303600-N corresponding to 7.55-7.27 cal . kyrs. BP) (Fig. 8b). The sediments that plot positively on PC2 include four of the Baltic Sea surface sediments from the Gotland Basin (excluding surface sediment sample 303600; Fig. 2), almost all of the sediment record from the Ancylus Lake phase in the Arkona Basin (excluding sediment depth 642.5 from core 318310 corresponding with 10.20 cal kyr BP and sediment depth 732.5 cm from core 318340 corresponding to 10.52 cal kyr BP), a portion of the samples from both phases of the Gotland Basin record and those from the early part of the Ancylus Lake/Littorina Sea transition from both basins. When plotted against age the scores on PC2 are mostly negative and fairly stable in the brackish phase in both basins of the Baltic Sea (Fig. 10b). Most of the recent (2008 and 1793-1948 AD) sediments of the Gotland Basin are an exception in this respect since the score on PC2 increases to positive values at this time (Fig. 10b). The scores on PC2 are much more variable for the sediments deposited during the Ancylus Lake phase (Fig. 10b) than for

the recent brackish phase. A positive score on PC2 for the sediments from the Ancylus Lake phase in the Arkona Basin is noted, with the exception of one sediment with an age of 10.20 cal kyr BP (Fig. 10b). For the Gotland Basin the scores on PC2 for the sediments deposited during the Ancylus Lake phase are more variable and mostly higher than in the brackish stage (Fig 10b), however, unlike in the Arkona Basin the scores on PC2 are mostly negative from about 10.35-8.77 cal kyr BP. Despite the differences in absolute scores for PC2 for the two basins, both profiles show similar temporal trends (Fig. 10b). As noted for PC1, a marked change in the scores on PC2 is evident in both basins at the Anyclus Lake/Littorina Sea transition (7.7-7.3 cal kyr BP) and immediately following the Yoldia Sea phase (c. 10.44 cal kyr BP; Fig. 10b). After the Anyclus Lake/Littorina Sea transition, the high resolution profile of the Gotland Basin record shows that the scores on PC2 first increase and subsequently sharply decrease to the negative scores that are common for the brackish phase (Fig. 10b). This transition takes place in c. 400 yr and coincides with the marked increase in the scores on PC1 (Fig. 10a). As the Yoldia Sea phase neared its end (10.6 cal kyr BP), the scores on PC2 increase to positive values in the Arkona Basin record (at 10.86 cal kyr BP) and in the records from both basins there is a sudden increase in the PC2 values during the early Ancylus Lake phase (c. 10.4 cal kyr BP in the Arkona Basin and c. 10.3 cal kyr BP in the Gotland Basin record) and then a subsequent decrease in values (Fig. 10b). In the Baltic Ice Lake phase the PC2 values are all negative, but then sharply increase at the Ancylus Lake regression (10.23 cal kyr BP; Fig. 10a). The PC2 score then returns to negative values until close to the Yoldia Sea/Ancylus Lake transition at 10.9 cal kyr BP when the score increases sharply once again to positive values (Fig. 10b).

4.3 Stable carbon isotopic composition of brGDGTs

The presence of the novel brGDGT IIIa" (Fig. 1), which has been linked to lacustrine production of brGDGTs (Weber et al., 2015), was found in specific sections of the Gotland Basin sediment record from core 303600-N (Table 2). In order to determine if the origin of this brGDGT is different from that of the other brGDGTs, we determined the ^{13}C content of the brGDGTs in the sections of the sediment core with a higher abundance of brGDGT IIIa" by ether cleavage and GC-IRMS analysis of their alkyl chains (see experimental). Unfortunately, it was not possible to obtain individual $\delta^{13}C$ data for the 5,13,16- and 6,13,16-trimethyloctacosanes (which are only partly separated by GC), and when these isomers were integrated together the resulting $\delta^{13}C$ values were identical to that of 13,16-dimethyloctacosane (Table 2).

Table 2 The average of triplicate analysis for $\delta^{13}C$ values of brGDGTs from selected sediment depths from core 303600-N from the Gotland Basin record.

Sediment depths (cm)	Age (cal kyr BP)	brGDGT-derived alkane(s)	Avg. $\delta^{13}C$ (‰)	STDEV	Avg. $\delta^{13}C_{TOC}$ (‰)	STDEV
234-243	8.21-8.43	13,16 dimethyloctacosane (a)	-28.4	0.28		
234-243	8.21-8.43	5,13,16- and 6,13,16 trimethyloctacosane (b+c)	-29.0	0.01	-28.1	0.1
309-323	10.03-10.23	13,16 dimethyloctacosane (a)	-28.8	0.26		
309-323	10.03-10.23	5,13,16 and 6,13,16 trimethyloctacosane (b+c)	-28.7	0.10	-27.7	0.4
351-363	10.34-10.39	13,16 dimethyloctacosane (a)	-27.4	0.14		
351-363	10.34-10.39	5,13,16 and 6,13,16 trimethyloctacosane (b+c)	-28.4	0.11	-26.3	0.2

5 Discussion

5.1 Provenance of brGDGTs in the Baltic Sea

The application of brGDGTs on marine sediments for paleoclimate studies can be complicated when diverse sources of brGDGTs, which can include soils (Weijers et al., 2007b; Bendle et al., 2010), peats (Weijers et al., 2006a), and riverine (Yang et al., 2012; Zell et al., 2013; De Jonge et al., 2014b; Warden et al., 2016a) and marine (Peterse et al., 2009; Weijers et al., 2014; Sinninghe Damste, 2016) in situ production, contribute to the marine sediments. Therefore, the main sources of brGDGTs to a study site should be assessed before using brGDGTs for paleoenvironmental studies (Yang et al., 2012; Zell et al., 2013; De Jonge et al., 2015b; Warden et al., 2016a). Previously, a study by Sinninghe Damsté (2016) discussed how the heterogeneity of brGDGT sources complicates their application for paleoclimate studies, especially in coastal sediments between the depths of 50-300m where in situ production of brGDGTs is widespread, likely due to the higher delivery of organic matter. This study explored several methods for determining the provenance of brGDGTs in a specific setting (Sinninghe Damsté, 2016). Since the average depth of the Baltic Sea is 55 m, in situ production within the sediments as well as the water column must be assessed before applying a soil calibration for MAT estimates based on brGDGTs. Various lines of evidence

suggest that autochthonous production of brGDGTs played an important role in the sedimentary system of the Baltic Sea during the Holocene and shall be discussed below.

Sinninghe Damste (2016) demonstrated that when the fractional abundances of the tetra-, penta- and hexamethylated brGDGTs from soils are plotted in a ternary diagram, the composition of these soil derived brGDGTs lies within a distinct area. By comparing brGDGTs in coastal sediments with soils using this diagram, it can be assessed whether the brGDGTs are derived from soils through riverine transport or from aquatic production. A ternary plot comparing the distribution of brGDGTs of the Baltic Sea sediments with the global soil data set (Fig. 11; cf. Sinninghe Damsté 2016) shows that very few of the Baltic Sea sediments plot on top of the global soil data set. Those that do include some of the Baltic Sea surface sediment samples, one sample from the Ancylus Lake phase of the Gotland Basin, and a portion of samples from the Ancylus Lake phase of the Arkona Basin, suggesting that in these cases a higher percentage of the sedimentary brGDGTs are soil derived (Fig. 11).

A larger fraction of the brGDGTs was hexamethylated during the lower salinity phases and a decrease in methylation of brGDGTs occurs moving from the Ancylus Lake into the brackish phase (Figs. 7 & 11). This trend is true for both basins but is less pronounced in the Arkona Basin than in the Gotland Basin. Relatedly, an increase in MBT_{5me} is observed over the Holocene with each phase change in the Baltic Sea. Additionally it should be noted that an increased presence of the hexamethylated brGDGT isomer IIIa' is seen in all of the lower salinity phases in the Baltic Sea for both the Gotland (2^{nd} most abundant brGDGT) and Arkona (most abundant brGDGT along with IIIa) basins during the Ancylus Lake phase and also in the Arkona Basin during the Baltic Ice Lake and Yoldia Sea phases (most abundant brGDGT along with IIIa and Ia). A higher abundance of IIIa' was also observed in the SPM of Yenisei River waters (De Jonge et al., 2014b) as well as Svalbard sediments (Sinninghe Damste, 2016) and thought to indicate in situ production. Therefore, this suggests in situ production is a factor in these basins during lower salinity times.

Previously it has been suggested that when the average value for the number of rings (#rings) of the tetramethylated and the 5- and 6- methyl pentamethylated brGDGTs exceeds 0.7 (value indicated by the gray dotted lines in Fig. 12) as was observed in the Svalbard fjord sediments (#rings = 0.8-1.0), the brGDGTs are predominantly derived from in situ production (Peterse et al., 2009; Sinninghe Damste, 2016). The #rings for the 5-methyl pentamethylated brGDGTs, calculated using equation [8], exceeds 0.8 for a short time period during the

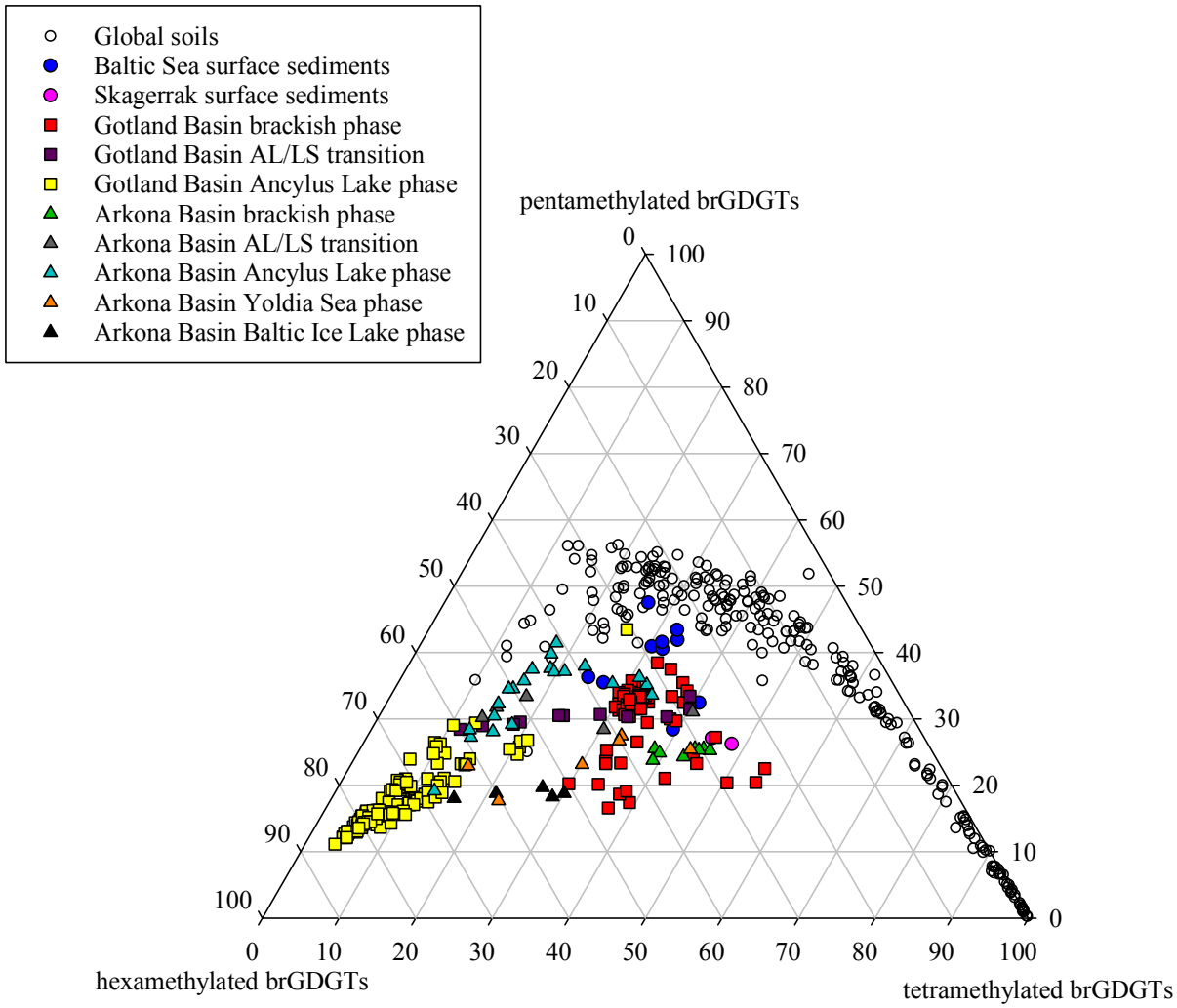

Fig. 11 Ternary diagram illustrating the fractional abundances of the tetra- (Ia-c), penta (IIa-c and II'a-c), and hexamethylated (IIIa-c and III'a-c) brGDGTs. The global soil dataset (open circles; De Jonge et al., 2014) is included for reference. Very few of the Baltic Sea sediments plot exactly on top on the global soil data demonstrating that for none of the complete sample sets brGDGTs are of 100% of soil origin (cf. Sinninghe Damsté, 2016). Only the samples from the Ancylus Lake phase of both basins and a few Baltic Sea surface sediments plot on top of or close to the global soil dataset indicating these samples have the largest contribution from terrestrially derived brGDGTs. The basins and phases of the Baltic Sea sediments are denoted by color and shape as indicated.

Ancylus Lake phase in both basins ~10.4 cal kyr BP (0.91±0.02 for the Gotland Basin and 0.88±0.12 for the Arkona Basin) and also during the Ancylus Lake/Littorina Sea transition in the Gotland Basin (0.85±0.06). Leading up to the Ancylus Lake/Littorina Sea transition (8.38-7.87 cal kyr BP) in the Gotland Basin the #rings for the 5-methyl pentamethylated brGDGTs are elevated (0.73±0.02) but do not reach the value of 0.8. The #rings for the 6-methyl pentamethylated brGDGTs, calculated using equation [9], in the Skagerrak surface sediments exceeds 0.7 (0.84±0.01) as it does in the Baltic Sea surface sediment in the Bothnian Bay (372820; 0.80), and although the overall average for the brackish phase of the Gotland Basin

is below 0.8, a section in the more recent past exceeds the threshold of 0.7 (1760-1961 AD; 0.83±0.05; Fig. 12b). In the brackish phase of the Arkona Basin the #rings for the tetramethylated brGDGTs, calculated using equation [7], also exceeds 0.7 (0.80±0.05) as do values for sediments from the more recent brackish phase in the Gotland Basin (0.77±0.01; 1786-1893 AD) and the surface sediment sample 349190 (0.77) located in the mouth of the Gulf of Finland (Figs. 12a-b). Therefore, the average value for the #rings indicates that in situ production is occurring in the brackish phase of both basins, the Ancylus Lake/Littorina Sea transition of the Gotland Basin (c. 10.4 cal kyr BP in both basins), as well as in the Skagerrak surface sediments and locations in the Baltic Sea basin close to sources of freshwater input (349190 and 372820; Fig. 2).

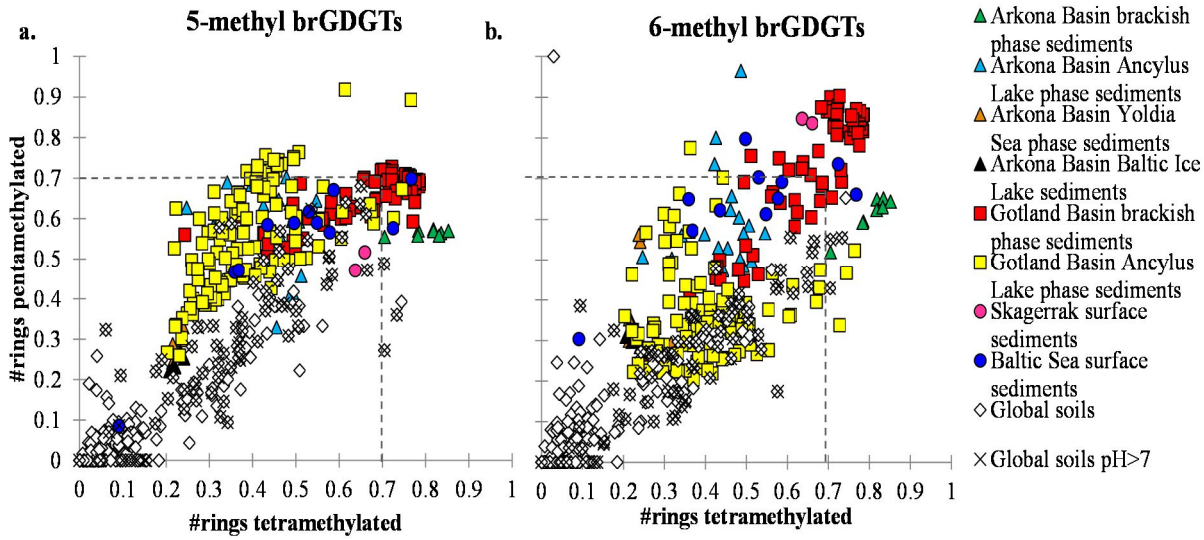

Fig. 12 Scatterplots of the number of cyclopentyl rings (#rings) in the tetramethylated brGDGTs vs. (a) 5-methyl pentamethylated brGDGTs, and (b) 6-methyl pentamethylated brGDGTs. The basins and phases of the sediments from this study are differentiated by symbol and color as indicated. Soils from the global data set with a pH greater than seven are indicated with an 'x'.

Since pH is the major control on the degree of cyclization, (DC'; Weijers et al., 2007b; Peterse et al., 2010) values for the #rings between 0.6-0.7, as observed for the Ancylus Lake/Littorina Sea transition in the Gotland Basin, the recent sediments from the Gotland Basin (1786-1893 AD) and surface sediments sample 349190, have been observed in alkaline soils (Sinninghe Damste, 2016). However, the often peat covered soils of the region surrounding the Baltic Sea basin have a slightly acidic pH; the average pH for topsoils (0-25 cm depth) is 6.1 according to a study on soils collected from 10 European countries surrounding the Baltic Sea basin (Reimann et al., 2000). Additionally, high pH soils tend to have higher amounts of 6-methyl brGDGTs (IR >0.7; De Jonge et al., 2014b), and the fact

that the Baltic Sea sediments have an average IR value of 0.41±0.10 points towards insignificant input of alkaline soils. The Baltic Sea surface sediment sample, 377850, located in the lower Bothnian Sea, is characterized by the lowest number of rings ($\#rings_{tetra}$=0.09, $\#rings_{penta}$ for the 5-methyl brGDGTs=0.09, $\#rings_{penta}$ for the 6-methyl brGDGTs=0.30; Figs. 12a-b). This surface sediment also has a much higher BIT index (0.31) compared to all other studied surface sediments, suggesting that it receives the highest contribution of soil-derived brGDGTs. Recently, a study on Baltic Sea surface sediments that compared brGDGT concentrations and leaf-wax *n*-alkanes proposed that the BIT index does reflect the relative contribution of soil organic matter in the surface sediments, indicating high soil organic matter input into the Bothnian Sea area (average 29%; Kaiser and Arz, 2016). They also asserted that this value was in agreement with previously published data that used lignin-phenols to estimate terrestrial organic matter contribution in the northern Baltic Sea (30%; Bianchi et al., 1997). The low #ring values for surface sediment sample 377850 are in agreement with the reported low pH of soils surrounding the Baltic Sea, which indicates that this sediment can be used as an end-member for the composition of soil derived brGDGTs. This suggests that especially for all other surface sediments and the sediments deposited during the brackish phase, the contribution of soil-derived brGDGTs has been low (<20%), whereas for sediments deposited during the other phases soil-derived brGDGTs account for 30-90% based on a simple two endmember mixing model. In summary, we conclude that for the time periods and regions mentioned above, the input of terrestrial material is likely relatively minor and the majority of brGDGTs are being produced in situ in either or both the alkaline pore waters of the marine sediments and the water column.

The novel hexa-methylated brGDGT IIIa", which we only detected in specific parts of the record, has been just recently been identified in sediments of a eutrophic Swiss mountain lake (Lake Hinterburg), where it's absence from soils of the watershed indicated an exclusively lacustrine source of this compound (Weber et al., 2015). Hence, the presence of brGDGT IIIa'' during certain periods of the Ancylus Lake phase in the Gotland Basin record as well as at times during the Ancylus Lake phase and the Yoldia Sea phase in the Arkona Basin, demonstrates that at these times at least some of the brGDGTs were produced in situ. Further information on the origin of brGDGTs may be derived from the stable carbon isotope composition of their alkyl moieties ($\delta^{13}C_{brGDGT}$).

A further check for potential in situ production is the determination of the $\delta^{13}C$ of the alkyl moieties of brGDGTs. In Lake Hinterburg the ^{13}C content of brGDGTs in the sediment (c. -43‰) was found to be substantially lower than (i) $\delta^{13}C_{brGDGT}$ values measured in soils

from the watershed (c. -27‰), and (2) the $\delta^{13}C$ of sedimentary TOC (-34‰) (Weber et al., 2015). Weber et al. (2015) postulated that this stark ^{13}C-depletion of brGDGTs arises from extensive microbial C recycling within the lake that leads to ^{13}C depletion in the dissolved and particulate C pools, which in turn serve as a C source for the aquatic brGDGT-producing microbes. Three intervals from the Gotland Basin sedimentary record with the highest fractional abundance of brGDGT IIIa", an indication of in situ production of brGDGTs (see above), were selected to determine if the majority of the brGDGTs from these periods were in in fact produced in situ. However, in contrast to Lake Hinterburg, the presence of the (supposedly) in-situ-produced brGDGT IIIa'' was not linked to such low $\delta^{13}C_{(brGDGT)}$ values in the Baltic Sea sections analysed (-29.0‰ to -27.4‰; Table 2), instead they seem rather consistent with a predominant soil origin of brGDGTs (cf. Pancost and Sinninghe Damsté, 2003; Weijers et al., 2010). However, the low TOC content (<1.1%) and lack of lamination in the shallower Ancylus Lake (Figs. 3-4), as well as the relatively higher $\delta^{13}C_{TOC}$ values (-26‰ to -28‰; Table 2) compared to Lake Hinterburg sediments (-34‰) indicate that the basin was probably not stratified or eutrophic during that period. It remain therefore ambiguous, whether the $\delta^{13}C_{(brGDGT)}$ values in the Ancylus Lake phase mainly reflect a terrestrial signal or are inherited from aquatic C pools. Given the presence of the "aquatic" brGDGT IIIa'' and the results of the two endmember mixing model we, however, reason that both in situ production and terrigenous input must have contributed to the brGDGTs deposited during the Ancylus Lake phase in the Gotland Basin.

After comparing the fractional abundances of the tetra-, penta- and hexamethylated brGDGTs from soils to the Baltic Sea sediments in the ternary diagram (Fig. 11), considering the (#rings) of the tetramethylated and the 5- and 6- methyl pentamethylated brGDGTs (Fig. 12a-b), using the abundance of the novel IIIa" brGDGT in the sedimentary record, and considering the $\delta^{13}C$ of the alkyl moieties of brGDGTs at that time, we conclude that in situ production of brGDGTs is contributing to the pool of brGDGTs in the Baltic Sea sediments over the Holocene to a varying extent.

5.2 Using brGDGTs for climate reconstructions in the Baltic Sea

The heterogeneity of brGDGT sources in the Baltic Sea basin will greatly complicate the use of brGDGTs as a temperature proxy. The $\delta^{13}C$ of the alkyl moieties of brGDGTs and the lower values for the #rings during the lower salinity phases of the Baltic Sea indicates a portion of the brGDGTs during these phases are terrestrially derived and so a soil calibration will be applied in an attempt to obtain MAT estimates. Evidence suggests that a change in the

provenance of the brGDGTs occurred over the Holocene and even though the recent brackish phase appears unsuitable for a soil calibration, perhaps another calibration, which takes into account in situ production of brGDGTs could be used for obtaining MAT estimates during this time. In the previous section it was established that in situ production of brGDGTs is contributing to the total pool of brGDGTs over the Holocene in the Baltic Sea basin, however, we proceeded to apply the new soil calibration based on individually quantified 5- and 6-methyl brGDGTs from De Jonge et al. (2014a) for reconstructing continental pH and MAT when there was evidence that a portion of the brGDGTs in the sediments were of soil origin. The novel marine coastal sediment calibration for calculating bottom water temperatures (BWT) from Dearing et al. (unpublished results) was applied on sediments where a soil calibration was deemed inappropriate due to the lack of soil-derived brGDGTs.

Surface sediment sample 377850 has the highest BIT index of the surface sediments (0.31) and a lower #rings than all other surface sediments, indicating this sediment most probably received a higher soil contribution than the other surface sediments. This could be because this sediment is close to a river mouth, although some of the other surface sediments in the Baltic Sea are even closer to a river mouth (i.e. 372820, 377830, and 349200) but do not have correspondingly higher BIT index values (Table 1; Fig. 2). Perhaps this site receives more terrestrial material or less in situ production is occurring in this region and so the terrestrial signal is not being overwhelmed by in situ produced brGDGTs. The CBT'-derived reconstructed pH [10-11] for this sediment is 6.4, which is close to the reported average of soils in the Baltic region (6.1; Reimann et al., 2000). The reconstructed temperature using the MAT_{mr} calibration [12] is 5.4°C and this value is similar to the reported measured MAT from the closest weather station, 4.5°C (reported measured MAT values are an average from over the period of 1890-2016; RIMFROST). Consequently, this appears to be a good site for collecting sediment cores for future brGDGT based climate reconstructions in the Baltic Sea area.

Since a soil calibration was not suitable for the other surface sediments, the newly developed coastal marine calibration for BWT was applied to all other surface sediments [13] (Dearing et al., unpublished results). For the Baltic Sea surface sediments, the resultant BWT varied substantially ranging from -0.4 to 9.4°C. Measured MATs from weather stations in Sweden and Finland close to these sites ranged from 1.4-8.1°C (RIMFROST). The correlation of the estimated BWTs and the MATs from the closest weather stations is quite high, R^2=0.82

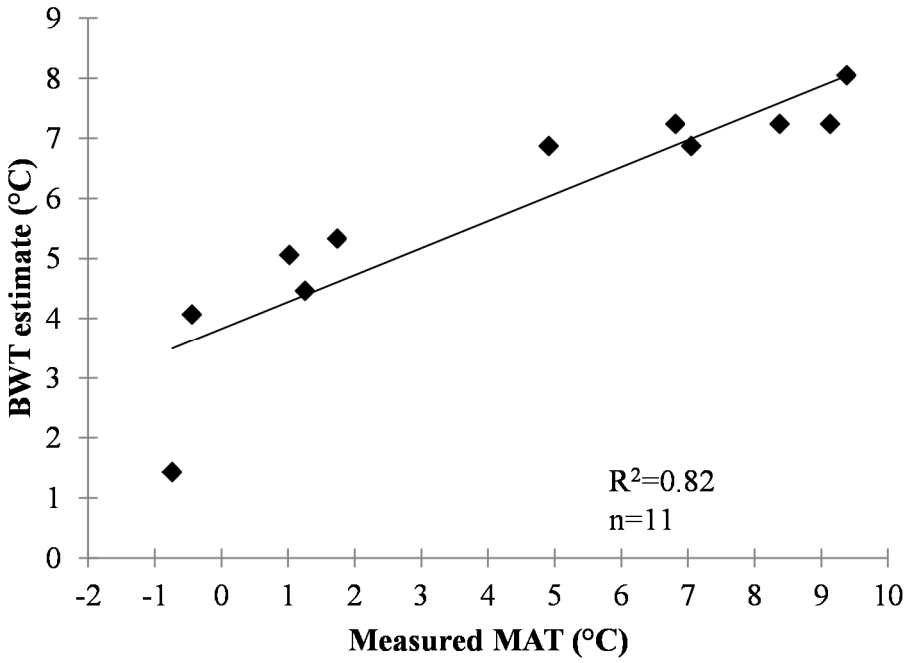

Fig. 13 Correlation of measured MATs from weather stations in Sweden and Finland (RIMFROST) close to sediment sample sites and the reconstructed BWTs (R^2=0.82, n=11).

(n=11, Fig. 13), providing some confidence in this new calibration. The derived BWTs from the northern Baltic Sea are the coldest, -0.4-1.3°C, and the MATs reported for the closest weather stations in Sweden ranged from 1.4-4.5°C (RIMFROST). The highest estimate for BWT is from the Arkona Basin, 9.4°C, and correspondingly the measured MAT from the closest weather station in Sweden was 8.1°C (RIMFROST). The resultant average BWT for the Skagerrak surface sediments, 16.6±1.5°C, is unrealistically high for BWT estimate (reported measured MAT average over 1890-2016 from the closest weather stations as reported at http://www.rimfrost.no/ was 6.8-7.8°C). It was previously found that MBT/CBT derived MAT from a sediment core in the Skagerrak compared best with summer temperatures (15.5°C; Rueda et al., 2009). Rueda et al. (2009) postulated that this could be due to transport of brGDGTs from the southern North Sea or alternatively that in this region the organisms that produce the brGDGTs are more active during the summer since Scandinavian soils are mostly snow covered during the winter months. The results from this study, however, indicate that the higher temperature estimates obtained using brGDGTs are likely due to in the input of in situ produced brGDGTs.

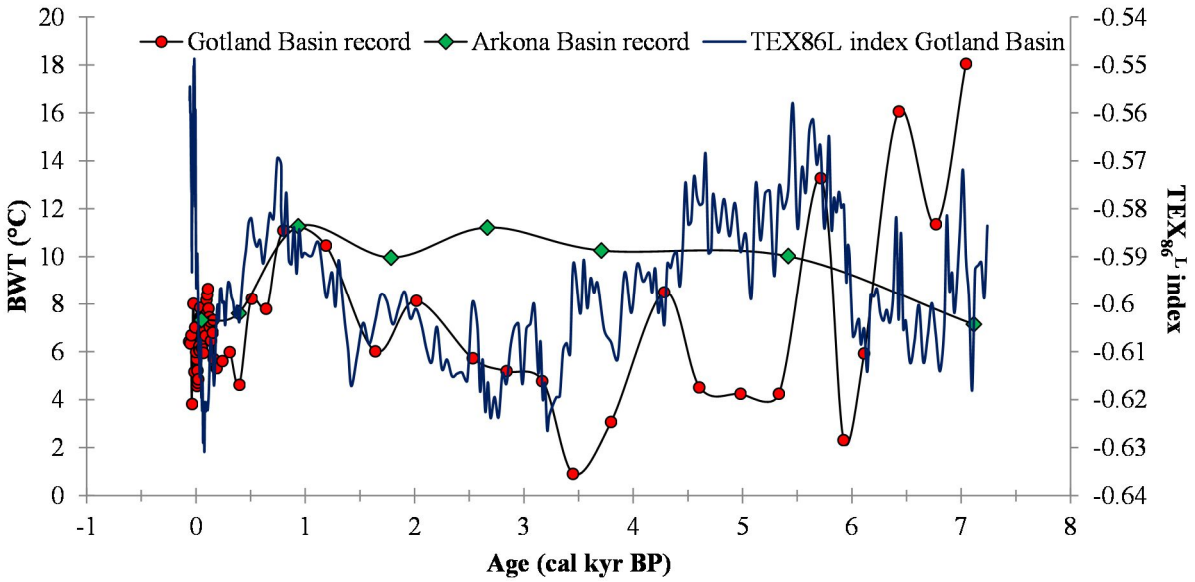

Fig. 14 Reconstructed BWT (°C) for both the Gotland (indicated by red circles) and Arkona (indicated by green diamonds) basins for the brackish phase (7.2-0 cal kyr BP). The previously published TEX^{86}_{L} index record (blue line) is shown for reference.

Because in situ production is the major source of brGDGTs during the brackish phase, the new marine coastal BWT calibration (Dearing et al., unpublished results) was applied to the records in both basins as well (Fig. 14). The records from both basins are in good agreement for the last 1,000 years (6.7±1.4°C in the Gotland Basin and 8.7±2.2°C in the Arkona Basin; Fig. 14). The measured MAT from a weather station close to the Arkona Basin, 8.1°C, is similar to the average of the estimated BWT from the brackish phase of the Arkona Basin record, 9.4±1.7°C (Fig. 14). From the weather station close to the Gotland Basin station the measured MAT, 7.2°C, is similar to the estimated average BWT from the Gotland Basin record during the brackish phase, 6.8±2.7°C (Fig. 14). Therefore, during the brackish phase of the Baltic Sea when the BIT index is low and the #rings for the tetra- and pentamethylated brGDGTs are high, the marine coastal sediment calibration performs well reconstructing temperatures (Fig. 14). Next, the BWT records from both basins were compared to a previously published TEX_{86}^{L} record (the TEX_{86}^{L} is sea surface temperature proxy based on the distribution of *Thaumarchaeotal* membrane lipids called isoprenoid GDGTs; Kim et al., 2010) from the same sediment cores making up the Gotland Basin record (Warden et al., in preparation) and shows fairly good agreement with the trends in the BWT reconstruction during the brackish phase, although the resolution for the BWT record is much lower throughout most of the brackish phase in both basins, but especially the Arkona Basin, making comparison difficult at times (Fig. 14).

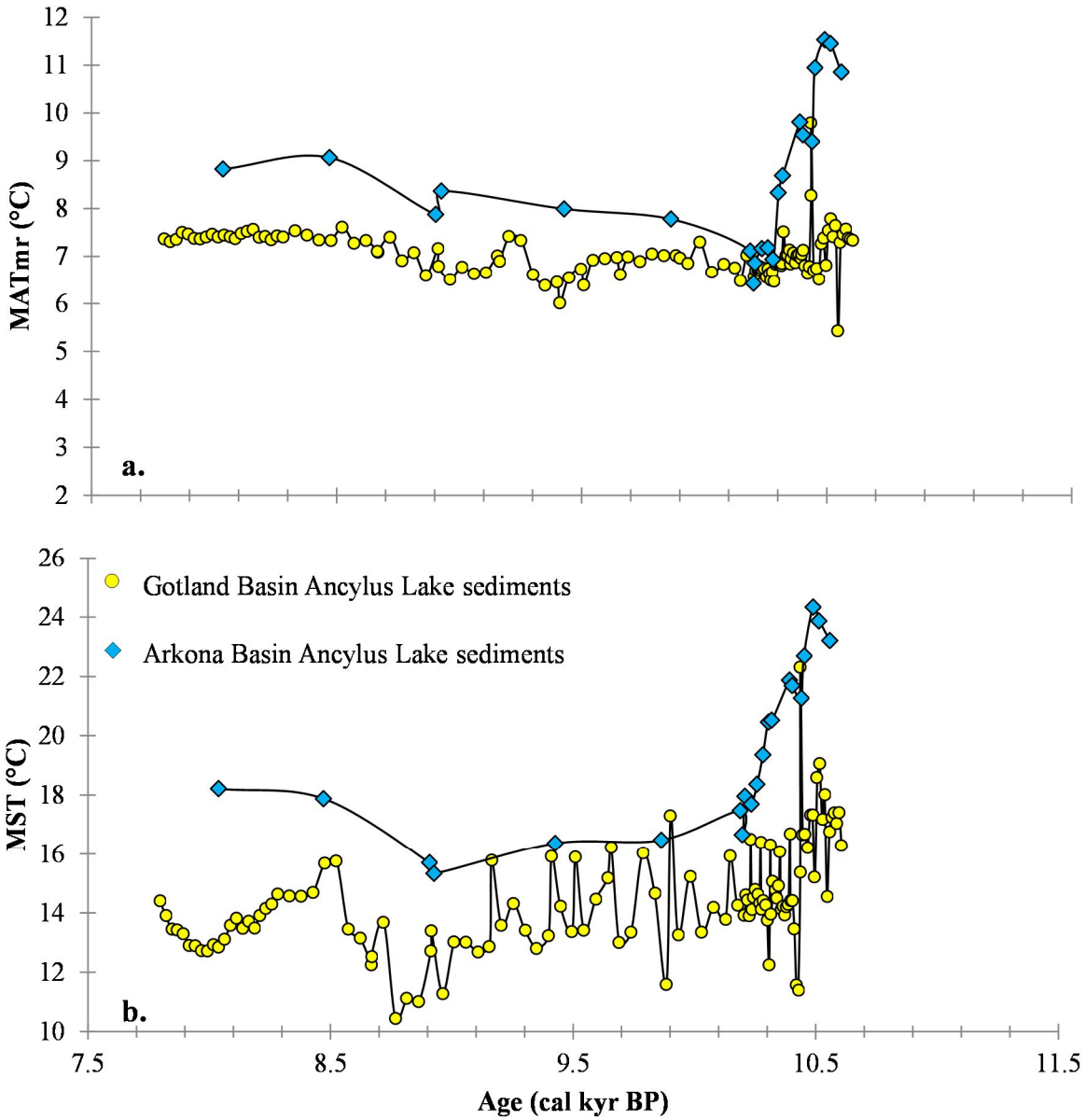

Fig. 15 Plot of reconstructed (a) MAT_{mr} (°C) and (b) MST (°C) with age (cal kyr BP) from the Ancylus Lake phase of both the Arkona (blue diamonds) and Gotland Basin (yellow circles).

Even though in the previous section it was determined that in situ production of brGDGTs is contributing to the total pool of brGDGTs over the Holocene in the Baltic Sea basin, some of the evidence presented indicates that a substantial portion (30-90%) of the brGDGTs during the lower salinity phases are of soil origin. Therefore, we proceeded to apply the new soil calibration based on individually quantified 5-methyl and 6-methyl brGDGTs from De Jonge et al. (2014a) for reconstructing continental pH and MAT in the region during the lower salinity phases of the Baltic Sea. Using equation [11] to reconstruct the average pH in the Gotland Basin over the Ancylus Lake phase, the resultant value,

6.9±0.3, was similar to those in the Arkona Basin during the Baltic Ice Lake phase, 6.5±0.1, the Yoldia Sea phase, 6.7±0.2, and the Ancylus Lake phase, 7.2±0.2. As previously stated a canvass of soils around the Baltic Sea region found the average pH of topsoils to be 6.1 (Reimann et al., 2000) and so the reconstructed values are slightly higher than those of the soils and this difference is likely due to the input of aquatically produced brGDGTs.

The average reconstructed MAT using the MAT_{mr} equation [12] are the same when the standard deviation is considered during the Ancylus Lake phase in both the Arkona, 8.7±1.6°C, and Gotland, 7.1±0.5 °C, basins (Fig. 15a). A temperature reconstruction from Lake Flarken in south-central Sweden based on a pollen-climate calibration model showed MAT was fairly stable around 7°C during the Ancylus Lake period of the Baltic Sea (Seppä et al., 2005). Therefore, the estimated air temperatures presented here using the new MAT_{mr} calibration for the lower salinity phases of the Baltic Sea are in good agreement with the previously published temperature reconstruction from south central Sweden (Seppä et al., 2005).

Since there are indications that in situ production could be a complicating factor during the Ancylus Lake period, an aquatic calibration might be a better choice for this portion of the record. Hence, we applied a modified version of the aquatic calibration [14] developed by Pearson et al. (2011) to calculate mean summer air temperatures (MST). The higher resolution Gotland Basin record reveals a high amount of variation between about 10.6-8.7 cal kyr BP in the estimated temperatures using the MST calibration as the reconstructed temperatures fluctuate by ~5°C in less than 100 year period (Fig. 15b). However, the calibration estimates summer lake temperature and variation within summer lake temperatures would be expected. The average MST for the Ancylus Lake phase in the Gotland Basin record, 14.5±1.8°C, is similar to the average for the Arkona Basin record, 19.4±2.8°C (Fig. 15b). The fact that the MST estimates derived using brGDGTs in both basins are similar increases the reliability of these summer temperatures estimates. These values are also similar to the instrumental summer temperatures reported for the Skagerrak regions in Rueda et al. (2009) (ranges between 14.2-16.3°C, average 15.5°C).

Weather stations in the region close to the Arkona Basin show higher measured MAT than weather stations to the north of that area, which is in agreement with what we see in the temperature reconstructions. For all three reconstructions the temperatures are slightly but consistently higher in the Arkona Basin record (Figs. 14 & 15 a-b), which is located more to the south than in the Gotland Basin record. Higher temperatures in both the MAT_{mr} and the MST estimates is apparent in the Arkona Basin between c. 10.60 cal kyr BP, which covers a

part of the early Ancylus Lake phase and could correspond to the warmer temperatures experienced during deglaciation. However, the increase in temperatures according to the MST seems too large for this time period (Figs. 15b) and so it could be that the increase in estimated temperatures seen during this time is a product of brGDGT distribution changes related to a shift in the provenance of brGDGTs that occurs during the transition between the Yoldia Sea phase and the Ancylus Lake phase. Both PC1 and PC2 increase in the Arkona Basin over each subsequent transition from the Baltic Ice Lake to the Yoldia Sea phase and then again during the Yoldia Sea/Ancylus Lake transition, lending credence to the idea that the increased production of in situ produced brGDGTs are affecting temperature estimates during this transition.

5.3 Changes in the BIT index and GDGT concentration in the Baltic Sea over the Holocene reflect environmental changes

The ternary plot of the three major GDGTs (Fig. 6) along with the BIT index, the summed concentration of brGDGTs, the amount of crenarchaeol (Fig. 5), and distribution of brGDGTs (Fig. 7-8 & 10) all demonstrate that the sedimentary GDGT composition is highly dependent on environmental conditions in the Baltic Sea over the Holocene and this has implications for paleoclimate studies based on brGDGTs. The sediments of the Baltic Ice Lake, Yoldia Sea phase and Ancylus Lake phase received a larger fraction of soil-derived brGDGTs, whereas in the sediments of the brackish phase brGDGTs are for a substantial part produced in situ. The BIT index has previously been interpreted to reflect soil organic matter input (of which a value close to 1 indicates terrestrial origin and a value close to zero indicates marine origin; Hopmans et al., 2004) However, in situ production of brGDGTs in rivers (Yang et al., 2013; Zell et al., 2013; 2014; De Jonge et al., 2014b) and lakes (Tierney and Russell, 2009; Sinninghe Damsté et al., 2009; Loomis et al., 2011; Buckles et al., 2014) can lead to a higher BIT index value that is not actually indicative of a higher portion of terrestrially derived brGDGTs. Additionally, crenarchaeol can be produced in soils resulting in a lower BIT index that does not actually reflect a higher contribution from aquatic organic matter (Weijers et al., 2006a; Peterse et al., 2010; Yang et al., 2011). Therefore, studies that examine the provenance of brGDGTs such as this one are necessary before using the BIT index to make inferences about terrestrial input.

The BIT index is consistently >0.30 in the Ancylus Lake phase of both basins as well as the Yoldia Sea phase and Baltic Ice Lake phase of the Arkona Basin and decreases in both basins during the transition from the Ancylus Lake phase to the brackish phase of the Baltic

Sea (Figs. 5c & f). This is in line with the increased marine input into the system corresponding with the opening of the Danish Straits, which allowed inflows of marine water into the basin. The concentration of crenarchaeol increased from the Ancylus Lake phase and moving into the Littorina Sea phase becoming more abundant than the brGDGTs as marine water continued to flow into the basin (Figs. 5b & e). The sum of the brGDGTs (μg g^{-1} TOC) decreased moving into the Littorina Sea phase, and since the discussion in the previous section indicated marine in situ production increased in the brackish phase, this suggests that the input of terrestrially derived brGDGTs lessened substantially at this time (Figs. 5a & d).

Table 3 BIT index values and ratio of (C_{23}+ C_{25})/total n-alkanes, demonstrating the dominance of *Sphagnum* plants indicating the presence of peat (Baas et al., 2000), for samples with BIT values above 0.7 from the Arkona Basin during the Ancylus Lake phase.

Sediment core	**Sediment core depth (cm)**	**Age (cal kyr BP)**	**BIT index**	**(C_{23}+ C_{25})/ total n-alkanes**
318340	540.5	8.91	0.7	0.25
318340	599.5	10.19	0.8	0.27
318340	634.5	10.28	0.8	0.23
318310	642.5	10.20	0.9	0.32

Several 'spikes' in the BIT index records occur in the basins during the lower salinity phases (Figs. 5c & f). In order to determine the causes of the BIT index 'spikes' towards higher values in the two basin records, the concentrations of brGDGTs and crenarchaeol were examined. The most recent BIT index 'spike' (c. 9.1 cal kyr BP) in the Gotland Basin record is caused by an increase in brGDGT concentration (μg g^{-1} TOC) and a concomitant decrease in the crenarchaeol concentration (Figs. 5a-c). In both basins a second BIT index 'spike' occurs around the same time (c. 10.2 cal kyr BP in the Arkona Basin and c. 10.3 cal kyr BP in the Gotland Basin). However, it appears that different processes are responsible for the increase in BIT index values in each basin (Figs. 5c & f). During this time in the Gotland Basin the amount of crenarchaeol (μg g^{-1} TOC) decreases relative to the sum of brGDGTs (μg g^{-1} TOC), possibly indicating a decline in marine input could be responsible for the increase in the BIT index (Figs. 5c & f). In contrast to the Gotland Basin, in the Arkona Basin the sum of brGDGTs (μg g^{-1} TOC) increases relative to crenarchaeol (μg g^{-1} TOC), suggesting either a proliferation of brGDGT-producing bacteria in the water column or sediments, or an increase in terrigenous input (Figs. 5a-f).

Peat usually contains higher concentrations of brGDGTs than soils (Weijers et al., 2011). In order to determine if peat erosion could have been responsible for the 'spikes' in the

BIT index towards higher values c. 10.2 cal kyr BP in the Arkona Basin, four sediment horizons from around the BIT 'spike' during the Ancylus Lake phase were analyzed for specific peat markers. A previous study by Baas et al. (2000) showed that *Sphagnum*, an abundant species in peat bogs, is characterized by a dominance of the C_{23} or C_{25} *n*-alkanes. Our results showed that the *n*-alkane distributions in all four sediments analyzed were dominated by the C_{23} and C_{25} *n*-alkanes (average ratio of C_{23}+ C_{25} compared with total *n*-alkanes is 0.27±0.04; Table 3) confirming the presence of *Sphagnum* and thus peat contribution to the Arkona Basin sediments during the Ancylus Lake phase. However, since the ratio of C_{23}+ C_{25} relative to total *n*-alkanes does not increase with increasing BIT index values, there is most likely not an influx of peat occurring during periods with higher BIT index values. A study by Kaiser and Arz (2016) found that the n-alkane distribution in sediments from the Baltic Sea indicated a contribution from peat in the northern and southern regions. Since peat is a possible source of brGDGTs to the basin c. 10.20 cal kyr BP, this could mean that the contribution of brGDGTs from peat during the deposition of the Ancylus Lake phase may further complicate temperature reconstructions at that time in Arkona Basin. A previous study demonstrated that the contribution of brGDGTs from peat leads to an overestimation of MAT, perhaps because shifts in the distribution of brGDGTs could be related to changing brGDGT producing communities with peat type and not solely temperature dependent (Weijers et al., 2011), although other studies have successfully used brGDGTs from peats for paleoclimate studies (Ballantyne et al., 2010; Zhou et al., 2011). Since peats usually contain high concentrations of brGDGTs, the presence of peat in the Arkona Basin is likely contributing to the higher BIT index values than in the Gotland Basin record during the Ancylus Lake phase. However, a higher abundance of crenarchaeol in the Gotland Basin than in the Arkona Basin occurs throughout most of the brackish phase as well as the freshwater phase and thus contributes to the lower BIT index values in the Gotland Basin during the Ancylus Lake phase (Figs. 5b-c & e-f). The increased amount of crenarchaeol in the Gotland Basin is perhaps surprising since the site is further from the connection to the North Sea, however, it has been shown that in large lakes crenarchaeol can be ubiquitous (Blaga et al., 2009; Powers et al., 2004). Since the Gotland Basin is located in the center of the Baltic Sea, which is similar to a large lake even during its brackish phase, perhaps a higher production of crenarchaeol in the Gotland Basin is contributing to the lower BIT index values observed in the Gotland Basin relative to the Arkona Basin over the Holocene (Figs. 5a-f). A study from the Black Sea, a large, stratified body of water with anoxic bottom waters and abundant sulfide below 100 m, demonstrated that different species

of marine Crenacrchaeota live in the suboxic zone compared with the low-sulfide conditions at the top of the sulfidic zone and a higher concentration of crenarchaeol was biosynthesized under low-sulfide conditions than in the suboxic zone (Coolen et al., 2007). Similarly, the Gotland Basin is also persistently stratified with an oxic upper layer and anoxic bottom waters and since iron-sulfide concentrations have been observed in the laminated sediments from the Littorina Sea phase deposited during anoxic times (Suess, 1979; Sternbeck and Sohlenius, 1997; among others), perhaps a sulfidic cheomcline existed in the Gotland Basin conducive to higher crenarchaeol production.

The increase of the BIT index in the Gotland Basin prior to the Ancylus Lake/Littorina Sea transition appears to be caused by a higher contribution of in situ produced brGDGTs. The changes in the BIT index and distribution of GDGTs at the transitional phases over the Holocene demonstrate the strong impact environmental changes can have on the amounts and provenance of brGDGTs in the Baltic Sea, which should be considered when brGDGT-based climate reconstructions extend over varying phases, especially during transitional times, in any region.

Conclusions

This study reveals that marked changes in GDGT distribution and the BIT index occurred concomitantly with the re-establishment of the connection between the Baltic Sea and the North Sea. These shifts are likely caused by variable contributions of terrestrial and in situ GDGT sources, as indicated by the BIT index, as well as the fractional abundances and the degree of cyclization in brGDGTs. The variable sources of brGDGTs over the Holocene confounds their use for temperature reconstructions in the Baltic Sea. After thorough assessment of GDGT provenance, however, MAAT estimates can still be meaningful if appropriate calibrations are applied. Our results further beg the question whether changes in brGDGT distribution, in turn, can be used to reconstruct environmental changes such as freshening and saltening of a basin that occurred in a region in the past. Hence, the factors controlling sedimentary brGDGT composition should be further investigated using suitable sedimentary records from other regions spanning known environmental changes to further explore this possibility.

Photo by Claudia Zell

CHAPTER 7

Examining the provenance of branched GDGTs in the Tagus River drainage basin and its outflow in the Atlantic Ocean over the Holocene to determine their usefulness for paleoclimate applications

Lisa Warden, Jung-Hyun Kim, Claudia Zella, Geert-Jan Vis, Henko de Stigter, Jérôme Bonnin, and Jaap S. Sinninghe Damsté

Biogeosciences, 13, 5719-5738, 2016

Abstract

The distributions of branched glycerol dialkyl glycerol tetraethers (brGDGTs), which are transported from the soils where they are predominantly produced to marine sediments via rivers, have been applied in reconstructing mean annual air temperatures (MAT) and pH of soils. However, paleoclimate reconstructions using sedimentary brGDGTs have proven difficult in arid regions including the Iberian Peninsula. Recently, six novel 6-methyl brGDGTs have been described using new analytical methods (in addition to the nine 5-methyl brGDGTs previously used for climate reconstructions), and so new pH and MAT calibrations have been developed that in a set of global soil samples were shown to improve the accuracy of reconstructions, especially in arid regions. Because of this we decided to apply the new method to separate the 5- and 6-methyl isomers along with the novel calibrations to a sample set from the Iberian Peninsula to determine whether it improves paleoclimate reconstructions in this area. This set includes samples that run in a transect from source to sink along the Tagus River and out to the deep ocean off the Portuguese margin spanning the last 6,000 years. We found that although pH reconstructions in the soils were improved using the new calibration, MAT reconstructions were not much better even with the separation of the 5- and 6-methyl brGDGTs. This confirmed the conclusion of previous studies that the amount of aquatically produced brGDGTs is overwhelming the soil derived ones in marine sediments and complicating MAT reconstructions in the region. Additionally, the new separation revealed a strong and until now unseen relationship between the new degree of cyclization (DC') of the brGDGTs and MAT that could be making temperature reconstructions in this and other arid regions difficult.

1. Introduction

Understanding past climate variability is important for predicting future climate change as well as how ecosystems, organisms and human society could be affected. The validation of climate proxies is imperative for the correct interpretation of climate archives and therefore also for the climate models building on these past climate data. Terrestrial environments play an important role in global climate, however, continental climate reconstructions are hindered by the lack of continental temperature proxies. In the future, changes in terrestrial climate are likely to have a large impact on human society just as they had in the past (e.g. Haug et al., 2003). Availability of trustworthy temperature data from the terrestrial environment will be essential for the development of reliable climate models.

The distribution of branched glycerol dialkyl glycerol tetraethers (brGDGTs, Fig. S1), a group of membrane-spanning lipids that occur in heterotrophic bacteria (Pancost and Sinninghe Damsté, 2003; Weijers et al., 2010) pervasive in peat (Weijers et al., 2006b) and worldwide in soils has proven useful as a tool to obtain high resolution, continental temperature reconstructions (Weijers et al., 2007b; Schouten et al., 2008; Bendle et al., 2010). Branched GDGTs are biosynthesized by bacteria (Sinninghe Damsté et al., 2011; 2014) living in soils and the distribution of brGDGTs in soils is affected by growth temperature and pH (Weijers et al., 2006b). More specifically, the degree of methylation of the brGDGTs (expressed as methylation of branched tetraethers index, MBT) relates to mean annual air temperature (MAT), and to a lesser extent soil pH, whereas the degree of cyclization (DC) of the brGDGTs (also expressed as the cyclization of branched tetraethers index, CBT) correlates solely with soil pH (Weijers et al., 2007b). MBT has recently been amended to become MBT' by eliminating the brGDGTs that rarely occur in soils (Peterse et al., 2012). These observations led to the development of a continental paleoclimate proxy based on the distribution of brGDGTs that has been applied in paleosoils (Peterse et al., 2009; Weijers et al., 2007b; 2011). Branched GDGTs that are produced in soils are washed by runoff into streams and rivers where they are transported to and deposited in river sediment and in coastal marine sediment that are under the influence of major river systems. In this way, brGDGTs have been used as recorders of the continental paleoclimate (Weijers et al., 2007a; Bendle et al., 2010; Hren et al., 2010; Keating-Bitonti et al., 2011).

Complications using brGDGTs as a proxy for MAT have arisen in some settings. In marine sediments receiving a low input of soil organic matter (OM), it was found that the distribution of brGDGTs and the reconstructed temperatures were quite different from that observed in regional soils (Peterse et al., 2009). Peterse et al. (2012) found in arid regions temperature is no longer an important control on the distribution of brGDGTs and therefore MAT reconstructions in these areas should be interpreted with care. In the Iberian Peninsula, Menges et al. (2014) found that MBT' was not correlated to MAT but instead correlated with the aridity index (AI), a parameter for water availability in soils, and mean annual precipitation (MAP). In drainage basins with varying soil sources that had different MATs (i.e. mountainous vs. lowland), it was found that the provenance of the soil matter must be considered when interpreting MAT reconstructions (Bendle et al., 2010). In-situ production of brGDGTs can occur within the river systems (Yang et al., 2012; Zell et al., 2013, De Jonge et al., 2014b) and cause brGDGT distributions and MAT reconstructions that differ from those in the soils of the source area. These complications make it vital to investigate how varying

environmental conditions, the transport of these terrestrially derived fossilized lipids, and in-situ production affect the implementation of brGDGTs for paleoclimate reconstructions.

Recently a set of six new brGDGT isomers that differ in the position of the methyl groups were identified and described (De Jonge et al., 2013). The relative abundance of these novel, 6-methyl brGDGTs are strongly dependent on pH and so by excluding them from the MBT' index (newly defined as MBT'_{5ME}) the correlation with MAT is improved (De Jonge et al., 2014a). The CBT index was also redefined in this study, as CBT', to include all of the pH dependent 6-methyl brGDGTs and consequently yielded a higher correlation with soil pH as a result (De Jonge et al., 2014a). De Jonge et al. (2014a) also developed, based on a dataset of globally distributed soils, a new pH calibration taking into account the new CBT' as well as new MAT calibrations, defined as MAT_{mr} and MAT_{mrs}. In a global soil set they were shown to improve the accuracy of reconstructions, especially in arid regions. These indices and calibrations were applied in a coastal sediment core in the Northern Kara Sea off Siberia in a study emphasizing the importance of examining the provenance of brGDGTs when using these lipids for paleoclimate reconstructions (De Jonge et al., 2015).

A comprehensive study has been previously performed on the present day transport of brGDGTs in the Tagus River basin from source to sink (Zell et al., 2014). The results from this study demonstrated that the distribution of brGDGTs in the riverine suspended particulate matter (SPM) did not reflect that of the soils, implying that due to the aquatic production in river and marine environments the use of brGDGTs for paleoclimate reconstructions in the region would be complicated (Zell et al., 2014; 2015). Here we examine if the assessment of the provenance of brGDGTs in the Tagus River basin can be improved by the application of the analytical methods allowing the separation of the 5- and 6-methyl brGDGTs (De Jonge et al., 2013). In addition, we examine if the provenance of brGDGTs changed over the Holocene and if the distribution of brGDGTs in the past reflected continental sources and thus past temperature and pH of the soils in the drainage basin of the river. To this end we compare the down core brGDGT distributions in Holocene sediments retrieved from four locations along a transect in the Tagus River basin, which includes the river floodplain (Tagus River Floodplain core), the offshore mudbelt (Mudbelt core), and marine sediments from the canyons (Lisbon Canyon Head core and Lower-Sétubal canyon core) (Fig. 1), and compare them to brGDGT distributions of soil and river SPM from the Tagus River watershed. This allows insight into the potential and limitations of using the novel MAT_{mrs}/CBT' proxies for climate reconstruction in this region and in river systems in general.

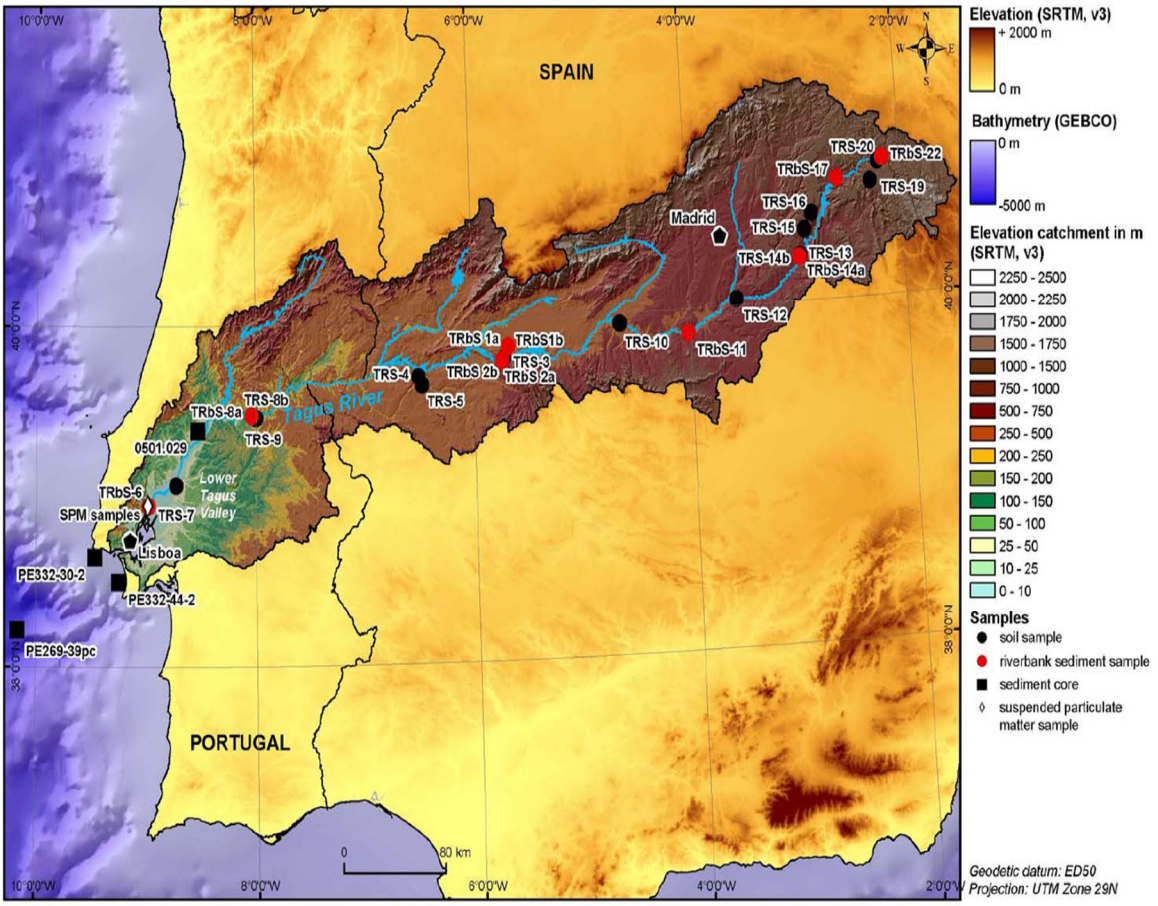

Fig. 1 The location of the study area on the Iberian Peninsula with the stations where the four sediment cores were sampled (indicated by black squares) along a transect from the Tagus River to off the Portuguese continental margin as well as the river SPM sampling site (indicated by a white diamond), riverbank sediment sampling sites (indicated by red circles), and soil sampling sites (indicated by black circles). The River SPM, riverbank sediments and soil samples were all collected for a previous study. Digital elevation data from Jarvis et al. (2006) and bathymetry from IOC-IHO-BODC (2003).

1.1 Study Area

The Tagus River drains the central part of the Spanish Plateau with an E-W orientation (Benito et al., 2003). The waters originate at an elevation of about 1600 m altitude in eastern Spain at the Iberian Range and the mouth of the river feeds into the Atlantic Ocean near Lisbon (Vis and Kasse, 2009). At 1,200 km long the Tagus River is the longest river of the Iberian Peninsula and it occupies 82 × 10^3 km^2 making it the third largest in catchment area (Benito et al., 2003). The Tagus Basin is surrounded by mountains on three sides with the Iberian Range to the east, the Central Range to the north, and the Toledo Mountains to the south. Present-day mean discharge at the Tagus River mouth is 400 m^3 s^{-1} (Vale and Catarino, 1996; Vaz et al., 2011) and the largest contribution of draining tributaries comes from the

Central Range in the North (Benito et al., 2003). The Tagus River is characterized by extreme seasonal and annual variability, including periods of flooding with 30 times the mean discharge and an annual discharge cycle characterized by two peaks in the winter (December and then again February to March) and a discharge minimum in the summer (August) (Benito et al., 2003). Since the 1940s dams have been built along the expanse of the Tagus River for water supply, hydropower, and flood prevention (Dias et al., 2002), which have likely impacted the transport of brGDGTs in the Tagus River system since their construction.

Where the Tagus River debouches into the Atlantic Ocean, the narrow continental shelf and steep continental slope are deeply incised by the Lisbon-Setúbal canyon system. The head of the Lisbon branch of that canyon system is located 13 km offshore from the Tagus River mouth at 120 m water depth. From that point, the canyon descends over a length of 165 km until it opens out onto the Tagus Abyssal Plain at 4860 m (Lastras et al., 2009). Even though the shelf is very narrow, sparse amounts of continental organic matter and clastic sediment reach the deep ocean in this region (Jouanneau et al., 1998; de Stigter et al., 2011; Vis et al., in press). This is because the Lisbon-Setúbal canyon is not a very dynamic system and has a weak down-canyon transport of sediments (Jouanneau et al., 1998; Jesus et al., 2010; de Stigter et al., 2011). A part of the continental shelf in this region is covered by mud deposits, which originate predominantly from the Tagus estuary (Jouanneau et al., 1998). According to this same study, the mouth of the much smaller Sado River is located further to the southeast and contributes only a relatively minor sediments volume to the shelf mud deposits.

Generally, the climate of the Tagus River Basin is characterized by seasonal variability and is considered continental Mediterranean (Le Pera and Arribas, 2004). Summers in the Tagus region are hot and dry and the winters are relatively mild and wet (Benito et al., 2003). During the summers, the climate regime in the Tagus Basin is controlled by the Azores high and in the winter by the westerlies (Benito et al., 2003). The MAT in the interior regions of the Tagus River basin varies from the highlands to the lowlands of the inner basin from 7.5 to 12.5°C, respectively and can increase up to 16°C along the Atlantic Coast (Le Pera and Arribas, 2004). The mean annual precipitation in the lowlands of the inner basin is mostly below 500 mm making it an arid region, however, some of the highest altitudes of the mountainous areas have a larger mean annual precipitation ranging from 750-1200 mm (Le Pera and Arribas, 2004).

The Iberian Peninsula is located between two major pressure systems, the Azores High and the Iceland Low, which make up the North Atlantic Oscillation (NAO). This climate phenomenon is caused by the varying pressure gradient in the North Atlantic and greatly

influences climate conditions all over Europe (Hurrell, 1995; Hurrell and VanLoon, 1997). Because of the Iberian Peninsula's advantageous position for studying the shifting NAO, the climate in this region has been intensively investigated (Zorita et al., 1992; Rodó et al., 1997; Trigo et al., 2004). Many of these studies are from an oceanic perspective, obtaining sea surface temperatures from marine sediments using the alkenone unsaturation indices (Abrantes et al., 2005, 2009; Rodrigues et al., 2009), coccolithophore assemblages (Cachao and Moita, 2000; Palumbo et al., 2013), and stable isotopic oxygen composition of foraminifera (Lebreiro et al., 2006 ; Bartels-Jónsdóttir et al., 2006; 2009). The terrestrial climate has been examined using continental paleoarchives such as speleothems (Munoz-Garcia et al., 2007; Martin-Chivelet et al., 2011; Stoll et al., 2013), tree rings (Andreu et al., 2007; Linan et al., 2012), and pollen (Huntley and Prentice, 1988; Lebreiro et al., 2006; Davis et al., 2003; Fletcher et al., 2007; Corella et al., 2013). The integrated continental and marine approach can give complimentary information to past climate in a region and by using the same proxy on the continent, in the ocean, and at the ocean-continent interface we would perhaps obtain a clearer picture of continental climate processes in an area rather than using separate studies or a multi-proxy approach.

2. Material and Methods

Sample collection. Soil samples, riverbank sediment samples, and river SPM from the Tagus River basin (Fig. 1b) were collected previously (Zell et al., 2014). These samples were complemented with four long sediment cores collected along a transect running from the Tagus River to the lower continental slope (Fig. 1). The Tagus River Floodplain core (0501.029) was collected in a low-energy backswamp of the present-day floodplain of the river at ~4 km west of the Tagus channel (Table 1). The sediment was collected using an Edelman hand auger for sediment above the groundwater table and a gauge for sediment below the groundwater table (Vis et al., 2008). The sediments were wrapped in the field for laboratory analyses. The other three cores were collected using a piston corer, during campaigns in May 2007 and March 2011 with RV *Pelagia* conducted by the NIOZ - Royal Netherlands Institute for Sea Research. The coring site for the Mudbelt core (64PE332-30-2) was to the west of the Tagus Estuary mouth, for the Lisbon Canyon Head core (64PE332-44-2) it was to the east of the Tagus Estuary mouth, and for the Lower Setúbal Canyon core (64PE269-39) it was on the crest of the northern levee of the lower Setúbal Canyon (Table 1).

Table 1 Stations, sediment core names, locations of sampling and water depth for each sediment core used in this study.

Station	Core name	Latitude [N]	Longitude [W]	Water depth [m]
0501.029	Tagus River Floodplain	39° 23' 07.80"	08° 31' 55.56"	0
64PE332-30-2	Tagus Mudbelt	38° 39' 02.20"	09° 28' 07.68"	82
64PE332-44-2	Lisbon Canyon Head	38° 30' 20.19"	09° 15' 04.87"	259
64PE269-39-4	Lower Setúbal Canyon	38° 13' 12.00"	10° 10' 00.00"	4217

Age models. The accelerated mass spectrometry (AMS) ^{14}C measurements of the three marine sediment cores were carried out at the BETA analytic laboratory (USA) on benthic or planktonic forams, gastropods or shells fragments (Table 2). As for the Tagus River Floodplain core, the radiocarbon dating material was performed for a previous study and consisted of mostly terrestrial botanical macrofossils, but other bulk material was used as well (Vis et al., 2008). In order to establish consistent chronologies for the four sediment cores, all the AMS dates were calibrated into calendar ages using the CALIB 7.0, available at http://radiocarbon.pa.qub.ac.uk/calib (Stuiver et al., 1998). For the three marine sediment cores, Marine13 was used for calibration data and curve selection, and Int-Cal13 was used for the Tagus River Floodplain core (Reimer et al., 2013). All radiocarbon dates mentioned have age spans at the 2σ range and are expressed as calibrated ages (cal. BP) (Table 2, Fig. S2).

Bulk isotope data Prior to bulk carbon isotope analysis, sediment was decalcified using a 2 N HCL solution for approximately 18 h. The sediment was rinsed three times using double-distilled water and then freeze dried again. Total organic carbon (TOC) and $\delta^{13}C_{TOC}$ (Table 3) were measured in duplicate using the Flash 2000 series Organic Elemental Analyzer (Thermo Scientific) equipped with a TCD detector. The $\delta^{13}C_{TOC}$ is expressed in relation to the Vienna PeeDee Belemnite (VPDB) standard and the isotope analysis precision was 0.1‰.

Lipid extraction and GDGT analysis. Between 1-3 g of freeze dried sediment was extracted using the Dionex™ accelerated solvent extraction (ASE) with dilchloromethane (DCM):methanol (9:1, v/v) as the solvent at a temperature of 100°C and a pressure of 1500 psi for 5 min with 60 % flush and purge 60 seconds. The extract was then collected and dried using Caliper Turbovap®LV. Next, using DCM, the lipid extract was dried over a column of anhydrous Na_2SO_4 and then blown down under a gentle stream of N_2. In order to quantify GDGTs, 1 µg of an internal standard (C_{46} GDGT; Huguet et al., 2006) was added to the total

lipid extract before it was separated over a column of Al_2O_3 (activated for 2 h at 150°C) into three fractions using hexane:DCM (9:1, v:v) for the apolar fraction, hexane:DCM (1:1, v:v) for the ketone fraction and DCM:MeOH (1:1, v:v) for the polar fraction. The polar fraction, which contained the GDGTs, was dried under a N_2 stream and then re-dissolved in hexane:isopropoanol (99:1, v:v) at a concentration 10 mg ml^{-1}. Finally it was passed through a 0.45 μm PTFE filter and analysed with high performance liquid chromatography-atmospheric pressure positive ion chemical ionization–mass spectrometry (HPLC-APCI-MS) with a separation method that allows the separation of 5- and 6-methyl brGDGTs (Hopmans et al., 2015). For the study of Zell et al., (2014) the samples were split into two different fractions before the analysis, the intact polar lipid (IPL) fraction and core lipid (CL) fractions. For the purposes of this study the IPL and CL fractions of the river SPM were analyzed separately on the HPLC-APCI-MS for GDGTs (Hopmans et al., 2015) and then the amount of GDGTs found in the CL and IPL fractions were combined. After analysis some of the GDGT based indices were recalculated for the entire sample set.

Calculation of GDGT-based proxies. The Roman numerals used to calculate the following GDGT-based proxies refer to the GDGTs indicated in Fig. S1. The 5-methyl brGDGTs and 6-methyl brGDGTs are distinguished by an accent on the 6-methyl brGDGTs. The GDGT indicated by IV is crenarchaeol, the isoprenoid GDGT specific to Thaumarchaeota (Sinninghe Damsté et al., 2002). The BIT index (Hopmans et al., 2003), which results in a value between 0 and 1 with those values closer to 0 designating a more marine signal and a value close to 1 indicating a more terrestrial signal, was calculated using the following formulae that specifically includes the novel 6-methyl brGDGTs according to De Jonge et al. (2015):

$$\text{BIT index} = (Ia+IIa+IIIa+IIa'+IIIa')/(Ia+IIa+IIIa+IIa'+IIIa'+IV) \quad (1)$$

The isomer ratio (IR) signifies the quantity of the penta- and hexamethylated 6-Me brGDGTs compared to the total brGDGTs and was calculated according to De Jonge et al., (2015):

$$IR=(IIa'+IIb'+IIc'+IIIa'+IIIb'+IIIc')/(IIa+IIb+IIc+IIIa+IIIb+IIIc+IIa'+IIb'+IIc'+IIIa'+IIIb'+IIIc') \quad (2)$$

The relative abundance of the penta- and hexamethylated 6-methyl brGDGTs are calculated according to (De Jonge et al., 2014b):

IR_{II}= IIa'/(IIa+IIa') (3)

IR_{III} = IIIa'/(IIIa+IIIa') (4)

The MBT'_{5Me} (which excludes the 6-methyl brGDGTs) was used to calculate MAT according to De Jonge et al., (2014a):

MBT'_{5Me} = (Ia+Ib+Ic)/(Ia+Ib+Ic+IIa+IIb+IIc+IIIa) (5)

MAT = -8.57 +31.45* MBT'_{5Me} (6)

The equation to determine DC (Sinninghe Damsté et al., 2009) was reformulated to specifically include the pentamethylated 6-methyl brGDGTs:

DC' = (Ib+IIb+IIb')/(Ia+Ib+IIa+IIb+IIa'+IIb') (7)

To calculate pH and MAT the novel MAT_{mr} /CBT' calibration was used (De Jonge et al., 2014a):

CBT' = ^{10}log[(Ic+IIa'+IIb'+IIc'+IIIa'+IIIb'+IIIc')/(Ia+IIa+IIIa)] (8)

pH = 7.15 + 1.59 * CBT' (9)

MAT_{mr} = 7.17 + 17.1 * [Ia] + 25.9 * [Ib] + 34.4 * [Ic] - 28.6 * [IIa] (10)

MAT_{mrs} = 5.58 + 17.91 * [Ia] – 18.77* [IIa] (11)

Statistical analysis. Using R software package for statistical analysis we employed principal component analysis (PCA) based on the correlation matrix. The PCA was performed on the fractional abundances of all 15 of the 5- and 6-methyl brGDGTs for the entire sample set along the transect from the land to the ocean.

3. Results

We report bulk and brGDGT data for four cores covering Holocene sedimentation in the Tagus River Basin and its outflow into the Atlantic. We compare these data with new results acquired through an improved LC method able to distinguish between the 5- and 6-methyl brGDGTs (De Jonge et al., 2013) on the soils, riverbank sediments, and SPM samples previously obtained by Zell et al., (2014).

3.1 Bulk parameters of the sediments

The age-depth models for the marine sediment cores (Fig. S2, Table 1) are based on radiocarbon dating of picked foraminifera, gastropods, and shell fragments. The data show that of the four sediment cores from the transect the Tagus River Floodplain sediments date to 6.7 cal. kyrs. BP, the Mudbelt sediments date to 5.8 cal. kyrs. BP, the Lisbon Canyon Head sediments date to 8.7 cal. kyrs. BP, and the Lower Setúbal Canyon penetrated the oldest strata (13.0 cal. kyrs. BP). Reported values for sediments from each location were averaged over the interval 0-6.0 cal. kyrs. BP, so as to avoid a bias in the data since not all of the sediment cores covered more than 6.0 kyrs.

The bulk carbon isotope data for the Tagus River SPM, riverbank sediments, and soils has been previously discussed in Zell et al., (2014). The TOC values for the Tagus River Floodplain sediments are relatively high and also highly variable with a range of 1.5-16 wt. % and a mean of 6.5±4.3 wt. % (average ± standard deviation) and the mean $\delta^{13}C_{TOC}$ was -27.0±1.0 ‰ (Fig. 2; Table 3). In the Mudbelt sediments the TOC is less variable than in the Tagus River Floodplain sediments, ranging from 0.6-1.2 wt. % and with an average of 0.9±0.2 wt. % (Fig. 2; Table 3). The average $\delta^{13}C_{TOC}$ in the Mudbelt sediments, -24.3±0.2 ‰, is higher than in the Tagus River Floodplain sediments. The average $\delta^{13}C_{TOC}$ of the Lisbon Canyon Head sediments, -23.0±0.6 ‰, is higher than the Mudbelt sediments and the TOC content is similar to that of the Mudbelt sediments, ranging from 0.25-1.5 wt. % with the mean of 0.9±0.3 wt. % (Fig. 2; Table 3). The average $\delta^{13}C_{TOC}$ values in the Lower Setúbal Canyon sediments (-23.4±1.5‰) are similar to those of the Lisbon Canyon Head sediments with a TOC content ranging from 0.51-0.85 wt. % with a mean value of 0.65±0.14 wt. % (Fig. 2; Table 3).

3.2 Concentrations and distributions of GDGTs

Tagus Soils and Riverbank Sediments. The average concentration of crenarchaeol is higher in the riverbank sediments (~8.7±7.8 µg gOC^{-1}) than in the soils (~1.4±1.1 µg gOC^{-1}) (Fig. 3a-b; Table 3). The same trend is true for the brGDGTs with the average concentration being higher in the riverbank sediments (~33.9±24.5 µg gOC^{-1}) than the soils (~6.8±6.5 µg gOC^{-1}) (Fig. 3a-b; Table 3). The values of the BIT index were similar to those previously reported (Zell et al., 2014) for both the soils and riverbank sediments and ranged from 0.3 to 1.0 with an average of 0.7±0.2 (Fig. 3c; Table 3). The re-analysis of the brGDGTs in the soils

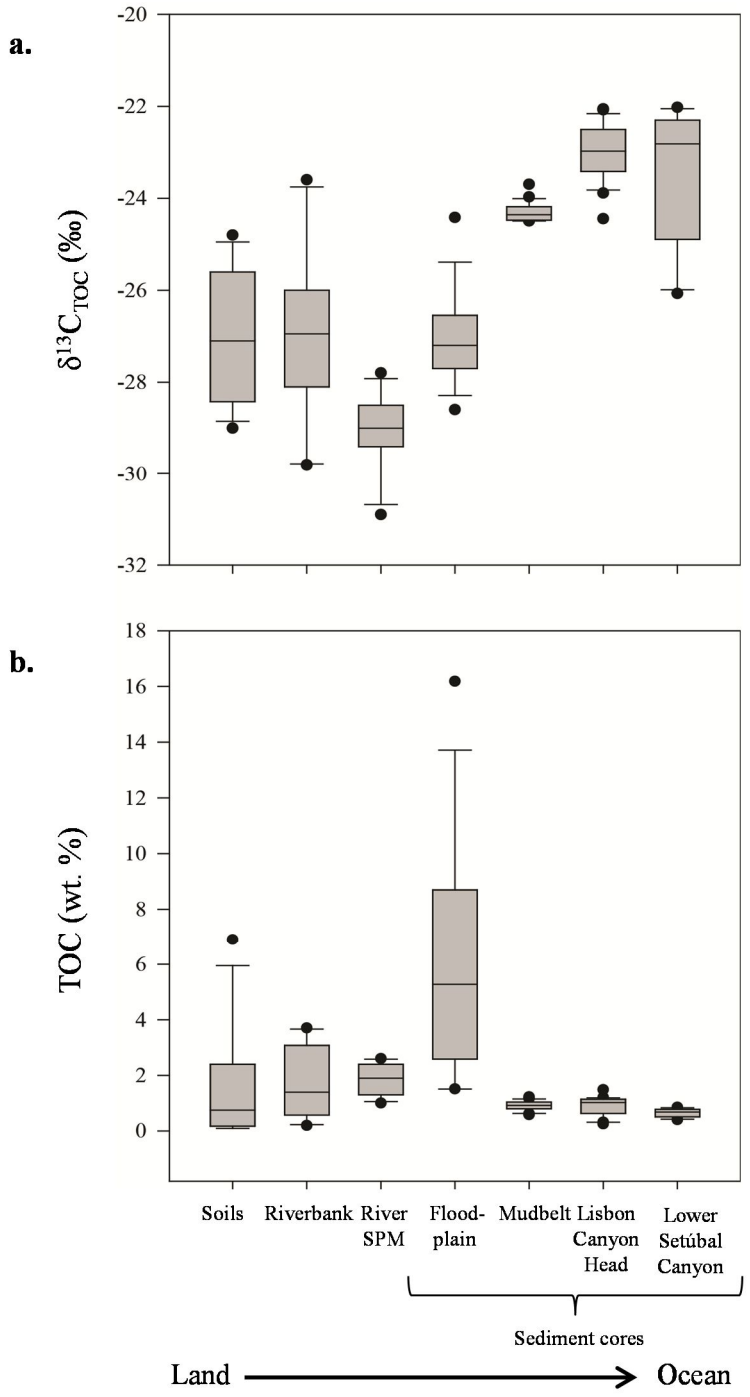

Fig. 2 Boxplots of (a) $\delta^{13}C_{TOC}$ (‰) of the organic carbon and (b) TOC (wt. %) for each sample set along the Tagus River source to sink transect. The increasing $\delta^{13}C_{TOC}$ values in the sediment core locations with increasing distance from the coast indicates that more of the organic carbon in these sediments is marine derived.

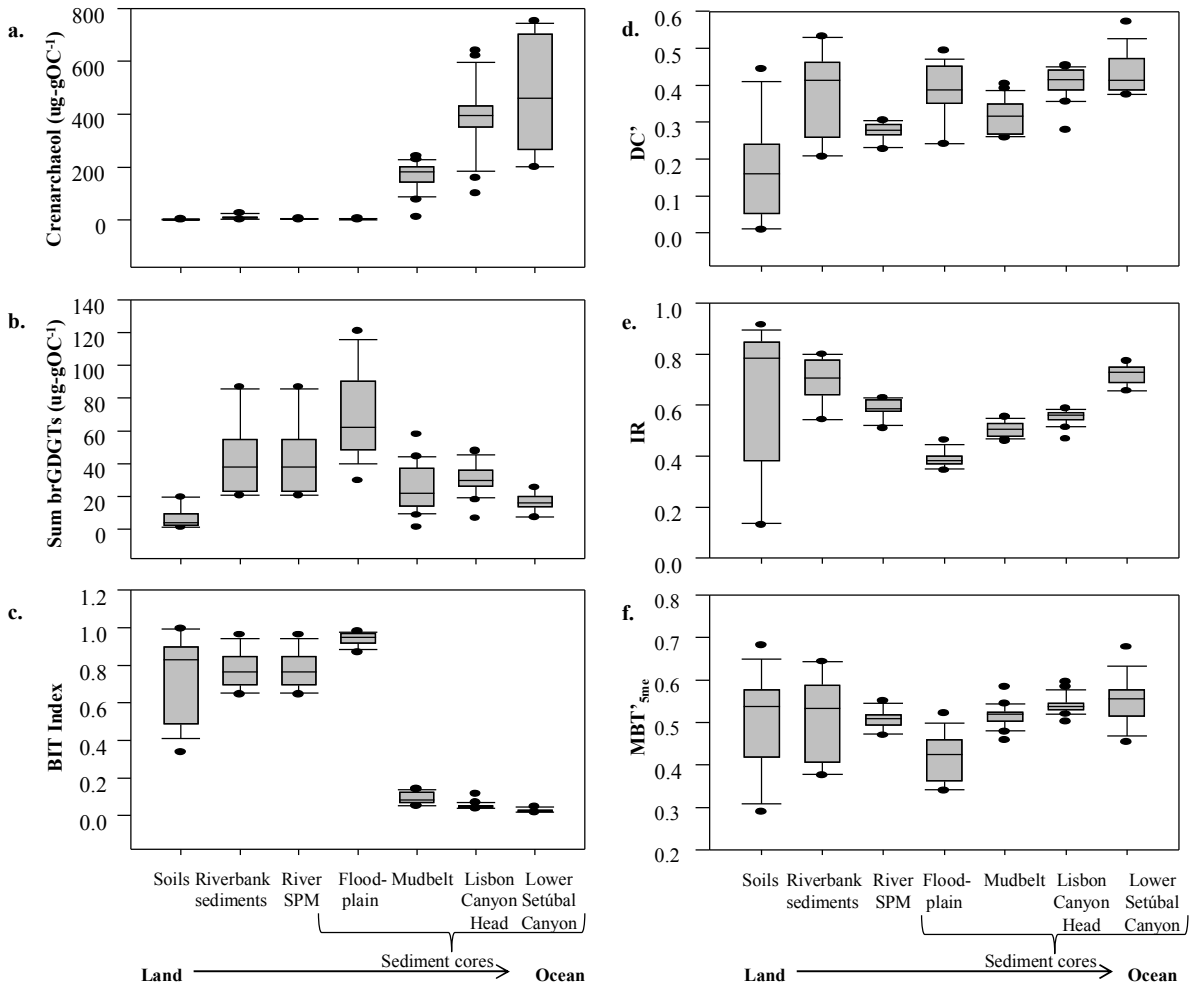

Fig. 3 Boxplots of (a) crenarchaeol concentrations (µg gOC^{-1}), (b) sum of brGDGTs (µg gOC^{-1}), (c) BIT index, (d) DC', (e) IR, (f) MBT'_{5me} for each sample set in the transect from the land to the ocean off the Portuguese coast.

reveals that the relative abundance of the novel 6-methyl brGDGTs is highly variable (ranging from 0.13-0.92) and can be quite high; the average values for the IR are 0.6±0.3 (Fig. 3e; Table 3). IR is even higher but less variable for the riverbank sediments with an average of 0.7±0.1 (Fig. 3e; Table 3). In general the penta- and hexamethylated brGDGTs show the same ratio of 5- and 6-methyl isomers (Fig. 4), however, in soils from an altitude of >350 m the 6-methyl brGDGTs are especially dominant (Fig. S3). Values for the new MBT'_{5me} index, which excludes the 6-methyl brGDGTs (cf. De Jonge et al., 2014a), of the soils and riverbank sediments are quite similar with an average of 0.5±0.1 in both cases (Fig. 3f; Table 3). The DC' ratio deviates between the soils and the riverbank sediments (Fig. 3d; Table 3). The DC' for the soils is highly variable but on average low (0.2±0.1); for the riverbank sediments it is higher with an average of 0.4±0.1 (Fig. 3d; Table 3).

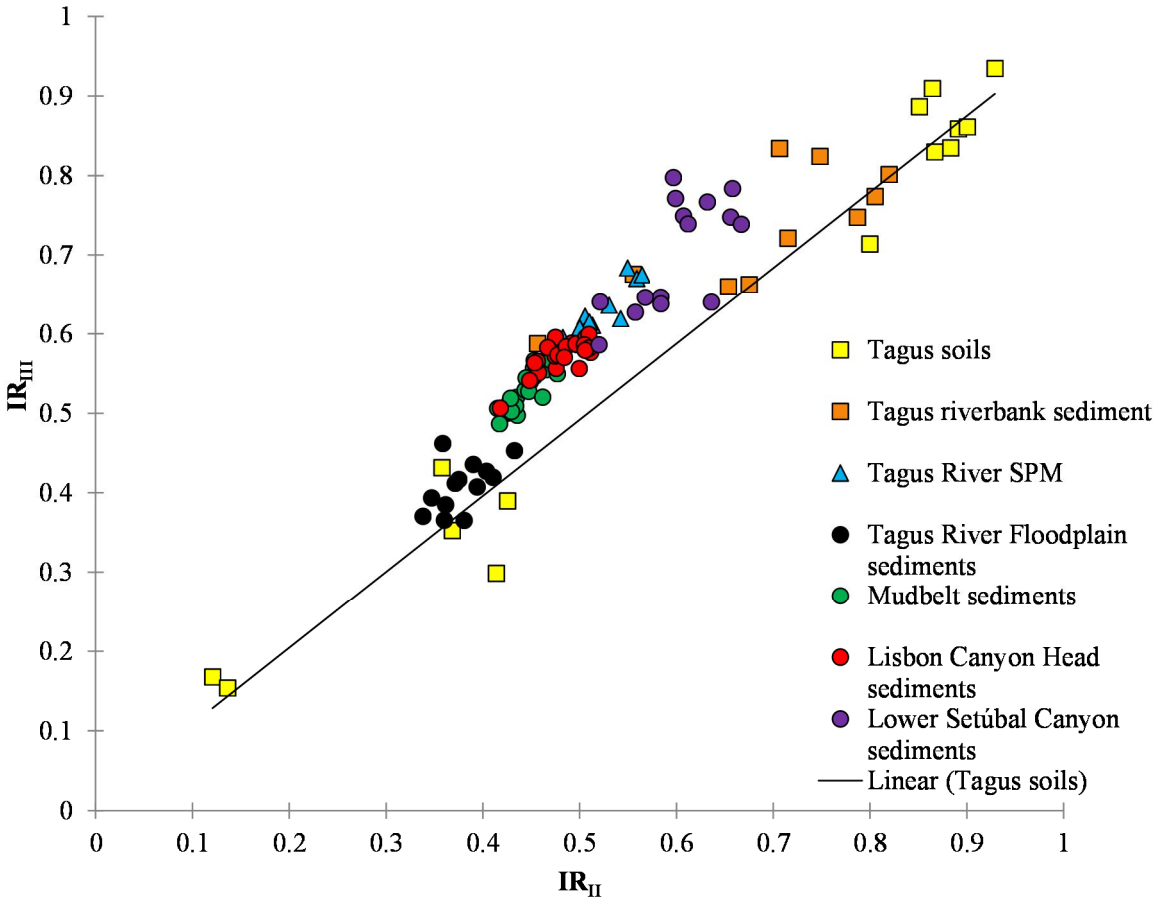

Fig. 4 Isomer ratio for the non-cyclized pentamethylated brGDGT (IR_{II}) plotted against that of the non-cyclized hexamethylated brGDGT (IR_{III}).

Tagus River SPM. The SPM was obtained from the Tagus Estuary near the mouth of the Tagus River once a month over the course of a year (excluding the month of August). Data from the Tagus River SPM showed that the summed brGDGT and crenarchaeol concentrations in the river SPM varied throughout the year and were on average 45±23 µg gOC^{-1}, and 9.8±6.8 µg OC^{-1}, (Figs. 3a-b; Table 3), respectively, resulting in only small variations in the BIT index (i.e. 0.8±0.1; Fig. 3c; Table 3). The distribution of brGDGTs (Fig. 5c) was relatively constant throughout the year as is evident from the values for MBT'_{5me} (0.5±0.0), DC' (0.3±0.0), and IR (0.6±0.0) for the river SPM (Figs. 3d-f; Table 3).

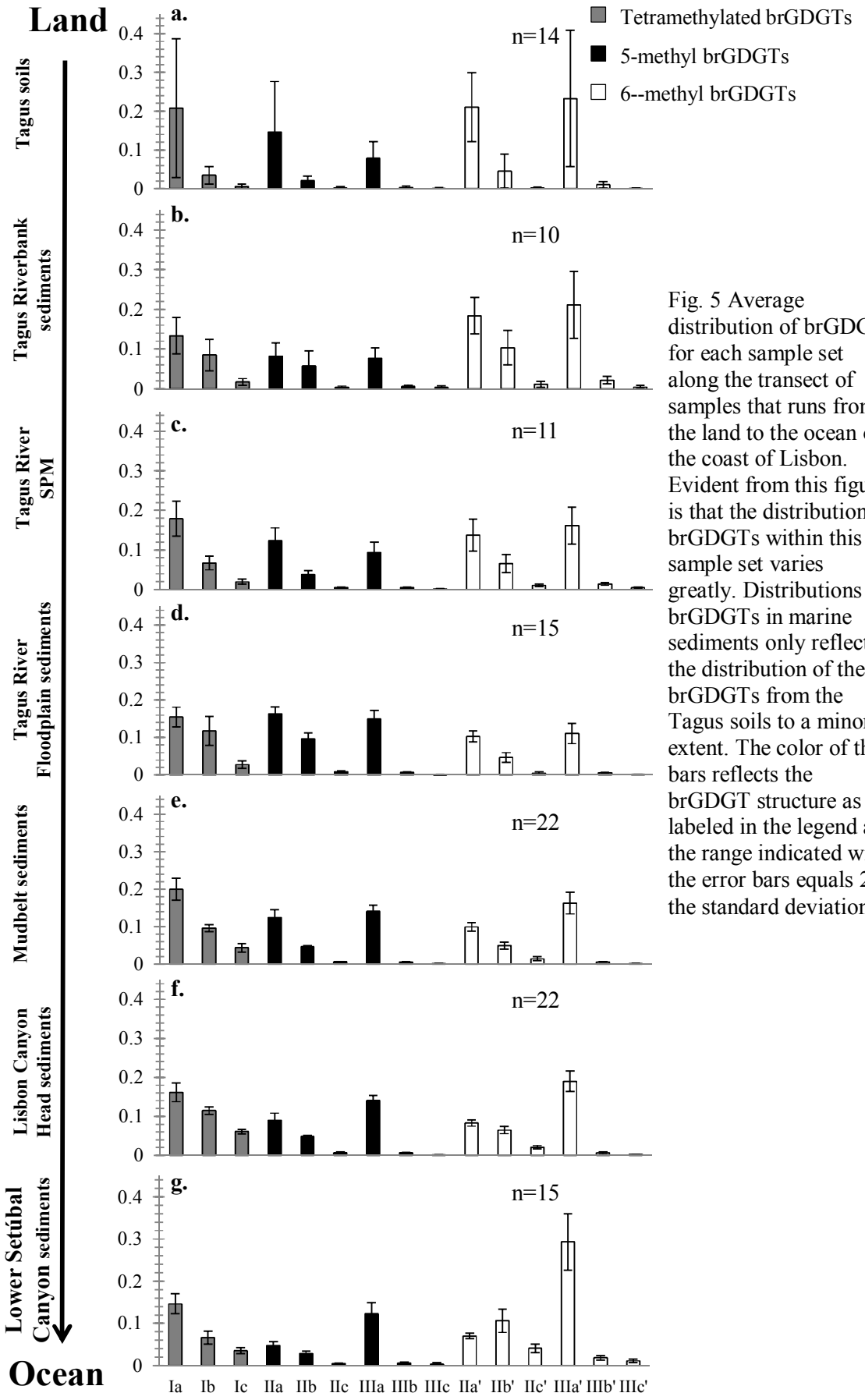

Fig. 5 Average distribution of brGDGTs for each sample set along the transect of samples that runs from the land to the ocean off the coast of Lisbon. Evident from this figure is that the distribution of brGDGTs within this sample set varies greatly. Distributions of brGDGTs in marine sediments only reflects the distribution of the brGDGTs from the Tagus soils to a minor extent. The color of the bars reflects the brGDGT structure as labeled in the legend and the range indicated with the error bars equals 2xs the standard deviation.

Tagus River Floodplain sediments. The average crenarchaeol concentration is fairly low in the Tagus River Floodplain sediments, 2.8±1.7 μg gOC^{-1}, conversely, the average sum of the brGDGTs in the sediments, 70±26 μg gOC^{-1}, is the largest out of the entire transect (Figs. 3a-b; Table 3). The BIT index is fairly high and constant throughout the sediment core with an average value of 0.9±0.0 (Fig. 3c; Table 3). The distribution of brGDGTs (Fig. 5d) is somewhat similar to that of the riverine SPM (Fig. 5c) and shows no major changes over the Holocene. The Tagus River Floodplain sediments has the lowest average values for MBT'_{5me}, 0.4±0.1, and IR, 0.4±0.0, of all the sediment records in the transect (Figs. 3e-f). The mean DC' throughout the sediments in this sample set is 0.4±0.1 (Fig. 3d; Table 3).

Mudbelt sediments. The average concentration of the brGDGTs in the mudbelt sediments, 25±14 μg gOC^{-1}, is lower than in the Tagus River Floodplain sediments, however, the concentration of crenarchaeol, 170±50 μg gOC^{-1}, is higher in the Mudbelt sediments (Figs. 3a-b; Table 3). This results in a lower mean value of the BIT index (i.e. 0.09±0.03; Fig. 3c; Table 3). The brGDGT distribution is relatively constant over the Holocene and is fairly similar to that of the Tagus River floodplain sediments with slightly higher fractional abundances of Ia and IIIa' (cf. Figs. 5d-e; Table 3). The average value of the MBT'_{5me} (0.5±0.0) is similar to the Tagus River SPM value (Fig. 3f). The average value of the DC' is 0.3±0.1 and the mean value of the IR is 0.5±0.0 (Figs. 3d-e; Table 3).

Lisbon Canyon Head sediments. The average sum of the brGDGTs, 31±9.3 μg g OC^{-1}, is about the same in the Lisbon Canyon Head sediments as in the Mudbelt sediments but the amount of crenarchaeol, 390±130 μg gOC^{-1}, is larger in the Lisbon Canyon Head sediments (Figs. 3a-b; Table 3). This results in lower BIT index values (0.05±0.02) than in the Mudbelt sediments (Fig. 3c; Table 3). The average brGDGT distribution (Fig. 5f) is fairly similar to that of the Tagus Floodplain and Mudbelt sediments and is relatively constant over the Holocene. The average of the MBT'_{5me} (0.5±0.0) is statistically identical to that in the Mudbelt sediments (Fig. 3f; Table 3). However, the average IR, 0.6±0.0, and DC', 0.4±0.0, are both a bit higher (Figs. 3d-e; Table 3).

Lower Setúbal Canyon sediments. The concentrations of the brGDGTs in these most distal sediments are quite low, on average 16±5.5 μg OC^{-1} (Fig. 3a; Table 3), while the amount of crenarchaeol in this sediment core is the highest out of the entire transect at 470±200 μg gOC^{-1} (Fig. 3b; Table 3). This results in a low average BIT index value of 0.02±0.01 (Fig. 3c; Table 3). The average distribution of brGDGTs in these sediments (Fig. 5g) is different from the marine sediments from the other two sites, with a higher fractional abundance of IIIa'. However, another component with the same molecular ion eluted at

around the same time as IIIa' in the Lower Setúbal Canyon sediments (which we determined was not the "mixed 5,6-dimethyl isomer"; cf. Weber et al., 2015), complicating integration and quantification. This indicates that the brGDGT results from these sediments must be interpreted with some caution. The average MBT'_{5me} (0.6±0.1) and DC' (0.4±0.1) are fairly similar to the Lisbon Canyon Head sediments averages but the average IR (0.7±0.0) is the highest of all sediments (Figs. 3d-f; Table 3).

3.3 PCA

In order to determine the variation in the distribution of brGDGTs, we performed principal component analysis (PCA) on the distributions of brGDGTs of all the samples examined. Most variation is explained by principal component 1 (PC1; 29.8 %) and is clearly related to the fractional abundance of the 5-methyl versus 6-methyl brGDGTs (Fig. 6a). With the exception of IIIc (which is typically a minor brGDGT with a fractional abundance of <1 %; Fig. 5), all of the 5-methyl brGDGTs score positively on PC1 and the 6-methyl brGDGTs score negatively. For the overall data set, PC1 is highly negatively correlated with the IR ratio (Fig. 7a, R^2=0.78). PC2 explains 25.6 % of the variance of the PCA. Branched GDGTs that score positively on PC2 are generally comprised of cyclized and more methylated brGDGTs (Fig. 6a). With the exception of IIIc (which is typically a minor brGDGT with a fractional abundance of <1 %; Fig. 4), all of the tetra- and penta-methylated brGDGTs containing no cyclopentane moiety (i.e. Ia, IIa, and IIa') score negatively on PC2. Consequently, PC2 is highly positively correlated with DC' for the whole data set (Fig. 7b, R^2=0.84).

4. Discussion

4.1 Environmental parameters affecting brGDGT distribution in Tagus soils

Evident from the earlier study by Zell et al. (2014) was that the distribution of the brGDGTs in Tagus soils varies widely. The primary environmental parameters influencing brGDGT distributions in soil (Weijers et al., 2006b), i.e. MAT and pH, did differ substantially in the Tagus River basin. MAT varies from 10-17°C and pH from 5.5-8.6 (Zell et al., 2014) and both parameters show a distinct correlation with altitude (R^2=0.93 and 0.73, respectively). Applying the brGDGT global soil calibration of Peterse et al. (2012), Zell et al. (2014) arrived at unrealistically low (0-10°C) estimated MATs using the brGDGT distributions. This was attributed to the arid conditions in the region (MAP<800 mm yr^{-1}), which has in other studies, including one that analyzed soils from the Iberian peninsula, been indicated as a likely cause for the discrepancy between actual and reconstructed MAT using brGDGT distributions

(Peterse et al., 2012; Dirghangi et al., 2013; Menges et al., 2014). Our re-analysis of the soils taking into account the novel 6-methyl brGDGTs now provides the possibility to re-evaluate these data. It is clear that the fractional abundances of the novel 6-methyl brGDGTs vary to a large extent. The IR_{II} and IR_{III} vary from 0.1 to 0.9 (Fig. 4) and some of the soils score very negatively on PC1 (Fig. 6b), which is predominantly determined by the fractional abundance of the 6-methyl brGDGTs. From the global soil brGDGT dataset (De Jonge et al., 2014a) it was evident that the main factor influencing the fractional abundance of the 6-methyl brGDGTs is soil pH with an increased abundance in high pH soils. In the Tagus River basin soil pH indeed shows a large variation, i.e. from 5.5 to 8.6, and this likely explains the large variation in IR. When we calculate the pH from the brGDGT distribution using the new equation (9) of De Jonge et al. (2014a), which is based predominantly on the fractional abundances of 6-methyl brGDGTs, we find a highly significant correlation between measured and reconstructed pH (R^2=0.89) following the 1:1 line (Fig. 8a). Differences in soil pH also affect the degree of cyclization of brGDGTs (Weijers et al., 2007b; De Jonge et al., 2014b) and indeed we find a significant positive correlation between DC' and soil pH (R^2=0.74). The effect of MAT is not clearly revealed in the dataset. For the global soil brGDGT dataset a strong relationship exists between MAT and MBT'_{5Me} (De Jonge et al., 2014a). Although we observe substantial variation for MBT'_{5Me} in soils (i.e. 0.3-0.7; Fig. 3f) for this dataset, we do not observe a statistically significant relationship of MAT with MBT'_{5Me}. Also, reconstructed MATs are far too low, i.e. 0.5–13°C using equation (6) and 2.6–11°C using equation (10). Evidently, the "cold bias" of the brGDGT distributions in the soils of the Tagus river basin (Zell et al., 2014) is not solved when 5- and 6-methyl brGDGTs are individually quantified.

Previously it was postulated that in this region aquatic in-situ production and arid conditions are complicating the use of brGDGTs for climate reconstructions (Menges et al., 2014; Zell et al., 2014). Within the soil sample set a strong negative relationship exists between the DC' and the measured MAT in the Tagus basin (R^2=0.79), whereas the degree of cyclization up until this point has only been reported to be related to pH and not to MAT (Weijers et al., 2007a). Conversely, though, the MAT_{mrs} reconstructed values for the soils have a positive correlation with DC' (R^2=0.51) and it is lower than with the measured MAT. Although at this point we are unsure if this association occurs in other arid areas as well, we do believe this strong relationship between the DC' and the MAT could be affecting the applicability of brGDGTs for temperature reconstructions in this region.

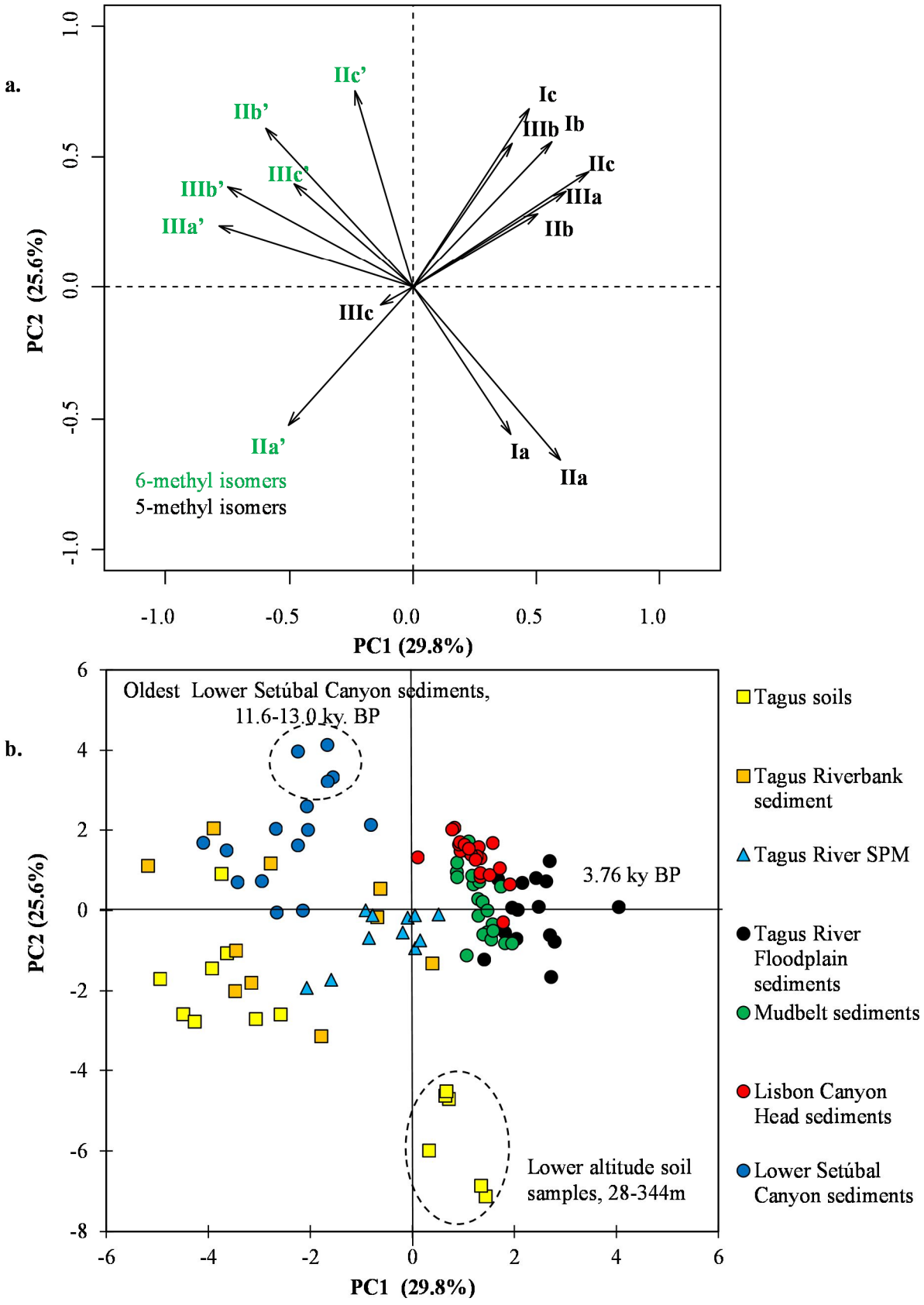

Fig. 6 Principal component analysis based on the fractional abundances of the 15 brGDGTs of samples in the transect that runs from inland to off the coast of Portugal plotting a) the scores of the brGDGT compounds on the first two principal components (PC) and b) the scores of the samples from each sample set used in this study.

4.2 Provenance of brGDGTs in the Tagus River and its outflow

The application of brGDGTs in marine sediments influenced by river outflows for reconstruction of the continental paleoclimate (e.g. Weijers et al., 2006b) rests on the premise that the distribution of the brGDGTs produced in the soils must be conserved throughout riverine transport to the sediments where they are archived. Therefore, we compare brGDGT distributions and concentrations from the rest of the sample set in the source-to-sink transect to determine if the soil signal is conserved during transport in the Tagus River basin. The PCA results (Fig. 6b) indicate that for the most part the distribution of brGDGTs from the river SPM and sediments along the transect is not similar to those from the soils or the Tagus Watershed. Sediments from three of the sample sets in the transect, the Tagus River Floodplain sediments, the Mudbelt sediments and the Lisbon Canyon Head sediments, all plot differently from the soils, and although the distributions of the Lower Setúbal Canyon sediments and the Tagus River SPM plot closer, there is still an offset from the soils. The The Tagus riverbank sediments plot the most closely to the soil samples in the Tagus River basin, however, again a slight offset still exists. So, even without considering the effects of environmental parameters on brGDGT distributions, we can already conclude that the brGDGTs in the sediments and river SPM only reflect the distribution of brGDGTs in the Tagus soils by a minor extent and, thus, it is unlikely that Tagus soils are a major source for brGDGTs in the marine sediments.

Using PCA (Fig. 6) we tried to determine what factors are causing the variation in the distribution of brGDGTs in the Tagus River basin. PC1 is primarily related to the predominance of 5-methyl versus 6-methyl brGDGTs (Fig. 6a) and thus pH (cf. De Jonge et al., 2014a). This was confirmed for the soils in the Tagus basin where the calculated pH based on the fractional abundance of predominantly 6-methyl brGDGTs shows good agreement with the measured pH (see Sect. 4.1). De Jonge et al. (2014b) showed that in the SPM of the alkaline waters of the river Yenisei 6-methyl brGDGTs also predominate, indicating that pH in all kinds of environmental settings determines the ratio between 5 and 6-methyl brGDGTs. The Tagus riverbank sediments, river SPM and the Lower Setúbal Canyon sediments score mostly negatively on PC1 as do soils from higher altitudes (>350 m) (Fig. 6b). The Mudbelt sediments, Lisbon Canyon Head sediments, the Tagus River Floodplain sediments, and the lower altitude soils (<350 m) have similar abundances of the 5- and 6-methyl brGDGTs or higher abundances of the 5-methyl brGDGTs and plot mostly positively on PC1. Since the Tagus River Floodplain sediments, the Mudbelt sediments, and the Lisbon Canyon Head sediments do not have a predominance of 6-methyl brGDGTs, this indicates that either they

received an equal contribution of soil derived organic matter from the lower altitude soils in the region (<350 m) as from the higher altitude region (>350m) or, more likely, that in-situ production of brGDGTs is a large source of brGDGTs in these sample sets.

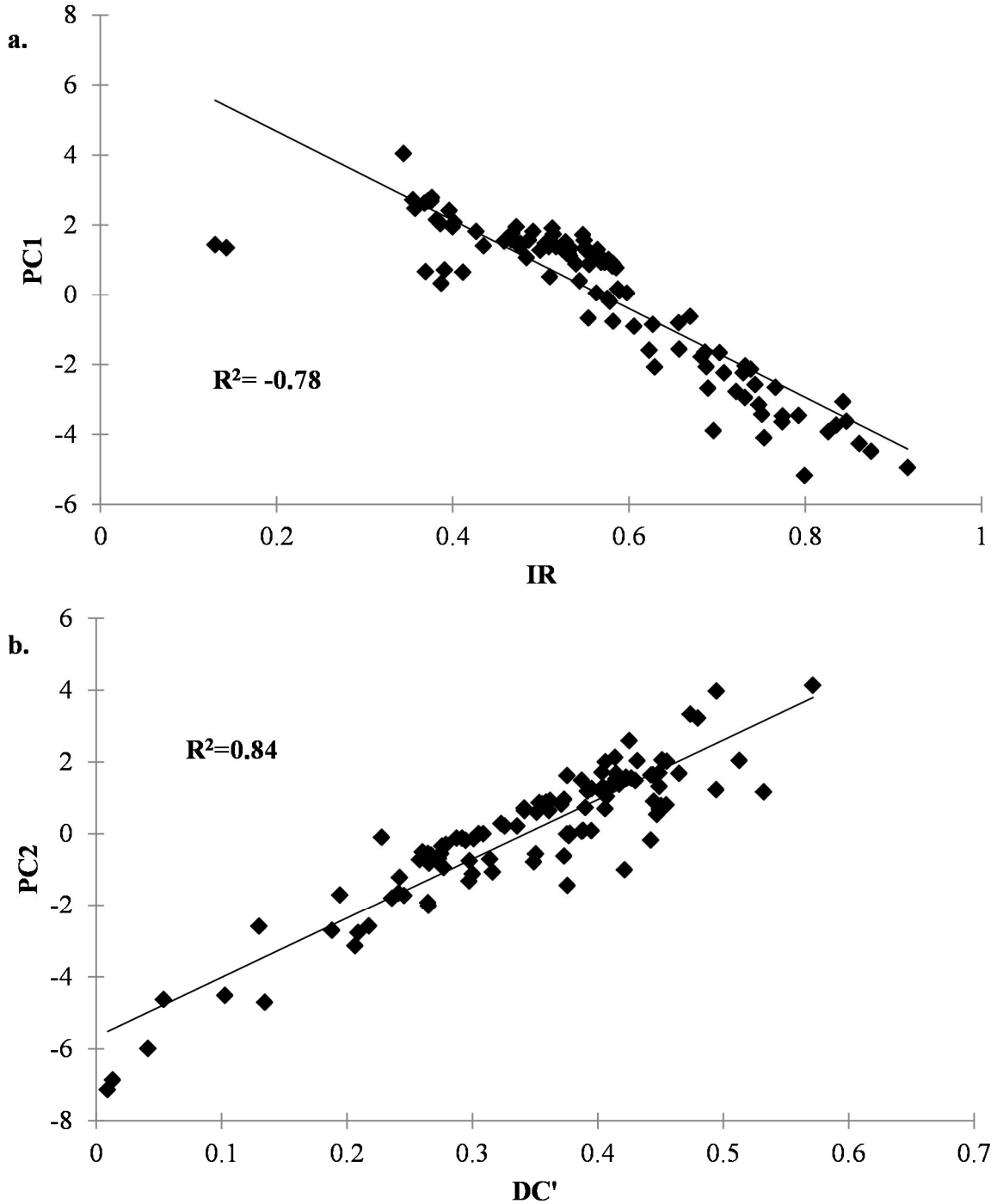

Fig. 7 Scatter plots of (a) PC1 against the IR (R^2=0.78) and (b) PC2 against DC' (R^2=0.84) for the entire set of samples used in this study.

PC2 also explains a substantial part of the variance in the dataset (25.6 %, Fig. 6b) and is correlated with DC' (R^2=0.84, n=109, Fig. 7b). Since pH is also the main driver of DC' (Weijers et al., 2007b), it suggests that differences in pH are also responsible for the variance seen in PC2. The samples that standout are the sediments from the Lower Setúbal Canyon core, which are the most marine sediments in the sample set, and plot most positively, and the lowest altitude soils (28-344 m), which plot the most negatively. These latter soils are characterized by a low measured pH. The oldest (11.6-13.0 kys BP) sediments of the Lower Setúbal Canyon score most positively on PC2. A high degree of cyclization of brGDGTs has been observed previously in marine sediments from a Svalbard fjord and attributed to marine in-situ production in the alkaline pore waters of marine sediments (Peterse et al., 2009; Weijers et al, 2014). Re-analysis of the Svalbard sediments for brGDGTs actually showed that this cyclization affects the tetra- and pentamethylated brGDGTs to a much larger extent than that of the hexamethylated brGDGTs (Sinninghe Damsté, 2016) and the same observation can be made for the sediments of the Lower Setúbal Canyon (Fig. 5g). Evidently, the high degree of cyclization of brGDGTs as a response to pH is not as clearly seen in the soils since the high altitude, high pH soils from the Tagus watershed (Fig. S3c) do not exhibit the pattern (i.e. fractional abundance of IIb' larger than that of IIa') observed in the Lower Setúbal Canyon sediments (Fig. 5g). This pattern is, to a lesser degree, also seen in the sediments of the Lisbon Canyon Head core (Fig. 5f). As mentioned earlier, the Lower Setúbal Canyon sediments also display a predominance of 6-methyl brGDGTs over the 5-methyl counterparts, especially with regards to the hexamethylated brGDGTs. In the Lower Setúbal Canyon sediments IIIa' is by far the most abundant brGDGT, consisting of 29 % of the entire brGDGT pool (Fig. 5g). This is comparable to Svalbard sediments (Sinninghe Damsté, 2016) where IIIa' is also the most abundant brGDGT. Taken together this clearly indicates the influence of in-situ production in the Lower Setúbal Canyon sediments. However, the degree of cyclization for Ia-c and IIa-c is not as high as observed for the Svalbard sediments, which still suggests some allochthonous input of brGDGTs even in these remote marine sediments.

Another way to determine if in-situ production is a factor affecting the brGDGT distribution in aquatic environments is by the calculation of reconstructed pH values. If in-situ production is heavily contributing to the brGDGT pool, then the reconstructed pH values should reflect that of the aquatic environment in which they were produced. The average reconstructed pH of the sample sets in the transect are relatively high with a clear trend to higher values with increasing distance from the river mouth (Fig. 9a), which would be in line with increased in situ production of brGDGTs in the alkaline pore waters of marine

sediments. However, these values are still within the range of the measured (5.5-8.5) and reconstructed (Fig. 9a) pH of the soils and so this does not prove in-situ production as a major contributor of brGDGTs in these sample sets. Conversely, the newly calculated DC', also a reflection of pH, is quite variable throughout the sample sets in the transect except for in the river SPM where it is fairly constant (Fig. 3d; Table 3). Since the DC' is lowest in the soils (0.2±0.1) and then higher in the rest of the samples in the transect (0.3-0.4), this suggests in-situ production is an issue (cf. Zell et al., 2014) in all of the sample sets (Fig. 3d; Table 3).

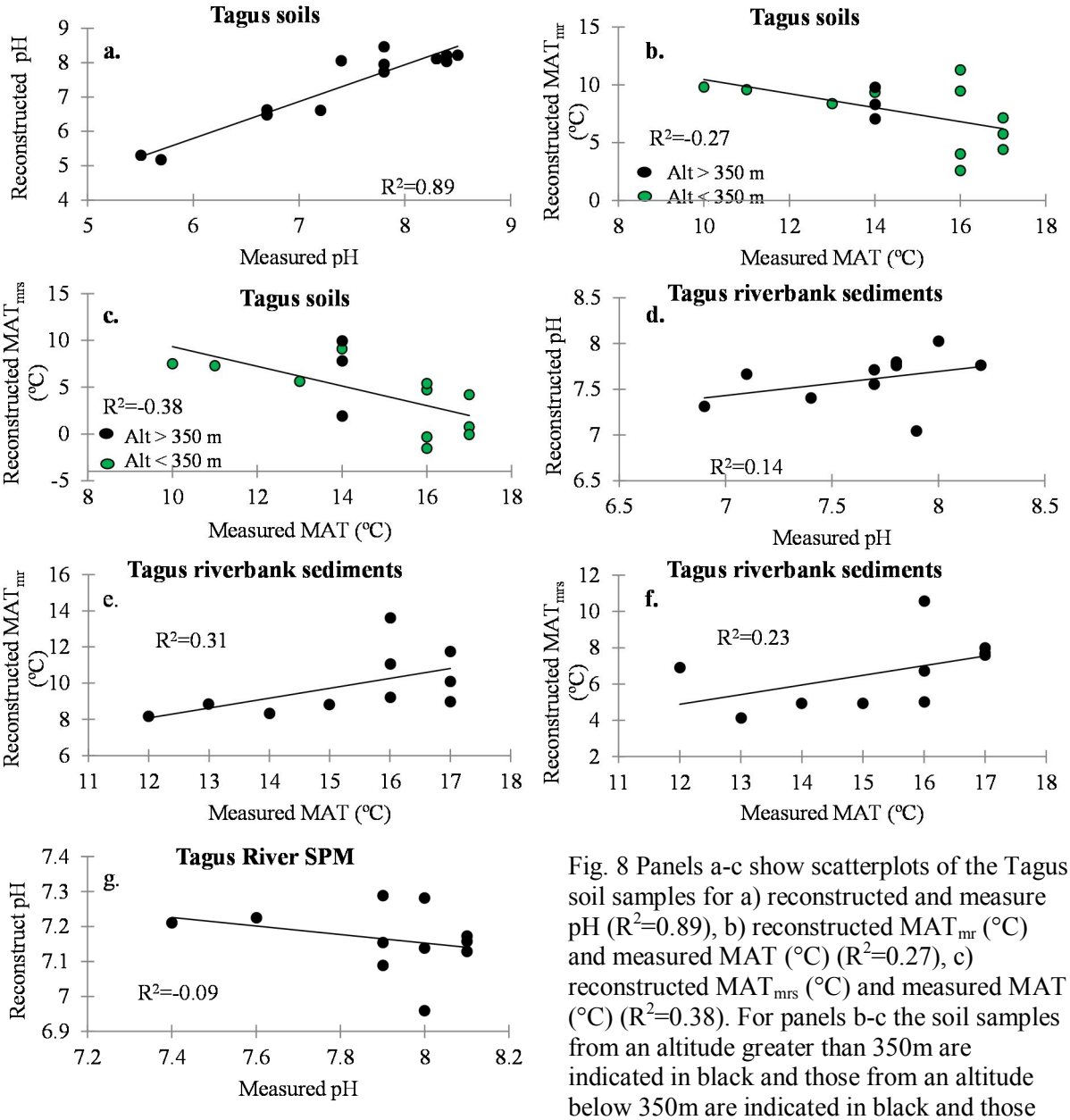

Fig. 8 Panels a-c show scatterplots of the Tagus soil samples for a) reconstructed and measure pH (R^2=0.89), b) reconstructed MAT_{mr} (°C) and measured MAT (°C) (R^2=0.27), c) reconstructed MAT_{mrs} (°C) and measured MAT (°C) (R^2=0.38). For panels b-c the soil samples from an altitude greater than 350m are indicated in black and those from an altitude below 350m are indicated in black and those from an altitude below 350m are indicated in green. Panels d-f show scatter plots of the Tagus riverbank sediments for d) reconstructed and measured pH (R^2=0.14), e) reconstructed MAT_{mr} (°C) and measured MAT (°C) (R^2=0.31), f) reconstructed MAT_{mrs} (°C) and measured MAT (°C) (R^2=0.23). Panel g is a scatter plot showing the reconstructed and measured pH for the Tagus River SPM samples (R^2=0.09).

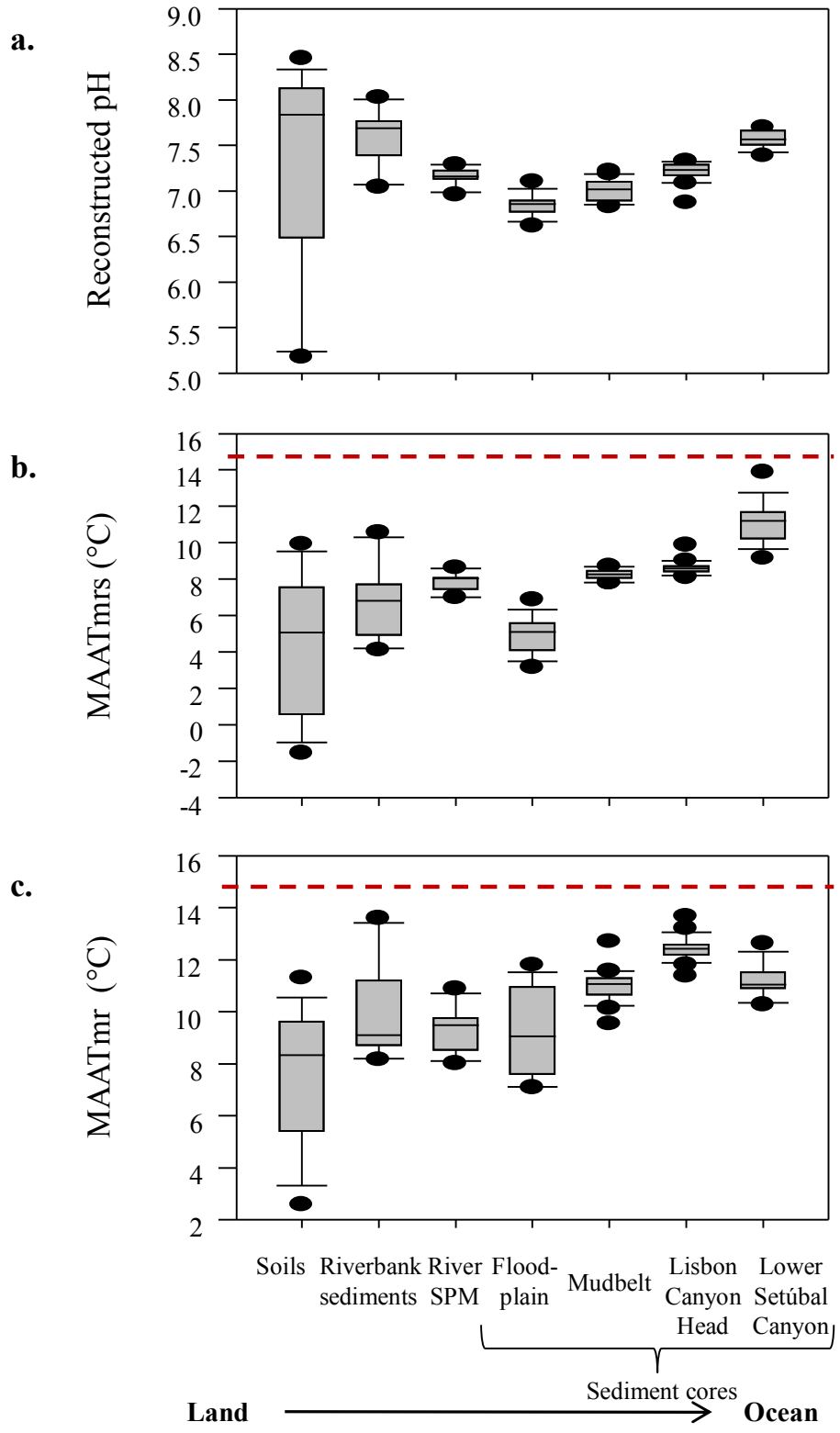

Fig. 9 Boxplots of all the sample sets within the transect from the land to the deep ocean off the Portuguese coast for (a) reconstructed pH, (b) MAT_{mrs} (°C) and (c) MAT_{mr} (°C). Red dotted line indicates estimated present day MAT for the Tagus River basin (14.6°C).

4.3 Branched GDGTs as indicators of terrestrial OM transport by the Tagus River

Classically, the assessment of the contribution of terrestrial OM to marine sediments is performed by measuring $\delta^{13}C_{TOC}$ (Hedges and Oades, 1997 and references cited therein). In the earlier study of the Tagus River system, Zell et al. (2014) determined that the average $\delta^{13}C_{TOC}$ of the riverine SPM (~-29 ±0.8‰), like the Tagus soils, are consistent with a predominant C_3 higher plants origin (Fry and Sherr, 1984). Additionally, this study found the $\delta^{13}C_{TOC}$ in marine surface sediments off the Portuguese coast in front of the Tagus River increase with increasing distance offshore by an increased contribution of ^{13}C-enriched marine OM. This trend is also evident for the Holocene sediments studied here. The most terrestrial sediments of the transect, i.e. from the Tagus River Floodplain, also have a $\delta^{13}C_{TOC}$ value (~27±1.0 ‰; Fig. 2a; Table 3) consistent with a predominant C_{origin} of higher plants. Moving offshore, the less negative $\delta^{13}C_{TOC}$ values of the Mudbelt sediments (-24±0.2 ‰), the Lisbon Canyon Head sediments (-23±0.6 ‰) and the Lower Setúbal Canyon sediments (-23±1.5 ‰) all indicate that the majority of the TOC off the Portuguese shelf is of marine origin (Fig. 2a; Table 3). So, as Zell et al. (2014) found with marine surface sediments off the Portuguese coast, the $\delta^{13}C_{TOC}$ (‰) averages from the sediments in our transect also increase with increasing distance offshore, demonstrating that the present trend in the $\delta^{13}C_{TOC}$ signal remained the same over the Holocene.

Zell et al. (2014) previously showed that in the present day Tagus River system the amount of brGDGTs (µg gOC^{-1}) increases from the soils to the riverbank sediment to the river SPM and explained this increase as proof of riverine in-situ production of brGDGTs. Concentrations of summed brGDGTs in surface sediments in transects from the Portuguese coast rapidly declined with increasing distance from the coast, suggesting that brGDGTs could still be used as tracer for terrestrial organic matter (Zell et al., 2015). The trends observed in these earlier studies are confirmed here for the Holocene. The Tagus River Floodplain sediments have the highest concentration of brGDGTs (67±26 µg gOC^{-1}) in the entire transect, much higher than in the soils (Fig. 3b; Table 3). However, the sediments in this core are somewhat a-typical for the Tagus Floodplain as some layers consist of peat as a result of the low-energy backswamp conditions in the vicinity, which could explain the difference in brGDGT concentrations from the surrounding soils. This could also be due to the addition of aquatically produced brGDGTs from the river during times of flooding although it should be noted that the concentration of brGDGTs is even higher than in riverine SPM (Fig. 3b). The summed brGDGT concentration decreases and is fairly similar among the Mudbelt sediments (25±14 µg gOC^{-1}) and the Lisbon Canyon Head sediments (31±9.3 µg

gOC^{-1}), and then decreases further moving away from the coastline to the Lower Setúbal Canyon sediments (16±5.5 µg gOC^{-1}) demonstrating the decrease in input of riverine brGDGTs moving away from the shoreline (Fig. 3b). However, even though the sum of the brGDGTs are lower in the marine sediment than in the Tagus River Floodplain sediments, the amount of brGDGTs in all four sediment cores are higher than in the Tagus soils (~6.8±6.5 µg gOC^{-1}) indicating the origin of the brGDGTs in the sediment cores are not all soil derived and pointing instead to riverine in-situ production as well as possibly in aquatic sediments (Fig. 3b).

A previous study by Zell et al., (2015) determined that in the surface sediments off the coast of Portugal the BIT index is influenced by both declining brGDGT concentrations and increased crenarchaeol production with increasing distance from the coast. For the Holocene sediments studied here, the average concentration of crenarchaeol in the Tagus River Floodplain sediments is low (2.8±1.7 µg gOC^{-1}) and similar to that of the Tagus soils (1.4±1.1 µg gOC^{-1}; Fig. 3a; Table 3). The crenarchaeol concentration increases in the sediments with increasing distance from the shoreline, signifying the increase in marine production with water depth and distance from the coast (Fig. 3a). Consequently, the BIT index is the highest in the Tagus River Floodplain sediments (0.94±0.03) out of the entire transect (Fig. 3c) and then the BIT index decreases within the sediments along the transect with increasing distance from the Portuguese coast potentially signifying a decrease in terrestrial input moving away from the shoreline.

4.4 Factors affecting the application of brGDGTs for paleoclimate reconstructions off the Iberian Peninsula

Despite the caveats with respect to in-situ production of brGDGTs in aquatic environments as described in the previous section, we tested how the new soil calibration based on individually quantified 5-methyl and 6-methyl brGDGTs (De Jonge et al., 2014a) performed to reconstruct continental MAT in this region. For this comparison we will consider the present day MAT of the entire Tagus River basin, 14.6±2.2°C (Zell et al., 2014), assuming that soil derived brGDGTs from along the whole river basin are contributing to the marine sediments. The assumption that the brGDGTs from the entire Tagus River basin are being contributed to oceanic sediments is probably invalid for modern times as the construction of dams along the Tagus River, which began in the 1940s, most likely prevents part of the terrestrial material from upstream making it downstream and out off the coast of Portugal. However, since we are not looking at marine surface sediments in this study but

instead sediments deposited during the Holocene, the placement of dams in the river should not affect our results except for with the riverine SPM. Despite the separation of the 5- and 6-methyl brGDGT isomers and the application of the new proxy, the reconstructed MATs using both riverine SPM and Holocene sediments is still substantially lower than 14.6°C (Figs. 9b and 9c), as noted for the Tagus basin soils (see Sect. 4.1). Using the MAT_{mrs} calibration, the reconstructed average temperature for the Lower Setúbal Canyon sediments (11.2±0.7°C) is the most similar to modern day MAT in the regions (Fig. 9b). Using the MAT_{mr} calibration, the average reconstructed temperature of the Lisbon Canyon Head sediments, 12.4±0.5° C, comes closest to the modern day MAT in the region (Fig. 9c).

Even though we used the new calibration to reconstruct MAT, it should be noted that the low BIT values (<0.15; Fig. 3c) of the Holocene sediments deposited at the three marine sites indicates that there were probably not enough soil-derived brGDGTs making it out to ocean and being deposited in the sediments over the Holocene for reliable climate reconstructions (cf. Weijers et al., 2014). When considering the summed concentration of brGDGTs along the entire transect, since the concentration is lowest in the soils this indicates that the origin of the brGDGTs may not be solely soil-derived. Therefore, even though the BIT index seems high enough for MAT reconstructions in the riverbank sediments and river SPM, in situ production of brGDGTs could be complicating the applications of brGDGTs for paleoclimate reconstructions throughout the transect of samples as was previously discussed (see Sect. 4.2). This further supports earlier conclusions from preceding studies (Yang et al., 2012; Zell et al., 2013) stating that the amount and origin of brGDGTs in a system needs to be examined along with the BIT index when determining if brGDGTs can be applied for MAT reconstruction.

5. Conclusions

We have established that the distribution of brGDGTs varies greatly within the Tagus River basin (Fig. 5) and although this may be partly explained by the varying contributions of higher altitude, which contain a greater proportion of 6-methyl isomers, versus lower altitude soils in the sample sets it is more likely due to the contribution of aquatically produced brGDGTs in some of the sample sets. In order to use sedimentary brGDGTs for paleoclimate reconstructions, the distribution of brGDGTs in the soils must be related to the MAT and conserved throughout riverine transport to the sediments where they are deposited, however, our results corroborate previous studies stating that most of the terrestrial matter is not making it out to the ocean and being deposited in sediments close to shore. The lack of soil derived

OM in offshore sediments along with the substantial input of aquatically produced brGDGTs is complicating MAT reconstructions from sedimentary, marine brGDGTs in this region.

Additionally, we confirm the findings of Zell et al., (2014; 2015) that in-situ production of brGDGTs is occurring in the river and marine systems of the Tagus River basin and go on to show that there are indications that it occurred in the past as well. Although in-situ production is complicating environmental reconstructions using marine sediments, another issue is that accurate MAT reconstructions using brGDGTs cannot currently be performed on the soils, even with the separation of the 6-methyl brGDGTs from the 5-methyl isomers using the new method and calibrations. Previous studies have concluded that paleoclimate reconstructions in arid regions using brGDGTs are complicated due to a breakdown in the relationship with MBT' and MAT (Peterse et al., 2012; Menges et al., 2014). In this study we confirm that there is not a strong relationship between the MBT'_{5me} and measured MAT in this arid region. However, we also do not observe the same relationship with MAP and MBT'_{5me} that has been previously reported between MAP and MBT' in arid regions and has been implicated in making reconstructions difficult. Instead, we see a strong relationship with the DC' and measured MAT in the area not observed before. We also see a predominance of 6-methyl isomers, previously only reported in river SPM, in the Tagus soils from greater than 350 m altitude. Although this might be a characteristic of arid soils and related to MAP since it is below 550 mm yr^{-1} in most of the soil samples above 350 m, the two highest elevation soil samples, which both have a MAP above 550 mm yr^{-1}, also demonstrate this trend. Future studies need to be performed in arid environments to determine if a strong relationship between MAT and DC' as well as a predominance of 6-methyl isomers are characteristics of arid regions and contributing to the complications found using brGDGTs for paleoclimate reconstructions. Also, higher elevation environments should be further studied to determine if a predominance of 6-methyl brGDGTs is a feature of higher altitudes and complicating climate reconstructions.

Because of these unique features in this region, perhaps the development of a local calibration could assuage difficulties in using brGDGTs as a paleoclimate proxy for soils in the Tagus River basin. This would not, however, solve the issue of in-situ produced brGDGTs overwhelming the amount of soil derived brGDGTs in aquatic sediments. We did find that the new CBT' and pH calibration do an excellent job reconstructing pH in the soils of the Tagus basin and since pH is related to other environmental factors such as MAP this will be useful for paleoclimate reconstructions in terrestrial sites over the Iberian peninsula where in-situ production is not a complicating factor.

Author contribution

J.H. Kim and J.S.S. Damsté designed the study, which was carried out by L. Warden who completed bulk carbon isotope and brGDGT analysis on samples along with C. Zell. C. Zell, H. Stigter, G.J. Vis and J.H. Kim collected samples for this study. J. Bonnin picked forams for dating. L. Warden and J.S.S. Damsté prepared the manuscript with contributions from all co-authors.

Acknowledgements

The research leading to these results has received funding from the European Research Council under the European Union's Seventh Framework Programme (FP7/2007-2013) / ERC grant agreement n° [226600]. JSSD is supported by funding from the Netherlands Earth System Science Center (NESSC) though a gravitation grant from the Dutch ministry for Education, Culture and Science. We thank the captain and crew of the R/V Pelagia for their support with sampling. We thank J. Ossebaar and E.C. Hopmans for their help with the HPLC-APCI-MS analysis, J. Ossebaar for his help with the element analyzer, and L.A.C. Rosales and A. Mets for help with sample preparation.

– SUPPLEMENTARY INFORMATION –

Part A: Sediment core descriptions

Tagus River Floodplain core (0501.029). Description has been previously published in:

Vis, G.-J., Bohncke, S. J. P., Schneider, H., Kasse, C., Coenraads-Nederveen, S., Zuurbier, K. and Rozema, J.: Holocene flooding history of the Lower Tagus Valley (Portugal), J. Quat. Sci., 25, 1222-1238, DOI: 10.1002/jqs.1401, 2010.

Mudbelt core (64PE332-30-2). Core 64PE332-30-2 retrieved from the Tagus Mudbelt consists of a fairly monotonous succession of dark olive gray homogeneous to weakly stratified sandy silt, gradually coarsening in downcore direction to silty sand. The silt and sand are composed of a mixture of siliciclastic material and bioclastic carbonate, with minute shell fragments but occasionally also intact bivalve and gastropod shells.

Lisbon Canyon Head core (64PE332-44-2). Core 64PE332-44-2 retrieved from the Lisbon Canyon head consists in its upper three meters of dark olive gray bioturbated clayey silt. Finely dispersed iron monosulphide, indicative of a strongly reduced state of the sediment, gives the sediment a dark mottled appearance. Below three meters depth the sediment turns to lighter shades of olive gray. Moving further downcore there is an increasing content of bioclastic carbonate sand. This sandy material, including foraminiferan shells and minute shell fragments, is found dispersed throughout the sediment but also locally concentrated in pockets produced by burrowing fauna. In the lower three meters towards the base of the core, the sandy material also occurs as discrete layers of a few centimeters thick, likely deposited by sediment gravity flows running down the canyon slopes. This is particularly the case for a coarse bioclastic sand layer at 778-797 cm depth, which has a sharply defined erosive lower boundary and fining upward succession typical of turbidite deposits.

Lower Setúbal Canyon core (64PE269-39). Core 64PE269-39pc was recovered from the crest of the large sediment levee bounding the lower Setúbal Canyon towards the north. In its upper half, considered in the present study and dated by AMS ^{14}C as of Holocene to Younger Dryas age, it consists of uniform olive-gray to gray bioturbated hemipelagic silty clay. From the presence of 2.5 cm of yellowish-grey oxidized sediment at the top of the core, with a thin rusty-brown iron oxide band marking the transition to reduced olive-grey sediment, it can be deduced that core recovery is fairly complete. In the lower half of the core, which on the basis of unpublished planktonic foraminiferal $\delta^{18}O$ results can be attributed to the Younger Dryas to

Last Glacial Maximum, silty layers of a few millimeters thick are found intercalated in the bioturbated hemipelagic silty clay. These silty layers are interpreted to represent deposition from sediment plumes spilling over the edges of the Setúbal Canyon in the wake of major down-canyon sediment gravity flows. The silty layers are particularly abundant in the lower part of the core, where they give the sediment a distinctly laminated appearance, further accentuated by intense black iron monosulphide coloring that comes along with the silty layers. The abundance of silty layers in the lower part of the core is indicative of a prevalence of deposition from sediment gravity flows along this part of the Portuguese margin during the late glacial sea level lowstand, contrasting with hemipelagic deposition during the Holocene.

Part B: Supplementary figures

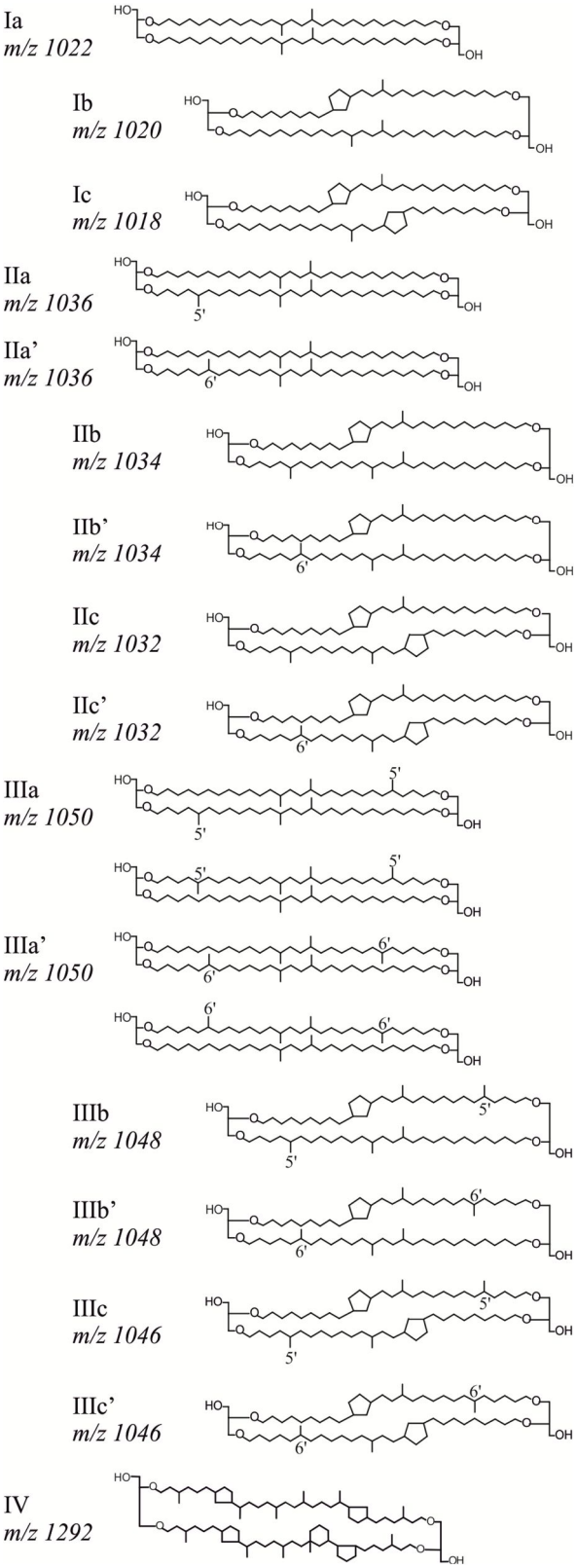

Figure S1 Chemical structures of all 15 brGDGTs (I-III) and crenarchaeol (IV) (De Jonge, et al., 2014a). The compounds indicated with a prime symbol are referred to as the 6-methyl brGDGTs and the ones not designated by the prime symbol are referred to as the 5-methyl brGDGTs.

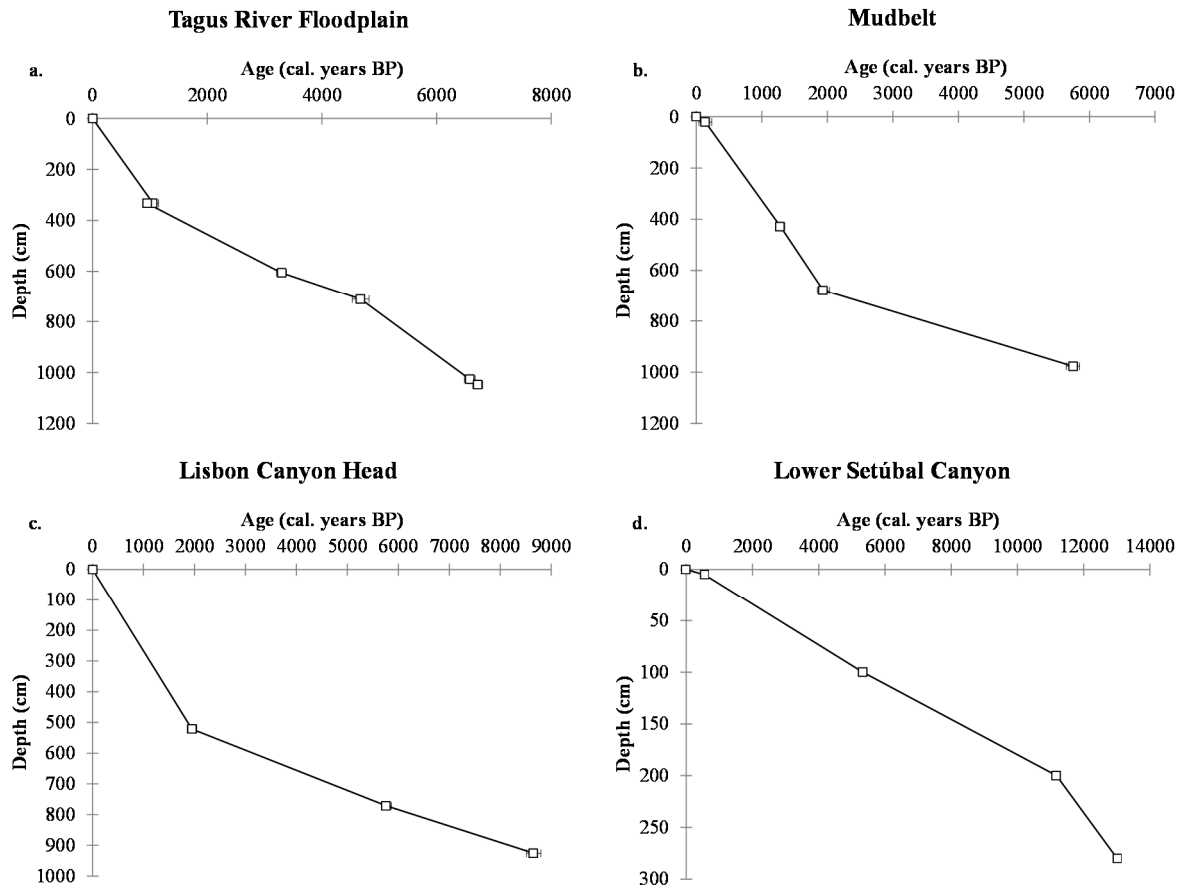

Figure S2 Depth age models for each sediment core used in this study based on the information summarized in Table 2. To create consistent chronologies for the four sediment cores, the dates were calibrated into calendar ages using the CALIB 7.0, available at http://radiocarbon.pa.qub.ac.uk/calib (Stuiver et al., 1998). The calibration data and curve selection utilized for the three marine sediment cores was Marine13 and for the Tagus River Floodplain core IntCal13 was implemented (Reimer et al., 2013). All radiocarbon dates mentioned are expressed as calibrated ages (cal. BP) and have age spans in the 2σ range.

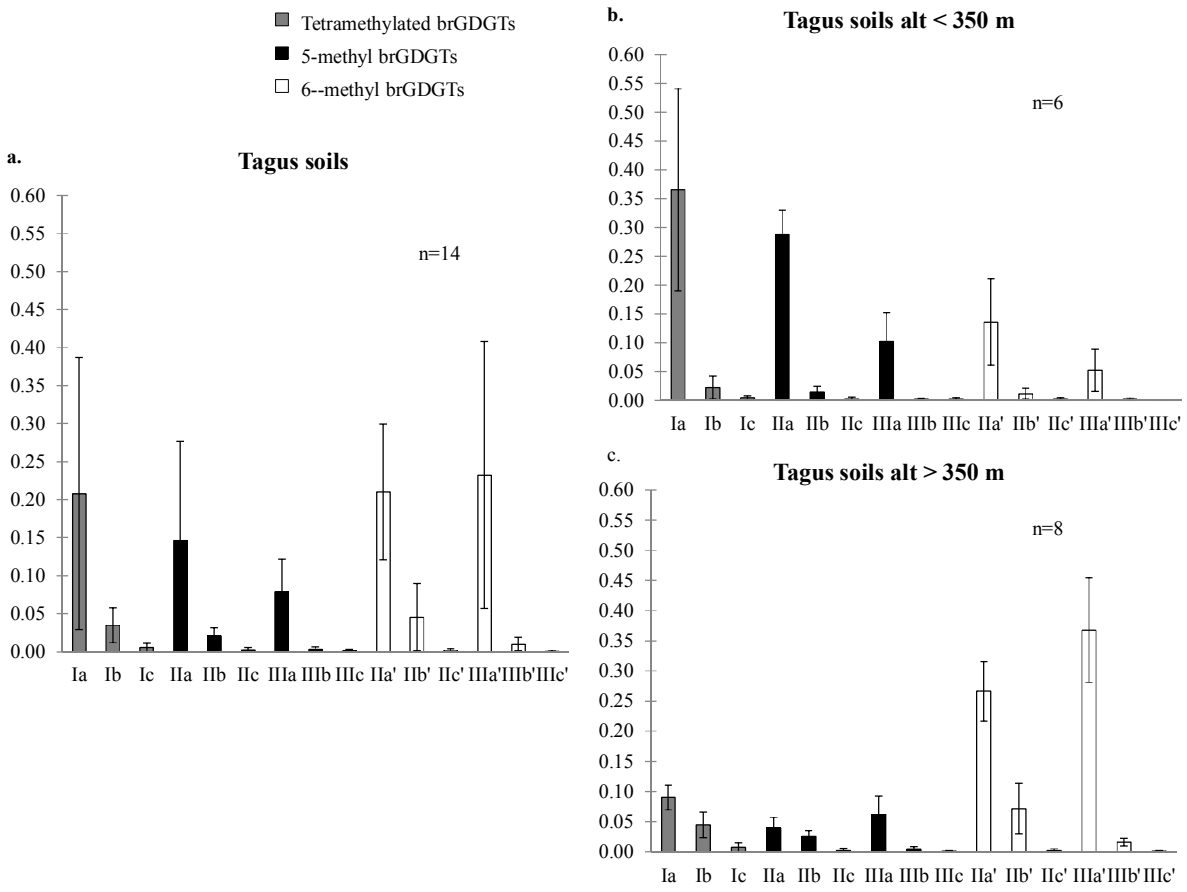

Figure S3 Averaged brGDGT distributions in soils of the Tagus River Basin are shown in panel a. Panels b-c show average brGDGT distributions for the Tagus soil samples based on altitude where Tagus soils sampled below 350 m (b) are considered low altitude and Tagus soils sampled above 350 m (c) are considered high altitude. Clearly the distribution of brGDGTs for low altitude samples is distinct from the distribution of brGDGTs for high altitude samples and the high altitude soil samples display a predominance of the 6-methyl over the 5-methyl brGDGT isomers. The colors of the bars reflect the brGDGT structure as labeled in the legend and the error bars represent 2xs the standard deviation.

Photo by René Heistermann

References, Summaries and Acknowledgments

References

Abrantes, F., Lebreiro, S., Rodrigues, T., Gil, I., Bartels-Jónsdóttir, H., Oliveira, P., Kissel, C., Grimalt, J.O. (2005). Shallow-marine sediment cores record climate variability and earthquake activity off Lisbon (Portugal) for the last 2000 years. Quaternary Science Review 24, 2477–2494.

Abrantes, F., Lopes, C., Rodrigues, T., Gil, I., Witt, L., Grimalt, J., Harris, I. (2009). Proxy calibration to instrumental data set: implications for paleoceanographic reconstructions. Geochemistry, Geophysics, Geosystems 9, Q09U07. doi:10.1029/2009GC002604.

Alheit, J., Möllmann, C., Dutz, J., Kornilovs, G., Loewe, P., Mohrholz, V., Wasmund, N. (2005). Synchronous ecological regime shifts in the central Baltic and the North Sea in the late 1980s. ICES Journal of Marine Science: Journal du Conseil 7, 1205-1215.

Alley, R.B., Mayewski, P.A., Sowers, T., Stuiver, M., Taylor, K.C., Clark, P.U. (1997). Holocene climatic instability: A prominent, widespread event 8200 yr ago. Geology 25, 483–486.

Andreu, L., GutiéRrez, E., Macias, M., Ribas, M., Bosch, O., Camarero, J.J. (2007). Climate increases regional tree-growth variability in Iberian pine forests. Global Change Biology 13, 1-12.

Andrén, T., Sohlenius, G. (1995). Late Quaternary development of the north-western Baltic Proper—Results from the clay-varve investigation. Quaternary International 27, 5-10.

Andrén, E., Andrén, T., Kunzendorf, H. (2000a). Holocene history of the Baltic Sea as a background for assessing records of human impact in the sediments of the Gotland Basin. The Holocene 10, 687–702.

Andrén, E., Andrén, T., Sohlenius, G. (2000b). The Holocene history of the southwestern Baltic Sea as reflected in a sediment core from the Bornholm Basin. Boreas 29, 233–250.

Arthur, M. A., Dean, W. E., Neff, E. D., Hay, B. J., King, J., Jones, G. (1994). Varve calibrated records of carbonate and organic carbon accumulation over the last 2000 years in the Black Sea. Global Biogeochemical Cycles 8, 195-217.

Arthur, M.A., Dean, W.E. (1998). Organic-matter production and preservation and evolution of anoxia in the Holocene Black Sea. Paleoceanography 13, 395–411.

Baas, M., Pancost, R., van Geel, B., Sinninghe Damsté, J.S. (2000). A comparative study of lipids in Sphagnum species. Organic Geochemistry 31, 535–541.

Bagge, O., Thurow, F., Steffensen, E., Bay, J. (1994). The Baltic cod. Dana (Denmark).

Bale, N.J., Hopmans, E.C., Zell, C., Sobrinho, R.L., Kim, J.-H., Sinninghe Damsté, J. S., Villareal, T.A., Schouten, S. (2015). Long chain glycolipids with pentose head groups as biomarkers for marine endosymbiotic heterocystous cyanobacteria. Organic Geochemistry 81, 1–7.

Ballantyne, A.P., Greenwood, D.R., Sinninghe Damsté, J.S., Csank, A.Z., Eberle, J.J., Rybczynski, N. (2010). Significantly warmer Arctic surface temperatures during the Pliocene indicated by multiple independent proxies. Geology 38, 603–606.

Ballard, R.D., Coleman, D.F., Rosenberg, G.D. (2000). Further evidence of abrupt Holocene drowning of the Black Sea shelf. Marine Geology 170, 253–261.

Banks, W. E., Antunes, N., Rigaud, S., d'Errico, F. (2013). Ecological constraints on the first prehistoric farmers in Europe. Journal of Archaeological Science 40, 2746–2753.

Bard, E., Tuna, T., Fagault, Y., Bonvalot, L., Wacker, L., Fahrni, S., Synal, H.A. (2015). AixMICADAS, the accelerator mass spectrometer dedicated to 14 C recently installed in Aix-en-Provence, France. Nuclear Instruments and Methods in Physics Research Section B: Beam Interactions with Materials and Atoms 361, 80-86.

Bartels-Jónsdóttir, H.B., Knudsen, K.L., Abrantes, F., Lebreiro, S., Eiríksson, J. (2006). Climate variability during the last 2000 years in the Tagus Prodelta, western Iberian Margin: Benthic foraminifera and stable isotopes. Marine Micropaleontology 2, 83-103.

Bartels-Jónsdóttir, H.B., Voelker, A.H., Knudsen, K.L., Abrantes, F. (2009). Twentieth-century warming and hydrographical changes in the Tagus Prodelta, eastern North Atlantic. The Holocene 3, 369-380.

Bauersachs, T., Speelman, E.N., Hopmans, E.C., Reichart, G.J., Schouten, S., Sinninghe Damsté, J.S. (2010). Fossilized glycolipids reveal past oceanic N2 fixation by heterocystous cyanobacteria. Proceedings of the National Academy of Sciences 45, 19190-19194.

Bellwood, P. (2005) First Farmers: The Origins of Agricultural Societies. (Blackwell, Oxford).

Bendle, J., Rosell-Melé, A., Ziveri, P. (2005). Variability of unusual distributions of alkenones in the surface waters of the Nordic seas. Paleoceanography 20, DOI: 10.1029/2004PA001025.

Bendle, J.A., Weijers, J.W., Maslin, M.A., Sinninghe Damsté, J.S., Schouten, S., Hopmans, E.C., Boot, C.S., Pancost, R.D. (2010). Major changes in glacial and Holocene terrestrial temperatures and sources of organic carbon recorded in the Amazon fan by tetraether lipids. Geochemistry Geophysics Geosystems 11.

Benito, G., Díez-Herrero, A., de Villalta, M.F. (2003) Magnitude and frequency of flooding in the Tagus basin (Central Spain) over the last millennium. Climate Change 58, 171–192.

Bennike, O., Rasmussen, P., Aaris-Sørensen, K. (2008). The harp seal (Phoca groenlandica Erxleben) in Denmark, southern Scandinavia, during the Holocene. Boreas 37, 263–272.

Berg, C., Listmann, L., Vandieken, V., Vogts, A., Jürgens, K. (2014). Chemoautotrophic growth of ammonia-oxidizing Thaumarchaeota enriched from a pelagic redox gradient in the Baltic Sea. Frontiers in Microbiology 5, 786.

Bianchi, T.S., Rolff, C., Lambert, C.D. (1997). Sources and composition of particulate organic carbon in the Baltic Sea: the use of plant pigments and lignin-phenols as biomarkers. Marine Ecology Progress Series 156, 25–31.

Björck, S. (1995). A review of the history of the Baltic Sea, 13.0-8.0 ka BP. Quaternary International 27, 19–40.

Björck, S., Kromer, B., Johnsen, S., Bennike, O., Hammarlund, D., Lemdahl, G., Possnert, G., Rasmussen, T.L., Wohlfarth, B., Hammer, C.U., Spurk, M. (1996). Synchronized terrestrialatmospheric deglacial records around the North Atlantic. Science 274, 1155–1160.

Blaga, C.I., Reichart, G.-J., Heiri, O., Sinninghe Damsté, J.S. (2009). Tetraether membrane lipid distributions in water-column particulate matter and sediments: a study of 47 European lakes along a north-south transect. Journal of Paleolimnology 41, 523–540.

Blaga, C.I., Reichart, G.-J., Schouten, S., Lotter, A.F., Werne, J.P., Kosten, S., Mazzeo, N., Lacerot, G., Sinninghe Damsté, J.S. (2010). Branched glycerol dialkyl glycerol tetraethers in lake sediments: Can they be used as temperature and pH proxies? Organic Geochemistry 41, 1225–1234.

Blanz, T., Emeis, K.-C., Siegel, H. (2005). Controls on alkenone unsaturation ratios along the salinity gradient between the open ocean and the Baltic Sea. Geochimica et Cosmochimica Acta 69, 3589–3600.

Blees, J., Niemann, H., Wenk, C.B., Zopfi, J., Schubert, C.J., Jenzer, J.S., Veronesi, M., Lehmann, M.F. (2014a). Bacterial methanotrophs drive the formation of a seasonal anoxic benthic nepheloid layer in an alpine lake. Limnology and Oceanography 59, 1410–1420.

Blees, J., Niemann, H., Wenk, C.B., Zopfi, J., Schubert, C.J., Kirf, M.K., Veronesi, M.L., Hitz, C., Lehmann, M.F. (2014b). Micro-aerobic bacterial methane oxidation in the chemocline and anoxic water column of deep south-Alpine Lake Lugano (Switzerland). Limnology and Oceanography 59, 311–324.

Bogucki, P., Nalepka, D., Grygiel, R., Nowaczyk, B. (2012). Multiproxy environmental archaeology of Neolithic settlements at Osłonki, Poland, 5500–4000 BC. Environmental Archaeology 1, 45-65.

Bonsall, C., Macklin, M. G., Anderson, D. E., Payton, R. W. (2002). Climate change and the adoption of agriculture in north-west Europe. European Journal of Archaeology 1, 9-23.

Bradley, R.S., Jonest, P.D. (1993). "Little Ice Age" summer temperature variations: their nature and relevance to recent global warming trends. The Holocene 3, 367–376.

Brander, K. (2000). Effects of environmental variability on growth and recruitment in cod (Gadus morhua) using a comparative approach. Oceanologica Acta 4, 485-496.

Brander, K. M. (2005). Cod recruitment is strongly affected by climate when stock biomass is low. ICES Journal of Marine Science: Journal du Conseil 3, 339-343.

Brassell, S.C., Eglinton, G., Marlowe, I.T., Pflaumann, U., Sarnthein, M. (1986). Molecular stratigraphy: a new tool for climatic assessment. Nature 320, 129–133.

Brassell, S.C. (1993). Applications of biomarkers for delineating marine paleoclimatic fluctuations during the Pleistocene. In Organic Geochemistry, Springer US, 699–738.

Breitburg, D. L., Pihl, L., Kolesar, S. E. (2001). Effects of low dissolved oxygen on the behavior, ecology and harvest of fishes: a comparison of the Chesapeake Bay and Baltic-Kattegat systems. In Coastal Hypoxia: Consequences for Living Resources and Ecosystems. (eds. N. N. Rabalais and R. E. Turner) 241-267 (American Geophysical Union, Washington, D.C.).

Brochier-Armanet, C., Boussau, B., Gribaldo, S., Forterre, P. (2008). Mesophilic Crenarchaeota: proposal for a third archaeal phylum, the Thaumarchaeota. Nature Reviews Microbiology 3, 245-252.

Buckles, L.K., Weijers, J.W., Verschuren, D., Sinninghe Damsté, J.S. (2014). Sources of core and intact branched tetraether membrane lipids in the lacustrine environment: anatomy of Lake Challa and its catchment, equatorial East Africa. Geochimica et Cosmochimica Acta 140, 106–126.

Cachao, M., Moita, M. T. (2000). Coccolithus pelagicus, a productivity proxy related to moderate fronts off Western Iberia. Marine Micropaleontology 1, 131-155.

Carter, T., Saarikko, R., Niemi, K. (1996). Assessing the risks and uncertainties of regional crop potential under a changing climate in Finland. Agricultural Food Science 5, 329–350.

Castañeda, I.S., Mulitza, S., Schefuß, E., dos Santos, R.A.L., Sinninghe Damsté, J.S., Schouten, S. (2009). Wet phases in the Sahara/Sahel region and human migration patterns in North Africa. Proceedings of the National Academy of Sciences 48, 20159-20163.

Chan, F., Barth, J.A., Lubchenco, J., Kirincich, A., Weeks, H., Peterson, W.T., Menge, B.A. (2008). Emergence of anoxia in the California Current large marine ecosystem. Science 319, 920–920.

Chivall, D., M'Boule, D., Sinke-Schoen, D., Sinninghe Damsté, J.S., Schouten, S., van der Meer, M.T. (2014). Impact of salinity and growth phase on alkenone distributions in coastal haptophytes. Organic Geochemistry 67, 31–34.

Chu, G., Sun, Q., Li, S., Zheng, M., Jia, X., Lu, C., Liu, J., Liu, T. (2005). Long-chain alkenone distributions and temperature dependence in lacustrine surface sediments from China. Geochimica et Cosmochimica Acta 69, 4985–5003.

Cline, J. D., Kaplan, I. R. (1975). Isotopic fractionation of dissolved nitrate during denitrification in the eastern tropical North Pacific Ocean. Marine Chemistry 4, 271-299.

Conte, M.H., Thompson, A., Lesley, D., Harris, R.P. (1998). Genetic and physiological influences on the alkenone/alkenoate versus growth temperature relationship in

Emiliania huxleyi and Gephyrocapsa oceanica. Geochimica et Cosmochimica Acta 62, 51–68.

Conte, M.H., Sicre, M.-A., Rühlemann, C., Weber, J.C., Schulte, S., Schulz-Bull, D., Blanz, T. (2006). Global temperature calibration of the alkenone unsaturation index ($U^{K'}_{37}$) in surface waters and comparison with surface sediments. Geochemistry, Geophysics, Geosystems 7.

Coolen, M.J., Muyzer, G., Rijpstra, W.I.C., Schouten, S., Volkman, J.K., Sinninghe Damsté, J.S. (2004). Combined DNA and lipid analyses of sediments reveal changes in Holocene haptophyte and diatom populations in an Antarctic lake. Earth and Planetary Science Letters 223, 225–239.

Coolen, M.J., Boere, A., Abbas, B., Baas, M., Wakeham, S.G., Sinninghe Damsté, J.S. (2006). Ancient DNA derived from alkenone-biosynthesizing haptophytes and other algae in Holocene sediments from the Black Sea. Paleoceanography 21, DOI: 10.1029/2005PA001188.

Coolen, M.J., Abbas, B., Van Bleijswijk, J., Hopmans, E.C., Kuypers, M.M., Wakeham, S.G., Sinninghe Damsté, J.S. (2007). Putative ammonia-oxidizing Crenarchaeota in suboxic waters of the Black Sea: a basin-wide ecological study using 16S ribosomal and functional genes and membrane lipids. Environmental Microbiology 9, 1001–1016.

Coolen, M.J., Saenz, J.P., Giosan, L., Trowbridge, N.Y., Dimitrov, P., Dimitrov, D., Eglinton, T.I. (2009). DNA and lipid molecular stratigraphic records of haptophyte succession in the Black Sea during the Holocene. Earth and Planetary Science Letters 284, 610–621.

Corella, J.P., Stefanova, V., El Anjoumi, A., Rico, E., Giralt, S., Moreno, A., Plata-Montero, A., Valero-Garcés, B. L. (2013). A 2500-year multi-proxy reconstruction of climate change and human activities in northern Spain: The Lake Arreo record. Palaeogeography, Palaeoclimatology, Palaeoecology 386, 555-568.

Craig, O.E., Forster, M., Andersen, S.H., Koch, E., Crombé, P., Milner, N.J., Stern, B., Bailey, G.N., Heron, C.P. (2007). Molecular and isotopic demonstration of the processing of aquatic products in northern European prehistoric pottery. Archaeometry 49, 135-152.

Craig, O.E., Steele, V.J., Fischer, A., Hartz, S., Andersen, S.H., Donohoe, P., Glykou, A., Saul, H., Jones, D.M., Koch, E., Heron, C.P. (2011). Ancient lipids reveal continuity in culinary practices across the transition to agriculture in Northern Europe. Proceedings of the National Academy of Sciences 108, 17910-17915.

Cramp, L.J., Evershed, R.P., Lavento, M., Halinen, P., Mannermaa, K., Oinonen, M., Kettunen, J., Perola, M., Onkamo, P., Heyd, V. (2014). Neolithic dairy farming at the extreme of agriculture in northern Europe. Proceedings of the Royal Society of London B: Biological Sciences 281, DOI: 10.1098/rspb.2014.0819.

Cranwell, P. A. (1985). Long-chain unsaturated ketones in recent lacustrine sediments. Geochimica et Cosmochimica Acta 49, 1545-1551.

D'Andrea, W.J., Lage, M., Martiny, J.B.H., Laatsch, A.D., Amaral-Zettler, L.A., Sogin, M.L., Huang, Y. (2006). Alkenone producers inferred from well-preserved 18S rDNA in Greenland lake sediments. Journal of Geophysical Research: Biogeosciences 111.

Danielssen, D.S., Svendsen, E., Ostrowski, M. (1996). Long-term hydrographic variation in the Skagerrak based on the section Torungen–Hirtshals. ICES Journal of Marine Science 53, 917–925.

Davis, B. A., Brewer, S., Stevenson, A. C., Guiot, J. (2003). The temperature of Europe during the Holocene reconstructed from pollen data. Quaternary Science Reviews 22, 1701-1716.

Dean Jr, W. E. (1974). Determination of carbonate and organic matter in calcareous sediments and sedimentary rocks by loss on ignition: comparison with other methods. Journal of Sedimentary Research 44, 242-248.

De Jonge, C., Hopmans, E.C., Stadnitskaia, A., Rijpstra, W.I.C., Hofland, R., Tegelaar, E., Sinninghe Damsté, J.S. (2013). Identification of novel penta-and hexamethylated branched glycerol dialkyl glycerol tetraethers in peat using HPLC–MS 2, GC–MS and GC–SMB-MS. Organic Geochemistry 54, 78–82.

De Jonge, C., Hopmans, E.C., Zell, C.I., Kim, J.-H., Schouten, S., Sinninghe Damsté, J.S. (2014a). Occurrence and abundance of 6-methyl branched glycerol dialkyl glycerol tetraethers in soils: Implications for palaeoclimate reconstruction. Geochimica et Cosmochimica Acta 141, 97–112.

De Jonge, C., Stadnitskaia, A., Hopmans, E.C., Cherkashov, G., Fedotov, A., Sinninghe Damsté, J.S. (2014b). In situ produced branched glycerol dialkyl glycerol tetraethers in suspended particulate matter from the Yenisei River, Eastern Siberia. Geochimica et Cosmochimica Acta 125, 476–491.

De Jonge, C., Stadnitskaia, A., Hopmans, E.C., Cherkashov, G., Fedotov, A., Streletskaya, I.D., Vasiliev, A.A., Sinninghe Damsté, J.S. (2015a). Drastic changes in the distribution of branched tetraether lipids in suspended matter and sediments from the Yenisei River and Kara Sea (Siberia): Implications for the use of brGDGT-based proxies in coastal marine sediments. Geochimica et Cosmochimica Acta 165, 200-225.

De Jonge, C., Stadnitskaia, A., Fedotov, A., Sinninghe Damsté, J.S. (2015b). Impact of riverine suspended particulate matter on the branched glycerol dialkyl glycerol tetraether composition of lakes: The outflow of the Selenga River in Lake Baikal (Russia). Organic Geochemistry 83, 241–252.

De Jonge, C., Stadnitskaia, A., Cherkashov, G., Sinninghe Damsté, J.S. (2016). Branched glycerol dialkyl glycerol tetraethers and crenarchaeol record post-glacial sea level rise and shift in source of terrigenous brGDGTs in the Kara Sea (Arctic Ocean). Organic Geochemistry 92, 42–54.

De Leeuw, J. W., van der Meer, F. W., Rijpstra, W. I. C., Schenck, P. A. (1980). On the occurrence and structural identification of long chain unsaturated ketones and hydrocarbons in sediments. Physics and Chemistry of the Earth 12, 211-217.

De Rosa, M., Gambacorta, A. (1988). The lipids of archaebacteria. Progress in Lipid Research 27, 153–175.

Dias, J.M.A., Jouanneau, J.M., Gonzalez, R., Araújo, M.F., Drago, T., Garcia, C., Oliveira, A., Rodrigues, A., Vitorino, J., Weber, O. (2002). Present day sedimentary processes on the northern Iberian shelf. Progress in Oceanography 52, 249-259.

Diaz, R. J. (2001). Overview of hypoxia around the world. Journal of environmental quality 30, 275-281.

Diaz, R. J., Rosenberg, R. (2008). Spreading dead zones and consequences for marine ecosystems. Science 321, 926–929.

Digerfeldt, G. (1988). Reconstruction and regional correlation of Holocene lake-level fluctuations in Lake Bysjön, South Sweden. Boreas 17, 165–182.

Dillon, J. T., Longo, W. M., Zhang, Y., Torozo, R., Huang, Y. (2016). Identification of double-bond positions in isomeric alkenones from a lacustrine haptophyte. Rapid Communications in Mass Spectrometry 30, 112-118.

Dirghangi, S.S., Pagani, M., Hren, M.T., Tipple, B.J. (2013). Distribution of glycerol dialkyl glycerol tetraethers in soils from two environmental transects in the USA. Organic Geochemistry 59, 49–60.

Döös, K., Meier, H. E. M., Döscher, R. (2004). The Baltic haline conveyor belt or the overturning circulation and mixing in the Baltic. AMBIO: A Journal of the Human Environment 33, 261-266.

Egge, E. S., Eikrem, W., Edvardsen, B. (2015). Deep-branching novel lineages and high diversity of Haptophytes in the Skagerrak (Norway) uncovered by 454 pyrosequencing. The Journal of Eukaryotic Microbiology 62, 121-140.

Eglinton, G., Hamilton, R.J. (1967). Leaf epicuticular waxes. Science 156, 1322–1335.

Emeis, K.-C., Struck, U., Blanz, T., Kohly, A., Voβ, M. (2003). Salinity changes in the central Baltic Sea (NW Europe) over the last 10000 years. The Holocene 13, 411–421.

Englebrecht, A.C., Sachs, J.P. (2005). Determination of sediment provenance at drift sites using hydrogen isotopes and unsaturation ratios in alkenones. Geochimica et Cosmochimica Acta 69, 4253–4265.

Epstein, B.L., D'Hondt, S., Quinn, J.G., Zhang, J., Hargraves, P.E. (1998). An effect of dissolved nutrient concentrations on alkenone-based temperature estimates. Paleoceanography 13, 122–126.

Eriksson, G. (2004). Part-time farmers or hard-core sealers? Västerbjers studied by means of stable isotope analysis. Journal of Anthropological Archaeology 23, 135-162.

Eriksson, G., Linderholm, A., Fornander, E., Kanstrup, M., Schoultz, P., Olofsson, H., Lidén, K. (2008). Same island, different diet: cultural evolution of food practice on Öland, Sweden, from the Mesolithic to the Roman Period. Journal of Anthropological Archaeology 27, 520-543.

Feeser, I., Dörfler, W., Averdieck, F. R., Wiethold, J. (2012). New insight into regional and local land-use and vegetation patterns in eastern Schleswig-Holstein during the Neolithic. In: Siedlung, Grabenwerk, Grossteingrab. Studien zu Gesellschaft, Wirtschaft und Umwelt der Trichterbechergruppen im nordlichen Mitteleuropa. Fruhe Monumentalitat und Soziale Differenzierung (eds. M. Hinz and J. Muller) Habelt, Bonn, 159-190.

Fietz, S., Huguet, C., Rueda, G., Hambach, B., Rosell-Melé, A. (2013). Hydroxylated isoprenoidal GDGTs in the Nordic Seas. Marine Chemistry 152, 1–10.

Fischer, A., Olsen, J., Richards, M., Heinemeier, J., Sveinbjörnsdóttir, Á.E., Bennike, P. (2007). Coast–inland mobility and diet in the Danish Mesolithic and Neolithic: evidence from stable isotope values of humans and dogs. Journal of Archaeological Science 34, 2125-2150.

Fletcher, W.J., Boski, T., Moura, D. (2007). Palynological evidence for environmental and climatic change in the lower Guadiana valley, Portugal, during the last 13,000 years. Holocene 17, 481–494.

Fornander, E., Eriksson, G., Lidén, K. (2008). Wild at heart: Approaching Pitted Ware identity, economy and cosmology through stable isotopes in skeletal material from the Neolithic site Korsnäs in Eastern Central Sweden. Journal of Anthropological Archaeology 27, 281-297.

Forstén, A., Alhonen, P. (1975). The subfossil seals of Finland and their relation to the history of the Baltic Sea. Boreas 4, 143–155.

France, R.L. (1995). Carbon-13 enrichment in benthic compared to planktonic algae: foodweb implications. Marine Ecology Progress Series 124, 307–312.

Frohlich, K., Grabczak, J., Rozanski, K. (1988). Deuterium and oxygen-18 in the Baltic Sea. Chemical Geology 72, 77–83.

Fry, B., Sherr, E. B. (1989). δ13C measurements as indicators of carbon flow in marine and freshwater ecosystems. In Stable isotopes in ecological research (196-229). Springer New York.

Fuhrman, J.A. (1992). Novel major archaebacterial group from marine plankton. Nature 356, 148–149.

Fujine, K., Yamamoto, M., Tada, R., Kido, Y. (2006). A salinity-related occurrence of a novel alkenone and alkenoate in Late Pleistocene sediments from the Japan Sea. Organic Geochemistry 37, 1074–1084.

Funkey, C.P., Conley, D.J., Reuss, N.S., Humborg, C., Jilbert, T., Slomp, C.P. (2014). Hypoxia Sustains Cyanobacteria Blooms in the Baltic Sea. Environmental Science & Technology 48, 2598–2602.

Gabriel, J. L., Chong, P. L. G. (2000). Molecular modeling of archaebacterial bipolar tetraether lipid membranes. Chemistry and Physics of Lipids 105, 193-200.

Giosan, L., Coolen, M.J., Kaplan, J.O., Constantinescu, S., Filip, F., Filipova-Marinova, M., Kettner, A.J., Thom, N. (2012). Early anthropogenic transformation of the Danube-Black Sea system. Scientific Reports 2, 582.

Gliozzi, A., Paoli, G., De Rosa, M., Gambacorta, A. (1983). Effect of isoprenoid cyclization on the transition temperature of lipids in thermophilic archaebacteria. Biochimica et Biophysica Acta (BBA)-Biomembranes 735, 234–242.

Griffies, S. M. (2004). Fundamentals of Ocean Climate Models (494), Princeton University Press, Princeton.

Gustafsson, B. G. (2000). Time-dependent modeling of the Baltic entrance area. 2. Water and salt exchange of the Baltic Sea. Estuaries 23, 253–266.

Gustafsson, B.G., Westman, P. (2002). On the causes for salinity variations in the Baltic Sea during the last 8500 years. Paleoceanography 17, 12–1.

Gustafsson, B.G., Schenk, F., Blenckner, T., Eilola, K., Meier, H.M., Müller-Karulis, B., Neumann, T., Ruoho-Airola, T., Savchuk, O.P., Zorita, E. (2012). Reconstructing the development of Baltic Sea eutrophication 1850–2006. Ambio 41, 534-548.

Haak, W., Lazaridis, I., Patterson, N., Rohland, N., Mallick, S., Llamas, B., Brandt, G., Nordenfelt, S., Harney, E., Stewardson, K., Fu, Q. (2015). Massive migration from the steppe was a source for Indo-European languages in Europe. Nature 522, 207-211.

Haug, G.H., Pedersen, T.F., Sigman, D.M., Calvert, S.E., Nielsen, B., Peterson, L.C. (1998). Glacial/interglacial variations in production and nitrogen fixation in the Cariaco Basin during the last 580 kyr. Paleoceanography 13, 427-432.

Haug, G.H., Günther, D., Peterson, L.C., Sigman, D.M., Hughen, K.A., Aeschlimann, B. (2003). Climate and the collapse of Maya civilization. Science 299, 1731–1735.

Hay, B.J. (1988). Sediment accumulation in the central western Black Sea over the past 5100 years. Paleoceanography 3, 491–508.

Hedges, J.I., Oades, J.M. (1997). Comparative organic geochemistries of soils and marine sediments. Organic Geochemistry 27, 319–361.

HELCOM (2010). Ecosystem Health of the Baltic Sea 2003–2007: HELCOM Initial Holistic Assessment. Baltic Sea Environmental Proceedings 122, 1-68.

Hoegh-Guldberg, O., Bruno, J.F. (2010). The impact of climate change on the world's marine ecosystems. Science 328, 1523–1528.

Hollander, D.J., Smith, M.A. (2001). Microbially mediated carbon cycling as a control on the δ 13 C of sedimentary carbon in eutrophic Lake Mendota (USA): new models for interpreting isotopic excursions in the sedimentary record. Geochimica et Cosmochimica Acta 65, 4321–4337.

Hopmans, E.C., Weijers, J.W., Schefuß, E., Herfort, L., Sinninghe Damsté, J.S., Schouten, S. (2004). A novel proxy for terrestrial organic matter in sediments based on branched and isoprenoid tetraether lipids. Earth and Planetary Science Letters 224, 107–116.

Hopmans, E.C., Schouten, S., Sinninghe Damsté, J.S. (2015). The effect of improved chromatography on GDGT-based palaeoproxies. Organic Geochemistry 93, 1-6.

Hordoir, R., Meier, H. E. M. (2012). Effect of climate change on the thermal stratification of the baltic sea: a sensitivity experiment. Climate Dynamics 38, 1703–1713.

Huguet, C., Hopmans, E.C., Febo-Ayala, W., Thompson, D.H., Sinninghe Damsté, J.S., Schouten, S. (2006). An improved method to determine the absolute abundance of glycerol dibiphytanyl glycerol tetraether lipids. Organic Geochemistry 37, 1036–1041.

Huguet, C., Fietz, S., Rosell-Mele, A. (2013). Global distribution patterns of hydroxy glycerol dialkyl glycerol tetraethers. Organic Geochemistry 57, 107–118.

Huntley, B., Prentice, I.C. (1988). July temperatures in Europe from pollen data, 6000 years before present. Science 241, 687–690.

Hurrell, J.W. (1995). Decadal trends in the North Atlantic oscillation. Science 269, 676–679.

Hurrell, J.W., Van Loon, H (1997). Decadal variations in climate associated with the north Atlantic oscillation. Climate Change 36, 301–326.

Hyvärinen, H., Donner, J., Kessel, H., Raukas, A. (1988). The Litorina and Limnaea Sea in the northern and central Baltic, in Problems of the Baltic Sea History. Annales Academiae Scientiarum Fennicae 148, 25–35.

International Council for the Exploration of the Sea (ICES) · Conseil International pour l'Exploration de la Mer (CIEM), Last accessed November 13, 2015: http://ocean.ices.dk/helcom/Helcom.aspx?MinData=5000&DataType=2&Mode=2

International Ocean Commission, International Hydrographic Organization, and British Oceanographic Data Centre (IOC/IHO/BODC) (2003). Centenary Edition of the GEBCO Digital Atlas, Published on CD-ROM on Behalf of the Intergovernmental Oceanographic Commission and the International Hydrographic Organization as part of the General Bathymetric Chart of the Oceans, British-Oceanographic-Data-Centre (Ed.), Liverpool, United Kingdom.

IPCC (2007). Climate Change 2007: The Physical Science Basis. Contribution of Working Group I to the Fourth Assessment Report of the Intergovernmental Panel on Climate Change. Solomon, S., D. Qin, M. Manning, Z. Chen, M. Marquis, K.B. Averyt, M.Tignor and H.L. Miller (eds.). Cambridge University Press, Cambridge, United Kingdom and New York, NY, USA.

Isaksson, S., Hallgren, F. (2012). Lipid residue analyses of Early Neolithic funnel-beaker pottery from Skogsmossen, eastern Central Sweden, and the earliest evidence of dairying in Sweden. Journal of Archaeological Science 39, 3600-3609.

Jarvis, A., Reuter, H.I., Nelson, A., Guevara, E. (2006). Hole-filled seamless SRTM data vol. 3, International Centre for Tropical Agriculture (CIAT).

Jensen, J.B. (1995). A Baltic Ice Lake transgression in the southwestern Baltic: Evidence from Fakse Bugt, Denmark. Quaternary International 27, 59–68.

Jensen, J.B., Bennike, O., Witkowski, A., Lemke, W., Kuijpers, A. (1999). Early Holocene history of the southwestern Baltic Sea: the Ancylus Lake stage. Boreas 28, 437–453.

Jesus, C.C., de Stigter, H.C., Richter, T.O., Boer, W., Mil-Homens, M., Oliveira, A., Rocha, F. (2010). Trace metal enrichments in Portuguese submarine canyons and open slope: anthropogenic impact and links to sedimentary dynamics. Marine Geology 271, 72–83.

Jones, G.A., Gagnon, A.R. (1994). Radiocarbon chronology of Black Sea sediments. Deep Sea Research Part I: Oceanographic Research Papers 41, 531–557.

Jones, P.D., Briffa, K.R., Barnett, T.P., Tett, S.F.B. (1998). High-resolution palaeoclimatic records for the last millennium: interpretation, integration and comparison with General Circulation Model control-run temperatures. The Holocene 8, 455–471.

Jones, P.D., Mann, M.E. (2004). Climate over past millennia. Reviews of Geophysics 42.

Jouanneau, J. M., Garcia, C., Oliveira, A., Rodrigues, A., Dias, J. A., Weber, O. (1998). Dispersal and deposition of suspended sediment on the shelf off the Tagus and Sado estuaries, SW Portugal. Progress in Oceanography 42, 233-257.

Kabel, K., Moros, M., Porsche, C., Neumann, T., Adolphi, F., Andersen, T.J., Siegel, H., Gerth, M., Leipe, T., Jansen, E., Sinninghe Damsté, J.S. (2012). Impact of climate change on the Baltic Sea ecosystem over the past 1,000 years. Nature Climate Change 2, 871–874.

Kaiser, J., Arz, H.W. (2016). Sources of sedimentary biomarkers and proxies with potential paleoenvironmental significance for the Baltic Sea. Continental Shelf Research 122, 102–119.

Kaneko, M., Kitajima, F., Naraoka, H. (2011). Stable hydrogen isotope measurement of archaeal ether-bound hydrocarbons. Organic Geochemistry 42, 166–172.

Karlson, K., Rosenberg, R., Bonsdorff, E. (2002). Temporal and spatial large-scale effects of eutrophication and oxygen deficiency on benthic fauna in Scandinavian and Baltic waters: A review. Oceanography and Marine Biology 40, 427–489.

Karner, M.B., DeLong, E.F., Karl, D.M. (2001). Archaeal dominance in the mesopelagic zone of the Pacific Ocean. Nature 409, 507–510.

Keating-Bitonti, C.R., Ivany, L.C., Affek, H.P., Douglas, P., Samson, S.D. (2011). Warm, not super-hot, temperatures in the early Eocene subtropics. Geology 39, 771–774.

Kim, J.-H., Schouten, S., Hopmans, E.C., Donner, B., Sinninghe Damsté, J.S. (2008). Global sediment core-top calibration of the TEX86 paleothermometer in the ocean. Geochimica et Cosmochimica Acta 72, 1154–1173.

Kim, J.-H., van der Meer, J., Schouten, S., Helmke, P., Willmott, V., Sangiorgi, F., Koc, N., Hopmans, E.C., Sinninghe Damsté, J.S. (2010). New indices and calibrations derived from the distribution of crenarchaeal isoprenoid tetraether lipids: Implications for past sea surface temperature reconstructions. Geochimica et Cosmochimica Acta 74, 4639–4654.

Knies, J., Cabedo-Sanz, P., Belt, S.T., Baranwal, S., Fietz, S., Rosell-Melé, A. (2014). The emergence of modern sea ice cover in the Arctic Ocean. Nature Communications 5.

Kononen, K. (1992). Dynamics of the toxic cyanobacterial blooms in the Baltic Sea. Finnish Institute of Marine Research 261, 3-36.

Krause-Kyora, B., Makarewicz, C., Evin, A., Flink, L.G., Dobney, K., Larson, G., Hartz, S., Schreiber, S., von Carnap-Bornheim, C., von Wurmb-Schwark, N., Nebel, A. (2013). Use of domesticated pigs by Mesolithic hunter-gatherers in northwestern Europe. Nature Communications 4.

Laamanen, M., Kuosa, H. (2005). Annual variability of biomass and heterocysts of the N2-fixing cyanobacterium Aphanizomenon flos-aquae in the Baltic Sea with reference to Anabaena spp. and Nodularia spumigena. Boreal Environment Research 10, 19–30

Laima, M. J., Matthiesen, H., Christiansen, C., Lund-Hansen, L. C., Emeis, K.-C. (2001). Dynamics of P, Fe and Mn along a depth gradient in the SW Baltic Sea. Boreal Environment Research 6, 317–333.

Lastras, G., Arzola, R.G., Masson, D.G., Wynn, R.B., Huvenne, V.A.I., Hühnerbach, V., Canals, M. (2009). Geomorphology and sedimentary features in the Central Portuguese submarine canyons, Western Iberian margin. Geomorphology 103, 310–329.

Lawson, J. W., Stenson, G. B., McKinnon, D. G. (1995). Diet of harp seals (Phoca groenlandica) in nearshore waters of the northwest Atlantic during 1990 – 1993. Canadian Journal of Zoology 73, 1805–1818.

Lebreiro, S.M., Francés, G., Abrantes, F.F.G., Diz, P., Bartels-Jónsdóttir, H.B., Stroynowski, Z.N., Gil, I.M., Pena, L.D., Rodrigues, T., Jones, P.D. (2006). Climate change and coastal hydrographic response along the Atlantic Iberian margin (Tagus Prodelta and Muros Ría) during the last two millennia. Holocene 16, 1003–1015.

de Leeuw, J.W., v.d. Meer, F.W., Rijpstra, W.I.C., Schenck, P.A. (1980). On the occurrence and structural identification of long chain unsaturated ketones and hydrocarbons in sediments. Physics and Chemistry of the Earth 12, 211–217.

Leipe T., Dippner J.W., Hille S., Voss M., Christiansen C., Bartholdy, J. (2008). Environmental changes in the central Baltic Sea during the past 1000 years: inferences from sedimentary records, hydrography and climate. Oceanologia 50, 23-41.

Leipe, T., Tauber, F., Vallius, H., Virtasalo, J., Uścinowicz, S., Kowalski, N., Hille, S., Lindgren, S., Myllyvirta, T. (2011). Particulate organic carbon (POC) in surface sediments of the Baltic Sea. Geo-Marine Letters 31, 175-188.

Lengger, S.K., Hopmans, E.C., Reichart, G.-J., Nierop, K.G., Sinninghe Damsté, J.S., Schouten, S. (2012). Intact polar and core glycerol dibiphytanyl glycerol tetraether lipids in the Arabian Sea oxygen minimum zone. Part II: Selective preservation and degradation in sediments and consequences for the TEX_{86}. Geochimica et Cosmochimica Acta 98, 244–258.

Le Pera, E., Arribas, J. (2004). Sand composition in an Iberian passive-margin fluvial course: the Tajo River. Sedimentary Geology 171, 261–281.

Linan, I.D., Gutierrez, E., Andreu-Hayles, L., Heinrich, I., Helle, G. (2012). Potential to explain climate from tree rings in the south of the Iberian Peninsula. Climate Research 55, 119–134.

Lindstrøm, U., Harbitz, A., Haug, T. Nilssen, K. T. (1998). Do harp seals Phoca groenlandica exhibit particular prey preferences? ICES Journal of Marine Science: Journal du Conseil 55, 941–953.

Lipp, J.S., Hinrichs, K.-U. (2009). Structural diversity and fate of intact polar lipids in marine sediments. Geochimica et Cosmochimica Acta 73, 6816–6833.

Liu, W., Liu, Z., Fu, M., An, Z. (2008). Distribution of the C37 tetra-unsaturated alkenone in Lake Qinghai, China: A potential lake salinity indicator. Geochimica et Cosmochimica Acta 72, 988–997.

Liu, W. G., Liu, Z.. H., Wang, H.Y., He, Y.X., Wang, Z., Xu, L.M. (2011). Salinity control on long-chain alkenone distributions in lake surface waters and sediments of the northern Qinghai-Tibetan Plateau, China. Geochimica et Cosmochimica Acta 75, 1693–1703.

Liu, X.-L., Lipp, J.S., Simpson, J.H., Lin, Y.-S., Summons, R.E., Hinrichs, K.-U. (2012a). Mono-and dihydroxyl glycerol dibiphytanyl glycerol tetraethers in marine sediments: identification of both core and intact polar lipid forms. Geochimica et Cosmochimica Acta 89, 102–115.

Liu, X.-L., Summons, R.E., Hinrichs, K.-U. (2012b). Extending the known range of glycerol ether lipids in the environment: structural assignments based on tandem mass spectral fragmentation patterns. Rapid Communications in Mass Spectrometry 26, 2295–2302.

Longo, W. M., Theroux, S., Giblin, A. E., Zheng, Y., Dillon, J. T., Huang, Y. (2016). Temperature calibration and phylogenetically distinct distributions for freshwater alkenones: Evidence from northern Alaskan lakes. Geochimica et Cosmochimica Acta 180, 177-196.

Loomis, S.E., Russell, J.M., Sinninghe Damsté, J.S. (2011). Distributions of branched GDGTs in soils and lake sediments from western Uganda: Implications for a lacustrine paleothermometer. Organic Geochemistry 42, 739–751.

Loomis, S.E., Russell, J.M., Ladd, B., Street-Perrott, F.A., Sinninghe Damsté, J.S. (2012). Calibration and application of the branched GDGT temperature proxy on East African lake sediments. Earth and Planetary Science Letters 357, 277–288.

Lougas, L. (1999). Postglacial development of fish and seal faunas in the Eastern Baltic water systems. The Holocene History of the European Vertebrate Fauna. Modern Aspects of Research 200.

Lougheed, B.C., Snowball, I., Moros, M., Kabel, K., Muscheler, R., Virtasalo, J.J., Wacker, L. (2012). Using an independent geochronology based on palaeomagnetic secular variation (PSV) and atmospheric Pb deposition to date Baltic Sea sediments and infer 14 C reservoir age. Quaternary Science Reviews 42, 43-58.

Lutze, G. F. (1965). Zur Foraminiferen-Fauna der Ostsee. Meyniana 14, 75-142.

MacKenzie, B. R., Köster, F. W. (2004). Fish production and climate: Sprat in the Baltic Sea. Ecology 85, 784–794.

Mann, M.E., Zhang, Z., Rutherford, S., Bradley, R.S., Hughes, M.K., Shindell, D., Ammann, C., Faluvegi, G., Ni, F. (2009). Global signatures and dynamical origins of the Little Ice Age and Medieval Climate Anomaly. Science 326, 1256–1260.

Marlowe, I.T., Green, J.C., Neal, A.C., Brassell, S.. C., Course, P.A. (1984). Long chain (n-C37–C39) alkenones in the Prymnesiophyceae. Distribution of alkenones and other lipids and their taxonomic significance. British Phycological Journal 19, 203–216.

Martin-Chivelet, J., Belen Munoz-Garcia, M., Edwards, R.L., Turrero, M.J., Ortega, A.I. (2011). Land surface temperature changes in Northern Iberia since 4000 yr BP, based on delta C-13 of speleothems, Global Planetary Change 77, 1–12, 2011.

Matear, R.J., Hirst, A.C. (2003). Long-term changes in dissolved oxygen concentrations in the ocean caused by protracted global warming. Global Biogeochemical Cycles 17.

Matthäus, W., Schinke, H. (1999). The influence of river runoff on deep water conditions of the Baltic Sea. *Hydrobiologia* 393**,** 1–10.

M'boule, D., Chivall, D., Sinke-Schoen, D., Sinninghe Damsté, J.S., Schouten, S., van der Meer, M.T. (2014). Salinity dependent hydrogen isotope fractionation in alkenones produced by coastal and open ocean haptophyte algae. Geochimica et Cosmochimica Acta 130, 126–135.

van der Meer, M.T., Sangiorgi, F., Baas, M., Brinkhuis, H., Sinninghe Damsté, J.S., Schouten, S. (2008). Molecular isotopic and dinoflagellate evidence for Late Holocene freshening of the Black Sea. Earth and Planetary Science Letters 267, 426–434.

van der Meer, M.T., Benthien, A., Bijma, J., Schouten, S., Sinninghe Damsté, J.S. (2013). Alkenone distribution impacts the hydrogen isotopic composition of the C37:2 and C37:3 alkan-2-ones in Emiliania huxleyi. Geochimica et Cosmochimica Acta 111, 162–166.

van der Meer, M.T., Benthien, A., French, K.L., Epping, E., Zondervan, I., Reichart, G.-J., Bijma, J., Sinninghe Damsté, J.S., Schouten, S. (2015). Large effect of irradiance on hydrogen isotope fractionation of alkenones in Emiliania huxleyi. Geochimica et Cosmochimica Acta 160, 16–24.

Menges, J., Huguet, C., Alcañiz, J.M., Fietz, S., Sachse, D., Rosell-Melé, A. (2014). Influence of water availability in the distributions of branched glycerol dialkyl glycerol tetraether in soils of the Iberian Peninsula, Biogeosciences 11, 2571-2581.

Möllmann, C., Kornilovs, G., Sidrevics, L. (2000). Long-term dynamics of main mesozooplankton species in the central Baltic Sea. Journal of Plankton Research 22, 2015–2038.

Möllmann, C., Kornilovs, G., Fetter, M., Köster, F. W., Hinrichsen, H.-H. (2003). The marine copepod, Pseudocalanus elongatus, as a mediator between climate variability and fisheries in the Central Baltic Sea. Fisheries Oceanography 12, 360–368.

Möllmann, C., Kornilovs, G., Fetter, M., Köster, F. W. (2005). Climate, zooplankton, and pelagic fish growth in the central Baltic Sea. ICES Journal of Marine Science: Journal du Conseil 62, 1270–1280.

Möllmann, C., Müller-Karulis, B., Kornilovs, G., St John, M. A. (2008). Effects of climate and overfishing on zooplankton dynamics and ecosystem structure: regime shifts, trophic cascade, and feedback loops in a simple ecosystem. ICES Journal of Marine Science: Journal du Conseil 65, 302-310.

Moros, M., Lemke, W., Kuijpers, A., Endler, R., Jensen, J.B., Bennike, O., Gingele, F. (2002). Regressions and transgressions of the Baltic basin reflected by a new high-resolution deglacial and postglacial lithostratigraphy for Arkona Basin sediments (western Baltic Sea). Boreas 31, 151–162.

Müller, P.J., Kirst, G., Ruhland, G., von Storch, I., Rosell-Melé, A. (1998). Calibration of the alkenone paleotemperature index $U^{K'}_{37}$ based on core-tops from the eastern South Atlantic and the global ocean (60 N-60 S). Geochimica et Cosmochimica Acta 62, 1757–1772.

Muñoz-García, M. B. (2007). Chronology of Termination II and the Last Interglacial Period in North Spain based on stable isotope records of stalagmites from Cueva del Cobre (Palencia)/Cronología de la Terminación II y del Último Periodo Interglacial en el norte de España a partir de los registros de isótopos estables de estalagmitas procedentes de la Cueva del Cobre (Palencia). Journal of Iberian Geology 33, 17-30.

Nakamura, H., Sawada, K., Araie, H., Suzuki, I., Shiraiwa, Y. (2014). Long chain alkenes, alkenones and alkenoates produced by the haptophyte alga Chrysotila lamellosa CCMP1307 isolated from a salt marsh. Organic Geochemistry 66, 90-97.

Nakamura, H., Sawada, K., Araie, H., Shiratori, T., Ishida, K.-I., Suzuki, I., Shiraiwa, Y. (2016). Composition of long chain alkenones and alkenoates as a function of growth temperature in marine haptophyte Tisochrysis lutea. Organic Geochemistry 99, 78-89.

Nelson, D. B., Sachs, J. P. (2014). The influence of salinity on D/H fractionation in alkenones from saline and hypersaline lakes in continental North America. Organic Geochemistry 66, 38-47.

Neumann, T., Schernewski, G. (2008). Eutrophication in the Baltic Sea and shifts in nitrogen fixation analyzed with a 3D ecosystem model. Journal of Marine Systems 74, 592-602.

Neumann, T. (2010). Climate-change effects on the Baltic Sea ecosystem: A model study. Journal of Marine Systems 81, 213-224.

Niemann, H., Stadnitskaia, A., Wirth, S.B., Gilli, A., Anselmetti, F.S., Sinninghe Damsté, J.S., Schouten, S., Hopmans, E.C., Lehmann, M.F. (2012). Bacterial GDGTs in Holocene sediments and catchment soils of a high Alpine lake: application of the MBT/CBT-paleothermometer. Climate of the Past 8, 889–906.

Ono, M., Sawada, K., Shiraiwa, Y., Kubota, M. (2012). Changes in alkenone and alkenoate distributions during acclimatization to salinity change in Isochrysis galbana: Implication for alkenone-based paleosalinity and paleothermometry. Geochemical Journal 46, 235–247.

O'sullivan, P.E. (1983). Annually-laminated lake sediments and the study of Quaternary environmental changes—a review. Quaternary Science Review 1, 245–313.

Palumbo, E., Flores, J.A., Perugia, C., Emanuele, D., Petrillo, Z., Rodrigues, T., Voelker, A.H., Amore, F.O. (2013). Abrupt variability of the last 24 ka BP recorded by coccolithophore assemblages off the Iberian Margin (core MD03-2699). Journal of Quaternary Science 28, 320–328.

Pancost, R.D., Sinninghe Damsté, J.S., de Lint, S., van der Maarel, M.J., Gottschal, J.C. (2000). Biomarker evidence for widespread anaerobic methane oxidation in Mediterranean sediments by a consortium of methanogenic archaea and bacteria. Applied Environmental Microbiology 66, 1126–1132.

Pancost, R.D., Sinninghe Damsté, J.S. (2003). Carbon isotopic compositions of prokaryotic lipids as tracers of carbon cycling in diverse settings. Chemical Geology 195, 29–58.

Parmanne, R., Rechling, O., Sjöstrand, B. (1994). Status and future of herring and sprat stocks in the Baltic Sea. Dana 10, 29–59.

Pearson, E.J., Juggins, S., Talbot, H.M., Weckstrom, J., Rosen, P., Ryves, D.B., Roberts, S.J., Schmidt, R. (2011). A lacustrine GDGT-temperature calibration from the Scandinavian Arctic to Antarctic: Renewed potential for the application of GDGT-paleothermometry in lakes. Geochimica et Cosmochimica Acta 75, 6225–6238.

Peterse, F., Kim, J.-H., Schouten, S., Kristensen, D.K., Koç, N., Sinninghe Damsté, J.S. (2009). Constraints on the application of the MBT/CBT palaeothermometer at high latitude environments (Svalbard, Norway). Organic Geochemistry 40, 692–699.

Peterse, F., Nicol, G.W., Schouten, S., Sinninghe Damsté, J.S. (2010). Influence of soil pH on the abundance and distribution of core and intact polar lipid-derived branched GDGTs in soil. Organic Geochemistry 41, 1171–1175.

Peterse, F., Prins, M.A., Beets, C.J., Troelstra, S.R., Zheng, H., Gu, Z., Schouten, S., Sinninghe Damsté, J.S. (2011). Decoupled warming and monsoon precipitation in East Asia over the last deglaciation. Earth and Planetary Science Letters 301, 256–264.

Peterse, F., Meer, J. van der, Schouten, S., Weijers, J.W., Fierer, N., Jackson, R.B., Kim, J.-H., Sinninghe Damsté, J.S. (2012). Revised calibration of the MBT-CBT paleotemperature proxy based on branched tetraether membrane lipids in surface soils. Geochimica et Cosmochimica Acta 96, 215-229.

Pitcher, A., Hopmans, E.C., Mosier, A.C., Park, S.-J., Rhee, S.-K., Francis, C.A., Schouten, S., Sinninghe Damsté, J.S. (2011). Core and intact polar glycerol dibiphytanyl glycerol tetraether lipids of ammonia-oxidizing archaea enriched from marine and estuarine sediments. Applied Environmental Microbiology 77, 3468–3477.

Powers, L.A., Werne, J.P., Johnson, T.C., Hopmans, E.C., Sinninghe Damsté, J.S., Schouten, S. (2004). Crenarchaeotal membrane lipids in lake sediments: A new paleotemperature proxy for continental paleoclimate reconstruction? Geology 32, 613–616.

Powers, L.A., Johnson, T.C., Werne, J.P., Castaneda, I.S., Hopmans, E.C., Sinninghe Damsté, J.S., Schouten, S. (2005). Large temperature variability in the southern African tropics since the Last Glacial Maximum. Geophysical Research Letters 32.

Powers, L., Werne, J.P., Vanderwoude, A.J., Sinninghe Damsté, J.S., Hopmans, E.C., Schouten, S. (2010). Applicability and calibration of the TEX86 paleothermometer in lakes. Organic Geochemistry 41, 404–413.

Prahl, F.G., Wakeham, S.G. (1987). Calibration of unsaturation patterns in long-chain ketone compositions for palaeotemperature assessment. Nature 330, 367-369.

Prahl, F.G., Muehlhausen, L.A., Zahnle, D.L. (1988). Further evaluation of long-chain alkenones as indicators of paleoceanographic conditions. Geochimica et Cosmochimica Acta 52, 2303–2310.

Prahl, F.G., Rontani, J.-F., Volkman, J.K., Sparrow, M.A., Royer, I.M. (2006). Unusual C35 and C36 alkenones in a paleoceanographic benchmark strain of Emiliania huxleyi. Geochimica et Cosmochimica Acta 70, 2856–2867.

Price, T. D. (2000). Europe's First Farmers.(ed. Price, T.D.) Cambridge University Press, Cambridge, 260-300.

Punning, J., Martma, T., Kessel, H., Vaikme, R. (1988). The isotopic composition of oxygen and carbon in the subfossil mollusc shells of the Baltic Sea as an indicator of palaeosalinity. Boreas 17, 27–31.

Rampen, S.W., Willmott, V., Kim, J.-H., Uliana, E., Mollenhauer, G., Schefuß, E., Sinninghe Damsté, J.S., Schouten, S. (2012). Long chain 1, 13-and 1, 15-diols as a potential proxy for palaeotemperature reconstruction. Geochimica et Cosmochimica Acta 84, 204–216.

Randlett, M.-E., Coolen, M.J., Stockhecke, M., Pickarski, N., Litt, T., Balkema, C., Kwiecien, O., Tomonaga, Y., Wehrli, B., Schubert, C.J. (2014). Alkenone distribution in Lake Van sediment over the last 270 ka: influence of temperature and haptophyte species composition. Quaternary Science Review 104, 53–62.

Rechka, J.A., Maxwell, J.R. (1988). Characterisation of alkenone temperature indicators in sediments and organisms. Organic Geochemistry 13, 727–734.

Reimann, C., Siewers, U., Tarvainen, T., Bityukova, L., Eriksson, J., Gilucis, A., Gregorauskiene, V., Lukashev, V., Matinian, N.N., Pasieczna, A. (2000). Baltic soil survey: total concentrations of major and selected trace elements in arable soils from 10 countries around the Baltic Sea. Science of the Total Environment 257, 155–170.

Reimer, P.J., Bard, E., Bayliss, A., Beck, J.W., Blackwell, P.G., Ramsey, C.B., Buck, C.E., Cheng, H., Edwards, R.L., Friedrich, M., Grootes, P.M. (2013) IntCal13 and Marine13 radiocarbon age calibration curves 0-50,000 years cal BP, Radiocarbon 55, 1869-1887.

Reinholdsson M., Snowball I., Zillén L., Lenz C., Conley D.J. (2013). Magnetic enhancement of Baltic Sea sapropels by greigite magnetofossils. Earth and Planetary Science Letters 366, 137-150.

Reissmann, J. H., Burchard H., Feistel R., Hagen E., Lass H.U., Mohrholz V., Nausch G., Umlauf L., Wieczorek G. (2009). Vertical mixing in the Baltic Sea and consequences for eutrophication–A review. Progress in Oceanography 82, 47–80.

Richards, M. P., Price, T. D., Koch, E. (2003). Mesolithic and Neolithic subsistence in Denmark: New stable isotope data. Current Anthropology 44, 288–295.

RIMFROST, Last accessed on September 13, 2016: http://www.rimfrost.no/

Rodó, X., Baert, E., Comín, F.A.(1997). Variations in seasonal rainfall in Southern Europe during the present century: relationships with the North Atlantic Oscillation and the El Niño-Southern Oscillation. Climate Dynamics 13, 275–284.

Rodrigo-Gámiz, M., Martínez-Ruiz, F., Rampen, S.W., Schouten, S., Sinninghe Damsté, J.S. (2014). Sea surface temperature variations in the western Mediterranean Sea over the last 20 kyr: A dual-organic proxy ($U^{K'}_{37}$ and LDI) approach. Paleoceanography 29, 87–98.

Rodrigues, T., Grimalt, J. O., Abrantes, F. G., Flores, J. A., Lebreiro, S. M. (2009). Holocene interdependences of changes in sea surface temperature, productivity, and fluvial inputs in the Iberian continental shelf (Tagus mud patch). Geochemistry, Geophysics, Geosystems 10. Q07U06, doi:10.1029/2008GC002367.

Rosell-Melé, A. (1998). Interhemispheric appraisal of the value of alkenone indices as temperature and salinity proxies in high-latitude locations. Paleoceanography 13, 694–703.

Rosentau, A., Harff, J., Oja, T., Meyer, M. (2012). Postglacial rebound and relative sea level changes in the Baltic Sea since the Litorina transgression. Baltica 25, 113–120.

Ross, D.A., Degens, E.T., MacIlvaine, J., (1970). Black Sea: recent sedimentary history. Science 170, 163–165.

Rößler, D., Moros, M., Lemke, W. (2011). The Littorina transgression in the southwestern Baltic Sea: new insights based on proxy methods and radiocarbon dating of sediment cores. Boreas 40, 231–241.

Rowley-Conwy, P. (2011). Westward Ho! The spread of agriculture from Central Europe to the Atlantic. Current Anthropology, 52, S431-S451.

Rowley-Conwy, P. (2013). North of the frontier: Early domestic animals in northern Europe. The origins and spread of domestic animals in Southwest Asia and Europe, 283-312.

Rueda, G., Rosell-Mele, A., Escala, M., Gyllencreutz, R., Backman, J. (2009). Comparison of instrumental and GDGT-based estimates of sea surface and air temperatures from the Skagerrak. Organic Geochemistry 40, 287–291.

Ryan, W.B., Pitman, W.C., Major, C.O., Shimkus, K., Moskalenko, V., Jones, G.A., Dimitrov, P., Gorür, N., Sakinç, M., Yüce, H. (1997). An abrupt drowning of the Black Sea shelf. Marine Geology 138, 119–126.

Sachs, J.P., Maloney, A.E., Gregersen, J., Paschall, C. (2016). Effect of salinity on 2H/1H fractionation in lipids from continuous cultures of the coccolithophorid Emiliania huxleyi. Geochimica et Cosmochimica Acta 189, 96-109.

Samuelsson, M. (1996). Interannual salinity variations in the Baltic Sea during the period 1954–1990. Continental Shelf Research 16, 1463–1477.

Schefuß, E., Ratmeyer, V., Stuut, J.-B.W., Jansen, J.F., Sinninghe Damsté, J.S. (2003). Carbon isotope analyses of n-alkanes in dust from the lower atmosphere over the central eastern Atlantic. Geochimica et Cosmochimica Acta 67, 1757–1767.

Schmoelcke, U. (2008). Holocene environmental changes and the seal (Phocidae) fauna of the Baltic Sea: coming, going and staying. Mammal Review 38, 231-246.

Schneider, R.R., Müller, P.J., Ruhland, G. (1995). Late Quaternary surface circulation in the east equatorial South Atlantic: Evidence from alkenone sea surface temperatures. Paleoceanography 10, 197–219.

Schouten, S., Hoefs, M.J.L., Koopmans, M.P., Bosch, H.-J., Sinninghe Damsté, J.S. (1998). Structural characterization , occurrence and fate of archaeal ether- bound acyclic and cyclic biphytanes and corresponding diols in sediments. Organic Geochemistry 29, 1305–1319.

Schouten, S., Hopmans, E.C., Pancost, R.D., Sinninghe Damsté, J.S. (2000). Widespread occurrence of structurally diverse tetraether membrane lipids: evidence for the ubiquitous presence of low-temperature relatives of hyperthermophiles. Proceedings of the National Academy of Sciences 97, 14421–14426.

Schouten, S., Hopmans, E.C., Schefuß, E., Sinninghe Damsté, J.S. (2002). Distributional variations in marine crenarchaeotal membrane lipids: a new tool for reconstructing ancient sea water temperatures? Earth and Planetary Science Letters 204, 265–274.

Schouten, S., Ossebaar, J., Schreiber, K., Kienhuis, M.V.M., Langer, G., Bijma, J. (2005). The effect of temperature and salinity on the stable hydrogen isotopic composition of long chain alkenones produced by Emiliania huxleyi and Gephyrocapsa oceanica. Biogeosciences Discussions 2, 1681–1695.

Schouten, S., Huguet, C., Hopmans, E. C., Kienhuis, M. V., Sinninghe Damsté, J. S. (2007). Analytical methodology for TEX86 paleothermometry by high-performance liquid chromatography/atmospheric pressure chemical ionization-mass spectrometry. Analytical Chemistry 79, 2940–2944.

Schouten, S., Eldrett, J., Greenwood, D.R., Harding, I., Baas, M., Sinninghe Damsté, J.S. (2008). Onset of long-term cooling of Greenland near the Eocene-Oligocene boundary as revealed by branched tetraether lipids, Geology, 36, 147–150.

Schouten, S., Rijpstra, W.I.C., Durisch-Kaiser, E., Schubert, C.J., Sinninghe Damsté, J.S., (2012). Distribution of glycerol dialkyl glycerol tetraether lipids in the water column of Lake Tanganyika. Organic Geochemistry 53, 34–37.

Schulz, H.-M., Schöner, A., Emeis, K.-C. (2000). Long-chain alkenone patterns in the Baltic Sea—an ocean-freshwater transition. Geochimica et Cosmochimica Acta 64, 469–477.

Schwab, D. J., Bennett, J. R., Liu, P. C. Donelan, M. A. (1984). Application of a simple numerical wave prediction model to Lake Erie. Journal of Geophysical Research: Oceans 89, 3586–3592.

Seifert, T., Kayser, B., Tauber, F. (1995). Bathymetry data of the Baltic Sea. Baltic Sea Research Institute, Warnemünde. Last accessed on January 14, 2017: http://www.io-warnemuende.de/topography-of-the-baltic-sea.html

Seppä, H., Hammarlund, D., Antonsson, K. (2005). Low-frequency and high-frequency changes in temperature and effective humidity during the Holocene in south-central Sweden: implications for atmospheric and oceanic forcings of climate. Climate Dynamic 25, 285–297.

Shennan, S., Downey, S.S., Timpson, A., Edinborough, K., Colledge, S., Kerig, T., Manning, K. Thomas, M.G. (2013). Regional population collapse followed initial agriculture booms in mid-Holocene Europe. Nature Communications, 4.

Sikes, E.L., Sicre, M.-A. (2002). Relationship of the tetra-unsaturated C37 alkenone to salinity and temperature: Implications for paleoproxy applications. Geochemistry, Geophysics, Geosystems 3, 1–11.

Sinninghe Damsté, J.S., Hopmans, E.C., Pancost, R.D., Schouten, S., Geenevasen, J.A.J. (2000). Newly discovered non-isoprenoid glycerol dialkyl glycerol tetraether lipids in sediments. Chemical Communications 17, 1683–1684.

Sinninghe Damsté, J.S., Schouten, S., Hopmans, E.C., van Duin, A.C., Geenevasen, J.A. (2002). Crenarchaeol the characteristic core glycerol dibiphytanyl glycerol tetraether membrane lipid of cosmopolitan pelagic crenarchaeota. Journal of Lipid Research 43, 1641–1651.

Sinninghe Damsté, J.S., Ossebaar, J., Abbas, B., Schouten, S., Verschuren, D. (2009). Fluxes and distribution of tetraether lipids in an equatorial African lake: Constraints on the application of the TEX_{86} palaeothermometer and BIT index in lacustrine settings. Geochimica et Cosmochimica Acta 73, 4232–4249.

Sinninghe Damsté, J.S., Rijpstra, W.I.C., Hopmans, E.C., Weijers, J.W.H., Foesel, B.U., Overmann, J., Dedysh, S.N. (2011). 13,16-Dimethyl Octacosanedioic Acid (iso-Diabolic Acid), a Common Membrane-Spanning Lipid of Acidobacteria Subdivisions 1 and 3, Applied Environmental Microbiology 77, 4147–4154.

Sinninghe Damsté, J.S.S., Rijpstra, W.I.C., Hopmans, E.C., Jung, M.-Y., Kim, J.-G., Rhee, S.-K., Stieglmeier, M., Schleper, C. (2012a). Intact Polar and Core Glycerol Dibiphytanyl Glycerol Tetraether Lipids of Group I.1a and I.1b Thaumarchaeota in Soil. Applied Environmental Microbiology 78, 6866–6874.

Sinninghe Damsté, J.S., Ossebaar, J., Schouten, S., Verschuren, D. (2012b). Distribution of tetraether lipids in the 25-ka sedimentary record of Lake Challa: extracting reliable TEX86 and MBT/CBT palaeotemperatures from an equatorial African lake. Quaternary Science Reviews 50, 43–54.

Sinninghe Damsté, J.S., Rijpstra, W.I.C., Hopmans, E.C., Foesel, B.U., Wüst, P.K., Overmann, J., Tank, M., Bryant, D.A., Dunfield, P.F., Houghton, K., Stott, M.B. (2014). Ether- and Ester-Bound iso-Diabolic Acid and Other Lipids in Members of Acidobacteria Subdivision 4, Applied Environmental Microbiology 80, 5207–5218.

Sinninghe Damsté, J.S. (2016). Spatial heterogeneity of sources of branched tetraethers in shelf systems: The geochemistry of tetraethers in the Berau River delta (Kalimantan, Indonesia). Geochimica et Cosmochimica Acta 186, 13-31.

Skoglund, P., Malmström, H., Raghavan, M., Storå, J., Hall, P., Willerslev, E., Gilbert, M.T.P., Götherström, A., Jakobsson, M. (2012). Origins and genetic legacy of Neolithic farmers and hunter-gatherers in Europe. Science 336, 466-469.

Skoglund, P., Malmström, H., Omrak, A., Raghavan, M., Valdiosera, C., Günther, T., Hall, P., Tambets, K., Parik, J., Sjögren, K.G., Apel, J. (2014). Genomic diversity and admixture differs for Stone-Age Scandinavian foragers and farmers. Science 344, 747-750.

Sluijs, A., Schouten, S., Pagani, M., Woltering, M., Brinkhuis, H., Sinninghe Damsté, J.S., Dickens, G.R., Huber, M., Reichart, G.-J., Stein, R., Matthiessen, J. (2006). Subtropical Arctic Ocean temperatures during the Palaeocene/Eocene thermal maximum. Nature 441, 610–613.

Song, M., Zhou, A., He, Y., Zhao, C., Wu, J., Zhao, Y., Liu, W., Liu, Z. (2016). Environmental controls on long-chain alkenone occurrence and compositional patterns in lacustrine sediments, northwestern China. Organic Geochemistry 91, 43–53.

Sørensen, L., Karg, S. (2014). The expansion of agrarian societies towards the north–new evidence for agriculture during the Mesolithic/Neolithic transition in Southern Scandinavia. Journal of Archaeological Science, 51, 98-114.

Sternbeck, J., Sohlenius, G. (1997). Authigenic sulfide and carbonate mineral formation in Holocene sediments of the Baltic Sea. Chemical Geology 135, 55–73.

de Stigter, H.C., Jesus, C.C., Boer, W., Richter, T.O., Costa, A., van Weering, T.C. (2011). Recent sediment transport and deposition in the Lisbon–Setúbal and Cascais submarine canyons, Portuguese continental margin, Deep-Sea Research Part II 58, 2321–2344.

Stoll, H.M., Moreno, A., Mendez-Vicente, A., Gonzalez-Lemos, S., Jimenez-Sanchez, M., Jose Dominguez-Cuesta, M., Edwards, R.L., Cheng, H., Wang, X. (2013). Paleoclimate and growth rates of speleothems in the northwestern Iberian Peninsula over the last two glacial cycles, Quaternary Research 80, 284–290.

Stora, J., Ericson, P. G. (2004). A prehistoric breeding population of harp seals (Phoca groenlandica) in the Baltic Sea. Marine Mammal Science 20, 115–133.

Stramma, L., Johnson, G.C., Sprintall, J., and Mohrholz, V. (2008). Expanding oxygen-minimum zones in the tropical oceans. Science *320*, 655–658.

Struck, U., Pollehne, F., Bauerfeind, E. & Bodungen, B. v. Sources of nitrogen for the vertical particle flux in the Gotland Sea (Baltic Proper)—results from sediment trap studies. J. Mar. Syst. 45, 91–101 (2004).

Stuiver, M., Reimer, P., Braziunas, T. (1998). High-precision radiocarbon age calibration for terrestrial and marine samples, Radiocarbon 40, 1127–1151.

Suess, E. (1979). Mineral phases formed in anoxic sediments by microbial decomposition of organic matter. Geochimica et Cosmochimica Acta 43, 339–352.

Sun, Q., Chu, G., Liu, G., Li, S., Wang, X. (2007). Calibration of alkenone unsaturation index with growth temperature for a lacustrine species, Chrysotila lamellosa (Haptophyceae). Organic Geochemistry 38, 1226–1234.

Sun, Q., Chu, G., Liu, M., Xie, M., Li, S., Ling, Y., Wang, X., Shi, L., Jia, G., Lü, H. (2011). Distributions and temperature dependence of branched glycerol dialkyl glycerol tetraethers in recent lacustrine sediments from China and Nepal. Journal of Geophysical Research: Biogeosciences 116.

Swart, P.K. (1991). The oxygen and hydrogen isotope composition of the Black Sea. Deep-Sea Research 38, S761-S772.

Tallavaara, M., Seppä, H. (2012). Did the mid-Holocene environmental changes cause the boom and bust of hunter-gatherer population size in eastern Fennoscandia? The Holocene 22, 215-225.

Ternois, Y., Kawamura, K., Keigwin, L., Ohkouchi, N., Nakatsuka, T. (2001). A biomarker approach for assessing marine and terrigenous inputs to the sediments of Sea of Okhotsk for the last 27,000 years. Geochimica et Cosmochimica Acta 65, 791–802.

Theroux, S., D'Andrea, W. J., Toney, J., Amaral-Zettler, L., Huang, Y. (2010). Phylogenetic diversity and evolutionary relatedness of alkenone-producing haptophyte algae in lakes: Implications for continental paleotemperature reconstructions. Earth and Planetary Science Letters 300, 311-320.

Theroux, S., Toney, J., Amaral-Zettler, L., Huang, Y. (2013). Production and temperature sensitivity of long chain alkenones in the cultured haptophyte Pseudoisochrysis paradoxa. Organic Geochemistry 62, 68-73.

Thiel, V., Jenisch, A., Landmann, G., Reimer, A., Michaelis, W. (1997). Unusual distributions of long-chain alkenones and tetrahymanol from the highly alkaline Lake Van, Turkey. Geochimica et Cosmochimica Acta 61, 2053–2064.

Tierney, J.E., Russell, J.M. (2009). Distributions of branched GDGTs in a tropical lake system: Implications for lacustrine application of the MBT/CBT paleoproxy. Organic Geochemistry 40, 1032–1036.

Tierney, J.E., Tingley, M.P. (2014). A Bayesian, spatially-varying calibration model for the TEX_{86} proxy. Geochimica et Cosmochimica Acta 127, 83–106.

Tikkanen, M., Oksanen, J. (2002). Late Weichselian and Holocene shore displacement history of the Baltic Sea in Finland. Fennia International Journal of Geography 180, 9–20.

Timpson, A., Colledge, S., Crema, E., Edinborough, K., Kerig, T., Manning, K., Thomas, M.G. Shennan, S. (2014). Reconstructing regional population fluctuations in the European Neolithic using radiocarbon dates: a new case-study using an improved method. Journal of Archaeological Science 52, 549-557.

Toney, J. L., Theroux, S., Andersen, R. A., Coleman, A., Amaral-Zettler, L., Huang, Y. (2012). Culturing of the first 37:4 predominant lacustrine haptophyte: geochemical, biochemical, and genetic implications. Geochimica et Cosmochimica Acta 78, 51-64.

Trigo, R.M., Pozo-Vazquez, D., Osborn, T.J., Castro-Diez, Y., Gamiz-Fortis, S., Esteban-Parra, M.J. (2004). North Atlantic oscillation influence on precipitation, river flow and water resources in the Iberian peninsula, International Journal of Climatology 24, 925–944.

Trouet, V., Esper, J., Graham, N.E., Baker, A., Scourse, J.D., Frank, D.C. (2009). Persistent positive North Atlantic Oscillation mode dominated the medieval climate anomaly. science 324, 78-80.

Uda, I., Sugai, A., Itoh, Y.H., Itoh, T. (2001). Variation in molecular species of polar lipids from Thermoplasma acidophilum depends on growth temperature. Lipids 36, 103–105.

Ukkonen, P. The early history of seals in the northern Baltic. In Annales Zoologici Fennici. Finnish Zoological and Botanical Publishing Board 39, 187-207.

Vahtera, E., Conley, D.J., Gustafsson, B.G., Kuosa, H., Pitkänen, H., Savchuk, O.P., Tamminen, T., Viitasalo, M., Voss, M., Wasmund, N., Wulff, F. (2007). Internal ecosystem feedbacks enhance nitrogen-fixing cyanobacteria blooms and complicate management in the Baltic Sea. AMBIO: A journal of the Human Environment 36, 186-194.

Vale, C., Catarino, F. (1996). Accumulation of Zn, Pb, Cu, Cr and Ni in sediments between roots of the Tagus estuary salt marshes, Portugal, Estuar. Estuarine, Coastal and Shelf Science 42, 393–403.

Van Soelen, E. E., Lammers, J. M., Eglinton, T. I., Sinninghe Damsté, J. S., Reichart, G. J., (2014). Unusual C35 to C38 alkenones in mid-Holocene sediments from a restricted estuary (Charlotte Harbor, Florida). Organic Geochemistry 70, 20–28.

Vaz, N., Mateus, M., Dias, J.M. (2011). Semidiurnal and spring-neap variations in the Tagus Estuary: Application of a process-oriented hydro-biogeochemical model, Journal of Coastal Research 64, 1619–1623.

Versteegh, G. J., Riegman, R., de Leeuw, J. W., Jansen, J. F. (2001). UK'37 values for Isochrysis galbana as a function of culture temperature, light intensity and nutrient concentrations. Organic Geochemistry 32, 785-794.

Vis, G.-J., Kasse, C., Vandenberghe, J. (2008). Late Pleistocene and Holocene palaeogeography of the Lower Tagus Valley (Portugal): effects of relative sea level, valley morphology and sediment supply, Quaternary Science Review 27, 1682–1709.

Vis, G.-J., Kasse, C. (2009). Late Quaternary valley-fill succession of the Lower Tagus Valley, Portugal. Sedimentary Geology 221, 19–39.

Vis, G.-J., Bohncke, S. J. P., Schneider, H., Kasse, C., Coenraads-Nederveen, S., Zuurbier, K. Rozema, J. (2010). Holocene flooding history of the Lower Tagus Valley (Portugal), Journal Quaternary Science 25, 1222-1238.

Vis, G.-J., Kasse, C., Kroon, D., Vandenberghe, J., Jung, S., Lebreiro, S.M., Rodrigues, T. (2016). Time-integrated 3D approach of late Quaternary sediment-depocenter migration in the Tagus depositional system: From river valley to abyssal plain. Earth-Science Reviews 153, 192–211.

Volkman, J.K., Eglinton, G., Corner, E.D., Forsberg, T.E.V. (1980). Long-chain alkenes and alkenones in the marine coccolithophorid Emiliania huxleyi. Phytochemistry 19, 2619–2622.

Volkman, J. K., Burton, H. R., Everitt, D. A., Allen, D. I., 1988. Pigment and lipid compositions of algal and bacterial communities in Ace Lake, Vestfold Hills, Antarctica. Hydrobiologica 165, 41-57.

Volkman, J.K., Barrerr, S.M., Blackburn, S.I., and Sikes, E.L. (1995). Alkenones in *Gephyrocapsa oceanica:* Implications for studies of paleoclimate. Geochim. Cosmochim. Acta *59*, 513–520.

Wacker, L., Lippold, J., Molnár, M., Schulz, H. (2013). Towards radiocarbon dating of single foraminifera with a gas ion source. Nuclear Instruments and Methods in Physics Research Section B: Beam Interactions with Materials and Atoms 294, 307-310.

Walsby, A. E. (1985). The permeability of heterocysts to the gases nitrogen and oxygen. Proceedings of the Royal Society of London B: Biological Sciences 226, 345–366.

Warden, L ., Kim, J-H., Zell, C., Vis, G-J., de Stitger, H., Bonnin, J., Sinninghe Damsté, J.S. (2016a). Examining the provenance of branched GDGTs in the Tagus River drainage basin and it outflow into the Atlantic Ocean over the Holocene to determine their usefulness for paleoclimate applications. Biogeosciences 13, 5719-5738.

Warden, L ., van der Meer, M., Moros, M., Sinninghe Damsté, J.S. (2016b). Sedimentary alkenone distributions reflect salinity changes in the Baltic Sea over the Holocene. Organic Geochemistry 102, 30-44.

Warden, L ., Moros, M., Nuemann, T., Shennan, A., Timpson, A., Sollai, M., Wacker L., Perner K., Häusler, K., Leipe, T., Kotilainen, A., Jansen, E., Schneider, R.R., Arz, H., Sinninghe Damsté, J.S., in review. Mid-Holocene warming triggered population increase and farming transition in the Baltic Region**.** Nature Geoscience.

Wasmund, N. (1997). Occurrence of cyanobacterial blooms in the Baltic Sea in relation to environmental conditions. Internationale Revue der gesamten Hydrobiologie und Hydrographie 82, 169–184.

Weber, Y., De Jonge, C., Rijpstra, W.I.C., Hopmans, E.C., Stadnitskaia, A., Schubert, C.J., Lehmann, M.F., Sinninghe Damsté, J.S., Niemann, H. (2015). Identification and carbon isotope composition of a novel branched GDGT isomer in lake sediments: Evidence for lacustrine branched GDGT production. Geochimica et Cosmochimica Acta 154, 118–129.

Weeks, S.J., Currie, B., and Bakun, A. (2002). Satellite imaging: Massive emissions of toxic gas in the Atlantic. Nature 415, 493–494.

Wefer, G., Berger, W.H., Bijma, J., Fischer, G. (1999). Clues to ocean history: a brief overview of proxies. In Use of Proxies in Paleoceanography, Springer Berlin Heidelberg, 1–68.

Weijers, J.W., Schouten, S., Spaargaren, O.C., Sinninghe Damsté, J.S. (2006a). Occurrence and distribution of tetraether membrane lipids in soils: Implications for the use of the TEX_{86} proxy and the BIT index. Organic Geochemistry 37, 1680–1693.

Weijers, J.W., Schouten, S., Hopmans, E.C., Geenevasen, J.A., David, O.R., Coleman, J.M., Pancost, R.D., Sinninghe Damsté, J.S. (2006b). Membrane lipids of mesophilic anaerobic bacteria thriving in peats have typical archaeal traits. Environmental Microbiology 8, 648–657.

Weijers, J.W., Schefuß, E., Schouten, S., Sinninghe Damsté, J.S. (2007a). Coupled thermal and hydrological evolution of tropical Africa over the last deglaciation. Science 315, 1701–1704.

Weijers, J.W., Schouten, S., van den Donker, J.C., Hopmans, E.C., Sinninghe Damsté, J.S. (2007b). Environmental controls on bacterial tetraether membrane lipid distribution in soils. Geochimica et Cosmochimica Acta 71, 703–713.

Weijers, J.W.H., Wiesenberg, G.L.B., Bol, R., Hopmans, E.C., Pancost, R.D. (2010). Carbon isotopic composition of branched tetraether membrane lipids in soils suggest a rapid turnover and a heterotrophic life style of their source organism(s). Biogeosciences 7, 2959–2973.

Weijers, J.W.H., Steinmann, P., Hopmans, E.C., Schouten, S., Sinninghe Damsté, J.S. (2011). Bacterial tetraether membrane lipids in peat and coal: Testing the MBT-CBT temperature proxy for climate reconstruction. Organic Geochemistry 42, 477–486.

Weijers, J.W., Schefuß, E., Kim, J.-H., Sinninghe Damsté, J.S., Schouten, S. (2014). Constraints on the sources of branched tetraether membrane lipids in distal marine sediments. Organic Geochemistry 72, 14–22.

Weisse, R., von Storch, H., Callies, U., Chrastansky, A., Feser, F., Grabemann, I., Guenther, H., Winterfeldt, J., Woth, K., Pluess, A., Stoye, T. (2009). Regional Meteorological–Marine Reanalyses and Climate Change Projections: Results for Northern Europe and Potential for Coastal and Offshore Applications. Bulletin of the American Meteorological Society 90, 849-860.

Westman, P., Sohlenius, G. (1999). Diatom stratigraphy in five offshore sediment cores from the northwestern Baltic proper implying large scale circulation changes during the last 8500 years. Journal of Paleolimnology 22, 53–69.

Wieland, K., Zuzarte, F. (1991). Vertical distribution of cod and sprat eggs and larvae in the Bornholm Basin (Baltic Sea) 1987-1990, ICES.

Wieland, K., Waller, U., Schnack, D. (1994). Development of Baltic cod eggs at different levels of temperature and oxygen content. Dana 10, 163–177.

Winterhalter, B. 1992. Late-Quaternary stratigraphy of Baltic Sea basins—a review. Bulletin of the Geological Society of Finland 64, 189–194.

Witkowski, A., Broszinski, A., Bennike, O., Janczak-Kostecka, B., Jensen, J. B., Lemke, W., Endler, R., Kuijpers, A. (2005). Darss Sill as a biological border in the fossil record of the Baltic Sea: evidence from diatoms. Quaternary International 130, 97–109.

Wolhowe, M. D., Prahl, F. G., Langer, G., Oviedo, A. M., Ziveri, P. (2015). Alkenone δD as an ecological indicator: A culture and field study of physiologically-controlled chemical and hydrogen-isotopic variation in C37 alkenones. Geochimica et Cosmochimica Acta 162, 166–182.

Wuchter, C., Schouten, S., Coolen, M.J., Sinninghe Damsté, J.S. (2004). Temperature-dependent variation in the distribution of tetraether membrane lipids of marine Crenarchaeota: Implications for TEX86 paleothermometry. Paleoceanography 19.

Wulff, F., Savchuk, O. P., Sokolov, A., Humborg, C., & Mörth, C. M. (2007). Management options and effects on a marine ecosystem: assessing the future of the Baltic. AMBIO: A Journal of the Human Environment 36, 243-249.

Xu, L., Reddy, C. M., Farrington, J.W., Frysinger, G. S., Gaines, R. B., Johnson, C. G., Nelson, R. K., Eglinton, T. I. (2001). Identification of a novel alkenone in Black Sea sediments. Organic Geochemistry 32, 633–645.

Yamamoto, M., Shiraiwa, Y., Inouye, I. (2000). Physiological responses of lipids in Emiliania huxleyi and Gephyrocapsa oceanica (Haptophyceae) to growth status and their implications for alkenone paleothermometry. Organic Geochemistry 31, 799–811.

Yang, H., Ding, W., Zhang, C.L., Wu, X., Ma, X., He, G., Huang, J., Xie, S. (2011). Occurrence of tetraether lipids in stalagmites: Implications for sources and GDGT-based proxies. Organic Geochemistry 42, 108–115.

Yang, G., Zhang, C.L., Xie, S., Chen, Z., Gao, M., Ge, Z., Yang, Z. (2012). Microbial glycerol dialkyl glycerol tetraethers from river water and soil near the Three Gorges Dam on the Yangtze River. Organic Geochemistry 56, 40-50.

Zachos, J.C., Schouten, S., Bohaty, S., Quattlebaum, T., Sluijs, A., Brinkhuis, H., Gibbs, S.J., Bralower, T.J. (2006). Extreme warming of mid-latitude coastal ocean during the Paleocene-Eocene Thermal Maximum: Inferences from TEX_{86} and isotope data. Geology 34, 737–740.

Zech, R., Gao, L., Tarozo, R., Huang, Y., 2012. Branched glycerol dialkyl glycerol tetraethers in Pleistocene loess-paleosol sequences: Three case studies. Organic Geochemistry 53, 38–44.

Zell, C., Kim, J.-H., Moreira-Turcq, P., Abril, G., Hopmans, E.C., Bonnet, M.-P., Sobrinho, R.L., Sinninghe Damsté, J.S. (2013). Disentangling the origins of branched tetraether lipids and crenarchaeol in the lower Amazon River: Implications for GDGT-based proxies. Limnology and Oceanography 58, 343–353.

Zell, C., Kim, J.-H., Balsinha, M., Dorhout, D., Fernandes, C., Baas, M., Sinninghe Damsté, J.S. (2014). Transport of branched tetraether lipids from the Tagus River basin to the coastal ocean of the Portuguese margin: consequences for the interpretation of the MBT'/CBT paleothermometer. Biogeosciences 11, 5637–5655.

Zell, C., Kim, J.-H., Dorhout, D., Baas, M., Sinninghe Damsté, J.S. (2015). Sources and distributions of branched tetraether lipids and crenarchaeol along the Portuguese continental margin: Implications for the BIT index, Continental Shelf Research 96, 34–44.

Zheng, Y., Huang, Y., Andersen, R. A., Amaral-Zettler, L. A. (2016). Excluding the di-unsaturated alkenone in the UK37 index strengthens temperature correlation for the common lacustrine and brackish-water haptophytes. Geochimica et Cosmochimica Acta 175, 36–46.

Zhou, H., Hu, J., Ming, L., Peng, P., Zhang, G. (2011). Branched glycerol dialkyl glycerol tetraethers and paleoenvironmental reconstruction in Zoigê peat sediments during the last 150 years. Chinese Science Bulletin 56, 2456–2463.

Zhu, C., Weijers, J.W., Wagner, T., Pan, J.-M., Chen, J.-F., Pancost, R.D. (2011). Sources and distributions of tetraether lipids in surface sediments across a large river-dominated continental margin. Organic Geochemistry 42, 376–386.

Zillén, L., Snowball, I., Sandgren, P., Stanton, T. (2003). Occurrence of varved lake sediment sequences in Varmland, west central Sweden: lake characteristics, varve chronology and AMS radiocarbon dating. Boreas 32, 612–626.

Zillén, L., Conley, D.J., Andrén, T., Andrén, E., Bjorck, S. (2008). Past occurrences of hypoxia in the Baltic Sea and the role of climate variability, environmental change and human impact. Earth-Science Reviews 91, 77–92.

Zink, K. -G., Leythaeuser, D., Melkonian, M., Schwark, L. (2001). Temperature dependency of long-chain alkenone distributions in recent to fossil limnic sediments and in lake waters. Geochimica et Cosmochimica Acta 65, 253–265.

Zink, K.-G., Vandergoes, M.J., Mangelsdorf, K., Dieffenbacher-Krall, A.C., Schwark, L. (2010). Application of bacterial glycerol dialkyl glycerol tetraethers (GDGTs) to develop modern and past temperature estimates from New Zealand lakes. Organic Geochemistry 41, 1060–1066.

Zorita, E., Kharin, V., Vonstorch, H. (1992). The Atmospheric Circulation and Sea-Surface Temperature in the North-Atlantic Area in Winter - Their Interaction and Relevance for Iberian Precipitation, Journal of Climatology 5, 1097–1108.

Summary

The better understanding society has about the global climate system the more educated choices that can be made for how to mitigate anthropogenically induced global climate change and its impacts on ecosystems. Knowledge about the climate system from before the instrumental data era comes from climate archives, such as marine and lake sediments, corals, tree rings, and speleothems to name a few, which contain measurable information about climate such as temperature, oxygen availability, salinity, etc. These indicators of past climate are called proxies. Proxy-records are used to extensively lengthen the climate record into the past. The information gathered about the past climate can be used to increase the robustness of climate models, helping to make predictions on future climate change and its impacts on ecosystems and societies more accurate. Therefore, proxy data must be accurate and so it is imperative to ensure the correct interpretation of climate archives and the reliability of climate proxies. This is done through applying the proxy in a variety of settings and comparing the results to instrumental data or data from another independent proxy to determine situations where it's application can be successful and to assess its limitations.

The focus of this thesis is on the use of organic biomarkers in the form of fossilized sedimentary lipids as proxies. Fossilized sedimentary lipids are useful as proxies because their preserved distribution in the sediments can reflect the environmental conditions (e.g. temperature) under which their source organism once lived. The research in this thesis is based on two different types of sedimentary lipids, long-chain alkenones and glycerol dialkyl glycerol tetraethers (GDGTs), both biomarkers for temperature. These biomarker proxies were examined to learn about past environments over the Holocene, in several regions, as well as to understand more about the proxy being applied. Additionally, indicators for anoxia or low oxygen conditions that can cause fish die offs, including laminations in the sediments and bulk isotope data, were examined as well.

Most of the research contributing to this thesis was performed on sediments from the Baltic Sea, a large brackish body of water with just a narrow connection to the North Sea that has experienced a complicated salinity history since the last deglaciation. Here sedimentary, alkenones, isoprenoid GDGTs (isoGDGTs), hydroxylated GDGTs (OH-GDGTs), and branched GDGTs (brGDGTs), were used to examine environmental changes in the region as well as the success and limitations of these proxies under changing environmental conditions such as occurred in the Baltic Sea over the Holocene. By comparing SST, indicators for anoxia and biomarkers for cyanobacteria (bloom forming microorganisms that when they die,

sink to the bottom of the basin and decompose consuming oxygen) from the Baltic Sea it was revealed that climate is the main controller of low-oxygen conditions in the basin. Therefore, increasing SSTs caused by global climate change could have disastrous effects for the Baltic Sea ecosystem. Additionally, a reconstruction of human population based on the abundance of human artifacts, when compared with SST estimates revealed evidence of the impact of climate on human population size and the transition to agrarian societies from 7,500-3,500 BP in the Baltic Sea region. In this study it is postulated that warmer temperatures intensified anoxia in the basin causing a decrease in marine resources while at the same time increased temperatures improved conditions in the region for farming. These changes triggered the switch from hunter-gather-fisher economy to agrarian, and this allowed for population growth.

The novel OH-GDGTs were discovered in the Baltic Sea recently and already established proxies based on these components were applied to surface sediment and archaeal cultures. A new index and new calibrations were developed for the region, as well. Several OH-GDGT based indices were applied to two sedimentary records in different regions of the basin (central and southern; i.e. the Gotland and Arkona basins) and the results were compared revealing that OH-GDGTs are a promising proxy for estimating SST in the Baltic Sea.

By examining the relationship between the distribution of alkenones and varying salinity regionally in the Baltic Sea, it was revealed that alkenone distributions co-vary with salinity changes. The alkenone distributions from the sediment records in the southern Baltic Sea (12.5-0.1 cal kyr BP) were also examined and it was found that the relationship between salinity and alkenone distributions that exists regionally in the Baltic Sea today also existed in the past, which suggests alkenone distributions can be used to examine paleosalinity. The rare, $C_{36:2}$ alkenone, believed to be an indicator of low-salinity conditions, was discovered in the Baltic Sea sediments and has not been reported in this basin before. Previously published data (hydrogen isotopic compositions of alkenones) from Black Sea sediments, which also contain the $C_{36:2}$ alkenone, was used to reconstruct salinity for the Black Sea over the Holocene, demonstrating that the $C_{36:2}$ alkenone is an indicator for low salinity conditions. Because the Black Sea has a similar salinity history to the Baltic Sea, these results were then used to make inferences about the composition of alkenone producing species and salinity changes in the Baltic Sea over the Holocene.

The provenance of brGDGTs were examined in two different sedimentary records in the Baltic Sea (from the Gotland and Arkona basins) and it was determined that the

provenance changed when the basin was reconnected to the North Sea and transformed from a freshwater lake to a brackish body of water. Despite evidence that in-situ production has occurred in the basin over the Holocene, it was determined which new calibrations were appropriate to apply in order to use the brGDGTs to reconstruct continental temperatures. Using enhanced chromatography methods, continental and bottom water temperatures along with pH were reconstructed over the Holocene. The resultant temperature estimates were similar in both basins, to previously published data from the region based on another proxy, and to present day instrumental data from the area. This study affirmed the importance of examining the origins of brGDGTs before using them for paleoclimate application, especially in regions that have undergone major environmental changes.

For a part of this thesis a re-examination of the provenance and distribution of brGDGTs in the soils, riverbank sediments, and river suspended particulate matter (SPM) from the Tagus River basin was performed using enhanced chromatography methods. Additionally, the distribution of brGDGTs in past sediments were studied by analyzing four sediment cores in a transect from the river to the deep ocean to determine if today's trends held true over the Holocene. Although mean annual air temperature estimates were not greatly improved upon, pH estimates based on the new methods and calibration were improved and new factors to be cautious of when applying brGDGTs for paleoclimate studies were revealed. This study also confirmed the importance of investigating the provenance of brGDGTs in a region before performing paleoclimate reconstructions.

The research contained in this thesis not only presents important findings about climate and its potential impacts on ecosystems and human societies, but also increases the knowledge base on sedimentary, fossilized, lipids used for paleoenvironmental studies, long-chain alkenones and GDGTs. Through applying proxies based on these fossilized lipids and comparing the estimates to previously published results based on an independent proxy, to instrumental data, or to the results from a different area in the same region, new knowledge was gained about the source organisms of these proxies and conditions that result in their successful application for paleoclimate studies. Proxy development and validation studies like the ones contained in this thesis are important for increasing the reliability of proxy data as well as the conjectures made about past and future climate based upon them.

Samenvatting

Hoe beter het inzicht van de samenleving is met betrekking tot het wereldwijde klimaatsysteem, hoe beter maatregelen om de door de mens veroorzaakte klimaatverandering en de effecten daarvan op ecosystemen te beperken zijn gemaakt kunnen worden. Kennis van het klimaat van voor de periode van instrumentele meetgegevens komt voornamelijk van klimaatarchieven, zoals mariene en meer sedimenten, koralen, jaarringen en ijskernen, die meetbare informatie over het klimaat, zoals temperatuur, beschikbaarheid van zuurstof, en zoutgehalte bevatten. Deze indicatoren van het vroegere klimaat worden ook wel proxies genoemd. Proxy-records worden gebruikt om ons inzicht in het klimaat van vroeger aanzienlijk uit te breiden. De verzamelde informatie over het vroegere klimaat kan worden gebruikt om de robuustheid van klimaatmodellen te verhogen, waardoor de toekomstige klimaatverandering en de effecten op ecosystemen en samenlevingen nauwkeuriger te voorspellen zijn. Daarom moeten proxy-gegevens nauwkeurig zijn en is het noodzakelijk de betrouwbaarheid van klimaat proxies te waarborgen en daarmee een juiste interpretatie van de klimaatarchieven te waarborgen. Dit gebeurt door de toepassing van de proxy in verschillende milieus te toetsen door de voorspellingen te vergelijken met instrumentele klimaatgegevens of gegevens bepaald met behulp van andere onafhankelijke proxies.

Het onderwerp van dit proefschrift is het gebruik van organische chemische fossielen in de vorm van sedimentaire lipiden als proxies. Omdat de distributie van deze lipiden vaak een afspiegeling zijn van de condities waaronder de micro-organismen die ze produceren ooit groeide, kunnen hiermee kwantitatief bepaalde parameters (zoals temperatuur) gereconstrueerd worden. Het onderzoek in dit proefschrift is gebaseerd op twee verschillende types van sedimentaire lipiden, alkenonen met lange ketens en glycerol dialkyl glycerol tetraethers (GDGTs), beide proxies voor temperatuur. Deze chemische fossielen werden bestudeerd om in verschillende gebieden meer te weten te komen over klimaatveranderingen gedurende het Holoceen. Tevens werd de toepasbaarheid van deze proxies getoetst. Indicatoren voor zuurstofgebrek, zoals bijvoorbeeld de gelaagdheid van sedimenten en bulk isotoop data, werden ook onderzocht.

Het grootste deel van het onderzoek beschreven in dit proefschrift werd uitgevoerd aan sedimenten van de Oostzee. Dit is een grote binnenzee die brak water bevat en momenteel slechts een beperkte verbinding met de Noordzee heeft. Sinds de laatste deglaciatie kent de Oostzee een sterk fluctuerend zoutgehalte. Sedimentaire alkenonen, isoprenoïde GDGTs (isoGDGTs), gehydroxyleerde GDGTs (OH-GDGTs), en vertakte GDGTs (brGDGTs),

werden gebruikt om veranderingen in het milieu van de Oostzee in het Holoceen te onderzoeken. Tevens werd de toepasbaarheid en mogelijke beperkingen van deze proxies onder veranderende omstandigheden gedurende het Holoceen onderzocht. Door het vergelijken van gereconstrueerde oppervlakte zeewatertemperaturen, proxies voor zuurstofgebrek en chemische fossielen voor cyanobacteriën (micro-organismen die vaak door een sterke bloei gekenmerkt worden en, wanneer ze sterven, naar de bodem zinken leidend tot een grote consumptie van zuurstof) bleek dat het klimaat de belangrijkste factor voor het veroorzaken van zuurstofarme omstandigheden in de Oostzee geweest is. Een verdere verhoging van de zeewatertemperatuur veroorzaakt door de voorziene wereldwijde klimaatverandering kan daarom rampzalige gevolgen voor het ecosysteem van de Oostzee hebben. Voor de periode van 7,500-3,500 BP, bleek uit een reconstructie van de menselijke bevolking op basis van archeologische gegevens in vergelijking met gereconstrueerde zeewatertemperaturen de beslissende invloed van klimaat op de dichtheid van menselijke bevolking rondom het Oostzeegebied. Uit deze studie volgt dat hogere temperaturen leidde tot zuurstofgebrek in de Oostzee die waarschijnlijk leidde tot veel lagere visstand. Tegelijkertijd zorgde de toegenomen temperatuur voor verbeterde omstandigheden voor het doen van landbouw. Deze veranderingen leidde tot een overgang van jager-verzamelaar-visser naar een agrarische economie, hetgeen de groei van de bevolking positief beïnvloedde.

De OH-GDGTs werden recent ontdekt in Oostzee sedimenten en bestaande proxies op basis van deze componenten werden toegepast op culturen van archaea en oppervlaktesedimenten uit de Oostzee om hun toepasbaarheid te testen. Tevens is een nieuwe index geformuleerd en zijn nieuwe kalibraties ontwikkeld voor deze regio. Verschillende OH-GDGT gebaseerde indices werden toegepast op twee sedimentaire archieven uit verschillende gebieden van de Oostzee (de Gotland en Arkona bekkens; in het midden en zuiden van de Oostzee). De resultaten laten zien dat OH-GDGTs een veelbelovend proxy kunnen zijn om zeewatertemperaturen te reconstrueren in de Oostzee.

Het onderzoek naar het verband tussen de verspreiding van alkenonen en het op regionale schaal variabele zoutgehalte in de Oostzee liet zien dat alkenoon distributies co-variëren met veranderingen in zoutgehalte. De alkenoon samenstelling in het sedimentaire archief (12,5-0,1 cal kyr BP) van de zuidelijke Oostzee werd eveneens onderzocht. Het bleek dat de alkenoon distributies variëren met het zoutgehalte, net als gevonden voor de oppervlaktesedimenten. Dit suggereert dat alkenoon distributies gebruikt kunnen worden om paleosaliniteit te reconstrueren. De zeldzame $C_{36:2}$ alkenoon, een indicator van een laag zoutgehalte, werd voor het eerst gevonden in de Oostzee sedimenten. Eerder gepubliceerde

gegevens (distributies en waterstofisotoop samenstelling van alkenonen) uit de Zwarte Zee sedimenten, die ook de $C_{36:2}$ alkenoon bevatten, werden gebruikt om het zoutgehalte te reconstrueren voor de Zwarte Zee in het Holoceen. Hieruit bleek de $C_{36:2}$ alkenoon inderdaad een betrouwbare indicator voor een laag zoutgehalte te zijn. Omdat de Zwarte Zee een soortgelijke geschiedenis heeft als de Oostzee omtrent zoutgehalte, werden deze resultaten vervolgens gebruikt om conclusies over de samenstelling van alkenoon producerende soorten en veranderingen in het zoutgehalte in de Oostzee in het Holoceen verder te onderbouwen. De herkomst van brGDGTs werd in twee verschillende sedimentaire archieven onderzocht in de Oostzee (Gotland en Arkona bekkens). Er werd vastgesteld dat hun herkomst veranderde toen het bekken weer verbinding kreeg met de Noordzee en omgevormd werd van een zoetwater meer naar een binnenzee met brak water. De toepassing van brGDGTs ligt in het feit dat ze gebruikt kunnen worden voor reconstructie van continentale temperaturen. Er zijn aanwijzingen dat er in situ productie van brGDGTs in de Oostzee zelf heeft plaatsgevonden. Daarom werden er verschillende kalibraties getest voor paleoklimaat reconstructie. Met behulp van een verbeterde methode voor de chromatografische scheiding van brGDGTs, werden zowel continentale en bodemwater temperaturen en pH gereconstrueerd gedurende het Holoceen. De resulterende temperatuurschattingen waren vergelijkbaar tussen beide bekkens, en in overeenstemming met eerder gepubliceerde gegevens uit de regio op basis van een andere proxy, en met instrumentale gegevens te presenteren uit het Oostzeegebied. Deze studie bevestigde het belang van het onderzoek naar de oorsprong van brGDGTs alvorens ze voor paleoklimaat reconstructie toe te passen, met name in regio's die in de loop van de tijd grote milieuveranderingen hebben ondergaan.

Het proefschrift besluit met een onderzoek van de herkomst en de verdeling van brGDGTs in de bodem, rivieroever sedimenten, en in de rivier zwevende deeltjes (SPM) van het Taag bekken op het Iberisch schiereiland. In tegenstelling tot eerder gepubliceerd werk is hier gebruik gemaakt van verbeterde chromatografie methoden. Tevens is de verdeling van de brGDGTs in sedimenten van het Holoceen onderzocht door het analysen van vier sedimentkernen in een transect van de rivier de Taag naar de diepe oceaan om te bepalen of de veranderingen in de distributies van de brGDGT die momenteel gezien worden karakteristiek zijn voor het gehele Holoceen. Jaarlijkse gemiddelde luchttemperatuur (MAT) schattingen zijn niet sterk verbeterd ten opzichte van eerdere methoden. De pH schattingen op basis van de nieuwe methode en kalibratie echter wel. Bovendien kwamen er nieuwe factoren aan het licht die bij het gebruik van brGDGTs in paleoklimaat studies van belang zijn.

Wederom bevestigt ook deze studie het belang van het onderzoek naar de herkomst van brGDGTs in een regio voor het uitvoeren van paleoklimaatreconstructies.

Het onderzoek in dit proefschrift presenteert niet alleen belangrijke bevindingen met betrekking tot het klimaat en haar mogelijke effecten op ecosystemen en menselijke samenlevingen. Het verhoogt ook de kennis over sedimentaire lipiden die gebruikt kunnen worden voor paleomilieu studies, met name met betrekking tot alkenonen en GDGTs. De toepassing van proxies op basis van deze fossiele lipiden en de vergelijking met eerder gepubliceerde resultaten gebaseerd op onafhankelijke proxies of instrumentele data heeft nieuwe kennis gegenereerd over de bron van deze componenten en toepassing van de proxies zodat zij succesvol gebruikt kunnen worden in paleoklimaat studies. Proxy ontwikkeling en validatie studies zoals die hier beschreven zijn zijn van belang voor het verhogen van de betrouwbaarheid van de proxy gegevens en daarmee van daarop gebaseerde klimaatreconstructies.

Acknowledgments

I am very grateful to Jaap for his guidance, for sharing his knowledge and his time, and for having incredible patience with me in the last year as the new addition to my life took precedence over my thesis for a while. I want to thank Stefan for always having an open door and being so approachable, and for his guidance and always being willing to share his knowledge. I want to thank Marcel for always taking the time to explain things to me and for opening the world of alkenones up to me. I want to thank Matthias for his ideas and all of the sediments that made my thesis possible and the fun times during his trips to Texel. I am thankful to Kim for motivating me with my first paper. I am grateful to Ellen for all of her help with the machines and providing some comedic relief in the lab.

I would like to thank the reading committee for their assessment of this thesis: Dr. Prof. Rich Pancost, Dr. Prof. Stephen Schouten, Dr. Isla Castañeda, Dr. Francien Peterse, and Prof. Dr. Gert-Jan Reichart.

I am grateful to all the technicians, Marianne, Irene, Jort, Anchelique, Monique, Kevin and Denise, for their help over the last five years. Anchelique, for good or for bad, you taught me everything I know about organic geochemistry methods! Thank you for your immense patience, your sense of humor, and your compassion. I really enjoyed having a lab bench near yours. Thank you, Monique, for all of your extensive help with the GC analysis and my dirty samples and even more I am grateful to have had you as a friend to talk with in the lab who shared my love of dogs. Jort, thank you for your help with the LC-MS and isotope analyzer, for always being approachable, for not making me feel stupid for asking a stupid question, and for your easy going nature and good sense of humor.

Thank you for everyone in the BGC who made my time here so much more enjoyable. A special thank you to Martina, as we started our Ph.D.'s at about the same time. Thank you for being a good friend, for always listening to my complaints and for sharing the work load with me. Thank you to the brGDGT girls, Claudia and Cindy, for answering all of the questions I was afraid to ask and for all of your help. Thank you, Yvonne and Cecile, for getting me kicked out of my first office that I shared with you and for our long (so very long) talks and the many laughs we had while I should have been working. Short Marc, I want to thank you for all of the fun we had in Urbino and beyond. I always enjoyed your dry sense of humor and appreciate how genuine you are. Thank you, Dave, for being you, and for all of the fun and late nights dancing. Thank you, Claudia, for always being a good friend. You are the sweetest, most genuine, and supportive person I have ever met. Thank you, Sandra, for

being so unique and interesting, for your sense of humor, the crazy stuff you said, and sharing my love of crime shows. Thank you, Marta, for always being up for hanging out, for giving good advice, talking to me and not acting annoyed when I went into your office looking for Eli, and just being such a kind person. Thank you, Sebastian, for all of the laughs while goofing around about our dreams of a Phil Collins radio station and our program to reach out to endangered youth among many others. Sometimes I don't even think we were laughing about the same things but that didn't matter. Thank you, Rodrigo and Isabela, for being such fun neighbors and sharing Artur with us. Thank you, Sabine and Darci, for the talks and entertainment in the lab as our benches were right near each other. Thank you, Denise, for all the fun conversations about weddings. Thank you, Nicole, for always being so fun and such a great hostess and stopping everything to give advice when I needed it. Thank you, Laura, for your dry sense of humor and for taking the time to offer advice. Thank you, Sebastiaan, for always being so friendly and easy to talk to. Thank you, Cindy, for being such a fun dancer. And thank you, Sophie, for being a great officemate, not allowing me to take anything too seriously in the end, for sharing your green thumb with our office children, and all the great talks. Having you start out as I was leaving made everything seem to come full circle.

As for people outside of the BGC, thank you Elke and Tom for all of the long walks we had. I appreciated so much having someone to meet every day, no matter the weather, for a long walk with the dogs. Thank you, Jenni, for all of the dog walks, talks and favors. Thank you, Sylvia, for all of your goofiness, compassion and charm and for convincing us to go to Greece for our honeymoon despite the immense amount of shark attacks. Thank you, Arno, for being so sweet and always willing to help out. Conversations with you, although long, were always enlightening and funny. Than you, Jacque, our fellow American that we met too late, and Jacob, for being so fun, kind and helpful. Thank you, Jolanda, for all of your help throughout our time at the NIOZ. Thank you, Christian, for seeing me when Catia didn't. And a special thanks to the Portuguese we met on Texel, our new favorite culture. Thank you, Luis and Sofia, for sharing your family with us. Time spent with you was always so enjoyable as you are such kind, sweet, caring people. Luis, your sense of humor and goofiness was always appreciated, as were your 'football' skills. And, Sofia, your sarcasm and sassiness are always welcome. One of my favorite memories from Texel was watching the world cup game with you guys, Arno and Eli. Thank you, Catia, for eventually seeing me, becoming such a good friend and fellow dog and Ceasar Millan lover, as well as always being crazy fun (and at times just crazy). Thank you, Catarina, for all of the walks and talks, for sharing your love of

dogs with me, and for all of your advice and empathy. Some of my favorite memories from my time on Texel are of dancing. I will always remember dancing at Eli's birthday party and my bachelorette party in De Koog, Claudia's bachelorette party in Amsterdam, at the American College University in Utrecht, Dave's going away party, and Catia's Ph.D. party. Thank you to everyone who danced with me!

Thank you to my family for being understanding when we moved thousands of miles away for four years. Thank you to all of the friends and family who visited us while we were here, that meant so much to us as we missed you all so much. Thank you also to my dad and mom for your expectations, your love and your support through the years. Thank you, Grandma Joan, for passing on to me through stories about your adventures with your sisters your love of travel. Without that I never would have come to the Netherlands to earn a doctoral degree. Thank you to my mom, Aunt Patrice and Aunt Sharyn, for holding my crying baby so I could work uninterrupted on this thesis. And thank you to my dogs, Isabel and Copper, for sitting by my feet as I wrote my thesis.

Eli, I have so much gratitude for you and that you are in my life. But on this occasion, I want to thank you for all of your support during my Ph.D., for always believing in me, for thinking I am smarter and more capable than I think I am, for considering me early on in your life decisions, for all of your advice, for listening to me moan and complain, for letting me get mad, and for taking on more than your fair share this past year so I could finish my thesis. Finally, Lauchlan, thank you for being with me these past two years as I wrote this thesis, first internally and then in a baby carrier sleeping as I bounced you and typed. Thank you for your companionship and for putting things into perspective for me during this stressful time. You have been a big distraction and a big motivation for me to finish and I appreciate you for both.

About The Author

Lisa Alexandra Warden was born in 1982 in Philadelphia, Pennsylvania, U.S.A. She received a B.S. in Marine Science and Master's degree in Science Education from Rutgers University. After teaching high school science for several years, Lisa decided to continue her own education. She began her Ph.D. in the Marine Microbiology and Biogeochemistry department of the Royal Netherlands Institute for Sea Research (NIOZ) under Prof. Jaap Sinninghe Damsté's supervision. Lisa's doctoral research is focused on paleoenvironmental applications of fossilized sedimentary lipids and the validation of proxies based upon these molecules. The results of her doctoral research are presented in this thesis.

Lisa currently lives in New Jersey with her husband, Eli, their son, Lauchlan, their two dogs, Isabel and Copper, and their cat, Mr. Rocky Balboa.